Generation and characterization of novel bifunctional protein and peptides for pharmaceutical applications

Baptiste Gouyou

Université Fédérale
Toulouse Midi-Pyrénées

THÈSE

En vue de l'obtention du
DOCTORAT DE L'UNIVERSITÉ DE TOULOUSE

Délivré par l'Université Toulouse 3 - Paul Sabatier

Présentée et soutenue par

Baptiste GOUYOU

Le 17 décembre 2020

Génération et caractérisation de nouveaux peptides et protéines bifonctionnels pour des applications pharmaceutiques

Ecole doctorale : **BSB - Biologie, Santé, Biotechnologies**

Spécialité : **MALADIES METABOLIQUES ET CARDIOVASCULAIRES**

Unité de recherche :
I2MC - Institut des Maladies Métaboliques et Cardiovasculaires

Thèse dirigée par
Philippe VALET et Mattia MATASCI

Jury

M. Pierre MARTINEAU, Rapporteur
M. André PELEGRIN, Rapporteur
M. Dario NERI, Examinateur
Mme Alessandra VILLA, Examinatrice
M. Philippe VALET, Directeur de thèse
M. Mattia MATASCI, Co-directeur de thèse

Acknowledgement

During the last 5 years (around 2 years as scientific associate and 3 as a PhD student) I worked at Philochem AG and learned a lot about multispecific biotherapeutics. It was a rich working experience where I had the ability to lead the projects presented in this thesis.

Therefore, I would like to thank Prof. Dr. Dario Neri, for giving me the chance to work at Philochem AG, for his support, his guidance and for allowing me to work on these exciting projects that I have presented in this thesis. Additionally, I would like to thank him for being part of the examination of my PhD.

I would also like to thank Prof. Dr. Philippe Valet, for giving me the chance to perform a collaborative PhD with his lab and Philochem AG. I would like to thank him for sharing his expertise on apelin and his support leading to the success of this PhD.

Since I was under his supervision, a special thanks belong to Dr. Mattia Matasci for his huge support during my PhD. He has helped me to grow as a scientist and taught me a lot about protein engineering and development. His expertise contributed a lot in the success of this PhD.

I am also grateful to Dr. Alessandra Villa, head of the biology group, who help me by discussing results and by giving me guidance to ensure the success and completion of the projects. Additionally, I would like to thank her for being part of the examination of my PhD.

I am very thankful to Dr. Samuele Cazzamalli who participated a lot on the success of my PhD by supporting with the chemistry and biodistribution experiments. And undoubtedly for the inspiring discussions we had, especially on the AAZ-IL2 and AlbuAPL projects.

Parts of this thesis have been achieved with the participation of external collaborators. Therefore, I am also very grateful to Prof. Dr. Marcus Franz and his team at Jena University, with whom we collaborated on the pulmonary hypertension project. His dedication for the experimental work was exemplary, the interactions we had on the

project were great and very useful. His collaboration lead to the success of this PhD project. Additionally, I would like to thank the team of Prof. Dr. Philippe Valet, especially Sophie Le Gonidec and Ophélie Pereira for their excellent work on the mouse experiment within the AlbuAPL project.

I would like to thank Philochem AG employees who helped me for the experimental work. Firstly, I would like to thank Tiziano Ongaro with whom I spent time performing biodistribution and cancer therapy experiments for both of our projects. Then I would like to give thanks to Jacopo Millul for his help on the chemistry, together with Dr. Samuele Cazzamalli, they both taught me to use LC-MS, HPLC and how to performed peptide chemistry. Anne Kershenmeyer, with whom I worked closely together with Dr. Mattia Matasci, was invaluable for her help with daily experiments in the laboratory. I would like to thank Lottie Howell for the organization of the lab. She ensured the availability of all the materials for the accomplishment of the experiments, an important work that people do not always recognize. Additionally, I would like to thank Dr. Roberto De Luca for his support on the biodistribution experiments. I am grateful to Sarah Ducellier who assisted me for the AAZ-IL2 project during her period at Philochem AG. Finally, I would like to thank Dr. Emanuele Puca and Jacqueline Mock for their assistance at ETH, especially for the ^{99m}Tc biodistribution experiments that have not been reported in this thesis.

Additionally, I would like to thank the people who made my days better during the period of time I worked at Philochem AG. Thus, I am grateful to Dr. Andreas Gloger, Louis Plüss, Dr. Florent Samain, Dr. Etienne Donckele, Jean-François Gosalbes and Eleonore Schmidt, who are currently working at Philochem AG but also Tina Frauenknecht, Bianca Scherer and Dr. Catherine Pemberton-Ross my former Philochem AG colleagues with whom I shared the office and kept me entertained whilst being productive at work.

In addition to the previously cited colleagues, I would like to thank all other Philochem AG employees who contributed to a nice working environment. They are Sheila Dakhel, Riccardo Corbellari, Lisa Nadal, Fred Peissert, Ilaria Biancofiore, Adriàn Gironda and Alessandro Sannino. I am grateful to Dr. Giovanni Neri and Dr. Isabelle Frouin from Philogen SpA for their work on the patent and the useful advice they gave me. I would also like to thank the clinical team, the proteomics team and the

administrative team of Philochem AG. Additionally, I would like to thank Dr. Sarah Wulhfard and Dr. Francesca Pretto for their part in recruiting me as a scientific associate 5 years ago and who taught me a lot about protein engineering and mouse work at Philochem AG.

Additionally, I would like to thank all ETHz PhD students and staff of Prof. Dario Neri for their support during the experiments I performed in their laboratory.

I would like to give thanks to Prof. Dr. André Pèlegrin and Prof. Dr. Pierre Martineau for accepting the roles of reporters for my PhD thesis and taking part in the examination of my PhD.

I wish all of the above successful careers and lives and hope to interact with them in the near future.

Finally, my deepest thanks go to Elodie who demonstrated to me once again how it is important to have a life partner and who supported me not just for these 3 years of PhD but also the 13 years that we have known each other. I also thank my parents and my brother who demonstrated their love and support despite the geographical distance between us.

Abstract

Multispecific molecules based on proteins or peptides represent a new generation of targeted biopharmaceuticals that hold great therapeutic promise. Engineered biotherapeutics drugs offer the possibility to combine multiple molecules with specific therapeutic functions featuring additional therapeutic activities, selective localization to the site of the disease and possibly extended half-life. Targeting disease-specific antigens with antibodies or small molecules has been an extensively explored strategy to selectively deliver therapeutically active payloads (e.g., cytokines, cytotoxic drugs or radionuclides) to the site of disease. The target antigen choice is of crucial importance for the successful development of targeted drugs. Alternative splice isoforms of fibronectin, such as the ones containing the extra-domain A (EDA), are extracellular matrix markers of tissue remodeling. EDA is overexpressed in different pathological conditions, including cancer and inflammatory diseases, but it is virtually absent from adult healthy tissues. Similarly, carbonic anhydrase IX (CAIX) is a cell surface tumor-associated antigen, which is overexpressed in 90% of renal cell carcinomas, but in healthy tissues his pattern of expression pattern is highly restricted to some gastrointestinal structures. Both EDA and CAIX represent excellent molecular targets for pharmacodelivery applications. Over the past two decades, a variety of cytokines or bioactive molecules have been fused to antibodies (e.g., immunocytokines and antibody drug conjugates) and small molecules (e.g., small molecule drug conjugates), in order to improve their therapeutic properties. Some of these bifunctional therapeutics have shown promising preclinical efficacy and have been further investigated in clinical trials for a variety of pathological conditions.

In this thesis, we used different methodologies to generate bifunctional therapeutics and performed initial evaluations of their therapeutic and pharmacokinetic properties.

Prompted by the postulated activity of interleukin 9 (IL9) in tumor immunity and resolution of chronic inflammation in arthritis, we have genetically engineered antibody-cytokine fusion proteins (immunocytokines) based on IL9 and the F8 antibody, which specifically recognize the EDA domain of fibronectin. An

immunocytokine variant showing improved *in vivo* targeting efficacy was further tested for therapeutic efficacy in various preclinical disease models.

In a second approach we have investigated the possibility of using small molecular ligands as targeting moieties for the pharmacodelivery of cytokines. To this aim we used the Sortase A enzyme to catalyze the covalent linkage between moieties containing specific peptidic sequences. The obtained product, termed AAZ-IL2, consisted in the fusion between acetazolamide, a CAIX ligand, and interleukin-2. Whereas AAZ-IL2 retained CAIX binding activity *in vitro*, it demonstrated only modest in vivo targeting efficacy.

Finally, we used a chemical assembly approach to generate a fusion molecule between a therapeutic peptide and a small molecule specific to human and mouse Albumin. Due to small size, peptides have very short half-life which limits their therapeutic use. To improve the pharmacokinetics of therapeutics, Albumin represents an attractive target, due to its very high abundance in blood. Albutag, a small ligand that selectively targets specific to Albumin, has been previously used to extend the half-life of various payloads. With the aim of enhancing the pharmacokinetic properties of a therapeutically relevant peptide, we have generated a new peptide-Albutag fusion molecule, and characterized it *in vitro* for Albumin binding affinity and *in vivo* for pharmacokinetic properties.

Altogether the research presented in this thesis may be of significance for the further development of bifunctional biopharmaceuticals with improved therapeutic and pharmaceutical properties.

Résumé

Les protéines ou peptides multi-spécifiques représentent une nouvelle génération de produits biopharmaceutiques prometteurs pour une application thérapeutique. Ces biomédicaments offrent la possibilité de combiner des molécules aux fonctions spécifiques comme l'ajout d'une activité thérapeutique, la localisation spécifique au sein de la maladie et une possible amélioration de la demi-vie. Le ciblage d'antigènes spécifiques aux maladies par le biais d'anticorps ou de petites molécules a largement été exploré pour la livraison sélective de charge thérapeutique (e.g., cytokine, cytotoxiques ou radionucléides) au sein de la maladie. Le choix de l'antigène est d'une importance cruciale pour le développement de molécules de ciblage. Les isoformes d'épissage alternatif de la fibronectine, comme celles contenant l'extra-domaine A (EDA), sont des marqueurs du remodelage de la matrice extracellulaire. Surexprimé dans différentes pathologies (cancer, maladies inflammatoires), EDA est pratiquement absent des tissus sains. De même, l'anhydrase carbonique IX (CAIX) est un antigène tumoral surexprimé à la surface de 90% des carcinomes des cellules rénales, mais dont l'expression dans les tissus sains est limitée à certaines structures gastro-intestinales. Ces antigènes représentent d'excellentes cibles moléculaires pour les applications de ciblage thérapeutique. Une variété de cytokines ou de molécules bioactives ont été fusionnées à des anticorps (immunocytokines et conjugués anticorps-médicament) et à de petites molécules (conjugués médicament-ligand à petite molécule), afin d'améliorer leurs propriétés thérapeutiques. Certaines molécules bifonctionelles ont démontré une efficacité préclinique prometteuse et sont actuellement en phase de recherche clinique pour différentes pathologies.

Dans le cadre de cette thèse, nous avons utilisé différentes méthodologies pour générer des molécules bifonctionnelles et évaluer leurs propriétés thérapeutiques et pharmacocinétiques.

Incités par la potentielle activité de l'interleukine 9 (IL9) dans l'immunité anti-tumorale et la résolution inflammatoire de l'arthrite, nous avons génétiquement généré des protéines de fusion anticorps-cytokines (immunocytokines) basées sur l'IL9 et l'anticorps F8, reconnaissant spécifiquement l'EDA. Une variante d'immunocytokine

avec la meilleure efficacité de ciblage *in vivo* a été testée de manière plus approfondie pour son efficacité thérapeutique dans divers modèles précliniques.

Par la suite, nous avons étudié la possibilité d'utiliser des ligands moléculaires pour la livraison pharmacologique des cytokines. Nous avons utilisé l'enzyme Sortase A pour catalyser une liaison covalente entre deux séquences peptidiques spécifiques. Le produit obtenu, appelé AAZ-IL2, est la fusion entre l'acétazolamide, ligand de CAIX, et l'interleukine-2. AAZ-IL2 a conservé une activité de fixation au CAIX *in vitro,* mais une modeste efficacité de ciblage *in vivo* a pu être démontrée.

Enfin, nous avons utilisé un assemblage chimique pour générer la fusion entre un peptide thérapeutique et une petite molécule spécifique à l'albumine humaine et murine. En raison de leur petite taille, les peptides ont une demi-vie très courte, limitant leur utilisation thérapeutique. Pour améliorer la pharmacocinétique de médicaments, l'albumine représente une cible intéressante, en raison de sa grande abondance dans le sang. L'Albutag, un ligand spécifique pour l'albumine, a été décrit comme pouvant prolonger la demi-vie de diverses molécules. Pour améliorer les propriétés pharmacocinétiques d'un peptide thérapeutique, nous avons généré une molécule de fusion peptide-Albutag, puis caractérisé son affinité pour l'albumine *in vitro* et ses propriétés pharmacocinétiques *in vivo*.

Dans l'ensemble, les recherches présentées dans cette thèse peuvent être importantes pour la poursuite du développement de produits biopharmaceutiques bifonctionnels ayant des propriétés thérapeutiques et pharmaceutiques améliorées.

Table of Content

1 Introduction

1.1 Biopharmaceuticals

1.1.1 Recombinant proteins as therapeutics

Proteins are macromolecules that consist of one or more amino acid chains. Within living organisms, they are involved in virtually every cellular process. Proteins were first described in the eighteenth century as a distinct class of biological molecules able to coagulate under heat or acid treatments. The first antibody-based therapeutic has been described in the 1890s when Emil von Behring and Erich Wernicke developed a serum therapy for the treatment of diphtheria. This discovery was awarded the Nobel Prize in Medicine and Physiology in 1901 [1, 2]. Further substantial progress in the field of therapeutic proteins was made in 1922 when insulin purified from animal pancreas was introduced for the treatment of severe type 1 diabetes mellitus. However, immunogenicity to this animal-derived product was often reported in a considerable percentage of patients, causing important side effects and partial loss of biological efficacy. Since 1982, human insulin is produced by recombinant DNA technology in bacteria, leading to a product with reduced immunogenicity and excellent efficacy [3]. The introduction of recombinant insulin and its clinical success set the basis for a new class of pharmaceutical products, i.e., recombinant therapeutic proteins. At the same time, the term “Biopharmaceuticals” was coined to describe a class of therapeutic proteins produced by genetic engineering techniques rather than by the conventional extraction from biological sources. This chapter is giving examples of different classes of therapeutic proteins that breakthrough and led to pharmaceutical products.

Therapeutic proteins generally display complex secondary and tertiary structures and require post-translational modifications that must be maintained for efficient therapeutic activity. Therefore, they are mainly produced by living organisms (e.g., bacteria, yeast, or mammalian cells), which are naturally able to properly fold and modify the produced proteins. The mode of action of therapeutic proteins is broad but generally limited to extracellular and cell surface interactions. Generally, proteins can have enzymatic or modulatory activities and exert their therapeutic function by (a)

replacing endogenous proteins that are abnormal or deficient, (b) activating/repressing existing pathways (c) provide novel functions or activities.

Enzymes are essential proteins for living organisms that act as metabolism effectors and defense weapons against microorganisms. They transform their cognate substrate into the desired product with high affinity and specificity. Therefore, if used in the correct setting, they can be very efficient therapeutics. Usually produced by recombinant technology, enzymes have been applied for the treatment of a wide range of medical conditions, including metabolic disorders caused by enzyme deficiencies, cancer and cardiovascular diseases, digestive system disorders, or acute poisoning, and bacterial infections. Successful enzyme products currently on the market include, for example, Lumizyme® (alglucosidase alfa) and Fabrazyme® (agalsidase beta) used as enzyme replacement therapy to treat patients with Pompe and Fabry diseases, respectively Erwinase® (L-asparaginase) or Oncaspar® (PEG-asparaginase) used in cancer treatment to deprive cancer cells of circulating asparagine and Activase® (recombinant tPA) used in the treatment of ischemic stroke, myocardial infarction, and pulmonary embolism [4–7]. Aside from their direct therapeutic applications, enzymes can be used as a tool for protein modification during the manufacturing of Biopharmaceuticals. In this thesis, we explored the use of an enzyme, termed Sortase A, for the generation of a multispecific product candidate. The results of this project are presented in Chapter 6.

Monoclonal antibodies (mAbs) represent the most important class of therapeutics that has been explored since 1975 when the hybridoma technology became available for their isolation. mAbs are complex glycoproteins that in humans are produced by B cells. Several technologies are currently available to generate therapeutic mAbs, including among other hybridoma technology, phage display, etc. mAbs can be designed to function in different ways. As such they are used to treat diverse disorders, including some type of cancer. They are highly specific proteins that can recognize cognate antigens with high affinity and selectivity. Clinical trials revealed antibodies as a powerful tool for (i) the neutralization of toxins or endogenous proteins, (ii) the activation or inhibition of cell receptors, and the corresponding signaling pathways (iii) for the delivery of bioactive payload at the site of the disease. Therapeutic mAbs represent a very successful class of biotherapeutics as of December 2019, seventy-

nine therapeutic mAbs have been approved for clinical use by the US FDA [8], and hundreds more are currently investigated in preclinical and clinical studies. The use of antibodies as therapeutics is extensively described from Chapter 2.1.3

Cytokines are a broad class of proteins that modulate the immune system response. Industrially produced by recombinant technology, this class of protein aid cell-to-cell communication in immune responses. By acting either as pro-inflammatory (e.g., IL2, TNF, IL12, IFN) or anti-inflammatory (e.g., IL10, IL22) mediators, cytokines play a critical regulatory role in the establishment and progression of many diseases. Consequently, if used as therapeutics, cytokines have great potential for treating a large variety of pathologies. Currently, several cytokine-based products are investigated in clinical trials, and some of them have reached market authorization. The first cytokine-based cancer immunotherapies were based on recombinant versions of interferon-alpha (IFNα) and interleukin-2 (IL2), which have been proven to be efficacious against a variety of cancers [9–16]. Due to their relatively small size, cytokines suffer from a fast body clearance. Consequently, cytokines generally need to be administered frequently and at high doses to obtain appropriate therapeutic efficacy; however, this often leads to systemic toxicities. In Chapter 2.1.1, more information about the therapeutic use of cytokines will be detailed, and in Chapter 2.2.2, strategies to improve their therapeutic efficacy will be explained.

Growth factors are small signaling proteins involved in different biological processes. Consequently, they hold great potential for clinical applications. Their therapeutic use is mainly seen in regenerative medicine, tissue repair, and wound healing. Being small-sized proteins, they suffer from low protein stability and short half-life but benefit from a rapid cellular internalization rate. Several recombinant growth factors are being evaluated in the clinic including, PDGF, VEGF, FGF, epidermal growth factor (EGF), keratinocyte growth factor (KGF), transforming growth factor-beta (TGF-β), granulocyte-macrophage colony-stimulating factor (GM-CSF), and others [17]. Despite their great potential as therapeutics, only a few growth factors have received market authorization. One example is Regranex® (Becaplermin, recombinant human-PDGF-BB) approved by the FDA in 1997 to treat diabetic foot ulcers.

Produced either chemically or by recombinant expression, therapeutic peptides are at the edge of biological therapeutic class. With a length of around 40 amino acids or

less, their 3D structure is less complex than the above described therapeutic proteins. Therapeutic peptides can be derivatives of endogenous human peptides (e.g., apelin, which will be discussed in Chapter 2.3.3) or be *de novo* discovered by the screening of synthetic display libraries (e.g., bicycle binders) [18, 19]. Due to their small size and flexible structure, therapeutic peptides potentially have improved tissue penetration, and thus may be of interest to reach challenging targets that cannot be reached by large protein therapeutics. However, their small size can be a double-edged sword. Indeed, since their weight is far below the renal clearance threshold, they are rapidly excreted from the body [20]. Besides, small peptides are usually prone to degradation by proteases, further reducing their *in vivo* therapeutic efficacy [21].

In order to improve the therapeutic efficacy of biologics and reduce their limitations, several modification strategies have been explored. For example, modification of proteins by fusion, conjugation and derivatization approaches have been applied to increase their half-lives. These modifications include but are not limited to Fc-fusion, albumin-fusion, PASylation, and PEGylation. These strategies aim at reducing dosage and side effects in patients while retaining the same therapeutic efficacy [22]. Additionally, antibody-engineering approaches have also been employed to arm antibodies with therapeutic payloads (e.g., cytotoxic drugs, cytokines, radionuclides, etc.). Such a strategy, allowing the targeted delivery at the site of the disease of the therapeutic payload, aims at limiting systemic toxicity and thus increase the product's therapeutic index [23–26]. Strategies to modify therapeutic proteins will be discussed in more details in Chapter 2.3

1.1.2 Current market of recombinant therapeutic proteins

Recombinant protein treatments are generally very expensive for both the patients and the healthcare system. On average, treatments based on therapeutic recombinant proteins are ranging from 10,000$ to over 100,000$ per therapeutic cycle or annually. For example, the cost per patient per year in 2017 for the treatment of rheumatoid arthritis with biologics, were 36,663$ (rituximab), 36,821$ (tocilizumab), 44,973$ (infliximab), and 46,532$ (abatacept) [27]. These high costs are mainly due to three factors: (i) the elevated costs of production (via fermentation of living cells) and quality controls, (ii) the necessity to cover the research and development expenses of the

current product, and (iii) the need for revenues to be reinvested into the research and development of new products [28].

Therapeutic proteins represent a huge market, consistent with the fact that they find applications in a broad range of disease such as cancer, autoimmune diseases, metabolic disorders, and others. Among the top ten best selling drugs, seven are monoclonal antibodies (mAbs). In 2018 mAbs had a market value of 115$bn, which is estimated to reach 300$bn by 2025. The seven best-selling mAbs in 2018 and 2019 were individually achieving revenues for more than 5$bn [8, 29]. Humira® (adalimumab), sold by AbbVie, was the best-selling drug in both 2019 (19.2$bn) and 2018 (19.9$bn), respectively. In 2019, Humira was followed by Keytruda® (pembrolizumab, Merck) 11.1$bn, Opdivo® (nivolumab, BMS) 7.2$bn, Avastin® (bevacizumab, Roche) 7.1$bn, Rituxan® (rituximab, Roche) 6.5$bn, Stelara® (ustekinumab, J&J) 6.4$bn and Herceptin® (trastuzumab, Roche) 6.1$bn [29].

Other therapeutic proteins, such as the recombinant cytokine manufactured by Biogen: Avonex® and Plegridy® (interferon beta), have generated 2$bn of revenues in 2018 [30]. Similarly, the sales of Ryzodeg®, a soluble formulation of insulin degludec and insulin aspart, reached 113$m in 2018 [31].

Additionally, the global peptide therapeutics market was valued at 25.0$bn in 2018 and expected to reach US 49.5$bn by 2027 [32]. More than 60 peptide-based drugs are already on the market, and several other therapeutic peptides are currently being evaluated in different phases of clinical trials [33].

1.1.3 Antibody therapeutics

1.1.3.1 Introduction to antibodies

The majority of monoclonal antibodies (mAbs) approved for therapeutic purposes are intact immunoglobulins G isotype (full IgGs). IgGs are heteromeric proteins characterized by a Y shape and composed of two heavy (HC) and two light (LC) chains connected via disulfide bridges. Functionally, they can be separated into variable (V) domains that bind the cognate antigen and constant (C) domains that determine the effector functions such as Fc receptor interactions and complement activation. The variable light (VL) and variable heavy (VH) domains, located at the N-terminal portions

of the light and heavy chains, respectively, contain the complementarity determining regions (CDRs). These clusters of hypervariable amino acid sequences are genetically rearranged *in vivo* to display a large diversity of structures, thus contributing to the antibody variability and specificity. The Fc fragment is composed of the remaining heavy portion of the antibody. This portion contains an N-glycosylation site at a conserved amino acid residue (asparagine 297). This posttranslational modification is essential for IgG-mediated effector functions, such as the interaction with Fc receptors and components of the complement system [34–36]. Different types of receptors, including Fc gamma receptors (FcγRs), and the neonatal Fc receptor (FcRn) can bind the Fc portion of IgGs. Whereas interaction with FcγRs triggers immune cell effector functions, binding to the FcRn regulates IgGs transport and recycling. Expressed mainly by monocytes or endothelial cells, the FcRn interacts with IgGs in the endocytic pathway and relocates them back to the cell surface, thus sparing them from lysosomal degradation [37–39]. From a pharmacological point of view, this recycling process has the advantage of extending the half-life of full IgG to several days, thus allowing for reduced dosing of mAbs while retaining efficient therapeutic activity [40]. In human six FcγRs family members have been identified, namely FcγRI (CD64), FcγIIA (CD32A), FcγRIIB (CD32B), FcγRIIC (CD32C), FcγRIIIA (CD16A), and FcγRIIIB (CD16B), which differ in their cellular expression pattern and ability to mediate effector cell responses [41]. Fc binding to an FcγR receptor leads either to activation or inhibition of downstream signaling. Activating FcγR induces antibody-dependent cell cytotoxicity (ADCC), degranulation, phagocytosis, and the release of cytokines or pro-inflammatory mediators. The four IgG human subclasses (namely IgG1, IgG2, IgG3, and IgG4) have different binding properties to FcγRs. Therefore, depending on the desired mode of action, distinct IgG subtypes are chosen for specific therapeutic applications. IgG1, 2, and 4 are the subclasses most frequently used for therapeutics. Since IgG1 antibodies trigger antibody-depended cellular cytotoxicity (ADCC) and complement-dependent cytotoxicity (CDC), they are mainly used in cancer therapy to recognize tumor-associated antigens. On the contrary, IgG2 and IgG4 are mainly used as blocking antibodies since they lack the ability to induce ADCC and CDC [42].

The generation of monoclonal antibodies started with the hybridoma technology first described by Kohler and Milstein in 1975 [2]. Hybridomas are immortalized cells

derived from the fusion of mouse B cell clones and myeloma cells, which produce a single antibody with unique specificity. Ten years later, the first monoclonal antibody, OKT3 (muronomab) [43], generated by hybridoma technology, received approval by the FDA for the treatment of transplant rejection [44]. However, early mAbs generated by hybridoma technology had only limited clinical success. Because of their murine nature, these early antibodies were poorly interacting with human FcRs leading to limited biological efficacy and short serum half-life. In addition to insufficient pharmacological parameters, they often induced immunogenicity via the production of human anti-mouse antibodies, resulting in anaphylactic reactions and serum sickness in patients [45–47].

Further developments in molecular biology made possible the generation of more human-like antibodies through the genetic combination of rodent- and human-derived antibody sequences. The first method developed resulted in the generation of mouse-human chimeric antibodies composed of murine variable domains and human constant chains to produce molecules that were composed of 70% human sequence [48]. The second method consisted of grafting only the murine complementarity-determining regions (CDRs) into human antibody scaffolds, resulting in antibodies with ca 85-90% human antibody sequences [49, 50]. More recently, transgenic animals were used in combination with hybridoma technology to obtain fully human mAbs. This technology, which was introduced in 1994 by the publication of the HuMabMouse [51] and XenoMouse [52] strains, relies on the immunization with the targeted antigen of mice genetically engineered to carry the human IgG locus (**Figure 1.1**).

Nowadays, several alternative methods for developing fully-human mAbs have been developed which rely on the *in vitro* screening of large synthetic libraries of antibody sequences. Phage display represents the first *in vitro* method described for the selection and generation [53]. In 2018 George P. Smith and Sir Gregory P. Winter were awarded the Nobel Prize in chemistry for their pioneer work in this field. In this technique, filamentous bacteriophages are genetically engineered to display on their surface recombinant antibody fragments. Large repertoires of antibody sequences in the synthetic library allow for the *in vitro* selection of specific and unique binders for a selected antigen, which following isolation, may be further matured *in vitro* to improve their antigen-binding affinity. This technique has led to the development of several

clinical grade antibodies that have been approved as therapeutics. For instance, Adalimumab (Humira®) was the first monoclonal antibody receiving FDA approval isolated from phage display libraries [8]. Additionally, our group has developed the antibodies F8, F16, and L19 antibodies from phage display technology [54–56]. These antibodies have been fused to cytokines to generate immunocytokines, some of which are currently under clinical evaluation. These biologics will be described in the following Chapters.

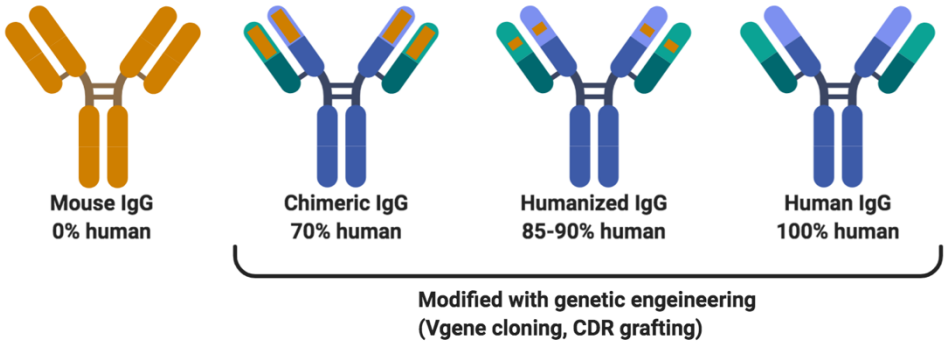

Figure 1.1: Representation of monoclonal antibodies developed as therapeutics. Orange parts represent murine sequences, whereas blue and green colors represent human sequences. Chimeric antibodies are 70% human (constant regions) and contain variable domains from mouse origin. Humanized mAbs are 85-90% human and contain only the hypervariable regions from mouse origin. Picture created using BioRender.com.

While full-size antibodies display an exceptional half-life and target affinity, their large size (150kDa) may limit their diffusion into the targeted tissue. Therefore, for specific therapeutic applications like pharmacodelivery, it may be suitable to engineer antibody fragments with reduced size but fully retaining the binding ability toward the cognate antigen. Several alternative antibody formats with different sizes have been proposed, which display diverse behavior in terms of body clearance, *in vivo* targeting performance, and stability (**Figure 1.2**).

Among alternative antibody formats, single-chain variable fragments (scFv) consist of the fusion between the variable heavy (V_H) and variable light (V_L) domains via a short 10-25 amino acidic linker. These single polypeptides result in small monomeric molecules of ca 27 kDa [57]. Therefore, scFvs retain the affinity toward the cognate antigen but lack valence-mediated avidity. Because of their small size, scFvs extravasate easily and diffuse more rapidly within tissues. At the same time, they are

more affected by renal clearance, and therefore, they generally have a short *in vivo* half-life.

The bivalent diabody format can be considered when a relatively small size (54kDa) combined with increased apparent affinity due to the avidity effect is required. In this case, using a shorter linker (3 to 12 amino acids) connecting the V_H and the V_L domains forces the molecule to fold as a non-covalent homodimer [58]. Therefore, the diabody format conserves fast body clearance but compared to scFvs, it generally shows increased *in vivo* targeting performances.

Another format that can be used is the small immune protein (SIP). This protein is a covalent homodimer, consisting of scFv genetically fused to the εCH4 domain of the secretory isoform s2 of human IgE. With its size of 75kDa, its pharmacokinetic profile stands between scFv and an IgG [59].

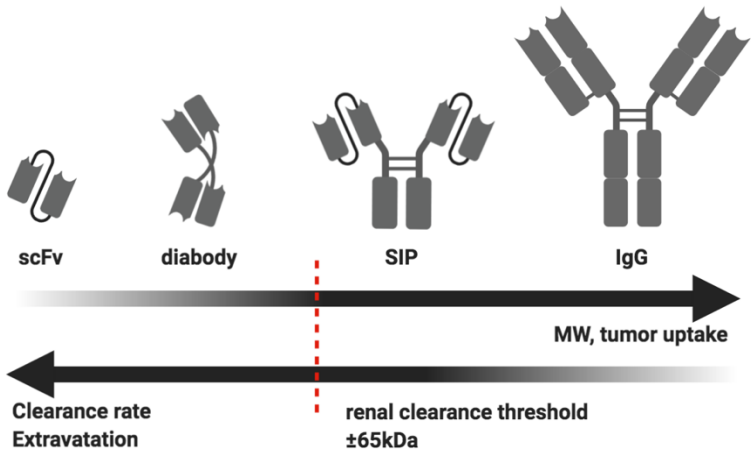

Figure 1.2: Comparison between antibody formats with their principal characteristics. From left to right: scFv, diabody, SIP and IgG. The figure is based on [60] and created with BioRender.com.

1.1.3.2 Monoclonal antibodies and on the market

Over the past thirty years, mAbs based therapeutics have been extensively developed, implemented, and used in the clinic to realize the great potential of targeted therapy. Nowadays, monoclonal antibodies represent a major modality of therapeutics for cancer and many other indications. Indeed, the versatility of antibodies for disease-associated antigen targeting make mAbs a perfect tool for a broad diversity of therapeutic approaches. Between 2018 and 2019, 18 new mAbs, antibody-drug

conjugates, and antibody fragments gained the FDA approval in the US (**Table 1.1**) for a total of seventy-nine approved therapeutic mAbs as of December 2019 [8].

As described in the previous chapters, mAbs are nowadays generated by several technologies (e.g., hybridoma, phage display, *etc.*) and can be therapeutically used via various mechanisms and strategies (see Chapter 2.1.2). Below we describe the mode of action of the six best-selling mAbs (**Table 1.2**).

Adalimumab (Humira®) was the first antibody approved by the FDA derived from phage display technology. It is an anti-TNFα antibody that exerts its therapeutic effect by preventing TNFα from interacting with its receptor. It is mainly used to treat rheumatoid arthritis, psoriasis, and Chron's disease, and it is commercialized since 2003 [8].

Nivolumab (Opdivo®), and pembrolizumab (Keytruda®), represent a new area in immunotherapies, the so-called immune checkpoint blockade (ICB) therapy. Both mAbs target the inhibitory T-cell surface receptor programmed cell death protein 1 (PD-1); therefore, the two antibodies block the PD-1 interaction with its ligands PD-L1/-L2 and reverse PD-1 pathway-mediated immunosuppression. Therefore, they are aimed at preventing T-cell exhaustion and enhance anti-tumor T cell activity. Nivolumab and pembrolizumab represent very successful examples of ICB therapy in cancer that are also explored in combination therapies [61–63].

Trastuzumab (Herceptin®) is a humanized antibody targeting the HER2/neu cells surface marker of breast cancer. The mechanism by which trastuzumab blocks the growth of HER2/neu overexpressing tumors may include both the inhibition HER2 mediated proliferation signaling, and ADCC mediated tumor cells lysis induced via its human Fc portion [64].

Bevacizumab (Avastin®) is a humanized antibody that targets the human vascular endothelial growth factor (VEGF). By blocking VEGF interaction with its cell surface receptor, Bevacizumab acts as an angiogenesis inhibitor, limiting blood supply to tumor tissue and resulting in tumor starvation and tumor growth inhibition [65].

Table 1.1: US FDA-approved monoclonal antibody on the market from 2018 to 2019. From [8], with editor permission.

mAb	Brand name	Company	Target	Format	Indication	US Approval
Burosumab	Crysvita	Kyowa Hakko Kirin/Ultragenyx Pharmaceutical Inc.	FGF23	Human IgG1	X-linked hypophosphatemia	2018
Lanadelumab	Takhzyro	Dyax Corp.	Plasma kallikrein	Human IgG1	Hereditary angioedema attacks	2018
Mogamulizumab	Poteligeo	Kyowa Hakko Kirin	CCR4	Humanized IgG1	Mycosis fungoides or Sézary syndrome	2018
Erenumab	Aimovig	Novartis	CGRPR	Human IgG2	Migraine prevention	2018
Galcanezumab	Emgality	Eli Lilly	CGRP	Humanized IgG4	Migraine prevention	2018
Tildrakizumab	Ilumya	Merck & Co. Inc./Sun Pharmaceutical Industries, Ltd.	IL-23 p19	Humanized IgG1	Plaque psoriasis	2018
Cemiplimab	Libtayo	Regeneron Pharmaceuticals Inc.	PD-1	Human mAb	Cutaneous squamous cell carcinoma	2018
Emapalumab	Gamifant	NovImmmune	IFNγ	Human IgG1	Primary hemophagocytic lymphohistiocytosis	2018
Fremanezumab	Ajovy	Teva Pharmaceutical Industries, Ltd.	CGRP	Humanized IgG2	Migraine prevention	2018
Ibalizumab	Trogarzo	Taimed Biologics Inc./Theratechnologies Inc.	CD4	Humanized IgG4	HIV infection	2018
Moxetumomab pasudodox	Lumoxiti	MedImmune/AstraZeneca	CD22	Murine IgG1 dsFv	Hairy cell leukemia	2018
Ravulizumab	Ultomiris	Alexion Pharma Inc.	C5	humanized IgG2/4	Paroxysmal nocturnal hemoglobinuria	2018
Caplacizumab	Cablivi	Ablynx	von Willebrand factor	Humanized Nanobody	Acquired thrombotic thrombocytopenic purpura	2019
Romosozumab	Evenity	Amgen/UCB	Sclerostin	Humanized IgG2	Osteoporosis in postmenopausal women at increased risk of fracture	2019
Risankizumab	Skyrizi	Boehringer Ingelheim / AbbVie Inc.	IL-23 p19	Humanized IgG1	Plaque psoriasis	2019
Polatuzumab vedotin	Polivy	Roche, F. Hoffmann-La Roche, Ltd.	CD79β	Humanized IgG1 ADC	Diffuse large B-cell lymphoma	2019
Brolucizumab	Beovu	Novartis Pharmaceuticals Corp.	VEGF-A	Humanized scFv	Macular degeneration	2019
Crizanlizumab	Adakveo	Novartis Pharmaceuticals Corp.	P-selectin	Humanized IgG2	Sickle cell disease	2019

Table 1.2: Top 10 best-selling monoclonal antibody drugs in 2018. From [8], with permission of the editor.

No.	Drug	Indication (1st US FDA Approval Year)	Company	2018 Revenue (USD)
1	Adalimumab (Humira)	Rheumatoid arthritis (2002) Psoriatic arthritis (2005) Ankylosing spondylitis (2006) Juvenile Idiopathic Arthritis (2008) Psoriasis (2008) Crohn's disease (2010) Ulcerative colitis (2012) Hidradenitis suppurativa (2015) Uveitis (2018)	AbbVie	$19.9 bn
2	Nivolumab (Opdivo)	Melanoma (2015) Non-small cell lung cancer (2015) Renal cell carcinoma (2015) Head and neck squamous cell (2016)	Bristol-Myers Squibb	$7.6 bn
3	Pembrolizumab (Keytruda)	Melanoma (2014) Head and neck cancer (2016) Non-small cell lung cancer (2015) Lymphoma (2018) Cervical cancer (2018) Microsatellite instability-high cancer (2018)	Merck & Co	$7.2 bn
4	Trastuzumab (Herceptin)	Breast cancer (1998) Gastric cancer (2010)	Roche	$7.0 bn
5	Bevacizumab (Avastin)	Colorectal cancer (2004) Non-small cell lung cancer (2006) Breast ERB2 negative cancer (2008) Renal cell carcinoma (2009) Glioblastoma (2011)	Roche	$6.8 bn
6	Rituximab, (Rituxan)	Non-Hodgkin's lymphoma (1997) Chronic lymphocytic leukemia (2010) Rheumatoid arthritis (2006) Pemphigus vulgaris (2018)	Roche	$6.8 bn
7	Infliximab (Remicade)	Crohn's Disease (1998) Rheumatoid arthritis (1999) Ankylosing spondylitis (2004) Ulcerative colitis (2005) Psoriatic arthritis (2005) Psoriasis (2006)	Johnson & Johnson	$5.9 bn
8	Ustekinumab (Stelara)	Psoriasis (2009) Psoriatic arthritis (2013) Crohn's Disease (2016)	Johnson & Johnson	$5.2 bn
9	Eculizumab (Soliris)	Paroxysmal nocturnal hemoglobinuria (2007) Atypical hemolytic uremic syndrome (2011) Generalized myasthenia gravis (2017) Neuromyelitis optica spectrum disorder (2019)	Alexion	$3.6 bn
10	Omalizumab (Xolair)	Asthma (2003) Chronic idiopathic urticaria (2014)	Roche	$3.0 bn

Rituximab (Rituxan®) is a chimeric antibody that has been approved by the FDA in 1997 for the treatment of lymphomas. It is a high-affinity binder of human CD20, a transmembrane protein highly expressed by over 95% of B cell lymphocytes but is absent on hematopoietic stem cells. Following Rituxan binding to cell surface CD20, Fc mediated effector functions results in the destruction of lymphocytes by several potential mechanisms, including CDC, ADCC, and direct lysis via NK cells [66].

1.1.3.3 Limitations

Therapeutic antibodies have become the predominant class of new drugs developed in recent years. However, despite their capacity to target specific antigens with high affinity, which generally results in fewer adverse effects, the generation and use of antibodies therapeutics still encounter several limitations. In the next paragraph, mAbs limitations and technological engineering advances to overcome them will be discussed.

An important limitation in the clinical use of mAbs that was predominantly observed with murine mAbs was immunogenicity. The immunogenic potential of murine antibodies has been initially addressed by the development of chimeric and humanized antibodies. More recently, *in vitro* technologies allowing the high throughput screening of fully human synthetic libraries or the use of transgenic mice strains carrying the human IgG locus have made possible the rapid generation of fully human antibodies with reduced immunogenic potential [36].

Treatment costs represent a substantial limitation in the widespread use of mAbs. At present, the elevated prices for monoclonal antibody therapies, mainly originating from the very high production costs and the need for high doses (often in the range of several grams/patient), makes it challenging, especially for certain countries, to use mAbs treatment for all potential patients [8, 36].

Pharmacological properties may limit mAbs therapeutic efficacy as they can impair efficient *in vivo* antigen targeting. Hence usually, the majority of injected protein leaves the body via excretory organs without interacting with the diseased cells. Poor *in vivo* targeting efficacy may result in suboptimal pharmacokinetics, lack of tissue penetration, and insufficient retention at the targeted tissue. These factors are influenced by various mAbs characteristics, including their size, shape, affinity, and

valency [36, 67]. Furthermore, low abundance and poor accessibility of the antigen at the disease site can negatively affect targeting efficiency. Whereas the large size of IgGs and their binding ability toward FcRn are factors that improve their *in vivo* half-life (range of days), these aspects may also be a handicap in penetration and diffusion through diseased tissues, especially in the case of solid cancers [68]. Depending on the therapeutic strategy and type of disease tissue to be targeted, mAbs affinity properties can pose some limitations. According to the "binding site barrier effect," high-affinity antibodies will bind tightly to a disease-associated antigen at first encounter. As a consequence, they will not diffuse deep inside diseased tissues until saturation of the more peripheral antigens is achieved [102]. Reduced affinity may allow better tissue penetration but may result in low residence time due to fast detachment of the antibody from the antigen. Ideally, a balance between high and low affinity should be found for each target.

Independently, from the antibody performances, mutations of the targeted antigen or modification in the downstream cell signaling can lead to acquired resistance to mAb therapy. This is particularly true for cancer cells that are particularly prone to mutagenesis and often develop resistance mechanisms to escape mAbs therapy. For example, mutations within the EGFR signaling pathway (e.g., *KRAS*, *NRAS*, *BRAF*, and *PIK3CA)* has been frequently reported to cause resistance to cetuximab in colorectal cancers [69]

Additional factors that may limit the therapeutic efficacy of mAbs may arise from their ability to appropriately interact with FcγRs to induce antibody-dependent cell-mediated cytotoxicity (ADCC). Indeed, the affinity between the Fc portion of an IgG and the FcγR receptors is often critical for immunotherapy efficacy. FcγR polymorphism can lead to a variable affinity between the Fc domain and the receptor allotypes, contributing to considerable differences in immune response among patients [70]. Similarly, IgG glycosylation at the Asn 297 residue in the Fc region is of crucial importance for the interaction of IgGs with FcγRs, and the type of carbohydrate moieties attached to this site can modulate the *in vivo* efficacy of antibodies. Accordingly, several strategies to modulate IgG glycosylation have been explored to enhance Fc effector functions, including genetic engineering of a manufacturing cell line, protein engineering, and modification of the manufacturing process and media [71]. Furthermore, mAbs have

to compete for FcγR binding with the high concentration of endogenous IgG in the blood, which is one reason why most mAbs have to be injected at very high doses to show therapeutic effect [72]. Finally, mAbs therapeutic efficacy may be mitigated by their ability to bind the inhibitory FcγRIIb receptor expressed by B-cells, macrophages, dendritic cells, and neutrophils [73].

1.1.4 Cytokines therapeutics

1.1.4.1 Introduction

Cytokines are small proteins important in cell signaling and play a complex regulatory function on inflammation and immunity. Cytokines act as immunomodulatory agents in an autocrine, paracrine, or endocrine fashion. By binding to specific receptors, they affect the behavior of target cells that may get activated or start a differentiation pathway. There are many types of cytokines, including interleukins (IL), interferons (IFN), tumor necrosis factors (TNF), chemokines, and lymphokines. Cytokines can be classified according to their functions. For example, some cytokines are primarily lymphocyte growth factors, other function as pro- or anti-inflammatory molecules, whereas other cytokines are involved in the polarization of the immune response to antigens. Regarding this last aspect, cytokines can be subdivided into type 1 (Th1-like) cytokines, mainly promoting a strong cellular immune response, and type 2 (Th2-like) cytokines, which mainly support a strong humoral immune response [74].

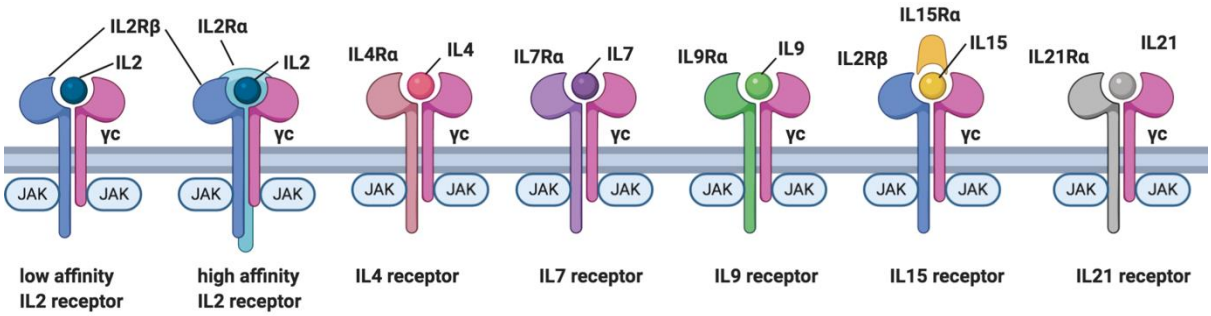

Figure 1.3: Representation of the γc receptor superfamily and their cytokines. Tyrosine kinase receptors from this family consist of a common γ chain (γc) and cytokine specific receptor partners. Upon activation via the corresponding cytokine, signal transduction is triggered via JAK/STAT. The figure was created with BioRender.com.

Cytokines are binding to a variety of different receptors, which are grouped into six major families: class I cytokine receptors, class II cytokine receptors, TNF receptors, IL-1 receptors, tyrosine kinase receptors, and chemokine receptors. Cytokine

receptors often include heterodimeric or heterotrimeric structures that combine unique cytokine-specific subunits with common receptor chains shared between different cytokines. There are three main shared cytokine receptors (i.e., gp130, γc, and βc). In this thesis, we mainly focused on cytokines that share the ability to bind to the common gamma chain receptor.

Table 1.3: Actions of γ_c family cytokines. From [75] with editor permission.

IL-2	• Promotes Th1, Th2, and Th9 differentiation and antagonizes Th17 and Tfh differentiation • Induces T cell and NK cell proliferation • Enhances Treg cell differentiation and function
IL-4	• Promotes B cell differentiation and Ig isotype switching • Promotes Th2 and Th9 differentiation • Proliferative effects on tissue-resident macrophages • Protection from helminth infection
IL-7	• Required for T cell development and homeostasis • Promotes memory $CD8^+$ T cell development • Essential for B cell development in mice but dispensable for B cell development in humans
IL-9	• Promotes mast cell proliferation • Augments mucus production by goblet cells
IL-15	• Essential for NK development, expansion, and survival • Promotes memory $CD8^+$ T cell development • Anti-cancer role for immunotherapy via actions on $CD8^+$ T cells and NK cells
IL-21	• Promotes B cell differentiation to plasma cells and augmenting Ig production • Actions on $CD8^+$ T cells and NK cells • Promotes Tfh differentiation and germinal center formation • Promotes Th17 differentiation • Inhibits Th9 differentiation
Ig: immunoglobulin, IL: interleukin, NK: natural killer, Tfh: T follicular helper, Th: T helper, Treg: T regulatory.	

The γc family of cytokines includes IL-2, IL-4, IL-7, IL-9, IL-15, and IL-21. Their receptor can be either heterodimeric or heterotrimeric being composed in addition to γc by one or two additional cytokine specific subunits (**Figure 1.3**). γc-containing receptors signal through the Janus family of tyrosine kinases (JAK)1 and JAK3, which then trigger signaling cascades via phosphorylation of specific members of the Signal Transducers and Activators of Transcription (STAT) family of transcription factors [75]. Gamma chain cytokines have a broad action in the human body by activating different immune cells. They participate in the immunosurveillance against cancer, mainly via their action on NK and CD8T cells (**Table 1.3**). However, when dysregulated, they are involved in the progression of different diseases such as asthma and autoimmune

diseases. With the advances of DNA recombination technologies, various γc-cytokines have been produced and administered exogenously in patients as therapeutics. Several cytokines are being investigated in the clinic for diverse diseases, and few of them have gained market authorization mainly for the treatment of cancer.

1.1.4.2 Cytokines in clinics and on the market

As cytokines are potent immunomodulators, they have been extensively investigated in the clinic to treat a variety of conditions, including cancer and inflammatory diseases (**Table 1.4**).

Recombinant interferon-α (IFNα) and interleukin-2 (IL2) were the first two cytokines biotherapeutics approved to treat cancers. IFNα is an important mediator of innate immunity during viral infection [76, 77], and has been involved in the survival, development, and activation of cytotoxic T-lymphocytes (CTL) [78]. IFNα (Intron A, Roferon A®) gained marketing authorization in 1986 for the treatment of some cancer types including hairy cell leukemia [14] follicular non-Hodgkin lymphoma [15] melanoma [16] and AIDS-related Kaposi's sarcoma [13] and later for the treatment of chronic hepatitis B and C. However, in cancer, IFNα is not widely used because its modest efficacy is associated with strong flu-like symptoms, including fever, headache, myalgias, arthralgias, nausea, and anorexia [77]. In 2019, Roche withdrew Roferon-A® from the market worldwide due to changes in clinical practice [79].

Interleukin-2, which will be described more in detail in chapter 2.3.2, is nowadays still used in the clinic. It has been approved for renal cell carcinoma treatment in 1992 and late-stage metastatic melanomas in 1998. Marketed under the brand name Proleukin®, IL2 exhibits an overall objective response rate of 14 to 16% and 5% of durable complete responses in advanced metastatic melanoma and renal cell carcinoma patients treated under high dose regime. However, since IL2 induces strong side effects at the therapeutic dose, including cytokine-storm and vascular leak syndromes, IL2 therapy is only possible for relatively fit cancer patients [9–12].

Table 1.4: Cytokines currently on the market. Based on [80–82]

Cytokine	Main biological functions	Indications	Example of Brand name	World first approvals in the world (Responsible Agency)	Companies having this cytokine or a derivative on the market
IL-1Ra	Binds IL-1 receptor without inducing signaling, natural IL-1 antagonist	Rheumatoid arthritis, neonatal-onset multisystem inflammatory disease	Kineret (Anakinra)	2001 (US)	Swedish orphan Biovitrum
IL-2	T-cell generation, homeostasis and proliferation stimulates NK cells.	Metastatic melanoma, renal cell carcinoma	Proleukin (Aldesleukin), Ontak (denileukin)	1992 (FDA and Fimea)	Novartis, Chiron, Eisei
IL-11	Promotes haematopoiesis, synergises with IL-3 and IL-4	Prevention of severe thrombocytopenia after myelosuppressive chemotherapy	Neumega (Oprelvekin)	1997 (FDA)	Wyeth Pharmaceuticals
IFN-α	Leukocyte interferon, anti-proliferative and anti-viral cytotoxic activity, increased expression of MHC class I antigen	Hairy cell leukaemia, AIDS-related Kaposi's sarcoma, hepatitis B/C, follicular lymphoma, malignant melanoma	Infergen, Intron-A, Roferon A	1986 (FDA)	Merk, Roche, Shering, Intermune, Interferon Sciences
IFN-β	Fibroblast interferon, similar activity to IFN-α	Relapsing multiple sclerosis	Avonex, Betaseron, Extavia, Rebif	1993 (FDA)	Bayer, Novartis, Biogen Idec, Merk Serono
IFN-γ	Modulates T-cell growth and differentiation promotes development of TH1 CD4+ cells	Chronic granulomatous disease, malignant osteoporosis	Actinmmune, Imukin	1994 (Fimea)	Intermune, Boehringer Ingelheim
G-CSF	Stimulates neutrophil development and differentiation	Chemotherapy-induced neutropenia	Granocyte (Lenograstim), Neupogen (Filgrastim)	1991 (FDA and Fimea)	AbZ-Pharma, Merckle Biotec, Ratiopharm, TEVA Pharma, Sandoz, Hospira, Apotex, Chugai-Sanofi-Aventis, Amgen
GM-CSF	Growth and development of macrophage and granulocyte precursors	Neutropenia under chemotherapy and bone-marrow transplant	Leucomax (Molgramostim), Leukine (Sargramostim)	1991 (FDA)	Berlex/Sanofi
TNF-α	Promotes inflammation, inhibition of tumorigenesis	Soft tissue sarcoma of the limb—administered via isolated limb perfusion	Beromun (Tasonermin)	1999 (EMA)	Boehringer Ingelheim

IFN-β exerts antiviral and antiproliferative properties similar to those of interferon alfa, recombinant preparations (IFN-β-1a: Betaseron®, and IFN-β-1b: Avonex®/Rebif®/Extavia®) are approved for the treatment of multiple sclerosis since 1993 [83]. Adverse reactions to IFN-β are similar to those of IFN-α, including fatigue, transient flu-like syndrome, and tachyphylaxis.

IFN-γ plays a key regulatory role in macrophage-mediated killing and granuloma formation in response to infection by intracellular pathogens. Recombinant IFN-γ (IFN-γ-1b) is currently approved only as an adjunct to antibacterial therapy in chronic granulomatous disease [84]. Adverse reactions to IFN-γ therapy include mild fever and flu-like symptoms, headache, and moderate injection site reactions.

IL11 is a growth factor that promotes the proliferation of megakaryocyte progenitors. Recombinant IL-11 is used in patients after certain chemotherapies to prevent thrombocytopenia by restoring the number of platelets [85]. Oprelvekin (recombinant IL11) is currently FDA-approved, although it is not widely used due to significant adverse effects, including dilutional anemia, fluid retention, congestive heart failure, arrhythmias, and anaphylaxis.

Tumor necrosis factor (TNF) is considered a major player in the inflammatory process. TNF binding to its two receptors (TNFR1 and TNFR2) results in the activation of T cells and NK cells cytotoxic effector functions [86]. Human recombinant TNF (trade name Beromun) is approved in Europe to treat advanced soft tissue sarcoma. However, due to its extreme toxicity, Beromun is used only in the isolated limb perfusion setting combined with melphalan chemotherapy [87].

1.1.4.3 Limitations

Cytokines play a central role in immune modulation; however, only a few cytokine therapeutics have reached market approval despite their great potential as therapeutic agents. The main limitation common to most cytokine therapeutics is the development of severe adverse effects in patients. Two main properties shared by most cytokines play a key role in the development of treatment-associated side effects. Firstly, cytokines exhibit a high degree of redundancy and pleiotropy. Thus, they modulate a wide range of functions in various cell types. Moreover, some cytokines may stimulate

the opposite biological effects in different cells. Furthermore, due to their small size, therapeutic cytokines are rapidly cleared from the body, and thus, to reach therapeutic efficacy, they need to be administered at high doses. While high doses may effectively enhance their therapeutic effects, they also worsen pleiotropic activities and systemic toxicity resulting in increased adverse effects in patients.

Protein engineering approaches have been extensively explored in order to reduce cytokine toxicity and increase their half-life. PEGylation, fusion to antibodies, or other proteins, and mutagenesis have been utilized to this aim.

The limitations of cytokine-based treatment are nicely summarized by the use of IL2 in cancer therapy. With its molecular weight of ca 15.5 kDa, exogenously-administered IL-2 (Proleukin) has an in vivo half-life of about 13 minutes in humans [88]. As a consequence, for effective cancer therapy, Proleukin needs to be administered repeatedly at high doses, which may cause a systemic response associated with severe side effects, limiting the use of IL2 therapy to the fittest portion of cancer patients [89].

1.2 Fusion proteins and bifunctional therapeutics

In the previous chapter, we have described the clinical benefits of intact therapeutic molecules and discussed their limitations. As single agents, both antibodies which can bind with high specificity their cognate antigen, and cytokines that are potent modulators of the immune reaction, have demonstrated relevant therapeutic activity. Several strategies have been explored to further potentiate these molecules by combining multiple functions on a single molecule. For example, technologies like genetic engineering, chemical conjugation, or enzymatic conjugation have been extensively used to functionalize antibodies. Antibodies armed with cytokines, cytotoxic drugs, radionuclides, or additional binding moieties, may represent more efficient therapeutics against various diseases. This chapter will discuss strategies for the multifunctionalization of therapeutic protein and provide examples of emerging classes of multispecific drugs, including Immunocytokines, bispecific antibodies, antibody-drug conjugates, small molecules drug conjugates, and albumin-binding based products.

1.2.1 Introduction to multispecific drugs

1.2.1.1 Concept

Multispecific drugs are resulting from the fusion of two or more binding moieties into a single molecule. These engineered molecules are being developed for the targeted delivery of bioactive payloads, to induce close contact between endogenous effectors and targets, or to extend the half-life of therapeutic molecules [90]. Multispecific drugs encompass extraordinary molecular diversity. They can be composed of small molecules, proteins, carbohydrates, lipids, or nucleic acids in any combination as a molecule of the same class (e.g., antibody and cytokine fusion) or hybrids between a molecule of different classes (e.g., antibody and cytotoxic fusion). Antibodies and small molecules represent the most frequently used targeting entities for the generation of multispecific drugs (**Figure 1.4**).

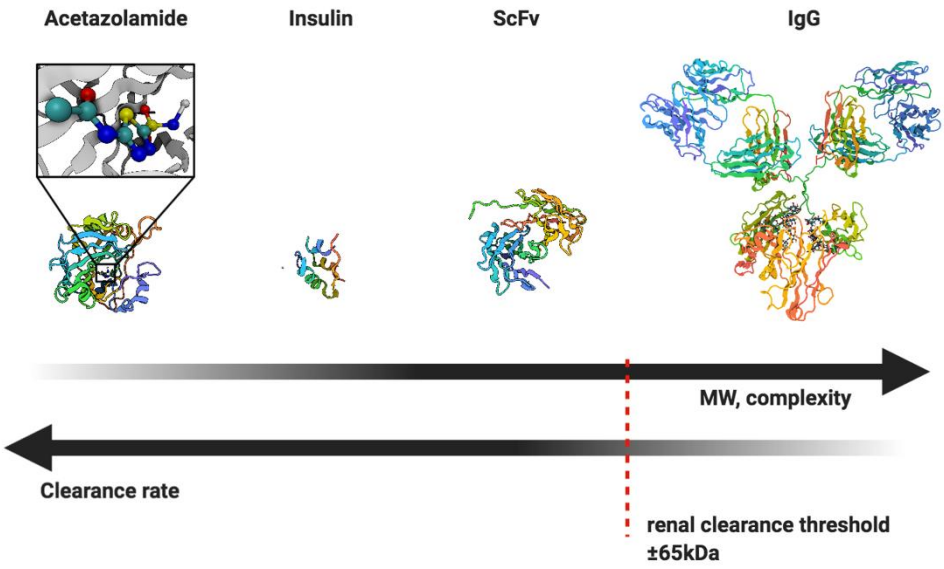

Figure 1.4: Size comparison between small molecules and proteins. Small molecules represent the smallest entities for pharmaceutical applications. Polypeptides (such as insulin) and single-chain Fv (ScFv) are more complex molecules but have a relatively fast clearance since their size lies under the renal clearance threshold (red dashed line). IgGs are complex structures and are above renal clearance. Therefore IgGs have an extended half-life compared to the other described products. 3D structures have been extracted from PDB number 3ML5, 1LPH, 6DSI, and 1IGY for acetazolamide in complex with mutant hCAVII, insulin, a scFv, and an IgG1, respectively. The figure was created by BioRender.com.

Whereas small molecules have been mostly used to deliver cytotoxic drugs and radionuclides, antibodies have been utilized with a higher versatility. In addition to

cytotoxic drugs (i.e., antibody-drug conjugates) and radionuclides (i.e., radioimmuno-conjugates), antibodies have been fused to bioactive proteins like cytokines, to generate so-called immunocytokines, to T-cell receptors for the production of CAR-T cells, or they have been engineered with different binding specificity resulting in bispecific antibodies (**Figure 1.5**)][23, 91–93].

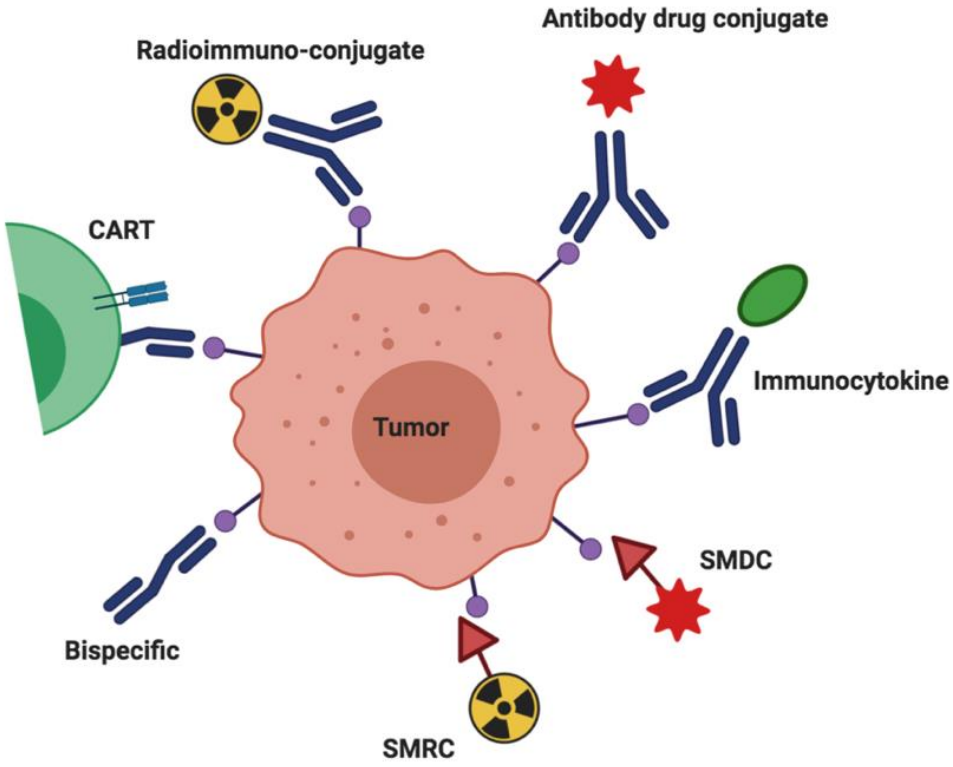

Figure 1.5: Representation of the use of antibodies and small molecular ligands for tissue-specific payload delivery. Selective for tumor-associated antigens, antibody, and small molecular ligands accumulate at the site of the disease. Radioimmuno-conjugates and small molecule radioconjugate (SMRC) acts by accumulating radioelements within cancer and can be used either as therapeutics or tracers for imaging. The same principle applies to the antibody-drug conjugate and small molecule drug conjugate (SMDC) armed with a cytotoxic payload. Immunocytokines allows the tissue-specific accumulation of immunomodulator payloads, mediating a localized immune response. Bispecific antibodies targeting tumor and T cells antigens mediate the engagement of target (tumor) and effector (cytotoxic T cells) cells. In comparison, CARTs are modified T cells expressing chimeric antigen receptors specific to tumor antigens, thus promoting their localization and activation at the cancer site. The figure was created with BioRender.com.

The classes of targeting moieties mentioned earlier exhibit specific advantages and limitations. The reduced size of small molecules allows better tissue penetration; furthermore, they usually do not induce immunogenicity and can be manufactured at relatively low costs. Because of their large size, antibodies extravasate and diffuse less efficiently within diseased tissues, but they usually have higher selectivity and

specificity toward their cognate antigens [94] (**Figure 1.4**). Whereas classical drugs usually do not have tissue specificity and diffuse in the whole body, multispecific drugs' main advantage is a better tissue specificity that may improve therapeutic activity while reducing systemic side effects [95]. Whereas the first small molecule multispecific drugs were approved for marketing before the full elucidation of their mechanism of action, during the last two decades, a number of prospectively developed multispecific drugs have reached market approval, including the bispecific antibodies catumaxomab, blinatumomab, emicizumab, and the antibody-drug conjugate gemtuzumab ozogamicin (**Table 1.5**), and several more are currently under clinical development [90].

Table 1.5: Approved multispecific drugs. From [90] with permission of the editor.

Drug	Date of first approval	Induces proximity of	Major indication
Thalidomide	1957	IKZF1 and IKZF3 with CRBN	Multiple myeloma
Cyclosporin	1983	Calcineurin and cyclophilin	Chronic dry eye
Tacrolimus	1994	Calcineurin and FKBP12	Organ transplant
Sirolimus	1999	mTOR and FKBP12	Organ transplant
Fulvestrant	2002	Estrogen receptor	Breast cancer
Lenalidomide	2005	IKZF1 and/or IKZF3 and CRBN	Multiple myeloma
Pomalidomide	2013	IKZF1 and/or IKZF3 and CRBN	Multiple myeloma
Gemtuzumab ozogamicin	2000	CD33-expressing cell and ozogamicin	AML
Catumaxomab	2009	EpCAM (cancer cell) and CD3 (T cell)	Malignant ascites
Blinatumomab	2014	CD19 (B-ALL cell) and CD3 (T cell)	B-ALL
Emicizumab	2017	Activated factor IXa and factor X	Haemophilia A

1.2.1.2 Limitations

Multispecific drugs are more complex with regards to their structure and mechanism of action than classical monospecific drugs. These factors pose additional challenges about their generation, structural optimization, pharmacokinetics, safety, manufacture, quality control, clinical development, and commercialization. In particular, their generation requires extensive efforts since two or more binding entities need to be developed, fused, and optimized as a single molecule. Furthermore, the lack of suitable animal models may pose unique challenges in their *in vivo* efficacy and toxicology assessment. As compared to monospecific drugs, the manufacture of multispecific drugs may be hampered by their increased tendency for aggregation, proteolytic degradation, physical instability, and low production yields [96–98]. Due to

their chimeric nature, engineered multifunctional protein drugs may elicit immunogenicity in the animals used for preclinical and toxicology studies and in humans. Furthermore, the increased size of multispecific small molecules may abrogate their compliance with the 'rule-of-5' characteristics [99], which may hinder oral availability, cellular uptake, and penetration of the blood-brain barrier. In general, multispecific drugs are also more challenging to administer and more expensive to be produced compared to traditional drugs. Selected examples of multispecific drugs and their limitations will be discussed in more detail in the next chapters.

1.2.2 Immunocytokines

1.2.2.1 Concept

Immunocytokines are a perfect example of an efficient multispecific biologic drug. While cytokines are highly potent immunomodulators, their systemic use can induce substantial toxicity. With the aid of a disease-specific antibody, cytokines can be selectively accumulated at the site of disease (e.g., tumor, inflamed joints of rheumatoid arthritis, psoriatic lesions). In this way, the therapeutic index of cytokines is enhanced by restricting their action to the tissue at which the therapeutic effect is required while sparing healthy organs from undesirable responses to the drug. The choice of the targeted antigen is crucial since its *in vivo* accessibility and expression pattern determines the efficacy of immunocytokines to localize at the disease site. Several companies are developing immunocytokines mainly for the treatment of cancer and inflammation conditions. For example, Roche has brought into clinical development, full IgG based immunocytokines targeting the extracellular tumor antigens CEA (cergutuzumab amunaleukin, CEA-IL2v) and FAP (RO6874281, FAP-IL2v) for the pharmacodelivery of an interleukin-2 variant [100, 101]. DI-Leu16-IL2 is an immunocytokine developed by Alopexx for the treatment of blood cancers, that consists of a humanized antibody targeting CD20 on B cells fused to human IL2 [102]. In alternative to tumor-specific cell surface markers, extracellular compounds can be efficiently used as targets for pharmacodelivery. For instance, Merck Serono has developed an IL12 based immunocytokine, termed NHS-IL12, which targets DNA released from necrotic tumors [103]. At Philochem, three clinical grade antibodies (i.e., F8, L19, and F16) have been developed which target extracellular matrix components, namely the alternatively spliced domains EDA (F8 antibody) and EDB (L19 antibody)

of Fibronectin, and the A1 domain (F16 antibody) of Tenascin-C. These antigens are neo-vasculature markers overexpressed during tissue remodeling. They are expressed in the disease tissues' perivascular structures undergoing remodeling but are virtually absent in healthy organs [54–56]. IL2 and TNF have been fused to the L19 antibody, targeting the EDB antigen, and the corresponding immunocytokines (L19-IL2 and L19-TNF, respectively) are currently in clinical development for melanomas, soft-tissue sarcomas, and gliomas (ClinicalTrials.gov Identifier: NCT03779230, clinicaltrial.gov identifier NCT02938299, EudraCT number 2015-002549-72, EudraCT number 2016- 003239-38). The F8 antibody, specific to the EDA domain of Fibronectin, has been used for the pharmacodelivery of IL-10. The corresponding immunocytokine (F8-IL10) is currently being tested in Phase II clinical trials for the treatment of rheumatoid arthritis and additional inflammatory conditions (ClinicalTrials.gov Identifier: NCT02270632) [104].

During initial development, the targeting efficacy of immunocytokines is usually assessed by radioiodine biodistribution, where radiolabeled protein preparations are intravenously injected into mice models of cancer or other diseases. Following administration, animals are sacrificed at defined time points to quantify radioactivity within the different organs. When fused to the L19 or the F8 antibody, cytokines accumulate into diseased tissues (e.g., tumors, arthritic joints, inflamed skin, or colon), with an efficiency comparable or even better than the one of the necked parental antibodies. Whereas certain cytokine fusions tested in our group, including those based on IL2, IL3, IL4, IL6, IL10, IL12, IL22, TNF, IFNα and G-CSF gave favorable biodistribution profiles [95, 105–117], other exhibited suboptimal pharmacokinetic parameters. Besides antigen accessibility, several additional factors are involved in the successful payload delivery to disease tissues. For example, cytokine trapping mediated by endogenous cytokine receptors expressed into normal tissues abrogated the efficient up-take of F8-IFNγ into tumors when the F8-IFNγ was injected at a comparable dose to other immunocytokines. Targeting performances could be restored when IFNγ knockout mice were used for the biodistribution experiment, or when the IFNγ receptors were pre-saturated by high dose injections of unlabeled F8-IFNγ [118]. A similar dose-dependent targeting efficacy was observed for other cytokines, including IL7, IL15, and GMCSF [119, 120]. Immunocytokine trapping by cytokine receptors could hinder pharmacodelivery at low doses and potentially cause

systemic toxicity in a therapy setting. Glycosylation is an additional parameter that may influence the targeting ability of immunocytokines. For instance, the high level of glycosylation of murine B7.2 resulted in the rapid elimination via the hepatobiliary route of the F8-B7.2 immunocytokine, consequently, in inefficient tumor targeting performances [121]. The manufacturing process can influence the protein glycosylation pattern, and in turn targeting efficacy. For instance, the differences in targeting performances of F8-IL9 preparations produced by two different fermentation methods could be attributed to variable content in terminal sialic acid on glycan residues, although the different preparations were fully immunoreactive in *in vitro* assays [122]. The size of immunocytokine can also influence its targeting efficacy. Indeed, whereas L19-IL12 and L19-TNF showed efficient tumor targeting *in vivo*, a triplespecific fusion between murine IL12, TNF, and the L19 antibody resulted in poor biodistribution properties, although the corresponding molecule having a MW of around 120 kDa, was efficiently binding its targeted antigen *in vitro* [123]. An additional crucial factor influencing the targeting potential of immunocytokines is the antibody format choice, which will be discussed in the next section.

1.2.2.2 Possible formats

Immunocytokines can be engineered using different antibody formats in order to modulate their biochemical properties (e.g., valency, size, Fc functionality). The antibody format can strongly influence the *in vivo* behavior of the molecule, with regard to extravasation, tissue penetration, and diffusion, retention time at the site of disease, or body clearance [124]. Usually, IgGs are used as a template for the generation of immunocytokines and can be engineered as intact full-size antibodies or antibody fragments. Some of the most common immunocytokine formats used in preclinical and clinical studies are presented in **Figure 1.6**.

Full-length IgGs have been extensively used to generate immunocytokines [23, 44, 66, 100, 109, 125, 126]. Using the IgG format, the cytokine can be attached either at the N- or C-termini of the heavy or light chain. As IgGs are bivalent, they show strong binding avidity toward the cognate antigen. Immunocytokines based on full-size IgGs are expected to have a circulatory half-life in the range of several days, due to recycling mechanisms mediated by the Fc portion. On the one hand, this may contribute to increased uptake into diseased tissue [127]. On the other hand, this could

induce systemic side effects due to off-target action of the payload. Furthermore, due to their large size, full-size IgG immunocytokines tend to have rather inefficient extravasation and tissue penetration. Interestingly, a half-life of only 1.6-8.2 hours has been reported for an IgG-based immunocytokines [126, 128]. The mechanisms leading to such a short half-life are not fully understood, but It has been hypothesized that cytokine-specific receptor-mediated clearance could be the cause [129].

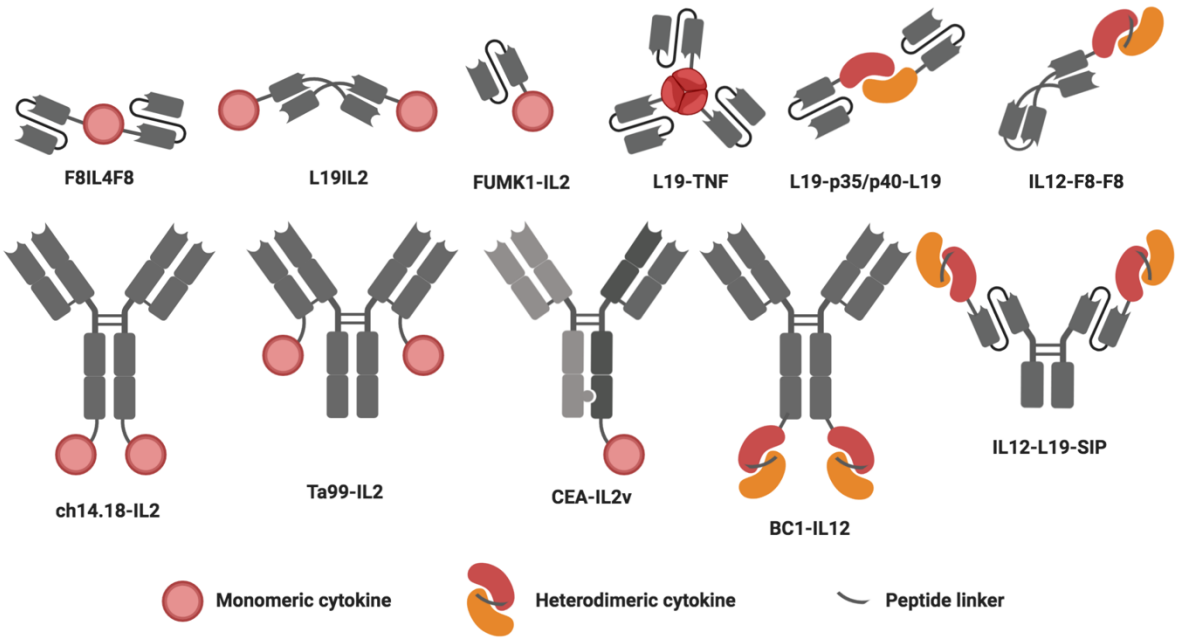

Figure 1.6: Examples of reported immunocytokines formats. The cytokine payload can virtually be attached at any N and C termini of intact or antibody fragments. Single-chain Fv (ScFv) antibody fragments have been used to generate F8IL4F8, FUMK1-IL2, L19TNF, and L19-p35/p40-L19. In comparison, diabodies have been used for the generation of L19IL12 and a tandem diabody for IL12F8F8. Intact IgGs have been used for the generation of the symmetrical immunocytokines ch14.18-IL2, Ta99-IL12, and BC1-IL12. In order to display a single cytokine moiety, an asymmetric IgG has been engineered with the "knob-into-hole" technology to generate CEA-IL2v. An additional format of antibody, the small immune protein (SIP), has been fused to IL12. These immunocytokines have been reported in [100, 106, 107, 109, 114, 129, 134–136]. The figure was created with BioRender.com.

Antibody fragments lacking the Fc portions are frequently used to engineer immunocytokines to reduce their residence time in the blood and thus increase tissue selectivity. Furthermore, due to their reduced size, antibody-fragment-based immunocytokines may improve extravasation and tissue penetration. One of the smallest antibody moieties used for immunocytokines is single-chain Fv fragments (scFv). As explained in chapter 2.1.3.1, the length of the linker between the VH and the VL domains promotes the folding of scFvs either as monomers or non-covalent dimers (diabody) [57, 130]. While the diabody format is particularly suitable for the

fusion of monomeric cytokines, monomeric scFvs can be used in the context of multimeric payloads (e.g., the trimeric TNF), in order to increase their binding valency while retaining a relatively small size [131]. In the design of immunocytokines based on antibody fragments, a compromise between efficient antigen targeting and rapid body clearance should be obtained to increase tissue selectivity and reduce systemic side effects. Biodistribution studies with radiolabeled immunocytokines have confirmed that at early time points, immunocytokines based on antibody fragments result in higher target to non-target organ ratios, compared to full-size IgG based products [59, 132, 133].

The choice of an appropriate antibody format also depends on the nature and structure of the cytokine payload, especially for homodimeric or heterodimeric cytokines. The heterodimeric IL12 cytokine composed of p35 and p40 subunits represents an example for which multiple immunocytokine formats have been investigated [107]. A single polypeptides format consisting of the p40, p35, and the L19 antibody in scFv format resulted in a monovalent immunocytokine with suboptimal targeting efficacy [95, 136]. A bivalent variant consisting of a covalent heterodimer between p40-scFvL19 and scFvL19-p35 showed improved targeting efficacy, but its manufacturability was hampered by the formation of p40-scFvL19 homodimers [136, 137]. More recently, a bivalent version consisting of the fusion of p40, p35, and the L19 antibody in single-chain diabody format resulted in both appropriate targeting efficacy and optimal manufacturability profile [114].

Another parameter to consider in the design of a novel immunocytokine is the bioactivity of the payload, i.e., the ability of the cytokine to interact with its receptor should not be impaired by the fusion to the antibody moiety. Whereas structural data about the cytokine/receptor complex may provide preliminary information for the engineering of a functional immunocytokine, the empirical testing in appropriate *in vitro* assays of multiple formats in which the payload is, for example, fused at the N- or C-termini of the antibody, is usually required.

Whereas several varieties of immunocytokine formats have been preclinically explored, to date, only full-size IgG and scFv-based immunocytokines have progressed into clinical trials [23].

1.2.2.3 Preclinical and clinical studies

Despite antibody-cytokine fusion candidates, based on a considerable number of cytokine payloads (e.g., IL2, IL12, IL15, GM-CSF, TNF, …), have shown promising preclinical results [95, 105–117], only a few payloads progressed into the clinic. Currently, only IL2, IL12, TNF, or IL10 based immunocytokines are being investigated in clinical trials for various indications [104, 128, 138–144].

IL2 based fusion proteins, which currently represent the most promising immunocytokines in the clinic, will be discussed in a dedicated chapter (Chapter 2.3.2.3). In this section, we will provide examples of preclinical and clinical outcomes for IL12 and TNF-based immunocytokines.

As mentioned in the previous chapter, the therapeutic efficacy and ability to localize at the site of disease for IL12 based immunocytokines strongly depend on the molecular arrangement of the various moieties in the fusion protein. Various IL12 immunocytokines have been engineered, which fully retain the ability of IL12 to activate NK cells and CD8+ T cells *in vitro* and *in vivo*. For example, our group is investigating IL12 fusions to antibody fragments, while two full-length IgG-based products are currently in clinical trials, namely NHS-IL12 [103, 145] and huBC1-IL12 [109]. NHS-IL12 tumor accumulation is mediated by the targeting of DNA released from necrotic tumor cells. Partial responses were observed in dogs with spontaneous tumors after a single injection of NHS-IL12 [146]. Its toxicity profile is being investigated in Phase I clinical trials, either as monotherapy (clinicaltrial.gov identifier NCT01417546) or in combination with the immune checkpoint inhibitor avelumab (clinicaltrial.gov identifier NCT02994953) [147]. BC1-IL12 recognizes an epitope on domain seven of fibronectin, which gets exposed via EDB expression during tissue remodeling [109, 148, 149]. BC1-IL12 tumor targeting and therapeutic efficacy have been confirmed in murine models of cancer [150]. In melanoma patients, BC1-IL12 stabilized disease progression for at least four months in 6 out of 11 patients, while only one patient achieved a partial response seventeen months later. Mainly minor adverse events were observed in this study, leading to the conclusion that BC1-IL12 was well tolerated [147].

As described in the previous chapter, TNF fused to an scFv is resulting in the formation of a stable non-covalent homotrimeric product [111, 131, 151–153]. Our group demonstrated that TNF fusion proteins could rapidly create hemorrhagic necrosis of the neoplastic lesions in mice. Tumor necrosis correlates with treatment efficacy and occurs within a few hours after injection [154]. However, when used as a single agent, TNF-based immunocytokines are not able to cure rodents of the tumor. A rim of residual tumor cells survives and is prone to regrowth once the treatment is ended. Nevertheless, TNF-based immunocytokines are highly potent, which makes them perfect candidates for combination therapies. Combination therapies are increasingly being used in cancer therapy to exploit the synergistic effect of certain drug combinations. Fibromun (L19-TNF) represents the only TNF-based product currently in clinical development. Developed by Philogen, Fibromun is the fusion of the anti-EDB antibody L19 in scFv format to human TNF [131, 155]. In preclinical studies, the murine homolog of Fibromun displayed excellent tumor-to-blood ratio of 100:1 and superior therapeutic activity compared to untargeted TNF, in a variety of murine models of cancer [123, 131, 134, 155–157].

In clinical trial phase I/II, monotherapy of Fibromun was well tolerated at doses up to 1mg per patient. Although a maximal tolerated dose (MTD) was not reached, tumor stabilizations were observed but not objective responses [158]. Another phase I study in patients with locally advanced extremity melanomas was conducted in the isolated limb-perfusion setting. In this setting objective responses were observed in 89 % of patients [159] at a dose 10-fold lower than the one used for recombinant TNF in similar procedures [160]. Furthermore, Fibromun localization at neovasculature structures within the tumors was confirmed by *ex vivo* immunohistochemical analysis [159]. Currently, L19-TNF (Fibromun), in combination with L19-IL2 (Darleukin), is evaluated in a Phase III trial for intralesional administration to stage IIIB/C melanoma patients (clinicaltrial.gov identifier NCT02938299, EudraCT number 2015- 002549-72) [161, 162]. Moreover, Fibromun is being tested in Phase III clinical studies for the treatment of patients with metastatic soft-tissue sarcoma in combination with doxorubicin (EudraCT number 2016- 003239-38).

1.2.3 Small molecule drug conjugates

1.2.3.1 Concept

Multispecific drugs based on small molecules have certain advantages over protein drugs, including low manufacturing costs, no immunogenicity, excellent bioavailability, and easier analytical characterization. Small molecule drug conjugates (SMDCs) are generally composed by a targeting ligand and a therapeutic payload, separated by a spacer that usually contains a cleavable bridge. The most commonly used therapeutic payloads are cytotoxic drugs and radionuclide. SMDC molecules are ideally designed to be stable in the bloodstream, but when they reach the targeting tissue, for example, the tumor microenvironment, their payload is released by linker cleavage. Some desired characteristics for optimal small ligands are high affinity and selectivity toward the targeted antigen and low toxicity. Small organic ligands having good affinity toward tumor-associated antigens are particularly suitable vehicles for pharmacodelivery. Because of their limited size, they can diffuse very rapidly and homogeneously into solid tumors, potentially reaching high tumor-to-organ ratios by combining extended residence time at the tumor site with rapid body clearance [163, 164]. SMDC products generally retain the affinity of the parental small molecule ligand toward the targeted antigen, while the linker used between the payload and the drug may influence its overall activity [165]. Some organic ligands have been described to be appropriate candidates for SMDC generation. Among them, folate analogs [166], prostate-specific membrane antigen (PSMA) binders [167], and ligands to carbonic anhydrase IX (CAIX) [168] will be described in the next chapter.

1.2.3.2 Selected examples of SMDC application

Used initially as a diuretic agent, acetazolamide (AAZ) is an inhibitor of carbonic anhydrase (CA) proteins and especially to the isoform 9 (CAIX). CAIX is a transmembrane protein that is overexpressed in certain types of cancer, such as renal cell carcinoma (RCC). AAZ has a strong affinity for CAIX (K_D = 8 nM), while a recently discovered acetazolamide derivative termed AAZ+, isolated from a DNA encoded libraries, has been characterized with a higher affinity (K_D = 0.200 nM) [169]. Biodistribution of near-infrared labeled AAZ and AAZ+ derivatives in RCC bearing mice displayed rapid and selective tumor uptake. In these experiments, AAZ+ showed

longer tumor residence time compared to the parental AAZ compound, compatible with its higher affinity to CAIX [169]. These results were further confirmed in quantitative biodistribution studies, using radiolabeled variants of AAZ and AAZ+ [170–173].

Various potent cytotoxic drugs have been coupled to AAZ or AAZ+ including, DM1, Monomethyl auristatin E (MMAE), cryptophycin-55 glycinate [165, 165, 168]. In preclinical models of RCC (SK-RC-52 bearing nude mice), AAZ coupled to DM1 displayed high tumor retardation when injected seven times every day compared to untargeted DM1, with good tolerability of the treatment [168]. Furthermore, AAZ and AAZ+ derivatives functionalized with the cytotoxic microtubule inhibitor MMAE, showed strong synergistic effects when administered in combination with IL2 or IL12 based immunocytokines (i.e., L19-IL2, and L19-IL12 respectively), or an anti-PD-1 check-point inhibitor [174].

Another SMDC of interest is the folate analog folate-vinblastin conjugate named Vintafolide and developed by Endocyte. Folate analogs target the folate receptor, which is overexpressed in many cancer types and metastasis [175, 176]. The use of Vintafolide in a clinical trial showed promising results for the treatment of ovarian cancer, especially in patients with high tumor expression of the folate receptor [177]. The product received conditional approval in Europe, but lack of efficacy in phase III clinical trials lead to discontinuation of its development [178].

Prostate-specific membrane antigen (PSMA) is a transmembrane protein virtually expressed in all prostate cancers, making it an excellent target for pharmacodelivery and imaging strategies using small molecular ligands. The EC1169 conjugate, developed by Endocyte, consists of a PSMA ligands conjugated via a stable enzyme cleavable linker to the cytotoxic agent tubulysin B hydrazide (TubBH). EC1169 has been investigated in Phase I clinical trials along with the companion diagnostic product ^{99m}Tc-EC0652, where it showed good tolerability and evidence of anti-tumor activity [177]. PSMA-ligands armed with radionuclides are also being investigated in the clinic. For example, treatment with the ^{177}Lu-labeled-PSMA-617 radiopharmaceutical resulted in >40% of objective response in patients with advanced prostate cancer [179].

The generation of small molecule ligands can be challenging, mostly depending on the nature of the target. The standard approach relies on the screening of large collections of compounds (“chemical libraries”) in which the single ligands are tested one by one for binding to the target of interest. Such an approach is time-consuming and labor-intensive besides requiring complex logistics, limiting screening capacities to libraries typically smaller than one million compounds [180]. The advent of DNA-encoded libraries has allowed the generation and screening of libraries of unprecedented size, thus facilitating the process of ligand discovery [169, 180–184]. More details on DNA-encoded libraries technology will be provided in Chapter 2.2.4.2.

1.2.4 Albumin binder therapeutics

1.2.4.1 Concept

A common limitation of many biologics, especially cytokines and peptides, is their fast body clearance limiting their therapeutic efficacy. Therapeutics that could stay in circulation for a longer period of time without causing systemic toxicity may be suitable to avoid the need for repeated injections. For these reasons, during the last decades’, technologies for half-life extension of therapeutic products have been extensively investigated (**Figure 1.7**).

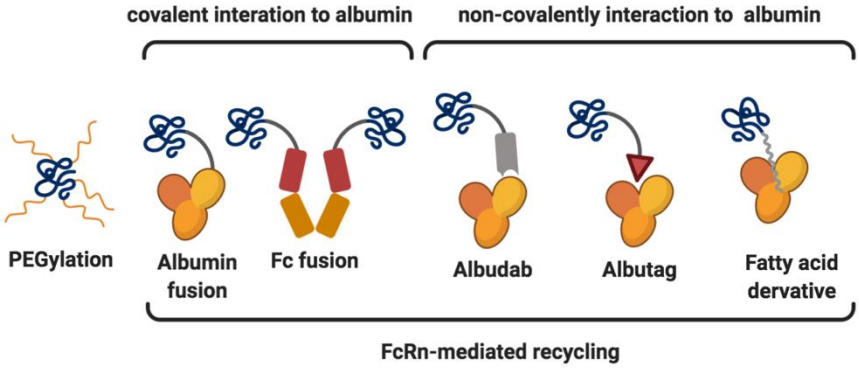

Figure 1.7: Representation of selected strategies for half-life extension. Pegylation has been extensively used for the extension of the half-life of proteins and peptides. The FcRn recycling process has been exploited by antibody Fc fragment fusion or albumin fusion. Additionally, more diligent strategies based on non-covalent interaction with albumin have been developed. Therefore, therapeutics have been fused to antibody fragments (e.g., AlbudAb®), small molecules (e.g., Albutag), or fatty acids (e.g., Insulin detemir), which are all interacting with albumin. Figure created with BioRender.com

A typical approach to increase the half-life of therapeutic proteins relies on increasing their size to minimize renal clearance [185]. To this aim, a commonly used approach is the conjugation of polyethylene glycol (PEG). The FDA currently has approved over

ten different PEGylated products; most of them rely on the random modification of lysine residues [186]. Such an approach generally leads to a heterogeneous mixture of pegylated proteins where each PEG-conjugate may differ in its activity and stability properties. Indeed, almost all PEGylated therapeutics result in decrease bioactivity compared to their parental non-PEGylated form [187]. More recently several technologies have been implemented for the site-specific pegylation of therapeutic proteins leading to more homogenous and active products [186].

The fusion of therapeutic proteins or peptide to the Fc domain of human IgG increases their circulating plasma half-life via neonatal Fc receptor (FcRn) binding and recycling [73]. Currently, 14 Fc-fusion drugs (including one biosimilar) are approved by the FDA to treat various clinical indications, including cancer, transplant rejection, inflammatory diseases, and monogenic disorders [188].

Albumin is the most abundant protein of the serum. Besides IgGs, albumin is also being recycled by the FcRn mechanism resulting in a half-life of about 19 days. Interestingly, albumin and IgGs bind to different sites on the FcRn, and they do not interfere with each other recycling process [190]. Therapeutic proteins can be either directly genetically fused to albumin or a non-covalently binding moiety specific to albumin, to improve their half-lives. Therefore, through fusion or binding to albumin, peptides or small proteins not only will have an increased size, superior to the renal clearance threshold but also they will follow the FcRn mediated recycling path of albumin. The approach based on non-covalent binding, rather than albumin fusion, may have the advantage that following the dissociation from albumin, the smaller multispecific drug will extravasate and penetrate the tissue more efficiently.

Antibody fragments raised against albumin have been extensively explored as fusion partners for half-life extension of therapeutic proteins. For example, the AlbudAb® half-life extension platform, developed by GSK, relies on the fusion to an anti-albumin domain antibody (AlbudAb®) [191]. This technology has been used for half-life extension of the GLP-1 receptor agonist Extendin-4 (GSK2374697) [192–194]. In clinical trials, GSK2374697 resulted in a half-life of 6–10 days (compared to ca 2.5 hours for Extendin-4), associated with the expected drug effects (e.g., reduction of postprandial glucose and insulin associated with a delayed gastric emptying) in healthy normal weight and healthy obese subjects [194].

Using fatty acids as a non-covalent albumin binding moiety has also been explored. For example, insulin detemir (Levemir®, approved in 2004) is an insulin analog that carries a C14 fatty acid chain attached to the terminal portion of its B-chain. The presence of the myristic acid allows a reversible interaction with serum albumin [195] and an extension of the insulin analog half-life from few minutes (for human insulin) to ca 8 h [196]. Recently, EPFL group of Professor Heinis has developed a technology for the half-life extension of therapeutic peptides. Their approach makes use of an albumin-binding ligand based on a peptide-fatty acid chimera. This heptapeptide-palmitoyl tag has high albumin binding affinity and increased solubility in aqueous solution. When the chimeric tag was conjugated to a cyclic peptide developed as factor XII inhibitor for anti-thrombotic therapy, a 24-fold half-life extension from 13 minutes to over five hours was observed in rabbits [197].

Chemical ligands targeting albumin have also been developed. For example, various small molecular albumin binders isolated from DNA encoded libraries have been described and used in preclinical studies [181, 198, 199]. In the next chapter, we will describe the Albutag, a small portable Albumin binder patented by Philochem AG.

1.2.4.2 Albutag technology

The discovery of small ligands is usually performed through the screening of chemical compound libraries, where the single library entities are tested one by one in a high throughput fashion. This procedure, which necessitates complex logistics, is usually limited to screening relatively small libraries (usually less than 1 million compounds). DNA-encoded chemical libraries (DECLs) represent a relatively new platform for ligand discovery, which allows the rapid screening of billions of compounds [169, 180–184]. DECLs consist of large organic molecule collections, which are individually coupled to an amplifiable DNA barcode [182]. DECLs are screened in a single test tube against proteins of pharmaceutical interest by affinity capture procedures. The identity of the isolated compounds is then determined by PCR amplification of the DNA barcodes and subsequent high-throughput sequencing [180, 200].

The small portable albumin binder, Albutag, has been isolated by DECL technology [181]. From the screening against albumin of a DECL containing 619 oligonucleotide compound conjugates, fourteen binder candidates were isolated [181]. The best

ligand, 4-(p-iodophenyl)butyric acid, was subsequently conjugated to lysine to introduce a negative charge, which was found to improve affinity towards albumin, and a reactive group to be used for further modifications. The final compound termed Albutag, a 4-(p-iodophenyl)butyric acid coupled to a D-lysine (**Figure 1.8**), forms kinetically stable complexes with both human serum albumin (HSA) and murine serum albumin (MSA) with a calculated K_D of 3.2 µM and 3.6 µM, respectively [181].

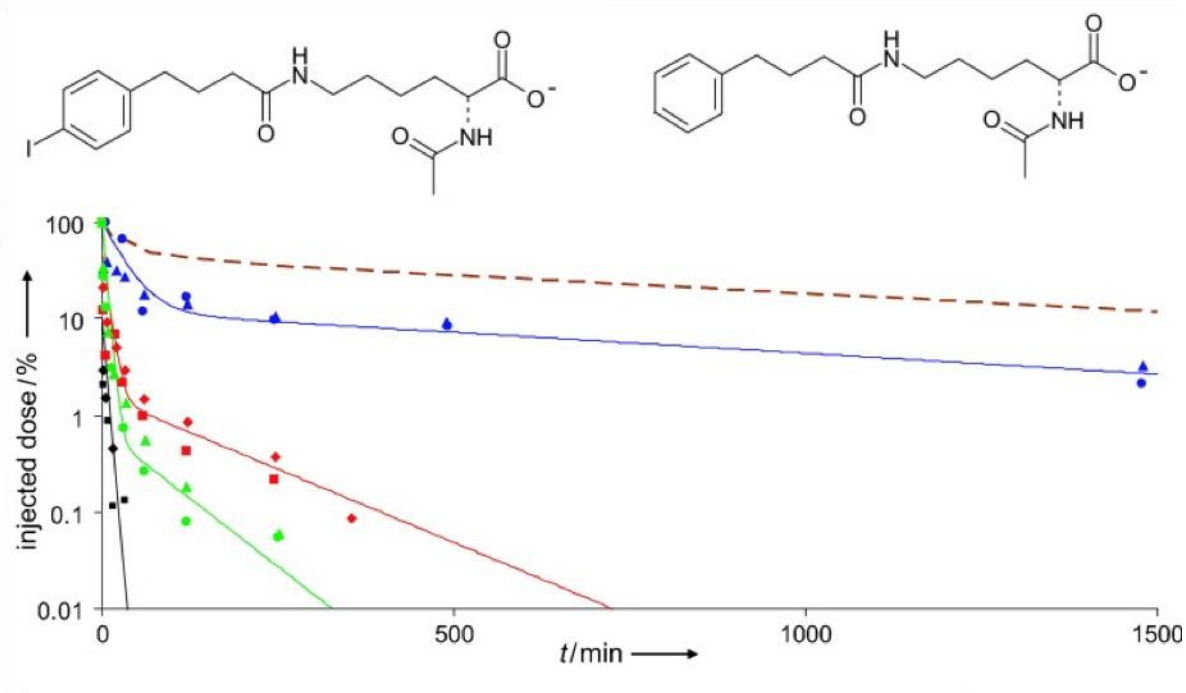

Figure 1.8: Albutag chemical structure and *in vivo* characterization of an Albutag-fluorescein conjugate. Left chemical structure of Albutag (428-D-Lys), and right structure of a control variant with a lower affinity toward albumin (622-D-Lys). The graph represents the pharmacokinetic profile of fluorescein (black), 428-D-Lys-FAM (blue), 622-D-Lys-FAM (red), and phenethylamine-FAM (green) after i.v. injection in mice. The plasma concentration-time course of 177Lu-labeled MSA is given for comparison (- - - -). Adapted from [181], with the permission of the editor.

When conjugated to fluorescein or 177Lu-DTPA, two contrast agents used for biomedical imaging, Albutag improved their in vivo circulatory half-life in mice by more than 100-fold [181] (**Figure 1.8**). Similarly, Albutag technology was applied to extend the half-life of a small antibody fragment specific for the EDA domain of fibronectin. The site-specific modification of the F8 antibody in scFv with Albutag resulted in a 10-fold increase in tumor uptake and a 35-fold slower clearance from blood in mice [198]. The versatility of the Albutag technology was further demonstrated in an alternative approach aimed at preventing cellular internalization of acetazolamide (a therapeutic agent inhibiting the activity of membrane-associated and intracellular carbonic

anhydrases described in Chapter 2.2.3.1). Avoiding acetazolamide internalization was expected to promote in vivo inhibition of membrane-bound carbonic anhydrases isoforms that are overexpressed in certain cancer types. The Albu-acetazolamide bispecific conjugate retained binding activity to both albumin and CAIX, and showed tumor growth retardation efficacy in renal cell carcinoma bearing mice [199].

Albutag is a highly versatile technology that can be used for different types of products, including small molecules and proteins. Since it results in significant extension of the half-life of the conjugated partner, dosage and administration schedule must be carefully optimized especially for highly potent or cytotoxic payloads. During this thesis, Albutag technology has been used to develop a long blood living peptide, described in chapter 7.

1.2.5 Other antibody derivatives of interest

Antibody-drug conjugate, bispecific antibodies, and immuno-radioconjugates represent important classes of multispecific biologics about which only a short overview will be given since they are not the main topic of my work.

1.2.5.1 Antibody drug conjugates

Over the last decade, Antibody-drug conjugates (ADC) have emerged as one of the most promising strategies for cancer treatment [25]. Currently, five ADC products are on the market for the treatment of different tumor types (i.e., Adcetris®, Mylotarg®, Kadcyla®, Besponsa®, and Polivy®) [25]. Similar to SMDCs, ADCs are tripartite drugs formed by a targeting moiety, here an antibody, a cytotoxic payload, and a cleavable linker [25, 201, 202]. Therefore, ADC products are potent oncolytic agents able to deliver highly cytotoxic compounds directly to cancer cells. Whereas ADC products are usually designed to internalize following antigen binding, and only after to release their payload in its active form within the targeted cells, non-internalizing products which specifically release their payloads extracellularly have shown considerable therapeutic efficacy [202]. The three ADC components (i.e., the antibody, the cytotoxic drug, and the linker) need to be judiciously chosen to generate a successful product. Highly affinity and specific antibodies are selected in combination with toxic components that typically have sub-nanomolar potency [25]. Currently, anti-microtubule agents are used in ca 70 % of the ADCs in clinical development. Since

this cytotoxic is has demonstrated efficacy only in few tumor types [91], additional drugs like DNA-damaging agents or the polymerase II inhibitor, α-amanitin, are being considered for the development of ADC products [25].

Traditionally, conjugation of the linker-drugs to an antibody takes place in a random fashion at accessible reactive amino acids such as lysines or cysteines. Therefore, highly heterogeneous products are generated where each sub-species may have distinct activity and pharmacokinetic properties. Furthermore, strict manufacturing procedures are required to ensure batch to batch consistency [25]. Various technologies for the site-specific conjugation of antibodies have been developed, including the specific modification of engineered cysteines or unnatural amino acids, and the use of enzymes that catalyze the modification of the antibody sugar chains or of specific short peptidic tags that can be engineered into the antibody sequence. For example, the SMAC-technology® developed by NBE therapeutics uses an engineered Sortase A enzyme to attach cytotoxic payloads at specific tags introduced on the C-termini of the antibody's heavy and light chain. In their setting, enzymatic conjugation occurred at 80-90% efficacy resulting in drug to antibody ratio (DAR) values of 3.4, while the use of specific affinity purification steps allowed the final isolation of highly homogeneous ADCs with a DAR of 4 [203].

1.2.5.2 Bispecific antibodies

Bispecific antibodies are engineered antibodies that can simultaneously bind two different antigens to induce close contact between cancer cells and cytotoxic effector cells. [23, 204]. The first binding moiety is usually specific for a tumor-associated antigen, whereas in most cases, the second one recognizes CD3 on T-cells. An MHC-independent cytolytic activity is then induced by the close contact and cross-linkage of the lymphocyte and the tumor cell.

A large variety of antibody formats ranging from tandem single-chain variable fragments (scFv) to full-length immunoglobulins with dual variable domains are used for the generation of bispecific antibodies [205]. Blincyto® (blinatumomab), a bispecific T cell engager (BiTE), was the first bispecific antibody that received marketing authorization. Blincyto® is designed to simultaneously target CD19 expressing B cell lymphomas and CD3 on T cells. In a phase II clinical trial, Blincyto® led to 81 complete

responses out of 189 patients suffering of acute lymphoblastic leukemia (Clinical trial NCT01466179) [206]. Based on these results, Blincyto® received FDA's accelerated approval in 2014.

1.2.5.3 Radioimmuno-conjugates

Although cancer treatment by radiation may result in high cure rates, radiotherapy is often associated with severe adverse events. Therefore, radionuclides have been coupled with cancer-specific antibodies to restrict irradiation to the tumor environment and reduce radiotoxicity in normal tissues [26]. Radiolabeled antibodies are used either for imaging purposes, in this case, γ (SPECT) or β^+ (PET)-emitting radionuclides (e.g., ^{99m}Tc and ^{18}F, ^{11}C, ^{124}I) are used, or for therapeutic applications using β^- emitters like ^{90}Y, ^{177}Lu, ^{131}I. Currently, two anti-CD20 products, namely Zevalin® and Bexxar®, are the only approved radioimmuno-conjugates against cancer [207, 208].

1.3 Therapeutic payloads used in this thesis

1.3.1 Interleukin-9

1.3.1.1 Interleukin-9 immunology

Interleukin-9 (IL9) is a pleiotropic cytokine that has been investigated for its pro and anti-inflammatory properties. This chapter will give an overview of its cellular sources and targets as well as its immunomodulatory functions.

At the onset of inflammation, IL9 is transiently expressed and rapidly disappears from the body [209–215]. IL9 is secreted by CD4+ T cells after stimulation by TGFB and IL4 [216]. Whereas IL9 was initially linked to T helper 2 (Th2) cells, more recently, a specific T cell subset that predominantly secrete IL9 has been characterized (i.e., Th9 cells) [217–219]. Also, other T helper subsets, namely Th17 and Treg cells, may express this cytokine [209, 219–221]. However, IL9 expression is not restricted to CD4+ T cells, since it has been reported to be also produced by activated mast cells and eosinophils. [222, 223], and more recently by group 2 innate lymphoid cells (ILC2) [211, 224].

Together with IL2, IL4, IL7, IL15, and IL21, IL9 belongs to IL2's superfamily of cytokines, which shares the common cytokine receptor γ chain (γc/IL2Rγ) for signal

transduction [225]. Through the interaction with its heterodimeric receptor, which consists of the specific IL-9 receptor α-chain (IL-9Rα) and the IL2Rγ chain, IL9 exerts its functions on multiple immune cell types [226, 227].

Cells of the lymphoid, myeloid, and mast cell lineages and epithelial cells of the lung and the gut have been reported to respond to IL-9 stimulation [209, 228, 229]. One of the main functions of IL9 is to promote the growth and function of mast cells, especially in response to pathogen infections [230–232]. IL9 stimulates mast cell production of TGFβ, which can induce pro-inflammatory downstream effects [233, 234], and in combination with FcεRI activation, IL9 can enhance mast cell expression of several cytokines, including IL1β, IL5, IL6, IL9, IL10, and IL13 [234, 235]. *In vitro* evidence also suggests that IL9 can stimulate the proliferation and/or differentiation of Th17 cells and enhance the suppressive effect of Treg cells [220]. Furthermore, IL9 can also promote the survival of ILC2 cells through an autocrine feedback loop [224].

Through its pro- and anti-inflammatory functions, IL9 has been suggested to play a critical role in the immune-pathogenesis of diverse inflammatory diseases and the modulation of immune tolerance [236, 237]. In the next chapter, the role of IL9 in pathological conditions will be described.

1.3.1.2 Interleukin-9 effect in various diseases

IL9 has originally been described to induce allergic airway inflammation and to promote the expulsion of parasites via its action on mast cells and epithelial cells, respectively [224, 230, 238, 239]. Furthermore, IL9 has been suggested to play a role in several other pathological conditions such as cancer and auto-immune disorders. However, studies aimed at identifying additional IL-9 functions have often provided conflicting results. Therefore, further investigation is needed to understand better the IL9 biology and its potential use as a therapeutic protein. This chapter will provide an overview of the role of IL9 in various pathological conditions.

The expression of IL9 and its receptor are elevated in the lungs of asthmatic patients. Staining of lung biopsies from patients with allergic and nonallergic lung diseases showed that IL9 and IL9R overexpression correlates with asthma phenotype and lung fibrotic conditions [240, 241]. The pathogenic functions of IL9 in asthma and lung inflammation have been mainly studied in animal models of airway inflammation [238,

242]. In a murine model of cystic fibrosis, IL9 has been reported to promote microbial-induced lung inflammation via a positive feedback loop resulting from the interaction between mast cells, ILC2, and TH9 cells [243]. Lung-specific overexpression of IL9 in transgenic mice spontaneously results in an airway inflammation phenotype which is characterized by eosinophils and mast-cell infiltration, mucus hypersecretion, bronchial hyperresponsiveness, increased thickness of the blood vessel walls, increased sub-epithelial deposition of collagen, and overexpression of inflammatory mediators (e.g., IL13 and histamine) [244–247]. Airway inflammation can be developed in IL-9 knockout mice [248]. However, antibody-mediated neutralization of IL9 has been described to ameliorate pathological inflammation in a pulmonary *Aspergillosis* cystic fibrosis mouse model [243]. IL9 depletion via antibodies also decrease lung inflammation and tissue damages caused by oxidative stress in a murine model of chronic obstructive pulmonary disease [249] and to suppress lung injury and pulmonary fibrosis in mice that were intranasally exposed to silica (e.g., decrease IL6, IL12 and TNFα levels) [241]. Controversially, one research group described a reduction in alveolar fibrosis in IL9 overexpressing mice that were intratracheally treated with silica particles [250]. Furthermore, despite the evidence from animal studies suggesting IL9 as a key modulator of allergic disease, treatment of patients with moderate to severe asthma with an IL9 blocking antibody (i.e., MEDI-528) did not show clinical benefits in a Phase IIb study and thus, the development of MEDI-528 for asthma was discontinued [251].

The role of IL9 in tumor growth is controversial whereas IL9 has been correlated to the progression of hematological malignancies both in mouse [252] and human [253], more recently, IL9 dependent anti-cancer activity have been reported in a variety of solid tumor models including melanomas [254] and colon carcinomas [255, 256]. According to its postulated immunomodulatory activity, IL9 based therapies have been investigated in cancer and inflammation preclinical models. In particular, Purwar and collaborators investigated the tumor immunity provided by IL9 in a preclinical therapeutic setting [254]. In the B16F10 melanoma models, they demonstrated the ability of recombinant IL9 to impair tumor cell growth by a mechanism dependent on mast cells but not on T or B cells. The authors obtained similar results when recombinant IL9 was administered to mice bearing Lewis Lung carcinoma tumors

suggesting potential use of IL-9 based therapies for the treatment of diverse cancer types.

Increased IL9 expression levels have been observed in a variety of autoimmune diseases, including Multiple Sclerosis (MS) [257] rheumatoid arthritis (RA) [258], Inflammatory Bowel Diseases (IBDs) [259], and systemic lupus erythematosus (SLE) [258, 260]. However, IL9 involvement in the pathological development of these diseases still needs to be elucidated since literature data on the corresponding preclinical models are often controversial. For example, it has been demonstrated that IL9 secreted by iNKT cells also induce the release of IL-10 and TGF-β and therefore decrease inflammation in the DSS-mediated colitis model [261]. However, in another mouse model of ulcerative colitis (oaxalone induce colitis), treatment with recombinant IL9 slowed the colon wound healing process compared to PBS, while IL9KO mice had a better overall wound healing profile [262]. Additionally, depletion of IL9 (via KO and anti-IL9 antibodies) in another colitis mouse model (TNBS induced colitis) led to protection against the establishment of colitis via conservation of the intestinal barrier integrity [263, 264]. Moreover, it has been reported that deficiency in IL9 or IL9R or treatment with anti-IL9 antibodies is protective against the development of experimental autoimmune encephalitis (EAE) [219, 265, 266], Whereas others described increased severity of EAE in IL9R knockout mice [220, 267]. Similarly, the role of IL9 in rheumatoid arthritis still remains unclear. In contrast, IL9 has been reported to be strongly overexpressed in the synovium of RA patients and correlates with the degree of tissue inflammation [268]. Recently, Rauber and collaborators have identified IL9 as a key player in the resolution of rheumatoid arthritis in the murine models of Antigen Induced Arthritis (AIA) and Serum Induced Arthritis (SIA) [269]. Accordingly, they proposed a mechanism by which IL9 would promote ILC2 proliferation through an autocrine loop, finally resulting in the activation of Treg cells and the suppression of inflammation.

1.3.2 Interleukin-2

1.3.2.1 Interleukin-2 immunology

Interleukin-2 (IL2) is considered a double sword-edge cytokine that acts as one of the main regulators of the immune system. Due to its immunostimulatory and

immunosuppressive functions, IL2 is a keeper of T cell homeostasis. IL2 has only a moderate affinity toward the heterodimeric variant of the IL2R (β and γ chains), expressed on naïve T cells. When T cells are activated, they increase the expression of the α chain of the IL2 receptor (CD25). Activated T lymphocytes are then displaying a heterotrimeric receptor (βγα), for which IL2 have a 50-fold higher affinity compared to IL2R βγ. By contrast, Tregs are constitutively expressing the high-affinity form of IL2R βγα, and thus outcompete naïve T cells for binding to IL2. Therefore, IL2 promotes the differentiation and proliferation of Tregs via the IL2Rβγα, in order to prevent autoimmunity [270], while it acts as a proinflammatory agent by stimulating the activation proliferation of cytotoxic CD8+ effector T cells and NK cells. Following pathogen challenge, IL2 stimulates the differentiation of CD4+ T helper cells into various effector T cell subsets and the generation of memory T cells, which are essential for long-lasting immunity [270]. For these reasons, IL2 immunological effects are dose-dependent; consequently, recombinant IL2 (Proleukin®) is used at a low dose to promote immune tolerance in chronic graft vs. host disease [271], while at high doses is used to enhance effector T-cell functions in cancer treatment [272].

1.3.2.2 Interleukin-2 treatment as a cytokine

IL2 is a potent inducer of cytotoxic T cells and NK cells and was the first therapeutic cytokine to be approved by the FDA for the treatment of metastatic melanoma and renal cell carcinoma (RCC) [272]. Its use at high doses produces a durable complete response in a small portion of patients. However, despite its therapeutic efficacy, repeated administration is generally associated with severe systemic toxicity, limiting its clinical use [273, 274].

Extensive efforts have been made to reduce IL2 toxicity and improve its therapeutic benefits. Several strategies are being explored to preferentially stimulate the expansion of Treg or effector T cells (Teff) [275]. These strategies include the generation of IL-2 mutants with a differential affinity towards the IL-2Rβγ or IL2Rβγα receptors [276–279], the use of antibody fragments specifically masking the epitopes of IL2 for the α, β, or γ subunits, once complexed with the cytokine [280–282], or the IL2 site-specific pegylation to promote binding to the distinct IL2 receptors [283]. For example, a site-specific PEGylated version of IL2 (namely, NKTR-214, bempegaldesleukin) has been developed by Nektar therapeutics [283, 284]. NKTR-

214, do not interact with CD25, which improves its specificity toward CD8+ Tcell compared to Tregs. Additionally, the six releasable PEG chains enhance the pharmacokinetics profile of IL2 (e.g., tolerability and half-life). As monotherapy, NKTR-214 resulted in tumor size regression and patient stabilization. Currently, combination treatments with NKTR-214 and immunotherapeutics, like immune check-point inhibitors, are under investigation [284].

Other approaches to increase the therapeutic efficacy of IL2 consists in the targeted delivery of IL-2 by fusing the cytokine to antibodies raised against disease-specific antigens. Antibody-based delivery of IL2 to tumors has shown the potential to improve its therapeutic index in immunocompetent mouse models of cancer, and several IL2 based immunocytokines are being currently investigated in the clinic [100, 138, 141, 285].

1.3.2.3 Interleukin-2 based Immunocytokines clinical studies

The fusion of IL2 to antibodies is being explored by different research groups and pharmaceutical companies, to improve the IL2 therapeutic index. In preclinical studies, IL2-based immunocytokines exhibited strong anticancer activity in different tumor models. However therapeutic efficacy is generally dependent on the tumor type, the nature of the immunocytokine, and its ability to selectively accumulate at the tumor site [56, 100, 101, 110, 134, 156, 286–289]. In this chapter, a selection of IL2-based immunocytokines will be described for their anti-cancer properties in preclinical and clinical studies.

The immunocytokine ch14.18-IL2 consists of the IgG chimeric antibody, ch14.18, and human IL2. The ch14.18 antibody is directed against ganglioside GD2, a marker of neuroectodermal tumors, that in healthy tissues is detectable only in the cerebellum and peripheral nerves. In preclinical studies, ch14.18-IL2 proved to be more effective than non-targeted IL2 in suppressing neuroblastoma growth and metastases dissemination [286]. Following these promising results, a humanized variant (i.e., Hu14.18-IL2), was developed in order to reduce immunogenicity and was tested in clinical trials. In a Phase II study in children with relapsed or refractory neuroblastoma, complete responses were observed only in patients with relatively small tumors

burdens (5 out of 23 patients), whereas no responses were detected in patients with the bulky disease [143].

Roche developed an IL2 mutein, called IL2v, with a reduced binding affinity toward CD25 [101]. Therefore, IL2 mediated immunosuppressive effects are impaired since IL2v does not signal through the IL2Rβγα of Tregs. Using the “knob-into-hole” technology [290], they fused IL2v to various antibodies (i.e., anti-CEA and anti-FAP), resulting in IgG based immunocytokines carrying a single IL2v moiety [100, 101]. While CEA is a marker of colorectal cancer, FAP overexpression is detectable in different cancer types. Currently, CEA-IL2v and FAP-IL2v immunocytokines are studied in clinical trials as monotherapies or in combination with anti-PD-L1 antibody (clinicaltrial.gov identifier: NCT02350673, NCT03063762, NCT03386721), anti-HER-2 antibody (clinicaltrial.gov identifier: NCT02627274), or anti-EGFR antibody (clinicaltrial.gov identifier: NCT02627274).

Merck also developed an immunocytokine based on a mutein of IL2 (NHS-IL2LT). The IL2LT mutein have lower vascular toxicity compared to wild type IL2, with increased specificity toward the high-affinity IL2 receptor [291] NHS-IL2LT consists of two IL2LT moieties fused to the C termini of the heavy chains of the NHS IgG antibody, which targets DNA released from the necrotic tumor [291, 292]. In a Phase I clinical trial, NHS-IL2LT treatment resulted in the stabilization of a portion of solid tumors. However, no objective response was observed in patients [138]

Our group decided to fuse IL2, in its wild type form, to various antibody fragments. As previously described, our group has developed clinical grade antibodies targeting splice isoforms of fibronectin (EDB and EDA) and tenascin-C (domain D) (i.e., L19IL2, F8IL2, and F16IL2, respectively) [141, 293]. Immunocytokines based on these antibodies fused to the wild type sequence of human IL2 showed promising therapeutic efficacy in various murine models of solid and hematological cancers, thus paving the way to their further development into the clinic [294]. Below are some relevant examples of clinical evaluation of L19IL2, and F16IL2 immunocytokines as monotherapy and in combination with other therapeutic modalities.

L19IL2 is a fusion protein between the L19 antibody in diabody format and IL2. L19IL2 has been extensively studied in murine models of cancer and has been investigated

in various clinical trials both as a single agent and in combination with other therapeutic modalities. The ability of L19-IL2 to specifically localize within tumors has been demonstrated by quantitative biodistribution studies in tumor-bearing mice [287]. Moreover, the *in vivo* targeting ability of the parental L19 antibody has been studied in humans, by imaging more than 100 patients with different types of cancer types [295–297]. In preclinical studies, the targeted accumulation of L19IL2 within tumors induced a strong infiltration of NK cells and T cells within the neoplastic mass, resulting in consistent tumor growth inhibition in various cancer mouse models [134, 156, 287, 288]. In clinical trials, the monotherapy administration of L19IL2 led to disease stabilization in 83% of renal cell carcinoma patients, associated with low toxicity [298]. Additionally, the combined intralesional administration of L19-IL2 and L19-TNF in melanoma lesions resulted in a considerable reduction of the lesions' size, making them suitable for surgical removal [299]. Systemic anti-cancer protective immunity was also hypothesized based on the observed concomitant reduction of both injected and adjacent, non-injected lesions [299]. Furthermore, a Phase Ib clinical trial (NCT02957019) is ongoing to evaluate L19-IL2 combined to rituximab in patients with relapsed or refractory diffuse large B-cell lymphoma.

Like L19, the F16 antibody, specific to the A1 domain of tenascin-C, proved to selectively localize at neo-vascular tumor sites in animal models and most human breast, lung, and head/neck cancers [56, 148, 289, 294, 300]. The F16-IL2 immunocytokine, which has a format similar to L19-IL2, has been evaluated in several clinical trials. F16IL2 has been tested in combination with low-dose cytarabine in Phase I clinical trial for patients with acute myeloid leukemia that relapsed after allogeneic hematopoietic stem cell transplantation [301]. Additionally, a clinical trial Phase Ib/II with F16-IL2 combined with doxorubicin has been performed in patients with advanced solid tumors and expansion into patients with metastatic breast cancer [293]. F16-IL2 was safely administered in both indication and showed some preliminary signs of anti-cancer activity [293].

1.3.3 Apelin

1.3.3.1 Apelin biology

Apelin is an endogenous peptide that acts as a ligand for the human APJ receptor and has been qualified as a peptide hormone [302]. Apelin has diverse functions on human physiology, such as cardiovascular regulation, body fluid homeostasis, and modulation of the insulin response [21, 303].

Apelin, short for APJ Endogenous Ligand, has been named for its ability to interact with the APJ receptor [304]. The apelin sequence is highly conserved between species, with the last 23 C-terminal amino acid residues being identical in mammals [303]. Apelin is expressed as a 77-amino acid peptide (preproapelin), which includes a putative 22-residues long N-terminal leader sequence and a 55-amino acid C-terminal domain which contains the receptor-binding site. Following secretion and signal peptide removal, apelin proprotein is further N-terminal processed to generate the three bioactive forms: apelin-36, apelin-17, and apelin-13 [303]. Additionally, the spontaneous cyclization of the N-terminal glutamine of apelin-13 can generate the pyroglutamated apelin-13 ([Pyr1]apelin-13). This peptide modification, which is common and does not impair peptide bioactivity, protects [Pyr1]apelin-13 from enzymatic lysis. While all described apelin variants are active, the shorter isoforms have higher affinity toward the APJ receptor and, therefore, are more potent [303]. Similar to other peptides, apelin is prone to enzymatic degradation. The angiotensin-converting enzyme 2 (ACE2) is known to cleave apelin isoforms at their C-terminal phenylalanine. Apelin-13 and [Pyr1]apelin-13 are then converted to apelin-13(1-12) and [Pyr1]apelin-13(1-12), which are still retaining the ability to activate APJ signaling [305, 306]. Amino acids responsible for receptor binding have been identified by alanine and D amino acid scanning. A representation of different APJ peptide ligands is given by **Figure 1.9**. Different optimized sequences leading to improved affinity toward APJ and increased half-life of the neopeptides have been identified [21, 307, 308]. These mutations might be of interest for the design of new APJ binders with more favorable pharmacological properties.

The short apelin-13 variant has been characterized for having a half-life in humans of approximately 8 minutes [309, 310]. Several factors contribute to such a short half-life,

including (i) renal filtration due to its small size, (ii) cellular internalization following binding to the APJ receptor [311, 312], and (iii) enzymatic degradation [313]. Due to its short half-life, a continuous apelin-13 infusion is required to achieve therapeutic efficacy, as discussed in the next chapter. However, strategies for apelin half-life extension have been explored.

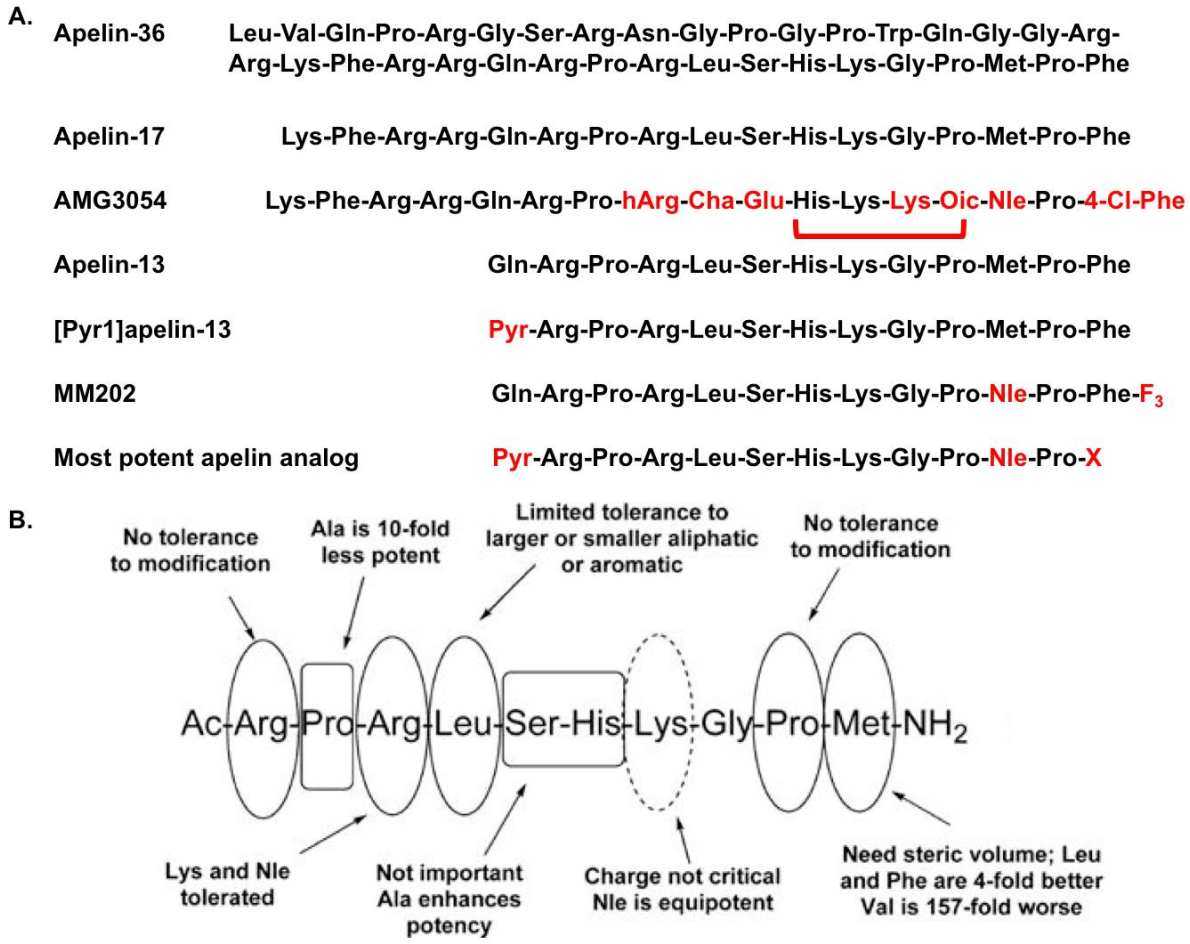

Figure 1.9: Examples of apelin peptide variants that efficiently activate the APJ receptor. (A) Mutated or modified amino acids compared to wild type sequences are represented in red. The apelin-55 can be cleaved, resulting in apelin-36 and apelin-17 and apelin-13. A post-translational modification results in the predominant apelin isoform [Pyr1]apelin-13. This isoform has longer blood half-life due to increased proteolytic resistance and is the most commonly used apelin peptide for therapeutic purposes. Amgen developed a modified variant of apelin-17, which contains multiple amino acid modifications and a lactam between the Glu10 and Lys13 residues. MM202 developed by GSK, features the substitution of Met11 with norleucine and the addition of a 3,4,5 trifluorophenylalanine (F_3) at the C-terminus. The most potent apelin variant has been identified by *in vivo* activity assay and is represented in this figure. (B) Summary of the essential or replaceable amino acids in the apelin-13 sequence, analysis has been performed by summarizing reported amino acid substitution screenings. Adapted from [21], with the permission of the editor.

Besides the amino acid sequence optimization with natural and non-natural amino acids, the fusion of apelin derivatives to other moieties has been explored to enhance apelin pharmacokinetics. For instance, an apelin-modified peptide agonist (MM202) has been fused to GSK's AlbudAb® (an antibody fragment which binds serum albumin), generating the MM202-AlbudAb conjugate. MM202 contains non-natural amino acids but conserves sequence similarity and functionality of endogenous apelin. Binding affinity toward APJ and albumin and *in vitro* and *in vivo* functionality of this bispecific molecule were fully retained [314]. In an alternative approach, apelin-13 has been fused to the Fc portion of human IgG to extend its half-life by FcRn-mediated recycling. Fc-apelin-13 had an extended half-life of about 33 hours in obese mice and retained biological apelin activity, including improved glucose disposal, amelioration of liver stenosis and heart fibrosis, and increased cardiac output [315].

As previously mentioned, apelin-based therapy would benefit from a half-life extension of the peptide; consequently, in section 7, the generation of a novel apelin product with extended half-life will be presented.

1.3.3.2 Therapeutic preclinical and clinical studies

The effect of apelin has been investigated in different pathological conditions, proving its high value for potential therapeutic applications. In this chapter, a selected number of apelin applications will be described, such as its use in metabolic diseases, cardiovascular diseases, and sarcopenia.

Endogenous apelin production decreases with aging in both humans and rodents. Aging is usually accompanied by progressive degeneration of skeletal muscle mass, a condition called sarcopenia. Since sarcopenia lacks early diagnostic tools and therapeutic interventions, it often results in the medical institutionalization of elderly individuals. Philippe Valet group discovered that old mice suffering from sarcopenia were recovering their muscle strength if treated with [Pyr1]apelin-13. Additionally, they discovered that apelin could stimulate muscle stem cells to enhance muscle regeneration [316]. Therefore, detection of apelin blood concentration has been proposed as an early marker of sarcopenia and its administration a potential therapeutic intervention for this aging-related disorder.

Apelin also impacts diverse metabolic diseases due to its ability to act on glucose and lipid metabolism and modulate insulin secretion. Preclinical data from obese insulin-resistant mice (due to high-fat diet) indicate that exogenous apelin administration improves this pathological condition [317–319]. In insulin-resistant mice, acute intravenous injection of apelin improves insulin sensitivity and increases glucose uptake by skeletal muscles and adipose tissues [320, 321]. Furthermore, chronic administration of apelin decreases insulinemia and abnormal fat retention in a hepatocyte independent manner [317–319]. The promising preclinical results on exogenous apelin administration led Philippe Valet and Pierre Gourdy to assess the efficacy of apelin in a clinical trial (ClinicalTrials.gov, NCT02033473). At a 30 nmol/kg dose, in healthy overweight men, [Pyr1]apelin-13 infusion significantly improved insulin sensitivity, while no adverse event could be detected by cardiovascular monitoring [322].

Additionally, apelin has been reported to have beneficial cardiovascular effects. Vasorelaxation [323], decrease arterial blood pressure and systemic venous tone [324–327], and increase cardiac contractility [328] have been observed in different preclinical models. Therefore, Japp and collaborators investigated vascular effects upon apelin infusion in humans. First, they treated healthy volunteers with an infusion of apelin-36 and [Pyr1]apelin-13. Both peptides induced vasodilatation and therefore decreased resistance of blood vessels. [310] Similar results were obtained in patients with chronic heart failure, where [Pyr1]apelin-13 infusion led to vasodilatation associated with an increased cardiac output [329].

Moreover, apelin has been reported to improve haemodynamic parameters in two models of pulmonary hypertension (i.e., the monocrotaline-induced model in rats and the genetic PPAR-γ knockout model in mice) [330–332]. Furthermore, Brash and collaborators reported that [Pyr1]apelin-13 administration in pulmonary hypertension patients ameliorated the pulmonary vascular resistance and increased cardiac output (ClinicalTrials.gov NCT01457170) [333]

In summary, the apelin peptide administration represents a potential treatment for various diseases such as heart failure, pulmonary arterial hypertension, type 2 diabetes associated with obesity, and sarcopenia.

1.4 Targets and animal models used in this thesis

1.4.1 Cancer models

1.4.1.1 Tumor bearing mice

The transition of a therapeutic candidate from *in vitro* characterization to the patient's bedside is particularly challenging in oncology. Cancer is a highly heterogeneous disease resulting from spontaneous mutations occurring in cells from various organs. Consequently, preclinical modeling of cancer requires a large variety of tumor models to mimic the different tumor types. To improve the standardization and reproducibility of experiments, immortalized tumor cell lines are widely used in oncology research. Rodent cancer models have become standard tools for the preclinical validation of anti-cancer agents. The main advantages of rodent models include the fact that mice are small and relatively easy to maintain and breed in captivity. Furthermore, they are genetically highly similar to humans [334–337]. The most commonly used mouse models in cancer research rely on the subcutaneous implantation into the flank of immunocompetent or immunocompromised host mice of cultured mouse (allograft) or human (xenografts) tumor cell lines, or in an alternative of mouse- or patient-derived tumor explants. Tumor growth is then monitored with calipers, allowing for rapid and cost-effective data assessment [334–337].

For the validation of anti-cancer therapeutic candidates, our group extensively uses tumor cell lines of different origins. Some examples relevant to this thesis include CT26, K1735M, SK-RC-52, and F9 cell lines. CT26 has been used as a model of undifferentiated colon carcinoma. This cell line has been isolated from mice exposed to N-nitroso-N-methylurethane-(NNMU), [338]. The K1735M cells is a murine model of melanoma, while the parental melanoma line, K1735, was generated by UV radiation of mice, the fast-growing K1735M line was derived from K1735 metastasis [339]. The SK-RC-52 is a preclinical model of human renal cell carcinoma generated from metastatic tumors obtained from patients under surgery [340]. The last cell line used is the F9, which is an embryonal carcinoma model. It has been generated from mouse testicular teratocarcinoma after implanting a six-day-old mouse embryo into adult mice testes [341, 342]. The generation method (UV and chemical) might have generated a more mutational burden in CT26 and K1735M. Thus these tumor models

might be more immunogenic into immunocompetent bearing mice compared to the F9 model. In our experience, these cell lines show robust and consistent growth once implanted into mice, which is of particular importance in order to compare the therapeutic performances of different products within different experiments [107, 108, 110, 110, 111, 134, 156, 174, 285, 289, 343]. The therapeutic efficiency of immunomodulatory products is usually largely tumor dependent, which is partially due to high variabilities among tumor cell lines with regard to their intrinsic immunogenicity, the expression of tumor antigens, and the composition of immune cells in the tumor microenvironment following tumor cell transplantation. Whereas certain tumor types (like the CT26) are highly immunogenic and consequently more responsive to cancer immunotherapy, poorly immunogenic tumors (like F9 and LLC) represent a more stringent test to evaluate the therapeutic potential of immunomodulatory products [344, 345]. Therefore, the use of multiple tumor models allowed us to identify highly promising anti-cancer immunocytokines, some of which have been further developed into clinical trials (e.g., L19IL2, L19TNF, F16IL2, described in chapter 2.2.2 and 2.3.2) [107, 108, 110, 110, 111, 134, 156, 174, 285, 289, 343, 346].

For the preclinical evaluation of immunomodulatory immunocytokines, the most common choice is to use syngeneic immunocompetent mice bearing tumor models (e.g., F9 murine teratocarcinoma cells in 129Sv mice) [341, 342]. As an alternative, nude mice are used to investigate the mechanism of action of immunocytokines and the therapeutic contribution of the different immune cell types, or the use of xenograft models (e.g., SK-RC-52), because immunodeficient mouse strains, B and T cells are lacking while the NK response is still present. [174, 285].

The immune cell population within the neoplastic tumor mass can differ depending on the parental tumor cell line. For example, untreated CT26 [134, 347] and K1735M [348] tumors have been reported to contain high levels of lymphocytes infiltrates, including CD8, NK, and Treg cells, while F9 teratocarcinoma generally contains only a limited number of immune cells [107, 108, 346, 349]. Accordingly, the terms cold and hot tumors are used to discriminate tumors with a high degree of lymphocyte infiltrates from tumors with a low content of effector T cells and NK cells but a high number of Tregs, respectively [350].

The tumor microenvironment composition can influence response to immunomodulatory drugs both in murine cancer models and in patients. There is increasing evidence highlighting the importance of the tumor microenvironment composition in determining the efficacy of cancer immunotherapy. Accordingly, monitoring the tumor immune microenvironment in patients' biopsies is increasingly being used to predict patients' prognosis and stratify patients for specific immunotherapies [351–354]. For example, analysis of tumor biopsies from patients treated with immune checkpoint inhibitors has been extensively applied to identify tumor microenvironment components associated with response or resistance to immune checkpoint blockade treatment. In particular, these studies highlighted the importance of the density and functional orientation of infiltrating T cells in providing an efficient response to this therapy [353].

1.4.1.2 Tumor specific antigens

For antibody-based cancer therapies, two type, of antigens may be considered, namely cell-surface antigens or the extracellular matrix components. Ideal antigen targets are either tumor-specific antigens (TSAs), which are arising from tumor-specific mutations or tumor-associated antigens (TAAs) representing normal proteins expressed at abnormal concentrations in cancer [355] (**Figure 1.10**). Additionally, optimal antigens should have no soluble isoforms that may interfere with tumor targeting and should be easily accessible *in vivo* [356]. Especially concerning this latter feature, angiogenic markers are particularly attractive. Tumor progression is generally accompanied by process of neovascularization, allowing the proliferating malignant cells to gain access to the circulation system. The newly formed blood vessels not only provide the tumor mass with nutrients and oxygen, promoting the expansion of the tumor and permit the extravasation of immune cells and therapeutic agents within the cancer mass. Remodeling of the extracellular matrix (ECM) is an essential event during angiogenesis [357]. The ECM represents a major structural component of the tumor microenvironment [358–360]. ECM is a highly dynamic three-dimensional structure composed of fibrillar proteins, glycoproteins, proteoglycans, and glycosaminoglycans. Besides providing physical support for cells to grow, the ECM influences diverse cellular functions, including migration, proliferation, and differentiation [361–363]. Whereas antibody-based therapies for cancer treatment are

predominantly based on targeting tumor-associated cell surface antigens, ECM components differentially expressed in cancer may represent optimal targets for therapeutic interventions. Indeed, ECM molecules are generally more stable and abundant than cell surface proteins. Furthermore, they are less prone to mutations as cancer progresses [364], therefore decreasing the risk of antigen loss or antigen-low escape mechanisms [92]. In the next paragraphs, examples of ECM and membrane-bound antigens used in this thesis for the pharmacodelivery of cytokines are presented.

Fibronectin (FN) is a major component of the ECM and plays important role in cell adhesion, migration, wound healing, and embryogenesis [362, 365]. FN expression is subject to alternative splicing events, generating up to 20 possible isoforms in humans. Three alternatively spliced domains have been identified, termed EDA, EDB, and IIICS, which are either fully (EDA, and EDB) or partially (IIICS) retained, or completely excluded in the different FN isoforms [366] (**Figure 1.10**). The EDA and EDB domains are virtually undetectable in healthy adult tissues but are highly overexpressed in tissues undergoing rearrangement and angiogenesis, like the neo-vasculature and stroma of many different tumors and the sites of chronic inflammation [361, 363, 367–369]. Besides an insoluble multimeric cellular variant that contains variable amounts of the EDA and EDB domains, FN also exists as a soluble dimer in plasma with a very low content of EDA and EDB [362]. Moreover, the alternatively spliced EDA and EBD domains are highly conserved between rodents and humans, facilitating the transferability of findings from preclinical studies into clinical applications. Consequently, our group has developed clinical grade antibodies targeting the EDA (i.e., F8) and EDB (i.e., L19) extradomains of fibronectin that are being currently used both in preclinical studies and clinical applications [54, 294, 369].

Carbonic anhydrases (CAs) represent a family of metalloenzymes associated with tumor progression, particularly the membrane-bound isoform CAIX [370, 371]. Fifteen isoforms have been described in humans, which differ in their pattern of expression, subcellular localization, and kinetic properties [370]. Carbonic anhydrases catalyze the interconversion of carbon dioxide and hydrogen carbonate, and as such, are involved in cellular pH regulation and the active transport of CO_2 and hydrogen carbonate across cellular membranes [370, 372]. CAIX is a transmembrane

homodimeric enzyme over-expressed in more than 90% of clear cell renal cell carcinoma (ccRCC) subtypes [370, 371, 373]. Furthermore, since CAIX is strongly upregulated under hypoxia conditions, many solid tumors express CAIX in their hypoxic regions (**Figure 1.10**). CAIX is detectable in healthy organs only in few structures of the gastrointestinal tract (e.g., stomach, duodenum, and gallbladder) [372].

Our group has extensively investigated CAIX as a tumor-specific cellular target and has developed small molecular ligands such as acetazolamide derivatives for pharmacodelivery purposes. Several SMDC and radioactive conjugates products targeting CAIX showed promising results in rodents and humans [164, 165, 168, 169, 171, 174, 374].

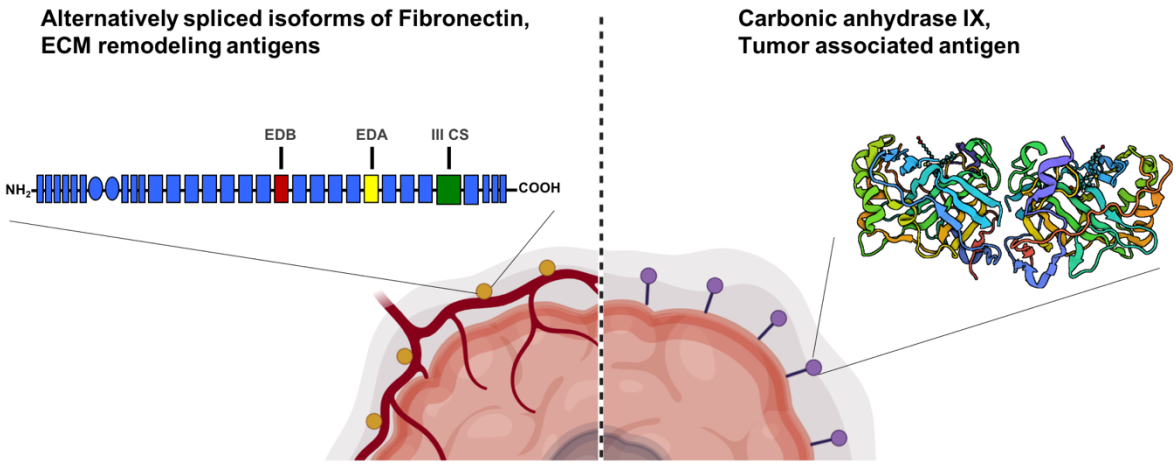

Figure 1.10: Comparison of antigen localization for the targeted delivery of payloads in cancer. ECM antigens such as EDA or membrane-bound antigens such as CAIX can be targeted by antibody or small molecules. The accessibility of ECM antigens is improved due to colocalization with newly formed blood vessels. Whereas improved tissue penetration is desired for membrane-bound antigens. Created with BioRender.com

1.4.2 Collagen induced arthritis as rheumatoid arthritis model

1.4.2.1 Collagen Induced Arthritis

Rheumatoid arthritis (RA) is a progressive autoimmune disease that primarily affects the joints and is associated with tissue damage such as cartilage degradation and bone erosion (**Figure 1.11**) [375, 376]. Its characteristic trait is a persistent inflammation of the synovial membrane and an invasive synovial tissue formation. Several cell types of the innate and acquired immune systems infiltrate the synovial

tissue and contribute to the inflammatory process including T cells, B cells, monocytes/macrophages, mast cells, and dendritic cells [377, 378]. Inflammation is followed by tissue morphology changes such as hyperplasia of the synovial tissue and the formation of a “pannus” at the cartilage-bone junction. Persistent inflammation is leading to articulation swelling, pain, and bone erosion [377–379]. Additionally, the pathogenesis of rheumatoid arthritis is accompanied by process of neovascularization.

Rheumatoid arthritis is affecting approximately 1% of the population worldwide [380–382]. Therefore, modeling of this disease is suitable to assess the preclinical efficacy of therapeutic candidates.

Among all preclinical rheumatoid arthritis models, the collagen-induced arthritis (CIA) mouse model is the most commonly used. In this model, rodents are immunized by two subcutaneous injections (within 18 days) at the base of the tail of an emulsion of bovine type II collagen in Completes Freund’s Adjuvant. Consequently, mice develop an autoimmune reaction against collagen II (the major cartilage component) that results in severe arthritis in multiple joints within two to three weeks. The CIA rodent model shares many of the pathological features of human rheumatoid arthritis, such as high synovial immune cell invasion, hyperplasia, cartilage degradation, bone erosion, and pain [383, 384]. This preclinical model led to the development of biological therapeutic intervention, such as the depletion of TNFα [385] or the immunocytokine F8IL10 [117].

1.4.2.2 EDA expression

Angiogenesis is a critical process in the pathogenesis of rheumatoid arthritis. Deposition of EDA(+) fibronectin, a marker of angiogenesis, have been reported in the stromal areas of vascular structures and the synovial lining layer of arthritis tissues from patients [386]. Furthermore, the level of EDA(+) fibronectin expression in synovial tissues has been correlated with the progression of joint destruction [387]. The CIA model of RA conserves the overexpression of EDA(+) fibronectin within the inflamed joints, allowing the use of this preclinical model to evaluate and validate therapeutic strategies based on EDA targeting for the pharmacodelivery of therapeutic payloads. EDA expression pattern in RA led our group to investigate the F8 antibody’s use for the targeted delivery of the anti-inflammatory cytokine IL10 (F8IL10) at the site of

arthritic lesions in CIA mice. Based on the positive results obtained in this preclinical model, F8IL10 has been further progressed into clinical development to treat rheumatoid arthritis [104, 117, 139].

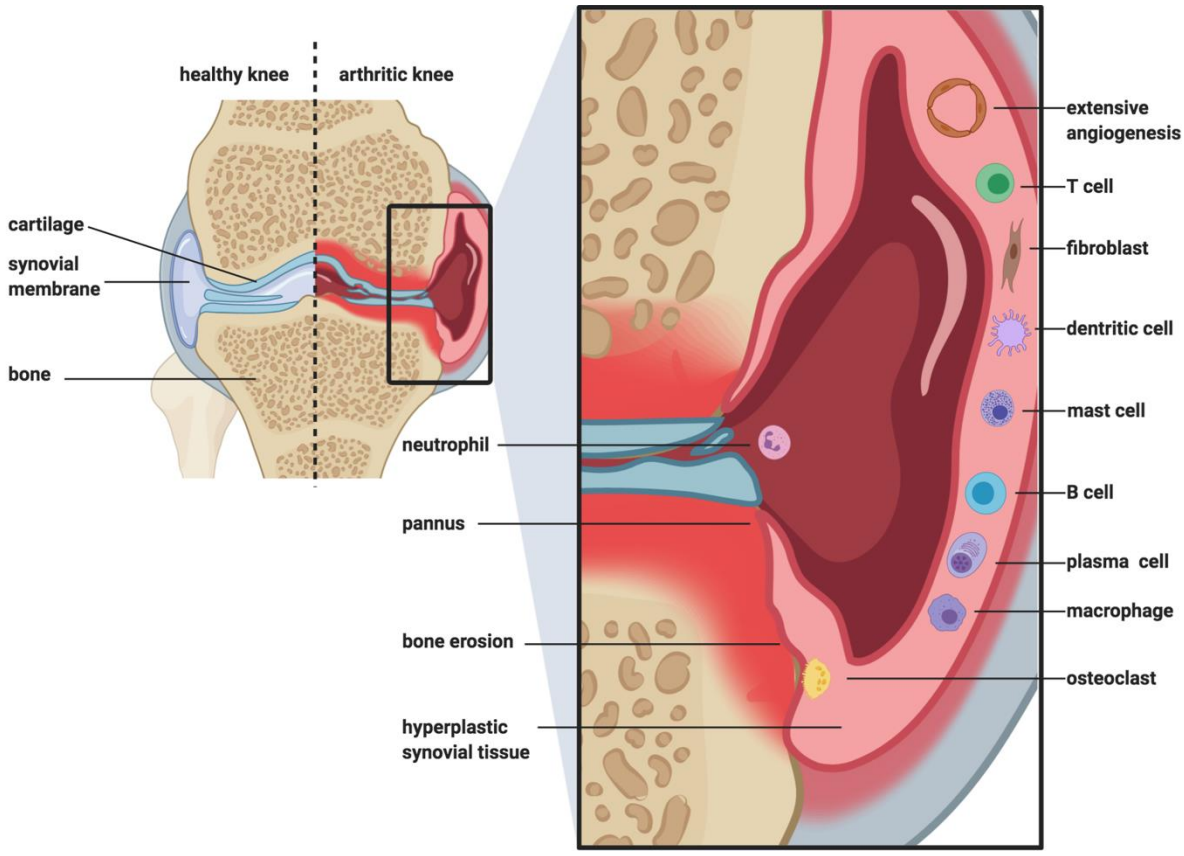

Figure 1.11: Comparison of a healthy joint and rheumatoid arthritis joint. The arthritic joint is characterized by forming a pannus, a hyperplastic synovial membrane infiltrated by inflammatory cells. Bone erosion is a consequence of persistent inflammation. This figure was created with BioRender.com.

1.4.3 Monocrotaline induced pulmonary hypertension

1.4.3.1 MCT

Pulmonary hypertension (PH) is a pathophysiological disorder that may involve multiple clinical conditions and is a pathological complication of most cardiovascular and respiratory diseases. PH is a disease defined as an increase in mean pulmonary arterial pressure (PAPm) ≥25 mmHg at rest [388]. Current treatment options for PH generally act by decreasing vascular tone and reducing pulmonary artery pressure, but no treatments can stop or reverse PH progression are available.

Therefore, modeling pulmonary hypertension in animal models is needed for the early discovery of new therapeutics. In this chapter, the monocrotaline (MCT)-induced PH model will be described to support its use in the experiments presented in chapter 5. MCT-induced PH is performed by injecting MCT, subcutaneously or intraperitoneally, into rodents [330]. In the liver, MCT is then metabolized by cytochrome-P450 into pyrrolic derivatives, which causes endothelial damages to pulmonary vasculatures [389]. Therefore about 18 days after MCT injection, rodents are subject to pulmonary vascular remodeling and thickening of the blood vessels accompanied by the obstruction of pulmonary vasculature [390, 391]. The difficulty for the blood to traffic via pulmonary vasculature causes an overload of the heart. Clinical signs of PH can be indirectly assessed by measuring haemodynamic parameters by right heart catheterization and echocardiography analysis.

Increasing evidence suggests an important role for inflammation in the pathogenesis of PH [392, 393]. However, the mechanisms by which inflammation may contribute to the pathophysiology of PH remain largely unclear. In animal PH models, immune cell depletion experiments led to the conclusion that inflammatory cells strongly contribute to pulmonary vascular remodeling. For example, it has been reported that depletion of macrophages is protecting against hypoxia-induced PH [392, 394–397], whereas the lack of Tregs activity has been postulated to be part of the pathogenesis of PH [398, 399]. Moreover, TH17 have been described to be part of PH pathogenesis via an IL6/IL21 signaling axis [400, 401]. Currently, a therapeutic intervention based on B cells depletion by the anti-CD20 monoclonal antibody, rituximab, is being tested in clinical trials to treat patients with systemic sclerosis-associated pulmonary arterial hypertension (SSc-PAH) (ClinicalTrials.gov, NCT01086540). Whereas immunomodulatory therapy for the treatment of PH conditions holds great potential it has been only poorly explored to date. In chapter 5, preliminary experimental results on a new immunomodulatory therapy in MCT-induced PH will be described.

1.4.3.2 Expression of EDA

PH pathogenesis is associated with a progressive remodeling of the vasculature in the lungs [402]. In an attempt to identify new markers of pulmonary hypertension, our group, in collaboration with the group of Prof. Marcus Franz studied lung tissue remodeling in the MCT-induced PH rat model [403]. Following confirmation of PH

induction by haemodynamics and histological analysis, gene expression and immunofluorescence studies were performed on diseased lung tissues. This study led to the identification of 9 significantly overexpressed genes known to be functionally involved in ECM remodeling. Furthermore, of the three proteins tested in immunofluorescence analysis (namely EDA(+)-fibronectin, B(+)-tenascin-C, and α-SMA), only EDA(+)-fibronectin showed increased deposition around vessel structures and within the parenchyma of the diseased lungs. Based on these results, EDA(+)-fibronectin was considered as a promising target for the antibody-based delivery of the IL9 cytokine to the site of PH lesions, as further described in Section 5.

2 Aim and structure of the PhD thesis

Multispecific drugs hold great potential as therapeutic products owing to increase target specificity. Enabling technologies are required to overcome the different challenges posed by their development and manufacturing.

The aim of this thesis was to develop and characterize diverse multispecific therapeutic prototypes. For this purpose, different technologies were applied, including: genetic engineering, enzymatic coupling, and chemical synthesis. In this thesis, four projects regarding the development and characterization of different multispecific therapeutics are presented.

The first project (Section 4) concerns the development of three IL9-based immunocytokines fused to F8 antibody moiety. Their ability to recognize the antigen has been assessed *in vitro* and *in vivo,* and the therapeutic efficacy of a selected immunocytokine variant has been further tested in cancer and rheumatoid arthritis mouse models. This work has been submitted and is currently under revision for publication in a peer-reviewed journal. The corresponding manuscript has also been deposited to the bioRxiv preprint server with the following DOI: 10.1101/2020.08.26.268292. This manuscript has been accepted for publication in "Experimental Biology and Medicine".

In the second project (Section 5), the therapeutic efficacy of the previously selected L9 based immunocytokine has been tested in a murine model pulmonary hypertension by collaborating with the group of Prof. Dr. Marcus Franz from the University Hospital

Jena. A manuscript summarizing the obtained results is currently in preparation, and a patent has been filed regarding the obtained results.

The third project (Section 6) is dealing with the development of a small molecule-cytokine conjugate (SMCC) representing a new class of bispecific molecules. The generated product termed AAZ-IL2 consists of the fusion between the CAIX ligand acetazolamide (AAZ) and the IL2 cytokine. The ability of AAZ-IL2 to bind its cognate target and localized *in vivo* at the tumor site has been assessed. This work resulted in a publication on ACS OMEGA with the following DOI: 10.1021/acsomega.0c03592

The fourth project (Section 7) summarizes the work done to develop an Albutagged therapeutic peptide, termed AlbuAPL. Three AlbuAPL variants were generated and characterized for their affinity for serum albumin. A preliminary assessment of the half-life of these products has been performed in mice in collaboration with the group of Prof. Philippe Valet Toulouse University. At the completion of the experiments, this project's results will be published in a peer-reviewed journal.

3 Antibody targeted delivery of IL9 in cancer and rheumatoid arthritis

Contribution of the authors: In this project I performed all the experimental work with the exception of the therapy study in the CIA model of rheumatoid arthritis experiment that has been performed by the Hooke Laboratories (US). The other authors helped me in the planning and realization of the project.

Antibody-based delivery of Interleukin-9 to neovascular structures: therapeutic evaluation in cancer and arthritis

Baptiste Gouyou[1], Tiziano Ongaro[1], Samuele Cazzamalli[1], Roberto De Luca[1], Anne Kerschenmeyer[1], Philippe Valet[2], Alessandra Villa[1], Dario Neri[3], Mattia Matasci[1]

Author affiliations:

1) Philochem AG, Libernstrasse 3, 8112 Otelfingen, Switzerland

2) Institut des Maladies Métaboliques et Cardiovasculaires, INSERM U1048, Université de Toulouse, UPS, Toulouse, France

3) Department of Chemistry and Applied Biosciences, Swiss Federal Institute of Technology, Zurich, Switzerland

Keywords: Tumor targeting, Rheumatoid arthritis targeting, Fibronectin, Immunocytokines, Interleukin-9

3.1 Abstract

Interleukin-9 (IL9) is a cytokine with multiple functions, including the ability to activate group 2 innate lymphoid cells (ILC2s), which has been postulated to be therapeutically active in mouse models of arthritis. Similarly, IL9 has been suggested to play an important role in tumor immunity. Here, we describe the cloning, expression and characterization of three fusion proteins based on murine IL9 and the F8 antibody, specific to the alternatively-spliced EDA domain of fibronectin. EDA is strongly expressed in cancer and in various arthritic conditions while being undetectable in the majority of healthy organs. IL9-based fusion proteins with an irrelevant antibody specific to hen egg lysozyme served as a negative control in our study. The fusion proteins were characterized by quantitative biodistribution analysis in tumor-bearing mice using radioiodinated protein preparations. The highest tumor uptake and best tumor:organ ratios were observed for a format in which the IL9 moiety was flanked by two units of the F8 antibody in a single-chain Fv format. Biological activity of IL9 was retained when the payload was fused to antibodies. However, the targeted delivery of IL9 to the disease site resulted in a modest anti-tumor activity in three different murine models of cancer (K1735M2, CT26, and F9), while no therapeutic benefit was observed in a collagen-induced model of arthritis. Collectively, these results confirm the possibility to deliver IL9 to the site of disease but cast doubts about the alleged therapeutic activity of this cytokine in cancer and arthritis, which has been postulated in previous publications.

3.2 Introduction

Interleukin-9 (IL9) is a multifunctional cytokine that has been originally identified as a T-cell and mast cells growth factor [238]. IL9 is secreted by mast cell and CD4+ T cells, including Th2, Th9, Th17, Treg, and NK cells [209] following stimulation by TGFβ and IL4 [216]. Its biological action is mediated by the heterodimeric receptor IL9-R comprising a specific IL-9 receptor α-chain and the common γ-chain cytokine receptor [404]. IL9 has been demonstrated to play an important role in a variety of physiological and pathological conditions, including pathogen immunity [212, 224], allergic inflammation [405, 406], and immune regulation of cancer progression [407, 408].

The role of IL9 in tumor growth is controversial whereas IL9 has been correlated to the progression of hematological malignancies both in mouse [252] and human [253], more recently IL9 dependent anti-cancer activity have been reported in a variety of solid tumor models including melanomas [254] and colon carcinomas [255, 256].

According to its postulated immunomodulatory activity, IL9 based therapies have been investigated in preclinical models of cancer and inflammation. In particular, Purwar and collaborators investigated the tumor immunity provided by IL9 in a preclinical therapeutic setting [254]. In the B16F10 melanoma models they demonstrated the ability of recombinant IL9 to impair tumor cell growth by a mechanism dependent on mast cells but not on T or B cells. The authors obtained similar results when recombinant IL9 was administered to mice bearing Lewis Lung carcinoma tumors suggesting a potential use of IL-9 based therapies for the treatment of diverse cancer types.

More recently, Rauber and collaborators have identified IL9 as a key player in the resolution of rheumatoid arthritis in murine models of Antigen Induced Arthritis (AIA) and Serum Induced Arthritis (SIA) [269]. In their proposed mode of action, IL9 would promote ILC2 proliferation through an autocrine loop, finally resulting in the activation of Treg cells via a GITR/GITRL and ICOS/ICOSL dependent mechanism. The authors used a gene therapy approach based on hydrodynamic gene delivery to mediate the recombinant expression of an IL9 cDNA construct in the treated mice. The *in vivo* levels of recombinant IL9 in arthritic mice were not measured, but a strong inhibition of disease progression, reduced tissue damage, and bone loss was reported compared to control mice treated with a mock construct.

Collectively, the published work on the therapeutic use of IL9 prompted us to develop and evaluate new IL9-based immunocytokines and test them in preclinical models of cancer and arthritic diseases.

Various cytokine-based therapeutics may benefit from a targeted delivery to the site of disease, helping spare normal organs [125, 409, 410]. We have previously described an antibody-IL9 fusion protein and reported an unexpected impact of protein glycoform variation on tumor targeting performance [122]. Specifically, we used the F8 antibody, which recognizes the alternatively-spliced EDA domain of fibronectin, a

marker of tumor angiogenesis, and of tissue remodeling [54]. F8 reacts with murine and human EDA with identical affinity since the target antigen features only three amino acid substitutions from mouse to man [54]. EDA is strongly expressed in the majority of solid tumors [368, 411], lymphomas [412] and in the bone marrow and chloroma lesions of acute leukemias [413] with a characteristic perivascular staining pattern, while the antigen is virtually undetectable in normal adult organs, exception made for the female reproductive system [116].

The tumor-targeting ability of the F8 antibody and its derivatives has been established using radiolabeled protein preparations and quantitative biodistribution analysis [54, 107, 117, 122, 156, 414]. Interestingly, pathological specimens from diseased tissues undergoing substantial remodeling (e.g., endometriosis, arthritis, psoriasis, atherosclerosis, vasculopathy and certain inflammatory bowel conditions) have been shown to be strongly positive for EDA(+)-fibronectin. The ability of F8 derivatives to preferentially localize at sites of chronic inflammation has been shown in mouse models [105, 106, 112, 116, 117, 415] and in patients with rheumatoid arthritis [416].

In this article, we describe the design, expression, and characterization of three recombinant formats of IL9-based fusion proteins, based on the EDA-targeting F8 antibody. IL9-fusions with the KSF antibody, specific for hen egg lysozyme, served as a negative control with irrelevant specificity in the mouse. The fusion proteins were characterized in terms of their biochemical parameters, IL9 activity, and tumor-targeting performance in biodistribution analysis after radioiodination. One of the formats, featuring the IL9 moiety flanked by two units of the F8 antibody in a single-chain Fv (scFv) format, exhibited the best tumor-targeting performance, with tumor:blood ratios > 10:1, twenty-four hours after intravenous administration. Whereas a low increase of immune cell infiltration within tumors was observed, IL9 fusion proteins displayed only minimal therapeutic activity in three immunocompetent mouse models of cancer (K1735M2, CT26, and F9) at the maximal tolerated dose. Similarly, no retardation of disease progression was observed in the collagen-induced model of arthritis in mice. These results confirm that IL9 can be efficiently delivered to sites of disease with high expression of EDA *in vivo* but cast doubts about the alleged translational therapeutic relevance of IL9 for the treatment of cancer and chronic inflammatory conditions.

3.3 Materials and methods

3.3.1 Cloning of IL9 based fusion proteins

The genes encoding the antibody fusion proteins used in this study were generated by the assembly of multiple PCR fragments using as starting templates cDNA encoding for the anti-EDA F8 antibody [21] or the irrelevant anti-hen-lysozyme KSF antibody [416], either in scFv or diabody formats, and the murine IL9 (AA 19-144). The assembled constructs were inserted into the HindIII/NotI sites of the pcDNA3.1 (Invitrogen) mammalian expression vector. Primers used for the amplification and assembly of the different constructs are listed in the supplementary **Table 3.1**.

The pcDNA3.1-F8IL9F8 vector contains the murine IL9 sequence flanked at both the N- and C- termini by a 10-mer peptidic linker and the F8 antibody in scFv format. A leader sequence from murine IgG was used for protein secretion.

The pcDNA3.1-KSFIL9KSF contains a similar insert where the two F8 moieties were replaced by two copies of the KSF antibody in scFv format.

The pcDNA3.1-F8IL9 and pcDNA3.1-IL9F8 carry an insert consisting of the F8 antibody in diabody format fused either to the N- (pcDNA3.1-F8IL9) or C- (pcDNA3.1-IL9F8) terminus of IL9 via a 15-mer amino acidic linker. As well in these two vectors, a murine IgG leader sequence was used for protein secretion.

3.3.2 Protein expression, purification and characterization

The IL9 based fusion proteins (F8IL9F8, KSFIL9KSF, F8IL9, and IL9F8) were expressed by transient gene expression in CHO cells [417]. For transfection 4×10^6 cells/mL cells were resuspended in ProCHO-4 Medium (Lonza) supplemented with 4 mM Ultraglutamine (Lonza). 0.625 μg of plasmid DNAs per million cells, followed by 2.5 μg polyethyleneimine per million cells (Polysciences) were added to the cells and gently mixed. Transfected cultures were incubated in a shaking incubator at 31°C with a 5% CO2 atmosphere shaking at 120 rpm for 6 days. The fusion proteins were purified by affinity chromatography using protein A affinity chromatography (Sino biological) according to the protocol provided by the supplier. Following elution, proteins were finally dialyzed against PBS. Purified proteins were characterized for

their size and homogeneity by SDS-PAGE and size exclusion chromatography, respectively. For SDS-PAGE analysis, proteins were run under reducing and non-reducing conditions on 10 or 12% acrylamide gels (Invitrogen) and stained using Coomassie blue. Size-exclusion chromatography was performed on an ÄKTA FPLC system using a Superdex 200 increase 10/300GL column (GE Healthcare). Protein binding affinity was performed by Surface Plasmon Resonance using a BIAcore X100 instrument using a CM5 chip coated with recombinant fibronectin 11A12 domain. Samples were injected as serial-dilution, using a concentration range from 1mM to 125nM. The melting temperature of the different fusion proteins was determined using a StepOne real-Time PCR system (Applied Biosystems) in combination with the Protein Thermal Shift™ kit (Applied Biosystems).

3.3.3 Immunofluorescence analysis of EDA expression

For biotinylation, 250 μg of fusion proteins was mixed to 50 μg of Biotin-NHS (Invitrogen) in a total volume of 1 mL. Reactions were gently agitated at room temperature for 1 hour prior to the removal of unreacted Biotin-NHS by size exclusion chromatography using PD-10 columns (GE Healthcare). Elution was performed using PBS. Immunofluorescence staining was performed on three different frozen tissues: F9 teratocarcinoma tumors from 129/Sv mice and healthy human basal and chorionic placenta. Frozen sections (8 μm) were fixed by ice-cold acetone and blocked with 20% fetal bovine serum in PBS. Detection of EDA positive fibronectin was performed using biotinylated fusion proteins, followed by Streptavidin Alexa 488 (Invitrogen). In parallel, the neovasculature marker CD31 was detected using either rat anti-mouse CD31 (BD Pharmingen) or mouse anti-human CD31 (eBiosciences) followed by Donkey Anti Rat-IgG-Alexa Fluor® 594 (Invitrogen), or Goat Anti Mouse-IgG-Alexa Fluor® 594 (Invitrogen), respectively.

3.3.4 *In vitro* bioactivity assay

The bioactivity of mIL9 based fusion proteins was tested by a proliferation assay using MC/9 cells (ATCC). These mast cells derived from mouse liver were expanded in suspension in DMEM, supplemented with 10% FBS, 10% rat T-Stim, 2mM UltraGlutamine, and 0.05mM –BetamercaptoEtOH. MC/9 cells were seeded at 40’000 cells per well in 96 wells plates in 200 μL of culturing medium (with 5% FBS and 2.5%

rat T-Stim). Murine IL9 based fusion proteins and commercial murine IL9 (Peprotech) were added to the cells in serial dilution (from 28 nM until 0.1 pM). After 70 hours of incubation at 37°C with 5% CO2 atmosphere, 20 μL of Cell Titer Aqueous One Solution (Promega) was added to the wells, and after incubation of 2 hours at 37°C the absorption at 492 nm was measured.

3.3.5 Radiolabeled biodistribution and tumor therapies

In vivo experiments on tumor models were performed in agreement with the Swiss regulations and under a project license granted by the cantonal veterinary office (ZH027/15 for biodistribution and ZH004/18 for therapies). F9 teratocarcinoma cells (ATCC) were grown in DMEM (Life Technologies) supplemented with 10% FBS using 0.1% gelatin-coated tissue culture flasks. 129/Sv mice (8 weeks old, Charles River) were injected on the right flank with 13×10^6 F9 teratocarcinomas. To assess tumor targeting in the F9 model, mice were grouped (n=3) when all tumors reached at least 200mm^3. *In vivo* targeting was evaluated by biodistribution analysis as described previously [418]. 100 μg of each fusion protein were radioiodinated with ^{125}I and Chloramine T hydrate and purified on a PD10 column (GE Healthcare), as described previously [418]. ~10 μg of radiolabeled proteins were injected into the lateral tail vein. Mice were sacrificed 24 h after injection. Organs were weighed, and radioactivity was counted using a Packard Cobra gamma counter (Packard, Meriden, CT, USA). Values are given as a percentage of the injected dose per gram of tissue (%ID/g ± standard error). K1735M2 melanomas were grown in DMEM (Life Technologies) supplemented with 10% FBS. C3H mice (8 weeks old, Janvier) were injected on the right flank with 5×10^6 cells. Treatment started as soon as an average tumor size of >100 mm^3 was reached; mice were randomized and grouped (n = 5 for IL9 based proteins, n = 4 for PBS). Mice were injected three times every second day with the test article intravenously (i.v.) in the lateral tail vein. 200 μg of F8IL9F8 or KSFIL9KSF were injected while PBS was injected at similar volume. CT26 colon carcinoma cells (ATCC) were grown in DMEM (Life Technologies) supplemented with 10% FBS. Balb/c mice (8 weeks old, Janvier) were injected on the right flank with 15×10^6 cells. For therapies experiments with the CT26 cells, treatment started as soon as an average tumor size of >120mm^3 was reached, mice were randomized and grouped (n = 5). Either 200 μg or 100 μg of F8IL9F8 or equivalent volume of PBS were injected i.v. with the same

schedule as the K1735M2 therapy. For F9 teratocarcinoma bearing mice, treatment started as soon as an average tumor size of >70 mm^3 was reached, mice were randomized and grouped (n = 5). 200 μg F8IL9F8 or KSFIL9KSF were injected and the same volume of PBS was injected for the control group were injected i.v. with the same schedule as the K1735M2 therapy. For the three models, tumor volume was measured every day, and the experiments were performed in a blind fashion. The therapy was discontinued by animal sacrifice when the weight loss exceeded -15% or tumor volumes was exceeding 1500 mm^3. Data are expressed as the mean volume ± SEM. Differences between therapy groups were analyzed by two-way ANOVA multiple comparisons (Bonferroni corrected) using GraphPad Prism (GraphPad Software, Inc.)

3.3.6 Immunofluorescence analysis for *ex vivo* targeting and immune cells infiltrates studies

For FITC labeling, 1 mg of the fusion protein was dialyzed in 0.1 M $NaCO_3$ pH 9 then mixed with 25 μg of FITC (ACROS organics) in a total volume of 0.5 mL. Reactions were gently agitated at 4°C overnight prior to the removal of unreacted FITC by size exclusion chromatography using PD-10 columns (GE Healthcare). Elution was performed using PBS. The *ex vivo* detection of the test articles was performed 24h after i.v. injection 160 μg of the FITC labeled proteins (F8IL9F8 and KSFIL9KSF) or PBS as control. Mice were sacrificed, and tumors were OCT embedded. Frozen sections (8 μm) were fixed by ice-cold acetone and blocked with 20% fetal bovine serum in PBS. Detection of the test articles was performed using a rabbit anti-FITC IgG (Biorad) followed by anti-rabbit IgG Alexa Fluor® 488 (Invitrogen). The neovasculature marker CD31 was detected using a rat anti-mouse CD31 (BD Pharmingen) followed by Donkey Anti Rat-IgG-Alexa Fluor® 594 (Invitrogen). Sections were counter-stained with DAPI.

For the analysis of immune infiltrate into the tumors, mice received F8IL9F8 (n=2), KSFIL9KSF (n=1), or PBS (n=1) according to the same setting used in the therapy experiments (e.g., dose, schedule, tumor volume). 24h after the last injection, K1735M2, and CT26 bearing mice were sacrificed, and the tumor was OCT embedded. Frozen sections (8μm) were fixed by ice-cold acetone and blocked with

20% fetal bovine serum in PBS. Detection of the immune cells infiltrates were performed using rat anti-mCD8 (Biolegend), rat anti-mCD4 (Biolegend), rat anti-mFoxP3 (Invitrogen) or rat anti-mCD335 (NKp46) (Biolegend). Goat anti-rat IgG Alexa Fluor® 488 (Invitrogen) was used as a detection antibody. Slides were counterstained with DAPI prior analysis. Sections were analyzed using an Axioskop2 mot plus microscope (Zeiss) pictures have been acquired with 10x magnification. For quantification of immune cell infiltrates, 6 field of each section were analyzed, and the percentage of stained area was calculated by ImageJ.

3.3.7 Rheumatoid arthritis therapy

For the collagen-induced arthritis (CIA) experiments in mice DBA/1J males (8-10 weeks old, Taconic Biosciences) were immunized by subcutaneous (s.c.) injection in the tail of an emulsion of bovine type II collagen in Completes Freund's Adjuvant (CFA) (Hooke Laboratories). 18 days later, a booster injection of bovine collagen/IFA (Hooke Laboratories) was given to the mice by s.c. injection in the tail. Mice were scored every other day. The final CIA score represents the scoring sum of all 4 paws (0 = normal 1 = one toe inflamed and swollen 2 = more than one toe, but not entire paw inflamed and swollen or mild inflammation and swelling of entire paw 3 = entire paw inflamed and swollen and 4 = very inflamed and swollen paw). CIA scoring was performed blind. At the onset of the disease, animals were randomized before receiving their first injection. 150 μg, or 50 μg (n=15) of F8IL9F8 (n=15) or PBS (n=15) were injected in a final volume of 150 μL three times every second day i.v. in the lateral tail vein. Dexamethasone was daily injected intraperitoneally (i.p.) at 0.5 mg/kg.

3.4 Results

All IL9 fusion proteins exhibit a good manufacturability profile.

Different IL9 based fusion proteins were successfully expressed by transient gene expression (TGE) in Chinese hamster ovary (CHO) cells (**Figure 3.1**). The purified fusion proteins exhibited favorable biochemical properties as confirmed by SDS-PAGE and size exclusion chromatography (**Figure 3.1 A-C**). EDA-binding kinetic was analyzed by surface plasmon resonance (SPR). SPR analysis showed comparable nanomolar range apparent K_D for all fusion proteins: 3.4 10^{-9} nM, 5.2 10^{-9} nM and 2.9

10^{-9} nM for F8IL9, IL9F8 and F8IL9F8 respectively (**Figure 3.1 A-C**). The bioactivity of the murine IL9 based fusion proteins has been assessed by their ability to stimulate the proliferation of MC/9 cells. In this assay, the three IL9 based fusion proteins showed similar activity with EC50 values of 38 pM (F8IL9F8), 21 pM (IL9F8), and 40 pM (F8IL9). The fusion of IL9 to the F8 antibody may slightly impair its function as a commercial mIL9 preparation showed a 10-fold higher biological activity (EC50 = 4 pM). The comparative analysis of N- or C- terminal IL9 fusions showed that the arrangement of the different moieties did not affect its biological activity (**Figure 3.1 D**). The single-chain Fv based variant of the fusion protein (F8IL9F8) displayed a 3°C increased melting temperature compared to the two variants based on the diabody format (**Figure 3.1 E**), suggesting better thermal stability. Indeed, when the F8IL9F8 variant was stored for up to 7 days at 4°C or 37°C or when tested over 3 cycles of freeze and thawing, no sign of aggregation, degradation, or protein loss could be detected by size exclusion chromatography or SDS-PAGE analysis, (data not shown). Taken together, these experiments suggest overall better stability of the F8IL9F8 fusion protein.

The format F8IL9F8 shows better *in vivo* targeting abilities.

In order to test whether the IL9 fusion proteins retains the ability to bind EDA+ fibronectin on newly formed vascular structures, we performed immunofluorescence experiments on EDA positive tissue sections (i.e., human placenta and F9 tumors) [54]. The three fusion proteins selectively bound to neovasculature structures in both murine F9 teratocarcinoma and human placenta sections as confirmed by the co-localization with an anti-CD31 neovascular marker (**Figure 3.2 E and F**). Subsequently, the *in vivo* targeting performance of the three IL9 fusion proteins was tested by biodistribution analysis in tumor-bearing mice. Purified fusion proteins were radiolabeled with Iodine 125, and 10 μg of each variant was injected into immunocompetent mice bearing F9 murine teratocarcinoma. The three variants were able to selectively localize to the tumor site at 24 hours post-injection (**Figure 3.2 A-D**). The F8IL9F8 variant with two scFv antibody moieties was found to be superior when compared to the two other variants (IL9F8 and F8IL9, respectively) in terms of biodistribution profile, with an increased accumulation at the tumor site and at least a 2-fold increase in the tumor to organ ratios (**Figure 3.2 A and B**). For further *in vivo*

investigation, we decided to focus on F8IL9F8 due to its better targeting performance. IL9 fusion proteins display a therapeutic effect depending on cancer type tested.

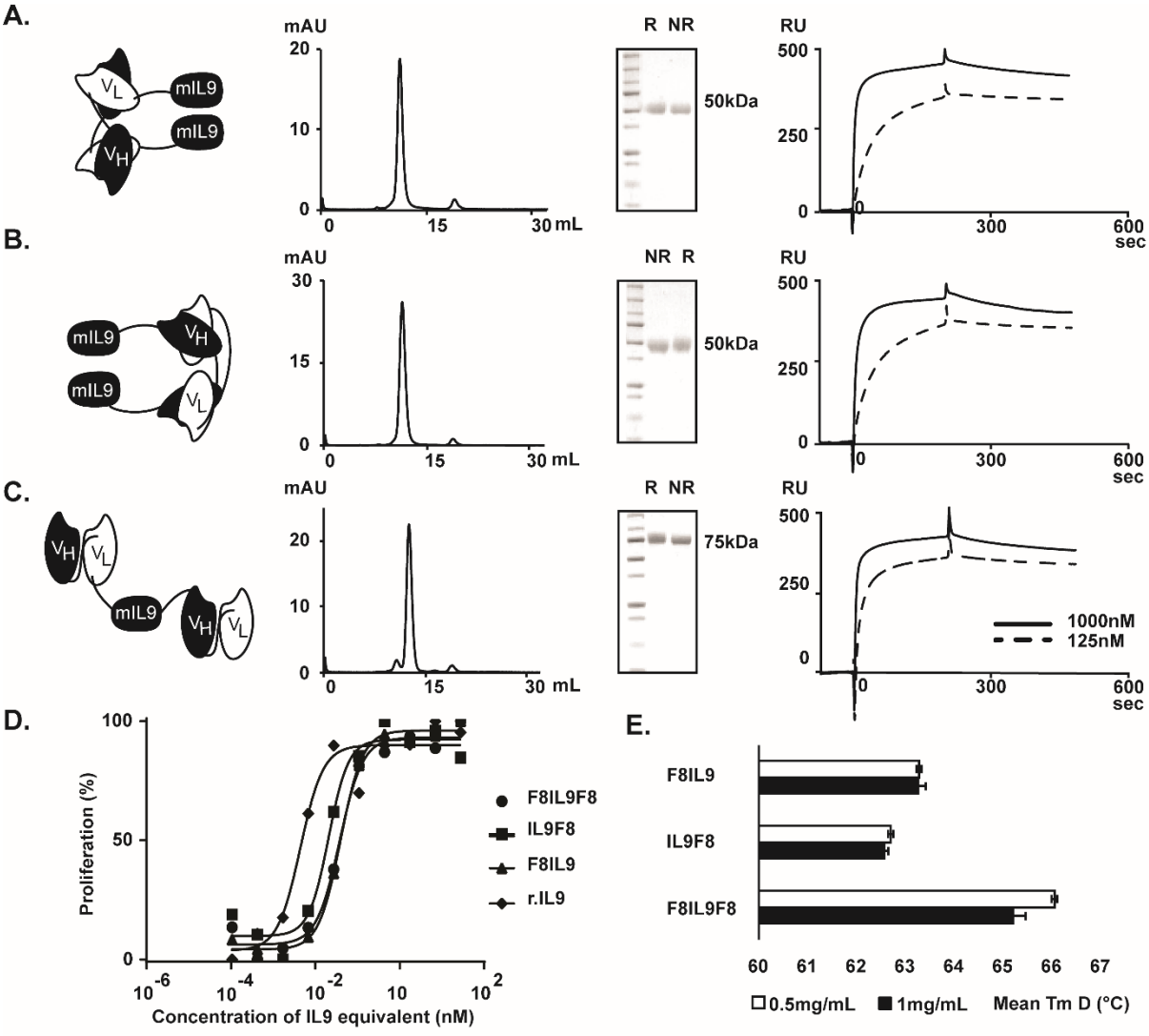

Figure 3.1: Cloning expression and characterization of IL9 based fusion proteins. IL9 fusion proteins have been expressed in CHO cells and characterized. From left to right: schematic representation of the IL9 based fusion protein, size exclusion chromatography profile, analytical SDS-PAGE analysis, SPR sensograms on EDA-coated sensor of (A) IL9F8, (B) F8IL9, (C) F8IL9F8. R: reducing conditions, NR: non-reducing conditions. (D) The proliferation of MC/9 has been assessed in the presence of serial dilution of (■) IL9F8, (▲) F8IL9, (●) F8IL9F8, and (◆) commercially available recombinant murine IL9 produced in bacteria. Data are presented as a percentage of maximal proliferation (mean of three replicates). (E) A thermal shift assay was performed on IL9 based fusion protein. Data are expressed in °C + Std. Error, melting temperature (Tm) was assessed at two different protein concentrations.

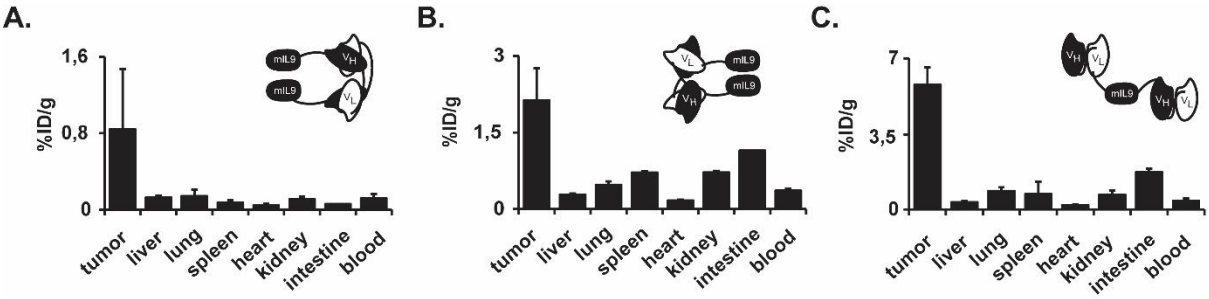

D.

	tumor/liver	tumor/lung	tumor/spleen	tumor/heart	tumor/kidney	tumor/intestine	tumor/blood
IL9F8	6.7	5.9	11.6	18.6	7.7	14.1	7.0
F8IL9	7.6	4.5	3.0	12.8	3.0	1.9	6.0
F8IL9F8	17.2	6.7	8.1	29.8	8.5	3.3	14.6

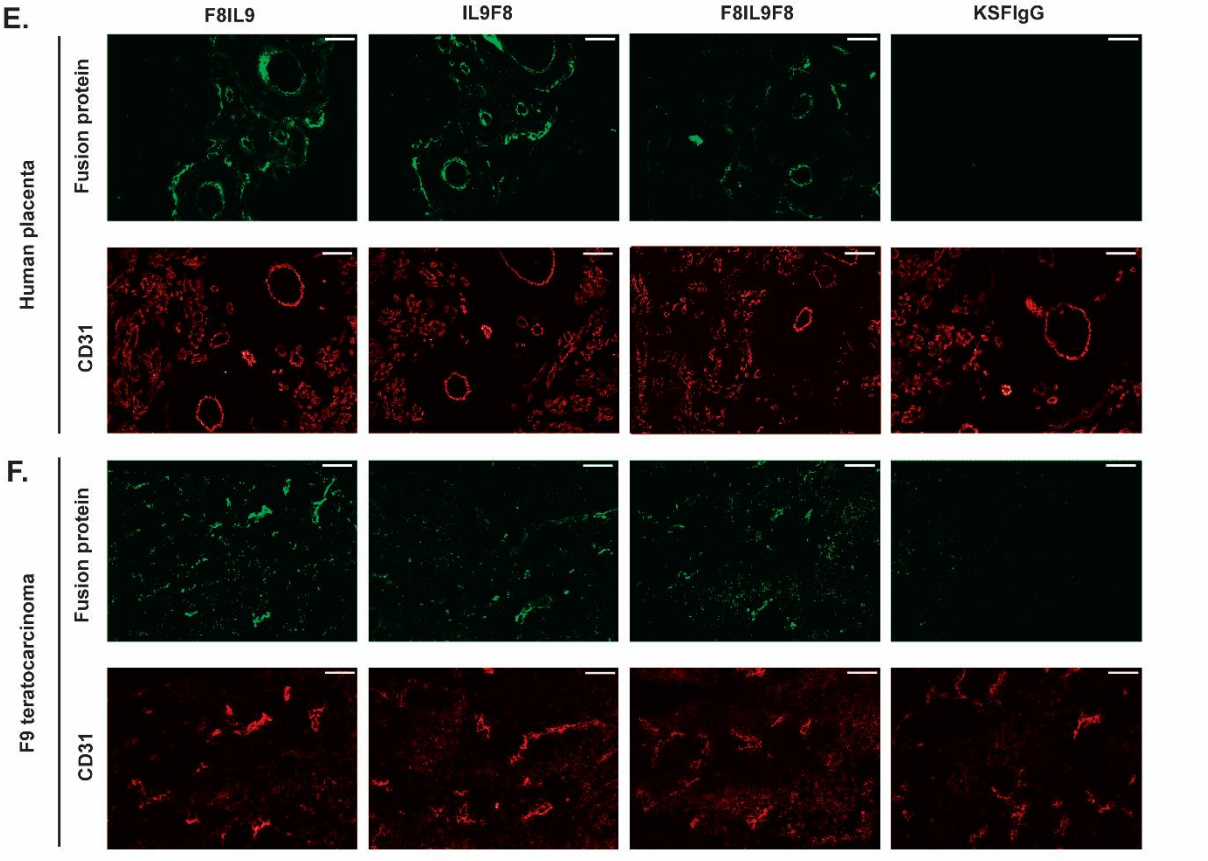

Figure 3.2: Tumor targeting performance of IL9-based immunocytokines. Quantitative biodistribution analysis of IL9 based fusion proteins. 10 μg of (A) IL9F8, (B) F8IL9, and (C) F8IL9F8 radiolabeled protein have been injected into the lateral tail vein of F9 tumor-bearing mice. Organs were collected, weighed, and the radioactivity was measured 24 hours after injection. Results are expressed as the percentage of injected dose per gram of tissue (% ID/g ± SEM), (n = 3 mice). (D) Table of tumor:organ ratios calculated from the average of the % ID/g. (E and F) Microscopic fluorescence analysis of (top panels) biotinylated IL9 based fusions proteins and (lower panels) anti CD31 antibody. Staining has been done against (E) healthy human placenta and (F) F9 Tumors grown in 129Sv mice, 10x magnification, and the scale bar represents 50 μm. The irrelevant KSF antibody in IgG format was used as negative control.

The therapeutic efficacy of F8IL9F8 was tested in three different cancer models: K1735M2 melanoma, CT26 colon carcinoma, and F9 teratocarcinoma.

Since previous studies showed the ability of IL9 or IL9-expressing Th9 cells to inhibit melanoma growth and reduce the number of melanoma-derived lung metastases in mice [254, 419], F8IL9F8 was initially tested in the EDA-positive K1735M2 melanoma model [156]. Compared to the saline group, F8IL9F8 treatment exhibited minor tumor growth retardation, which was statistically significant at the endpoint of the therapy (**Figure 3.3A**). Both F8IL9F8 and KSFIL9KSF treatments were well tolerated by mice, which displayed minimal and reversible weight loss. However, no substantial differences in tumor growth retardation and body weight change was observed between the treatments with targeted F8IL9F8 and the untargeted variant KSFIL9KSF (based on the irrelevant anti-hen egg lysozyme antibody KSF) (**Figure 3.3A**). The CT26 model, recently described as an immunologically "hot" tumor [345], was investigated due to earlier reports demonstrating *in vivo* growth impairment of CT26 tumors ectopically expressing IL9 [255, 256]. In order to investigate the dose-dependence effect of IL9 therapy, mice received three injections of F8IL9F8 at different doses, i.e., 100 μg or 200 μg. Both treatment regimens resulted in a similar tumor growth retardation when compared to the saline group, and no apparent signs of toxicity were reported (**Figure 3.3B**). However, similar to K1735M2 melanoma also in the CT26 model, no tumor eradication and mouse cure could be achieved with F8IL9F8. No therapeutic benefit of F9IL9F8 was observed in comparison to the saline group or mice treated with KSFIL9KSF in the F9 teratocarcinoma model. Interestingly, in this particular tumor model treatment with F8IL9F8 and KSFIL9KSF resulted in the highest body weight loss (**Figure 3.3C**).

To confirm the *in vivo* targeting ability of F8IL9F8 in these therapies setting, *ex vivo* immunofluorescence studies were performed. In parallel to the therapy studies, additional K1735M2, CT26, and F9 tumor bearing mice were injected with FITC labeled fusion protein variants, sacrificed 24 hours and tumors were analyzed for the localization of the injected fusion proteins within the tumor mass. Preferential accumulation of F8IL9F8 around the neovasculature structures was observed for the three tumor models tested. By contrast, no signal was observed for KSFIL9KSF or PBS injected mice, confirming the efficient and selective tumor targeting of the F8IL9F8 protein (**Figure 3.3D**).

IL9 treatment is modifying the immune phenotype of tumors

The two models, responsive to IL9 therapy (i.e., K1735M2 and CT26), were analyzed for immune cells infiltrates at the end of therapeutic treatment. Multiple representative pictures for each treatment group were analyzed by ImageJ to quantify the percentage of the positive area following staining for CD4+ T, CD8+ T, Treg, and NK cells. A general increase in immune cells could be detected in both K1735M2 and CT26 tumors treated with IL9-fusion at 200 μg per injection (**Figure 3.4**), however to a degree considerably lower when compared to our previous reports with other targeted immunocytokines and different tumor models [95, 107, 134, 287, 294, 420, 421]. Interestingly, in K1735M2 melanomas, a comparable increment in CD4+T and CD8+T cells was observed treated with either F8IL9F8 or KSFIL9KSF, whereas a slight increment in NK cells was observed only for F8IL9F8. Furthermore, no relevant changes in the infiltration of Treg cells could be observed between the 3 tested articles (**Figure 3.4 A-C**). Similar results were obtained for the CT26 colon carcinoma model, with a moderate increase of infiltrated CD4, CD8, and NK cells (**Figure 3.4 B**).

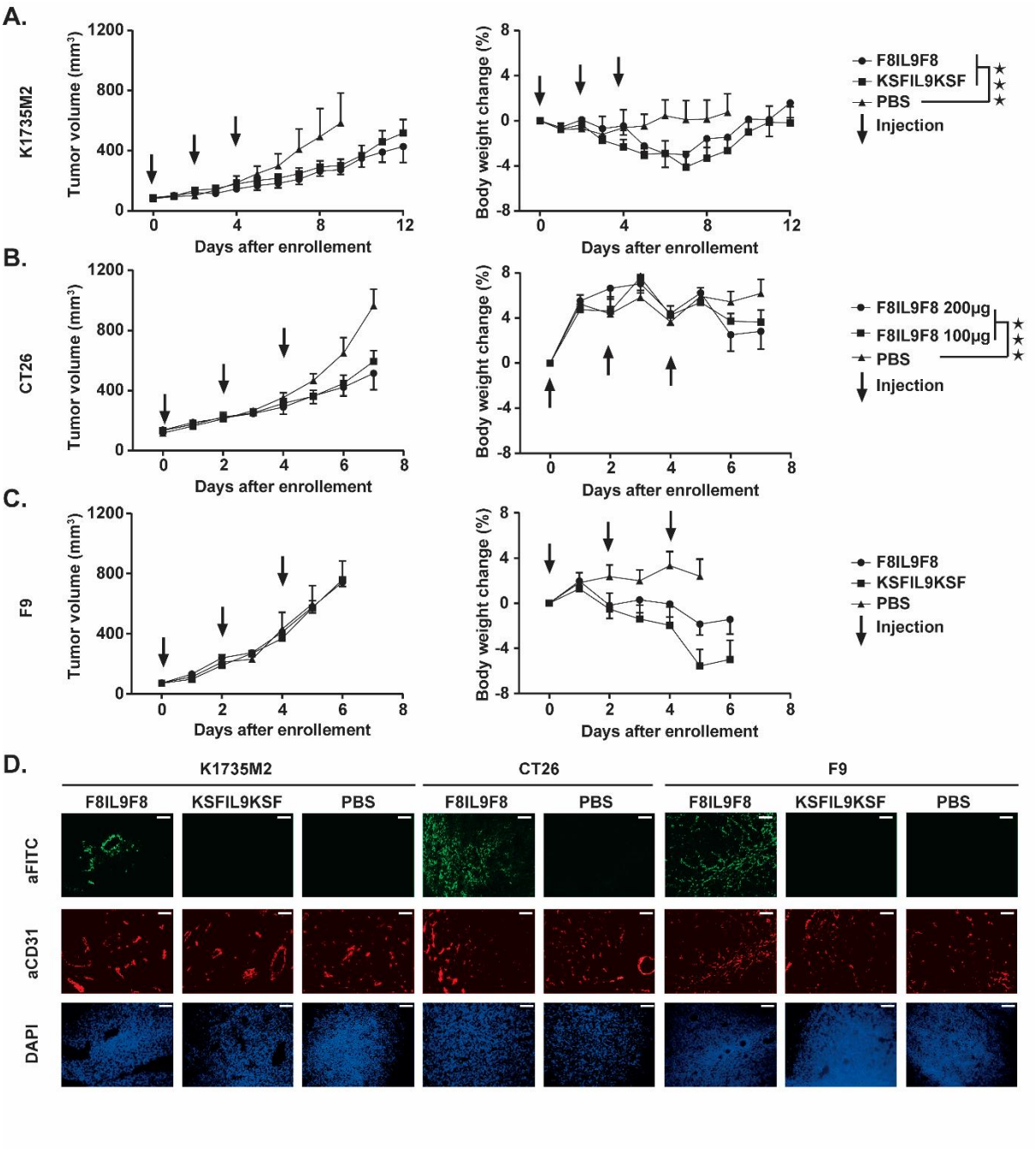

Figure 3.3: Therapeutic performance of IL9 based immunocytokines in C3H bearing K1735M2 melanoma, in Balb/c bearing CT26 colon carcinoma, and in Sv129 bearing F9 teratocarcinoma. Comparison of F8IL9F8, KSFIL9KSF injected at 200 µg, and PBS, treatment started when K1735M2 reached an average volume of 100 mm^3 borne in C3H (n = 5 mice for F8IL9F8 and KSFIL9KSF and n=4 for PBS) (A) Comparison of F8IL9F8 injected at 200 µg, at 100 µg and PBS, treatment started when CT26 tumors reached a volume of 120 mm^3 borne in Balb/c mice (n = 5 mice per group) (B) and comparison of F8IL9F8, KSFIL9KSF injected at 200 µg, and PBS, treatment started when F9 tumors reached an average volume of 72 mm^3 borne in Sv129 (n = 5 mice per group) (C). For all therapy experiments, mice were injected three times every second day i.v. in the lateral tail vein. Data represent mean tumor volume ± SEM (A-C left panel), body weight change ± SEM (A-C right panel). Statistical analysis was performed on tumor volumes using a 2-way Anova with a Bonferonni post-test ★: p-value < 0.05, ★ ★: p-value < 0.01, ★ ★ ★: p-value < 0.001, ns: not significant. Microscopic immunofluorescence analysis of the targeting ability of F8IL9F8, compared to KSFIL9KSF and PBS on the three tested cancer models, 10x magnifications and the scale bar represents 50 µm (D).

Delivery of IL-9 at the site of the disease did not provide a therapeutic benefit as an anti-inflammatory agent in collagen-induced arthritis mouse model.

The therapeutic potential of F8IL9F8 for the treatment of rheumatoid arthritis (RA) has been assessed in the CIA murine model. The disease was induced by two injections of a Bovine collagen preparation at distinct time points, which led to rapid development of the disease. Mice were scored every other day using the standard scoring system. For each paw, mice received 1 score for one toe inflamed and swollen, 2 for more than one toe, but not entire paw inflamed and swollen or mild inflammation and swollen paw, 3 for the entire paw inflamed and swollen, and 4 for the very inflamed and swollen paw. At the onset of the disease, F8IL9F8 was injected either at high (150 μg/dose) or low (50 μg/dose) dose, and dexamethasone or PBS treatments were used as positive and negative controls, respectively. Whereas the positive control dexamethasone effectively reduced the diseases score already after 3 days from the beginning of the treatment, the disease progression in the animal treated either with 50 or 150 μg/dose F8IL9F8 was comparable to one of the mice in the saline group (**Figure 3.5A**). In agreement with the arthritic score increase, mice treated with F8IL9F8 or PBS showed a more prominent, yet reversible, body weight loss when compared to the positive control group treated with dexamethasone (**Figure 3.5B**).

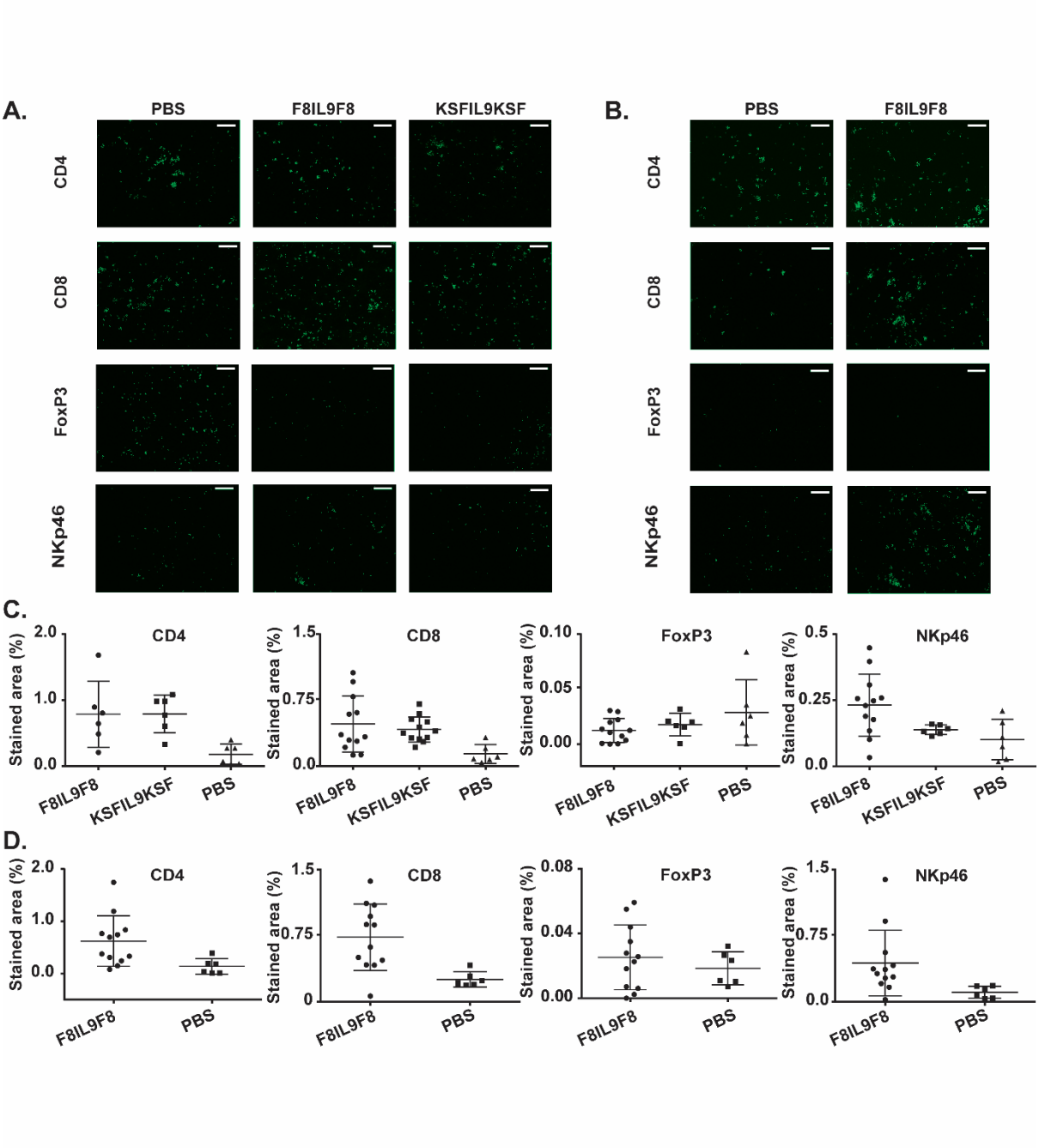

Figure 3.4: Immunofluorescence analysis of tumor-infiltrating immune cells in K1735M2 melanoma and CT26 colon carcinoma. Immunocompetent mice bearing K1735M2 (A and C) and CT26 (B and D) were injected three times every second day i.v. with 200 μg F8IL9F8, or 200 μg KSFIL9KSF or PBS. Mice were sacrificed 24h after the last injection and tumor sections were stained for $CD4^+$ cells (CD4), $CD8^+$ cells (CD8), Tregs (FoxP3) and NK cells (NKp46) (n = 2 mice for F8IL9F8 n=1 for KSFIL9KSF and PBS). Microscopic analysis of a representative section for each immunofluorescence, 10x magnification, and the scale bar represents 50 μm (A and B). Quantification of the percentage of the stained area using Image J. For each stained section, six representative areas were quantified and plotted as single dots. Bars correspond to mean values with standard deviation (C and D). The full set of pictures used for quantification of area are represented in **Figure 3.S1**.

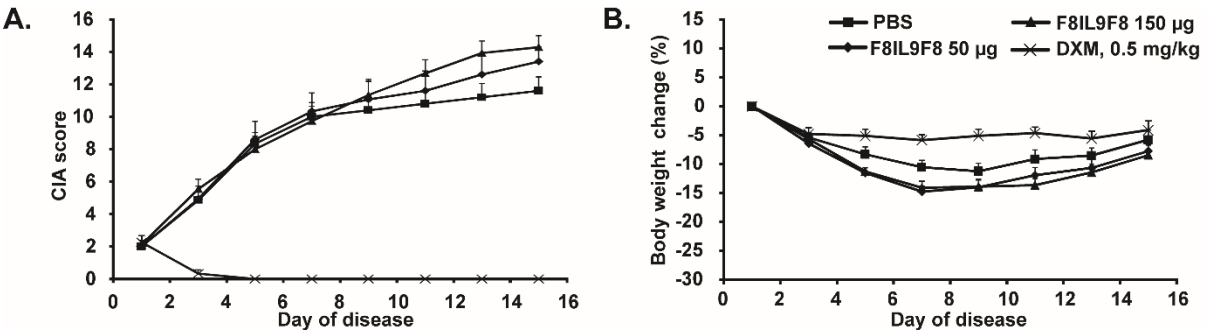

Figure 3.5: Therapeutic performance of F8IL9F8 in collagen-induced arthritis (CIA) DBA/1 mice. Comparison of F8IL9F8, Vehicle (PBS), and dexamethasone treatment in collagen-induced arthritis DBA/1 mice. At the onset of the disease (day 1), arthritic mice were injected three times every second day i.v. in the lateral tail vein with F8IL9F8 (150µg or 50µg) or Vehicle (PBS). dexamethasone was daily administrated (0.5mg/kg) i.p. from the onset of the disease. (n = 15 mice per group). Data represent from the onset of the disease mean CIA score ± SEM (A), body weight change from day 1 in percentage + SEM (B).

3.5 Discussion

We have generated and characterized three novel formats for antibody fusions with murine IL9. All three immunocytokine variants based on the F8 antibody, specific to the alternatively spliced EDA domain of fibronectin, could be expressed and purified to homogeneity. The products retained antigen-binding properties as well as *in vitro* IL9 biological activity. The F8IL9F8 product exhibited the best tumor-targeting performance (6% ID/g in the tumor at 24h), with a tumor:blood ratio of 14.6. The percent injected dose per gram of tissue of IL9-fusions that could be delivered to tumors in mice was comparable to results obtained for other F8-fusion proteins with other cytokine payloads (e.g., IL2, IL4, IL6, IL10, IL12, TNF, interferon-alpha) [107, 111, 115, 117, 118, 349, 422]. However, unlike other F8 derivatives immunocytokines [107, 111, 115, 117, 118, 349, 422], F8IL9F8 did not display a potent anti-cancer activity *in vivo*. Similarly, F8IL9F8 was not active in a mouse model of arthritis.

The function of IL9 in tumor immunity is controversial [229, 423, 424]. It has been generally suggested that IL9 may inhibit the growth of solid tumors by activating the innate or adaptive immune response [425, 426], while as a lymphocyte growth factor, it may promote the progression of hematological malignancies [253, 408]. However, since IL9 has also been reported to promote the proliferation of multiple solid tumor models (like pancreatic cancer, lung cancer, and colitis-associated cancer) [427–429], its anti-cancer activity may be context and tumor type-specific [229, 423, 424].

In this study, we have used three syngeneic immunocompetent models of solid cancer known to express the EDA antigen (i.e., K1735M2 melanoma, CT26 colon carcinoma, and F9 teratocarcinoma, respectively). When compared to saline treatment, a moderate anti-tumor effect could be observed *in vivo* only in the K1735M2 and CT26 models. However, targeting of F8IL9F8 did not result in improved therapeutic efficacy compared to the untargeted KSFIL9KSF at corresponding doses.

The anti-tumor function of IL9 on melanoma was initially postulated by Purwar and collaborators, who showed that adoptive transfer of IL9-producing Th9 cells in mice bearing B16F10 melanoma tumors was highly efficient in preventing tumor progression [254]. Accordingly, injection of recombinant IL9 resulted in impaired tumor growth, although to a lesser extent. More recently, Park and collaborators used B16F10 melanoma cells, ectopically expressing soluble or membrane-bound forms of IL9, to demonstrate the ability of IL9 to inhibit lung metastases [430]. A similar approach was used by Do Thi and collaborators. In this case, CT26 colon cancer cells engineered to ectopically express a membrane-bound IL9, showed tumor growth retardation when compared to mock-transfected CT26 cells [255, 256].

The exact mechanisms underlying IL9 mediated anti-tumor immunity are not fully understood. Whereas a prominent increase of CD4+ and CD8+ T and NK cells have been reported in tumor models ectopically expressing IL9 [255, 430], the work of Purwar suggest a key role played by mast cells since IL9 mediated tumor growth inhibition was abrogated in Kit W-sh mice (mast cells deficient mice) [254]. With our approach, we expected that high IL9 concentrations at the tumor site, resulting from the antibody-mediated targeted delivery of IL9, could contribute to a strong pro-inflammatory environment, ideally favoring anti-cancer immunity and tumor eradication. Even though *in vivo* targeting of IL9 to the subendothelial matrix of the tested tumor models was successful, only moderate tumor growth retardation could be obtained. Similarly, only a very modest increase in tumor-infiltrating CD4+ T, CD8+ T, and NK cells could be observed in the two IL9 responsive models (i.e., K1735M2 and CT26). Similar findings have been reported by our groups: other F8 delivered payloads (e.g., IL17, IFNα, and calreticulin) could increase immune cells infiltration without leading to noticeable anti-cancer efficacy in immunocompetent mice [343, 431, 432]. By contrast, other immunocytokines (e.g., IL2, IL12, IL15, TNF) can promote

strong neoplastic mass immune cell infiltration and strong anti-tumor efficacy [123, 134, 287, 349, 421, 433]. In a more recent study, Rauber and collaborators showed that IL9 could resolve chronic inflammation in two different models of arthritis (i.e., AIA in IL9 deficient mice and SIA models) [269]. They identified IL9-producing ILC2 cells as the main mediators of the resolution of the chronic inflammation and proposed a mechanism by which IL9 would support ILC2 proliferation and survival by an autocrine loop. In our study, we did not observe a therapeutic benefit when F8IL9F8 was administered to arthritic mice. Both differences in the murine arthritis models and therapeutic approach used may account for the divergent results.

The CIA model was chosen since, in this model, we previously demonstrate strong EDA expression in the arthritic paws that were efficiently targeted by various F8 based immunocytokines [106, 117, 415]. Recombinant F8IL9F8 was administered after the onset of the disease in order to mimic as close as possible a potential clinical setting. By contrast, the studies of Rauber are based on non-standard therapy experiments that would be difficult to be directly translated into clinical practice. IL9 was delivered by the hydrodynamic gene transfer (HDGT) approach, which does not allow control over the timing and concentration of overexpressed IL9. Furthermore, in their AIA study, IL9 deficient mice were used, in which a chronic form of arthritis is developed, without signs of resolution. It should be noticed that whereas restoration of IL9 expression in the knockout mice could resolve chronic inflammation, no therapeutic benefit was observed in the wild type mice. Finally, in their serum-induced arthritis model (SIA), IL9 delivery by HDGT was performed 5 days before disease induction, this would mimic a prophylactic rather than a therapeutic approach. The potential therapeutic benefit mediated by IL9 prior to the onset of the disease is in line with the recent finding that in the same SIA model, ILC2 adoptive transfer attenuated arthritis only if performed before SIA induction [434].

The therapeutic results obtained in the preclinical models of cancer and arthritis with F8IL9F8 were unexpected, particularly considering the previous results published by Purwar and Rauber [254, 269]. Although, it remains to be tested whether the anti-cancer and anti-arthritis activity of F8IL9F8 can be improved by combining it with other immunocytokines or through a prophylactic approach, respectively. Currently, we do

not believe that IL9 represents a suitable payload for the development of anti-tumor or anti-arthritis immunocytokines.

3.6 Supporting information

Table 3.1: Primers used for PCR amplification of IL9 based immunocytokines.

Payload	Fragment	Forward Primer	Backward Primer
F8IL9F8	Fragment-1	TCCTCCTGTTCCTCGTCGCTGTGGCTACAGGTGTGCACTCGGAGGTGCAGCTGTTGGAGTCTGGG	ACCTCCACCGCCAGAACCACTTCCGCCTGATTTGATTTCCACCTTGGTCCCTTG
	Fragment-2	TCAGGCGGAAGTGGTTCTGGCGGTGGAGGTCAGAGATGCAGCACCACATGGGG	CCCCCTGAACCACTGCCTCCAGATGGTCGGCTT
	Fragment-3	GCAGTGGTTCAGGGGGCGGTGGAGAGGTGCAGCTGT	TTTTCCTTTTGCGGCCGCTTATTTGATTTCCACCTTGGTCCC
	Fragment-1/2	CCCAAGCTTGTCGACCATGGGCTGGAGCCTGATCCTCCTGTTCCTCGTCGCTGTGGC	CCCCCTGAACCACTGCCTCCAGATGGTCGGCTT
	Fragment-2/3	CAGAGATGCAGCACCACATGGGGA	TTTTCCTTTTGCGGCCGCTTATTTGATTTCCACCTTGGTCCC
KSFIL9KSF	Fragment-1	ATTAAAGCTTCCACCATGGGCTGGAGCCTGATCCTCCTGTTCCTCGTCGCTGTGGC	ACCGCCAGAGCCACCTCCGCCTGAACCGCCTCCACCACTCGAGACGGTGACCAGGG
	Fragment-2	AGGCGGTTCAGGCGGAGGTGGCTCTGGCGGTGGCGGATCGTCTGAGCTGACTCAGGA	CTCTGACCTCCACCGCCAGAACCACTTCCGCCTGAGCCTAGGACGGTCAGCTTGGT
	Fragment-1/2	ATTAAAGCTTCCACCATGGGCTGGAGCCTGATCCTCCTGTTCCTCGTCGCTGTGGC	CTCTGACCTCCACCGCCAGAACCACTTCCGCCTGAGCCTAGGACGGTCAGCTTGGT
	Fragment-3	ATGGGGAATTCGAGACACCAATTACCTTATTGAA	TAATGCGGCCGCTTATCATCCCAGCACTGTCAGCTT
F8IL9	Fragment-1	ATTAAAGCTTCCACCATGGGCTGGAGCCTGATCCTCCTGTTCCTCGTCGCTGTGGC	GCCAGAGCCACCTCCGCCTGAACCGCCTCCACCTTTGATTTCCACCTTGGTCCC
	Fragment-2	CAGGCGGAGGTGGCTCTGGCGGTGGCGGATCACAGGGGTGTCCAACCTTG	TAATGCGGCCGCTTATCATATCTTGCCTCTCATCCCTCT
	Fragment-1/2	ATTAAAGCTTCCACCATGGGCTGGAGCCTGATCCTCCTGTTCCTCGTCGCTGTGGC	TAATGCGGCCGCTTATCATATCTTGCCTCTCATCCCTCT
IL9F8	Fragment-1	TCCTCCTGTTCCTCGTCGCTGTGGCTACAGGTGTGCACTCGCAGAGATGCAGCACCACA	GCCAGAGCCACCTCCGCCTGAACCGCCTCCACCTGGTCGGCTTTTCTGCCTTTGCAT
	Fragment-1'	ATTAAAGCTTCCACCATGGGCTGGAGCCTGATCCTCCTGTTCCTCGTCGCTGTGGC	GCCAGAGCCACCTCCGCCTGAACCGCCTCCACCTGGTCGGCTTTTCTGCCTTTGCAT
	Fragment-2	CAGGCGGAGGTGGCTCTGGCGGTGGCGGATCAGAGGTGCAGCTGTTGGAGTCT	TAATGCGGCCGCTTATCATTTGATTTCCACCTTGGTCCC
	Fragment-1/2	ATTAAAGCTTCCACCATGGGCTGGAGCCTGATCCTCCTGTTCCTCGTCGCTGTGGC	TAATGCGGCCGCTTATCATTTGATTTCCACCTTGGTCCC

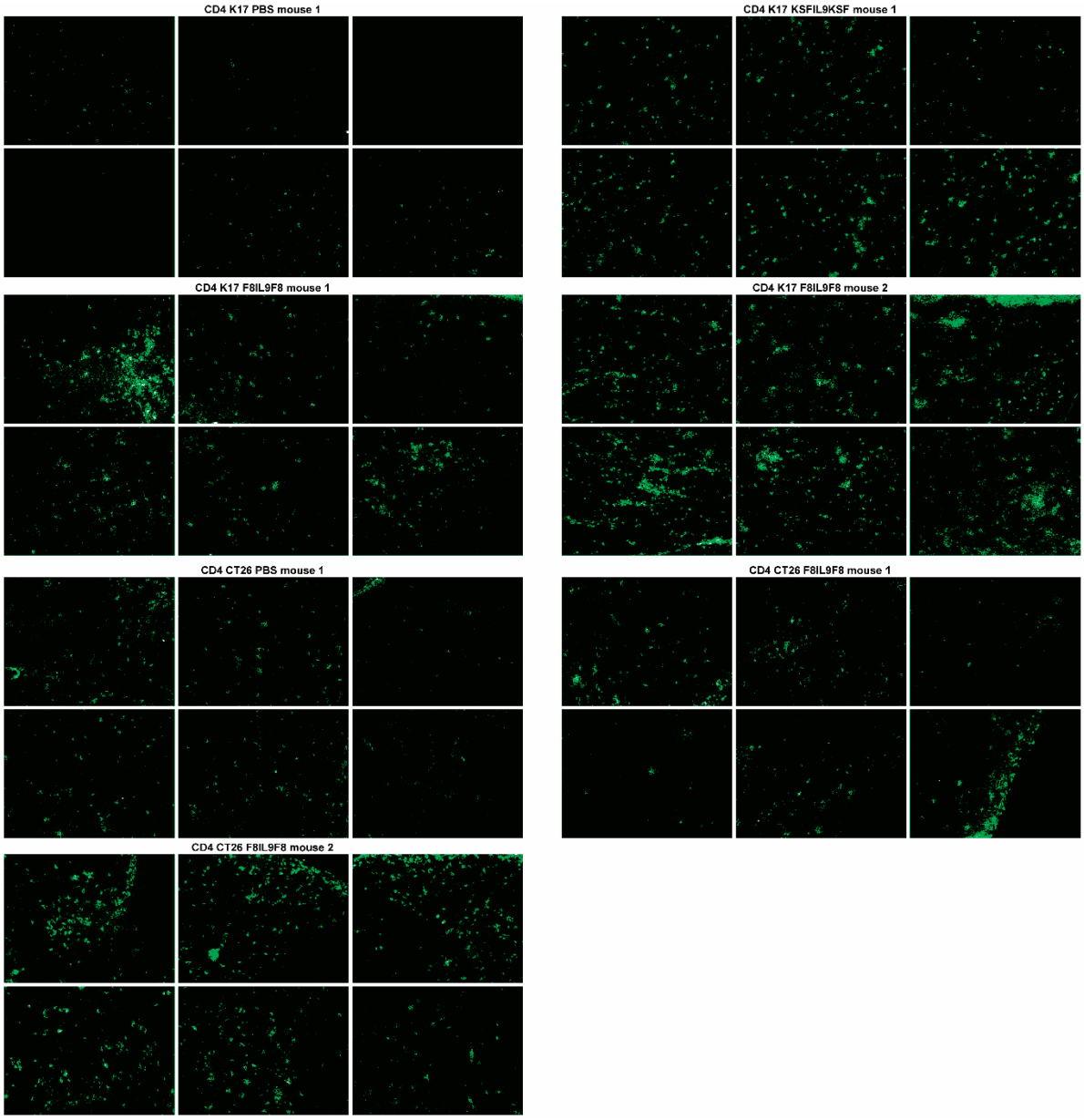

Figure 3.S1: Immunofluorescence analysis of tumor-infiltrating immune cells in K1735M2 melanoma and CT26 colon carcinoma. Immunocompetent mice bearing K1735M2 and CT26 were injected three times every second day i.v. with 200 μg F8IL9F8, or 200 μg KSFIL9KSF or PBS. Mice were sacrificed 24h after the last injection and tumor sections were stained for CD4+ cells (CD4), CD8+ cells (CD8), Tregs (FoxP3) and NK cells (NKp46) (n = 2 mice for F8IL9F8 n=1 for KSFIL9KSF and PBS, six sections for each animal). Microscopic analysis of tumor-infiltrating lymphocytes used for quantification via ImageJ.

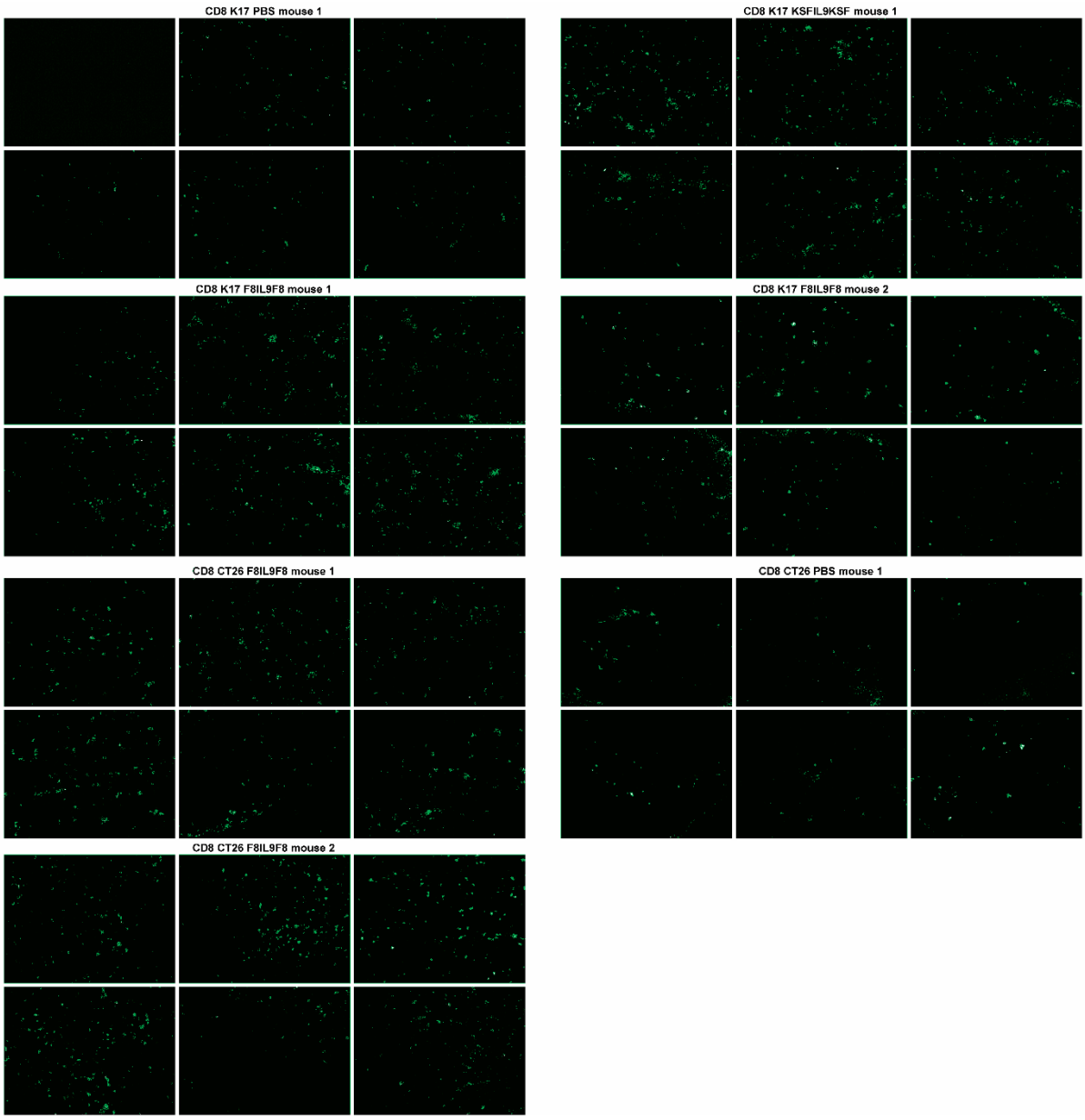

Figure 3.S1: (continued)

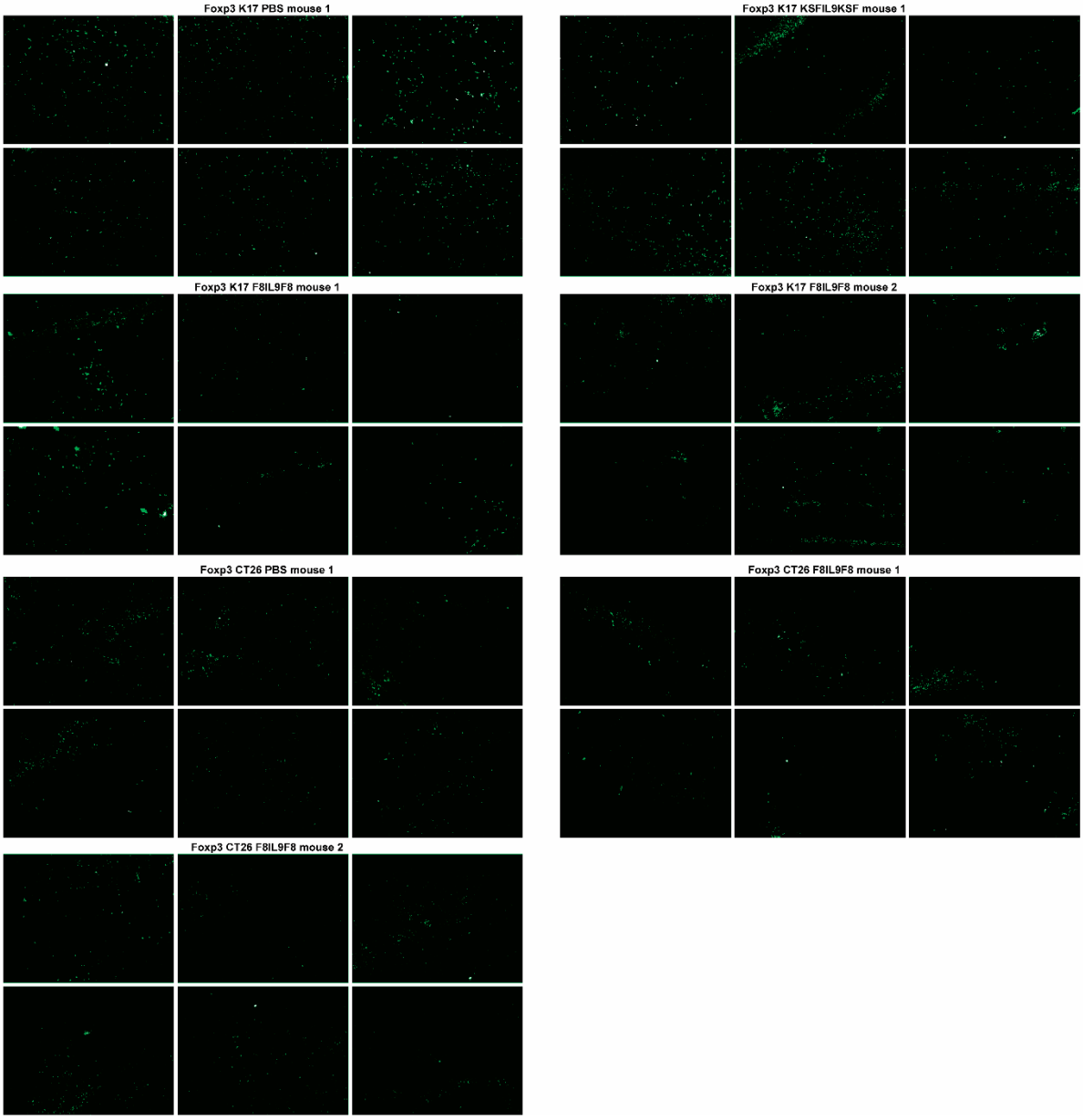

Figure 3.S1: (continued)

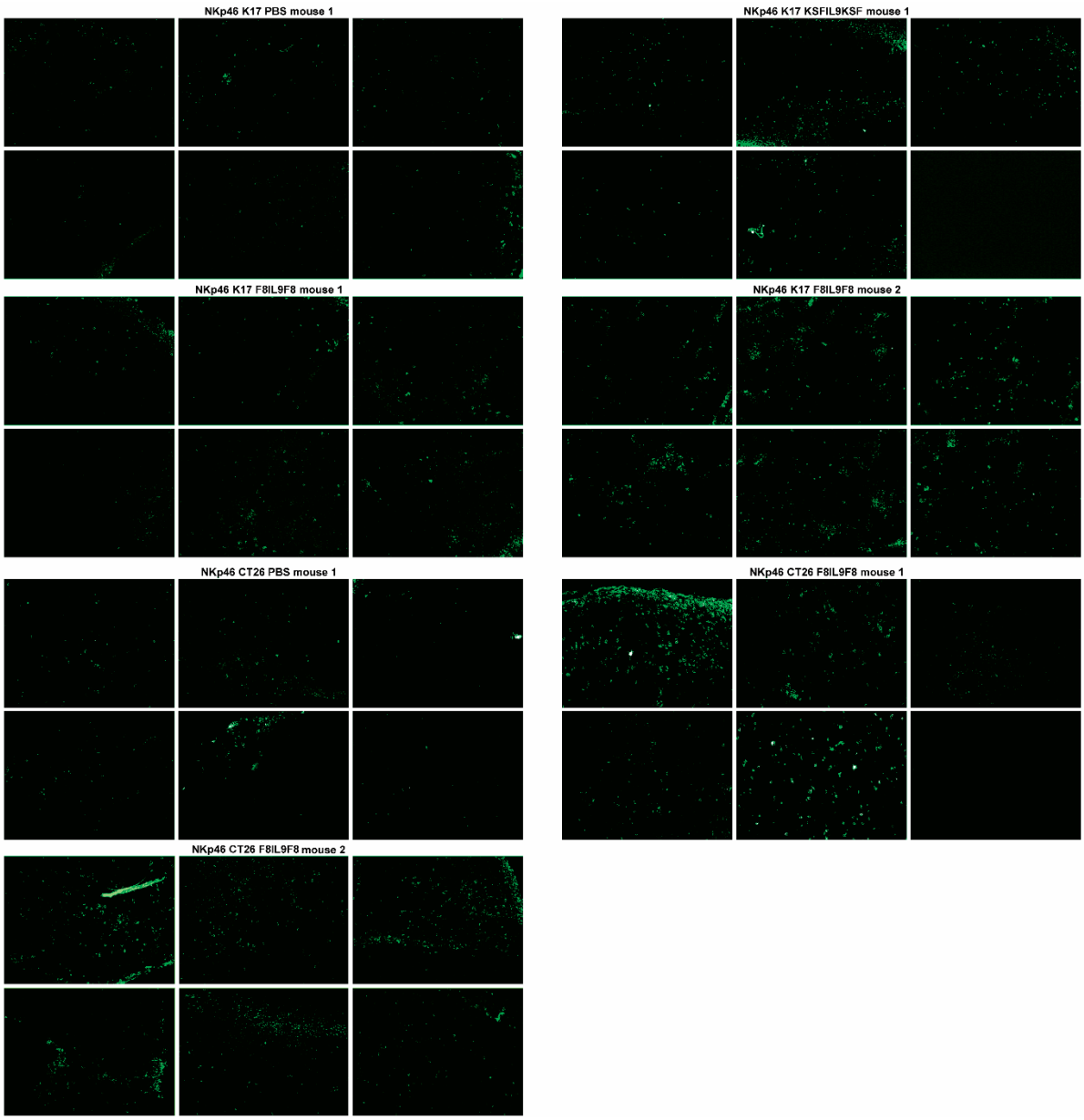

Figure 3.S1: (continued)

4 Antibody targeted delivery of IL9 in pulmonary hypertension

Contribution of the authors: In this work I prepared and characterized the different proteins used for the PH therapy studies. The *in vivo* experiments and tissue analyses have been performed by the group of Prof. Dr. Marcus Franz from the University Hospital Jena.

Therapeutic evaluation of IL9 antibody-based delivery in monocrotaline-induced pulmonary hypertension

Keywords: Pulmonary hypertension, monocrotaline, Fibronectin, Immunocytokines, Interleukin-9

4.1 Abstract

Pulmonary hypertension (PH) is a heterogeneous disorder characterized by a chronic increase in pulmonary artery pressure and associated with poor prognosis. Since only limited therapeutic options are available, there is great interest in developing new treatment strategies. Interleukin 9 (IL9) is a pleiotropic cytokine with both pro- and anti-inflammatory functions which role in pulmonary hypertension has been poorly investigated. The aim of this work was to evaluate in a murine model of PH the therapeutic activity of F8IL9F8, an immunocytokine which has been recently engineered for improved *in vivo* targeting efficacy. F8IL9F8 consists of IL9 fused to the F8 antibody, specific to the alternatively-spliced EDA domain of fibronectin. EDA is a marker of angiogenesis and tissue remodeling, which is strongly overexpressed at PH lesions in rodent models. The efficacy of F8IL9F8 in attenuating PH development in the monocrotaline-induced PH model in mouse was compared to the dual endothelin receptor antagonist macitentan or an IL9 based immunocytokine with irrelevant antibody specificity. Our study may provide preliminary pre-clinical evidence for the use of F8IL9F8 as a new therapeutic agent for the treatment of PH.

4.2 Introduction

Pulmonary hypertension (PH) is a pathophysiological disorder that may involve multiple clinical conditions and is a complication of the majority of cardiovascular and respiratory diseases. PH is a disease defined as an increase in mean pulmonary arterial pressure (PAPm) ≥25 mmHg at rest [388]. PH patients are classified into five different clinical groups, depending on the pathogenesis and prognosis of the disease, which are also defining the treatment strategies to be used [388, 402]. The five PH groups are defined as (1) pulmonary arterial hypertension (PAH), (2) PH due to left heart disease, (3) PH due to chronic lung disease and/or hypoxia, (4) chronic thromboembolic PH (CTEPH), and (5) PH due to multifactorial and unclear mechanisms.

Current treatment options for PH generally act by decreasing vascular tone and thereby reducing pulmonary artery pressure, but no treatment able to stop or reverse PH progression is available. Therefore, PH is generally associated with poor prognosis and limited therapeutic options. Indeed, whereas specific therapies are available for

group 1 PAH (e.g., prostanoids, endothelin receptor antagonists, phosphodiesterase inhibitors), and group 4 CTEPH (soluble guanylate cyclase agonist), for the other groups, the standard of care is limited to managing symptoms or to treat the underlying disease (cardiovascular or pulmonary disorders) [435]. Since mortality rates of PH patients are still high despite the available specific treatments, there is a scientific and clinical need to identify novel therapeutic interventions for pulmonary hypertension.

During PH disease progression, increased vasoconstriction and remodeling of the pulmonary vasculature occurs, resulting in PAP elevation and the clinical manifestations of the disease [402, 436]. Pulmonary vascular remodeling, involving all layers of the vessel walls, is a key component of PH pathogenesis [402]. Recently, the group of Prof. Marcus Franz has identified EDA(+)-fibronectin expression as a remodeling marker of PH in rats [403]. Interestingly, EDA overexpression has been reported in a variety of inflammatory conditions characterized by substantial tissue remodeling (e.g., endometriosis, arthritis, psoriasis, atherosclerosis, vasculopathy, and certain inflammatory bowel conditions) [105, 106, 112, 116, 117, 361, 363, 367, 387, 415]. On the contrary, EDA is virtually undetectable in normal adult organs, with the exception of the female reproductive system [116]. Thus, EDA can be considered as an excellent molecular target for antibody-based pharmacodelivery of immunomodulatory payloads (e.g., cytokine) directly to the site of disease [112, 411]

Antibody-cytokine fusion proteins (i.e., immunocytokines) are increasingly being evaluated in preclinical and clinical settings for the treatment of cancer and chronic inflammation [105, 106, 112, 116, 117, 415, 416]. Our group has extensively investigated the use of the F8 fully human antibody, specific to EDA(+)-fibronectin, for the targeted delivery of a variety of cytokines (e.g., F8-IL10 and F8-IL4) at sites of chronic inflammation in mouse models [105, 106, 112, 116, 117, 415] and in patients with rheumatoid arthritis [416]. Since murine and human EDA differ only in three amino acid substitutions, F8 is particularly suitable for *in vivo* pharmacodelivery applications because it recognizes the cognate antigen in mouse and man with identical affinity [54].

Interleukin-9 (IL9) is a pleiotropic cytokine mainly secreted by CD4+ T cells after stimulation by transforming growth factor-beta (TGFB) and IL4 [216]. IL9 signaling is mediated by a heterodimeric receptor consisting in the cytokine specific IL-9-receptor

α-chain (IL-9Rα) dimerized with the common γ-chain receptor (γc) [236]. IL9 has been shown to activate T cells, eosinophils, type 2 innate lymphoid cells (ILC2), and mast cells [226, 227]. Beside playing a regulatory role in autoimmunity and allergic reactions, IL9 has been suggested to be involved in anti-parasitic and anti-tumor responses, and in the formation of immune tolerance [221]. Whereas several biological functions have been attributed to IL-9, its involvement in PH has not been investigated so far, and results from preclinical models of lung fibrosis are controversial [241, 250].

F8IL9F8 is a newly developed immunocytokine, consisting of one murine IL9 moiety flanked by two units of the F8 antibody in a single-chain Fv format (**Figure 4.1**). F8IL9F8 has been recently engineered to improve *in vivo* targeting efficacy. Consistent with the reported IL-9 anti-tumor activity [254], F8IL9F8 treatment resulted in mild tumor growth delay in murine models of melanoma and colon cancer [437].

In this study, we have evaluated the therapeutic efficacy of the recently developed immunocytokine, F8IL9F8, in the MCT-induced model of PH in mice. Disease severity has been evaluated by assessing haemodynamic and echocardiographic parameters as well as by *ex vivo* histological and immunofluorescence analysis of lung and heart sections to assess tissue damages and immune cell infiltrations. Surprisingly, different than the untargeted IL9 control (i.e., KSFIL9KSF), F8IL9F8 treatment exhibited a therapeutic advantage compared to the standard of care MACI. While we are reporting a preliminary study on the therapeutic use of IL9 in PH, our findings suggest that F8IL9F8 is a potential candidate for the treatment of PH.

4.3 Materials and methods

4.3.1 Expression plasmids

The plasmids pcDNA3.1-F8IL9F8 and pcDNA3.1-KSFIL9KSF were used for the production of the F8IL9F8 and KSFIL9KSF fusion proteins, respectively. The 2 vectors were generated by inserting into the HindIII-NotI sites of pcDNA3.1 (Invitrogen), a PCR assembled sequence consisting of the murine IL9 (AA 19-144) flanked on both N- and C- termini by either the F8 (raised against the EDA domain of fibronectin) [54] or the KSF (raised against the hen egg lysozyme) [431] antibodies in scFv format. In the

assembled gene, the antibody moieties are fused to the IL9 cytokine by the meaning of 10 amino acids linkers. **Figure 4.1A** shows a schematic representation of the expression plasmids and the corresponding fusion protein.

4.3.2 Protein expression and purification

The IL9 based fusion proteins (F8IL9F8, KSFIL9KSF) were expressed by transient gene expression (TGE) in Chinese Hamster Ovary (CHO) cells [417]. For routine cultivation, cells were kept at 37°C with a 5% CO2 atmosphere under shaking conditions. One day prior to transfection, CHO cells were seeded at 2 x 10^6 cells/mL in PowerCHO-2CD (Lonza) medium supplemented with 4 mM Ultraglutamine (Lonza). The next day, the cells were recovered by centrifugation and resuspended in ProCHO-4 Medium (Lonza) supplemented with 4 mM Ultraglutamine (Lonza) at a density of 4 × 10^6 cells/mL cells. Transfections were performed in glass bottles by adding 0.625 μg of plasmid DNA and 2.5 μg polyethyleneimine (1mg/mL in water pH 7) (Polysciences) per million cells. The transfected cultures were maintained at 31°C in a shaking incubator with 5% CO2 and with agitation at 120 rpm. The supernatant from 6 days old cultures was collected by centrifugation, and the fusion proteins were purified by a single step of Protein A affinity chromatography (Sino biological) and finally formulated in PBS via dialysis.

4.3.3 Protein analysis

Dodecyl sulfate-polyacrylamide gel electrophoresis (SDS-PAGE) and size-exclusion chromatography Superdex 200 increase 10/300GL column (Amersham Biosciences) were used for characterization of protein size and purity. Analysis of the F8IL9F8 affinity to its cognate antigen was performed by Surface Plasmon Resonance (BIAcore X100, GE Healthcare). Samples were injected as serial-dilution (from 2000nM to 7.8nM) on a fibronectin 11A12 domain coated CM5 chip (GE Healthcare). ELISA was used to confirm the binding of KSFIL9KSF to hen egg Lysozyme. Briefly, hen egg lysozyme (Sigma) was coated overnight at a concentration of 3 mg/mL on Maxisorp plates (ThermoFisher Scientific). Captured KSFIL9KSF (triplicate of serial dilutions from 1000nM to 31.3nM) was detected with Protein A-HRP (GE Healthcare) using BM-Blue POD (Roche) as the substrate for horseradish peroxidase. Absorbance was

measured at 450nm vs 620nm using a microplate reader (Ledetect 96, Dynamica Scientific). Results are expressed as an average of triplicate measurements.

4.3.4 Mouse model of MCT-induced PH and treatment schedule

All experiments were conducted according to the National Institute of Health Guidelines for the Care and Use of Laboratory Animals (8th edition), to the European Community Council Directive for the Care and Use of Laboratory Animals of 22 September 2010 (2010/63/EU), the current version of the German Law on the Protection of Animals and the guidelines for animal care. The study protocol was approved by the appropriate State Office of Food Safety and Consumer Protection (TLLV, Bad Langensalza, Germany local registration number: UKJ17- 003).

Animals were obtained from ZET facility (Zentale Experimentelle Tierhaltung) of the University Hospital Jena (UKJ, Jena, Germany). Prior to PH induction, mice were allowed to acclimatize for at least 7 days with ad libitum access to food and water as well as controlled light/dark cycles.

PH was induced in C57BL/6 mice (bodyweight: 25-30g), using the MCT method. As summarized in **Figure 4.2** the following experimental groups were investigated: sham induced controls (n=6) MCT induced PH (n=8), MCT induced PH + MACI (n=7), MCT induced PH + F8IL9F8 (n=6), MCT induced PH + KSFIL9KSF (n=6).

The *sham induced controls* were injected with 30µl NaCl not containing MCT at day 1 (single dose intraperitoneally, i.p.). These mice did not develop PH and thus served as healthy controls. The other 4 experimental groups were injected with MCT to induce PH (single dose intraperitoneally, i.p. 60mg/kg body weight volume 30µl). Animals in the "*MCT + MACI"* group received the drug from day 14 to day 28 (once daily per os 15mg/kg body weight). Animals in the "*MCT + F8IL9F8"* group received F8IL9F8 3 times on day 14, 16, and 18 (intravenously, i.v. 200µg/injection volume 155 µl). Accordingly, animals in the "*MCT + KSFIL9KSF"* group received KSFIL9KSF 3 times on day 14, 16 and 18 (intravenously, i.v. 200µg/injection volume 135 µl). To prevent infection and inflammatory alterations of the lungs, mice in all groups received Enrofloxacin (Baytril) 2.5% ad water from day 1 to 14 after MCT injection. All animals were weighed and examined twice weekly for clinical monitoring of well-being. The clinical condition was assessed using an established score (clinical severity score =

CSS) from 1 to 5 (1 = no signs of clinical alterations, 2 = low-grade impairment, 3 = mid-grade impairment, 4 = high grade impairment, 5 = exitus) obtained by evaluating spontaneous activity, reaction to exogenous stimuli and posture.

4.3.5 Echocardiographic assessment

The echocardiographic assessment was performed on day 28 (**Figure 4.3**) using the Vevo 770 Rodent-Ultrasound-System, Visual Sonic, Canada, 17MHz probe RMV176. Before echocardiography, mice were anesthetized with isoflurane for a duration time of less than 10 minutes (isoflurane-CP, 2.5V%, FiO2 1.0, oxygen per inhalation-flow dosage). Body temperature and respiratory rate were continuously monitored. All surrogate parameters of right ventricular (RV) morphology and function were assessed, among others, RV basal and medial diameters (in mm), RV length (in mm), and RV fractional area change (FAC, in %).

4.3.6 Right heart catheterization

On day 28, after MCT injection, mice of all experimental groups were deeply anesthetized with a single dose of 100mg/kg body weight ketamine and 10mg/kg body weight Xylazin in approximately 60µl each administered i.p.. Right heart catheterization using a 1.4F micro conductance pressure-volume catheter (Model 10 SPR-839 Millar Instruments Inc PowerLab system, ADInstruments Ltd., Oxford, UK) was performed via the right vena jugularis interna to measure the systolic right ventricular pressure and thereby verify the success of the experimental setting. Mice were then sacrificed in deep anesthesia and analgesia to carry out cardiac blood collection after thoracotomy and to harvest the organs.

4.3.7 Histological assessment of lung and right ventricular cardiac tissue damage

For the assessment of PH associated lung tissue damage, a defined sum-score system was used, which was recently established and validated in our group [403, 438]. Microscopic evaluation was carried out using 4 µm thick H&E as well as Sirius Red stained lung tissue sections according to standardized protocols. The applied sum-score integrates the following histopathological features frequently occurring in PH: percentage of atelectasis area, percentage of emphysema area, degree of media hypertrophy of peribronchial arteries, presence of perivascular cellular edema of

peribronchial arteries, and degree of media hypertrophy of small arteries. Finally, the scoring can range between 0 and 12, with the maximum value reflecting the highest level of tissue damage. Right ventricular cardiac tissue damage was evaluated by assessing the two most evident features, which are inflammation (immune cell infiltration) and cardiac interstitial fibrosis. Occurrence of these phenomena was semi-quantitatively assigned to the following levels: 0 = not detectable, 1 = weakly detectable, 2 = moderately detectable, 3 = strongly detectable. All histological analyses were performed independently and blinded by two experienced scientists.

4.3.8 Immunofluorescence staining of CD45 (pan-leukocyte antigen) and CD68 (macrophage marker) in lung and right ventricular cardiac tissue

Immunofluorescence labeling of CD45 and CD68 was performed using 4 µm cryostat sections, which were fixed in ice-cold acetone for 10 min. For the detection of CD45, the rat-anti-mouse monoclonal antibody 30-F11 (BD Biosciences, Heidelberg, Germany) was applied (dilution for lung tissue: 1:200 dilution for cardiac tissue: 1:150) and allowed to incubate for 60 minutes at room temperature. For the detection of CD68, the rat-anti-mouse monoclonal antibody FA-11 (Bio-Rad Laboratories, GmbH, München, Germany) was used (dilution for lung tissue: 1:200 dilution for cardiac tissue: 1:150) and allowed to incubate for 60 minutes at room temperature. As a next step, rinsing in TBS-T washing buffer was performed three times, and sections were then incubated with Cy3-conjugated AffiniPure Donkey Anti-Rat IgG (Jackson Immunoresearch Laboratories Inc., Pennsylvania, USA) for 45 minutes at room temperature (dilution 1:400). After rinsing in TBS-T buffer and distilled water, sections were mounted in Vectashield H1200 mounting medium containing DAPI (Linaris biologische Produkte GmbH, Wertheim-Bettingen, Deutschland, blue fluorescence) and stored at –20°C. Antibody specificity control staining was performed in accordance but by omitting the primary antibodies. Immunofluorescence labeling was analyzed with the Axiophot microscope with the AxioVision Release 4.8 software (both Carl Zeiss, Germany). The magnification of microscopic images is 20-fold.

4.3.9 Immunofluorescence staining of EDA(+) fibronectin in lung and right ventricular cardiac tissue

For detection of EDA(+) fibronectin by immunofluorescence, again 4 µm cryostat sections were fixed in ice-cold acetone for 10 min. Blocking of endogenous biotin was performed with the DAKO Biotin Blocking System according to the manufacturer´s instructions (DAKO Deutschland,GmbH, Germany). The biotinylated SIP-F8 antibody was applied as a primary antibody in a dilution of 1:50 and allowed to incubate overnight at 4°C. In the next step, Cy3 labeled Streptavidin (Southern Biotech, Birmingham, USA) was added for 45 minutes in a dilution of 1:200 at room temperature. Antibody specificity control staining was performed in accordance but by omitting the primary antibodies (data not shown). Finally, sections were mounted using Vectashield H1200 containing DAPI-stain (Linaris biologische Produkte GmbH, Wertheim-Bettingen, Deutschland) and stored at –20°C. Analysis of immunofluorescence labeling was performed by the Axiophot microscope with the AxioVision Release 4.8 software (both Carl Zeiss, Germany). The magnification of microscopic images is 40fold for lung and 20fold for cardiac tissue.

4.3.10 Statistics

Statistical analyses were performed using IBM SPSS statistical software, version 25.0 (IBM SPSS Statistics for Windows. Armonk, NY, USA). Data are expressed as mean ± standard deviation. Mann-Whitney-U test was used to test for significant differences between the different groups.

4.4 Results

Production and characterization of IL9 based immunocytokines.

The F8IL9F8 and KSFIL9KSF fusion proteins consist of two scFv antibody moieties sequentially fused to the N- and C-termini of the murine interleukin 9, by the meaning of 10 amino acid long linkers. The fully human F8 antibody recognizes both the human and murine extra domain EDA of fibronectin with comparable affinity [54]. The KSF antibody (specific to the hen egg lysozyme) was used as a negative control antibody. The two fusion proteins were transiently produced in Chinese Hamster Ovary (CHO) cells at yields of about 20 mg/L. **Figure 4.1A** shows the cloning strategy chosen for

the expression of the two immunocytokines, while **Figure 4.1B** illustrates the domain assembly of the corresponding polypeptides. The sequential arrangement of two scFv moieties to both termini of IL9 resulted in highly stable proteins with suitable properties for *in vivo* studies. F8IL9F8 and KSFIL9KSF were purified to homogeneity by protein A affinity chromatography and were well behaved in SDS-PAGE and size exclusion chromatography analysis (**Figure 4.1 B and C right panels**). As expected, F8IL9F8 fully retained binding activity to the cognate EDA antigen as determined by Surface Plasmon Resonance (SPR), with an apparent K_D of 2.9 10^{-9} nM. Similarly, KSFIL9KSF binding to the irrelevant antigen hen egg lysozyme was confirmed by ELISA (**Figure 4.1 B and C left panels**).

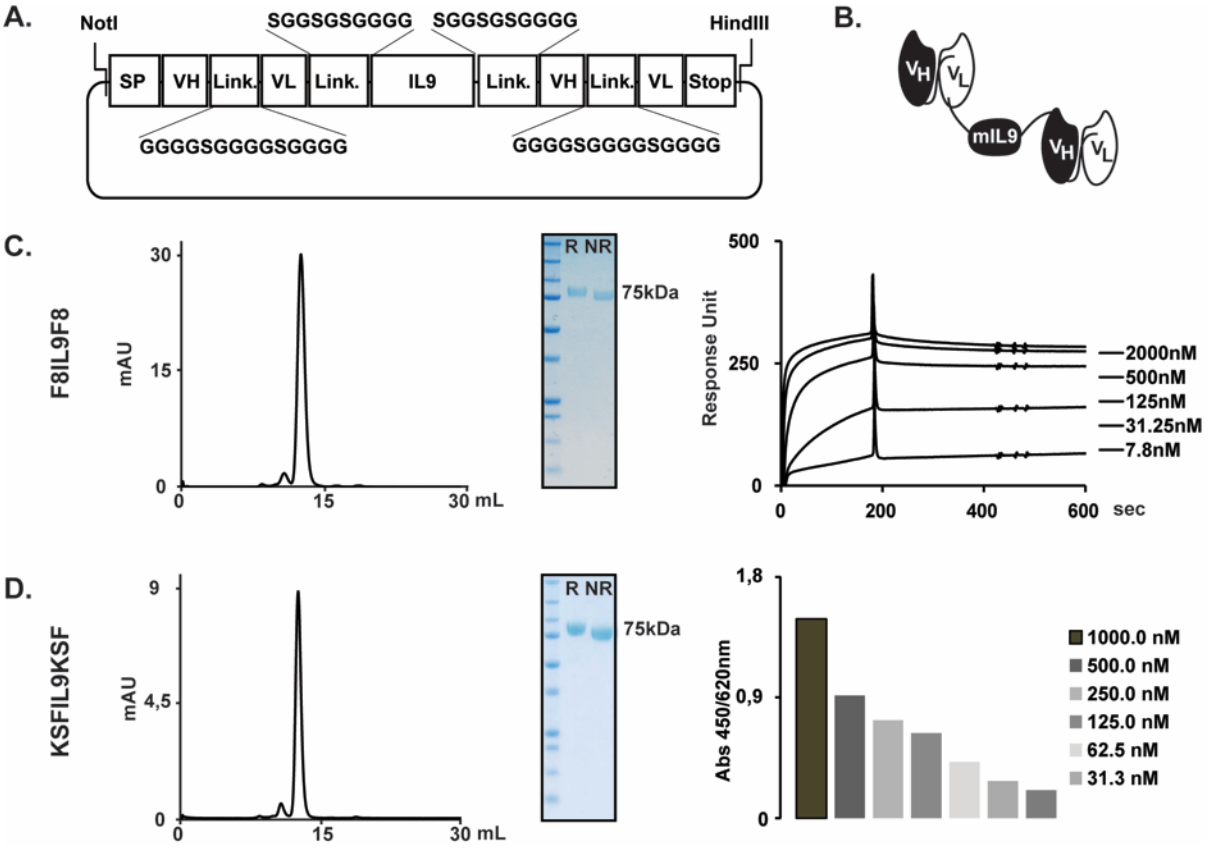

Figure 4.1: F8IL9F8 and KSFIL9KSF cloning expression and characterization. F8IL9F8 and KSFIL9KSF have been genetically engineered and produced in mammalian CHO cells. Cloning strategy of the IL9-based fusion proteins (A). Schematic representation of the domain structure of the IL9-based immunocytokines (B). Characterization of the F8IL9F8 (C) and KSFIL9KSF (D) purified proteins. From left to right: size exclusion chromatography profile, analytical SDS-PAGE analysis, SPR sensograms on EDA-coated CM5 chip for F8IL9F8, or ELISA on Lysozyme coated Maxisorp for KSFIL9KSF. R: reducing condition, NR: non-reducing condition SP: signal peptide, VH: variable heavy chain, VL: variable light chain, Link.: peptidic linker, STOP: codon stop.

Experimental design of IL9 treatment on MCT-induced PH in mice.

Pulmonary hypertension could be successfully induced in C57BL/6 mice using the MCT method. 14 days after monocrotaline intraperitoneal (i.p.) injection, mice developed pulmonary hypertension with a suitable grade for therapeutic intervention. Mice were then treated either with (Macitentan) MACI (15 mg/kg daily), F8IL9F8, or its control KSFIL9KSF (both 200 µg/injection, three times every second day) (**Figure 4.2A**). Successful PH induction in the MACI induced mice was confirmed by the increase in right ventricular systolic pressure (RVPsys) and clear signs of right heart overload and dysfunction as assessed by echocardiography (**Figure 4.2 and 4.3**). To determine PH severity in the different treatment groups, a variety of surrogate parameters of right ventricular (RV) morphology and function were assessed, including RV basal and medial diameters (in mm), RV length (in mm), and RV fractional area change (FAC, in %).

Effect of IL9 on haemodynamic parameter of MCT-induced PH

The therapeutic efficacy of F8IL9F8 was tested in the MCT induced model of PH in mouse and compared to both to the untargeted control KSFIL9KSF (an immunocytokine with irrelevant specificity in the mouse and therefore qualified as untargeted control), and MACI, a dual endothelin receptor antagonist proven to effectively reduce pulmonary artery pressures and therefore used as an approved standard therapy also in humans. Heart overload was assessed for each treatment group at 28 days after PH induction by recording RVPsys through right heart catheterization (**Figure 4.2C**). Compared to the sham group, RVPsys was significantly elevated in all MCT-induced PH groups ($p<0.05$), except for the group treated with F8IL9F8 ($p=0.068$). Both F8IL9F8 and MACI treatments lead to a significant reduction in RVPsys ($p=0.025$ and 0.028, respectively) when compared to the MCT group. Additionally, the group treated with F8IL9F8 displayed a significantly reduced RVPsys compared to the group treated with KSFIL9KSF ($p=0.047$). Therefore, the targeted delivery of IL9 by F8IL9F8 in the MCT murine model of PH is ameliorating right heart overload pressure in a manner similar to MACI treatment.

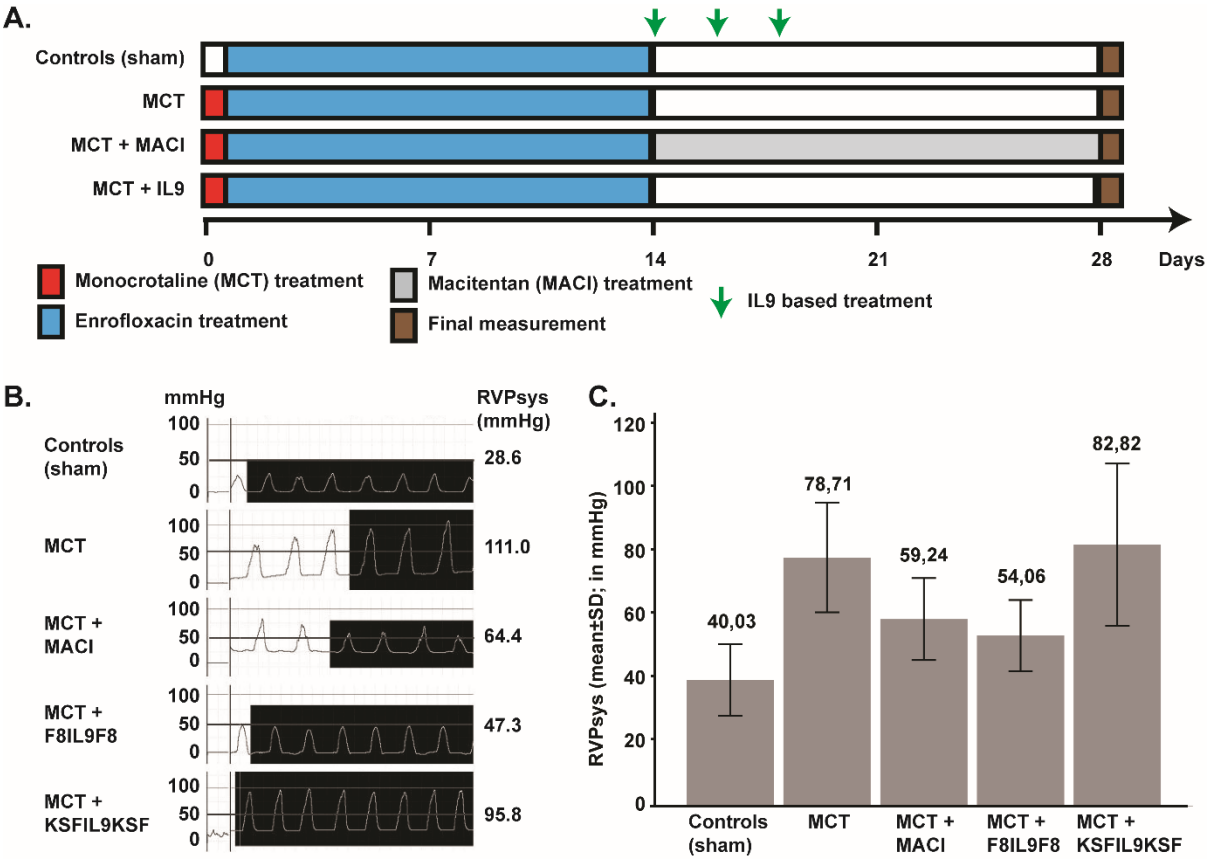

Figure 4.2: Treatment of MCT-induced PH mice with IL9 based fusion protein and MACI and effect on haemodynamic results after right heart catheterization. Experimental design of the MCT-induced PH mouse model and treatment schedule. Exception made for sham-induced controls (no PH), PH in mice was induced with a single injection of MCT, 60mg/kg i.p. on day 0. From day 1 to 14, mice in all groups received Enrofloxacin 2.5% ad water, to prevent infection and inflammatory alterations of the lungs. Starting from day 14, mice received treatment with MACI (15 mg/kg daily) or IL9 based fusion proteins (200 µg every second day). On day 28, echography, RV-catheter, and organ harvesting were performed. Groups are composed by Sham (n=6) MCT induced PH (n=8) MCT induced PH + MACI (n=7) MCT induced PH +F8IL9F8 (n=6) MCT induced PH + KSFIL9KSF (n=6) (A). Representative right ventricular pressure (RVP) curves for one mouse per treatment group as recorded by invasive right heart catheterization. The second column shows the typical right ventricular morphology curve, and the third column provides the average cyclic maximum values (equates to systolic RVP = RVPsys) for each individual animal as calculated using LabChart software (in mmHg) (B). Chart representing the mean RVPsys (mean + standard deviation) of each treated group, performed by invasive right heart catheterization. Values presented on top of the graph are the mean value, calculated with LabChart software (in mmHg) (C).

Effect of IL9 on echocardiographic parameters of MCT-induced PH.

Heart morphology and function were assessed at day 28 for each treatment group by echocardiography. RV basal and medial diameters, as well as the RV length, have been used as surrogate markers of RV-dilatation in response to pressure overload, while RV fractional area change was quantified and used as a surrogate marker of RV functions. While the RV basal diameter was significantly increased in all MCT-induced PH groups ($p<0.05$) compared to the sham group, only treatment with F8IL9F8 lead

to a significant decrease of the RV basal diameter value compared to MCT-induced PH groups (p=0.014) (**Figure 4.3A**). F8IL9F8 treatment resulted in a RV medial diameter comparable to the one of the sham-treated group (p=0.128), while in all the other MCT-induced PH groups, RV medial values were significantly increased compared to sham (p<0.05). Importantly, both the RV basal and medial diameter values in the F8IL9F8 group were significantly reduced compared to KSFIL9KSF treatment (p=0.010 for RV basal diameter and p=0.037 for RV medial diameter) (**Figure 4.3B**). The RV length was significantly increased in all MCT-induced PH groups compared to sham (p<0.05), except when mice were treated with F8IL9F8 (p=0.100). Additionally, in the group treated with F8IL9F8, RV length diameters were significantly reduced compared to the untreated or KSFIL9KSF-treated groups (p= 0.006 and p=0.016, respectively) (**Figure 4.3C**). RV systolic function was evaluated by calculating RV FAC values and by defining right ventricle dysfunction by RV FAC ≤35%. Compared to sham induced controls, the RV FAC values were significantly reduced in all MCT-induced PH groups (p<0.05), except the group treated with F8IL9F8 (p=0.337). Both MACI and F8IL9F8 treatments showed a significant improvement in the RV FAC values compared to MCT-induced mice without treatment (p=0.032 and p=0.046, respectively). Surprisingly, no significant differences in the RV FAC was observed between F8IL9F8 and KSFIL9KSF treatment (p=0.068) (**Figure 4.3D**). In summary, also the echocardiographic parameters evaluated in this study demonstrate the therapeutic efficacy of F8IL9F8 for the treatment of PH in the MCT-induced murine model.

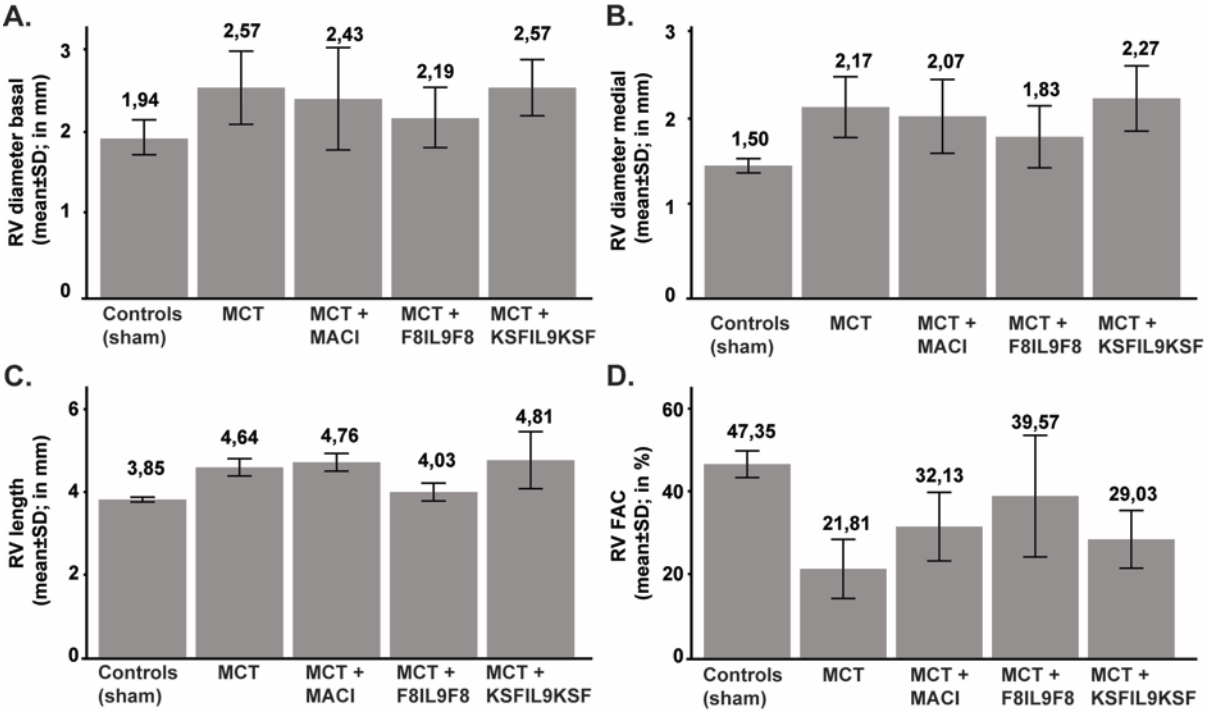

Figure 4.3: Echocardiographic assessment of treatment effect on MCT-induced PH mice. On day 28, Echography was performed in order to compare IL9-based fusion protein treatment to sham and MACI in MCT-induced PH mice. Echocardiographic measurement was performed using Vevo 770 Rodent-Ultrasound-System, Visual Sonic, Canada, 17MHz probe RMV176. Chart representing the basal (A) and medial (B) right ventricular diameter (RV diameter) values (mean ± standard in mm), right ventricular length (RV length) (C) values (mean ± standard in mm), and right ventricular fractional area change (RV FAC) (D) values (mean ± standard in %) in the 5 experimental groups.

Effect of IL9 on lung and right ventricular cardiac tissue damage in MCT-induced PH

Tissue samples from the lungs and right ventricles of all 33 animals investigated in this study underwent detailed histological analysis, as described above. For lung tissue, a semi-quantitative sum-score system including all relevant histopathological parameters occurring in PH, was applied. The level of tissue damage in general (sum-score) was significantly increased when comparing the sham group with the MCT-induced PH groups ($p<0.05$ for all groups). Most notably, when comparing the MCT-induced PH group without treatment with the treatment groups, only the administration of F8IL9F8 led to a significant decrease and thereby attenuation of tissue damage in the lungs ($p=0.007$). **Figure 4.4** shows representative histological phenomena (**Figure 4.4A**, H&E, as well as Sirius red stains) and summarizes the results of semi-quantitative lung tissue analysis illustrating the sum-score (**Figure 4.4G**) as well as its single parameters (**Figure 4.4B to F**). When focusing on the latter, especially media

hypertrophy of both peribronchial (**Figure 4.4D**) and small (**Figure 4.4F**) arteries, is significantly diminished exclusively in the F8IL9F8 group ($p<0.05$). Comparison of MACI with F8IL9F8 treatment reveals a relevant decrease of emphysema area ($p=0.018$). In the MACI treated group, perivascular cellular edema of peribronchial arteries was significantly decreased compared to the KSFIL9KSF group ($p=0.033$). A comparison of the F8IL9F8 and the KSFIL9KSF group revealed a significant reduction in the emphysema area ($p=0.030$), media hypertrophy of peribronchial arteries ($p=0.043$), and the histological sum-score in general ($p=0.004$) in the F8IL9F8 group.

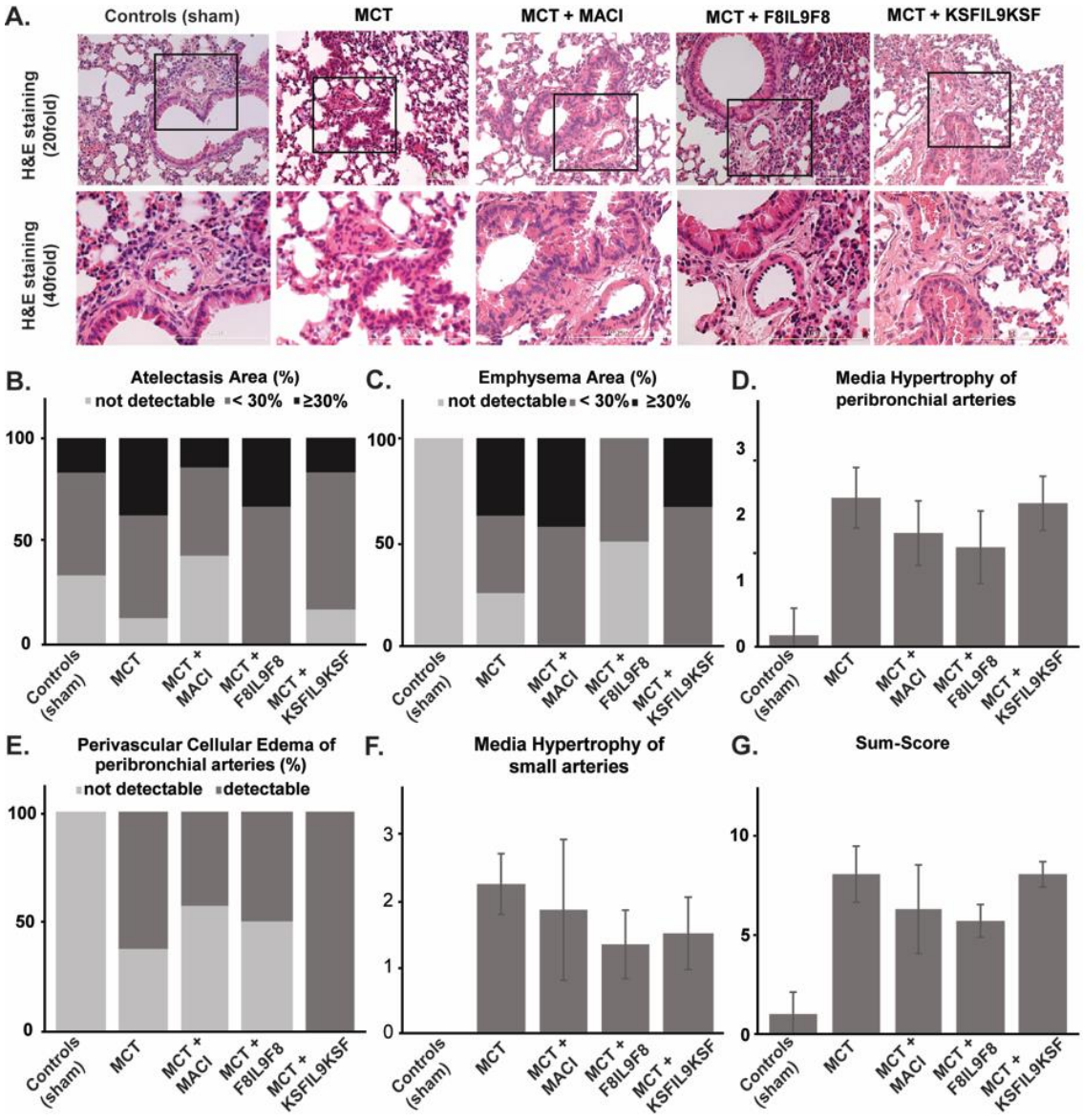

Figure 4.4: Assessment of histological damage in lung tissue: evaluation of different treatment effects on MCT-induced PH in mice. Lung tissue samples were subjected to detailed histological analysis to compare IL9-based fusion protein treatment to sham and MACI in MCT-induced PH mice. The assessment was performed by microscopic analysis using a defined sum-score system. Representative microscopic images of H&E, as well as Sirius red stains (A), illustrate

the clear differences in the extent of tissue damage in comparison of the 5 experimental groups (A). Graphs show results of a semi-quantitative assessment of the following single parameters contributing to the sum-score for the different groups: atelectasis areas (%) (B), emphysema area (%) (C), media hypertrophy of peribronchial arteries (mean ± standard) (D), perivascular cellular edema of peribronchial arteries (%) (E), media hypertrophy of small arteries (mean ± standard) (F). The sum-score integrating evaluation results for all single parameters is given in (G) (mean ± standard).

Histological analysis of right ventricular cardiac damage was performed with a focus on the assessment of inflammation and cardiac interstitial fibrosis by semi-quantitatively scoring as described above. In general, histological cardiac damage in the mouse model of MCT-induced PH is not as obvious as seen in the corresponding rat model (data not shown). When comparing the 5 different experimental groups in this study, there is a significant increase of both inflammation and fibrosis in the MCT-induced PH groups compared to the sham group ($p<0.05$ for all groups except for inflammation in the group treated with MACI). When comparing the MCT-induced PH group with the under-treatment groups, there are no significant differences in the MACI as well as the F8IL9F8 group (p=n.s.) and a slight but significant augmentation of tissue damage in the KSFIL9KSF group ($p<0.05$ for both inflammation and fibrosis). In the MACI group, compared to the KSFIL9KSF treated group, there was a significant reduction of inflammation ($p=0.045$) and fibrosis ($p=0.043$). Histopathological changes in right ventricular cardiac tissue in the comparison between the 5 experimental groups are illustrated in **Figure 4.5**.

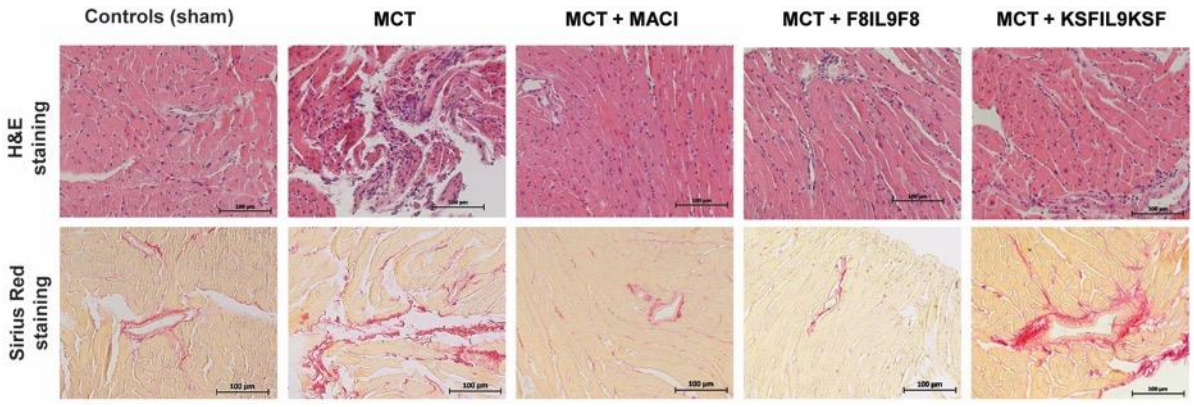

Figure 4.5: Histopathological changes in right ventricular cardiac tissue in comparison to the different experimental groups. Right ventricular cardiac tissue samples were subjected to histological analysis to compare IL9-based fusion protein treatment to sham and MACI in MCT-induced PH mice. Representative microscopic images of H&E, as well as Sirius red stains, illustrate the clear differences in the extent of tissue damage in comparison to the 5 experimental groups.

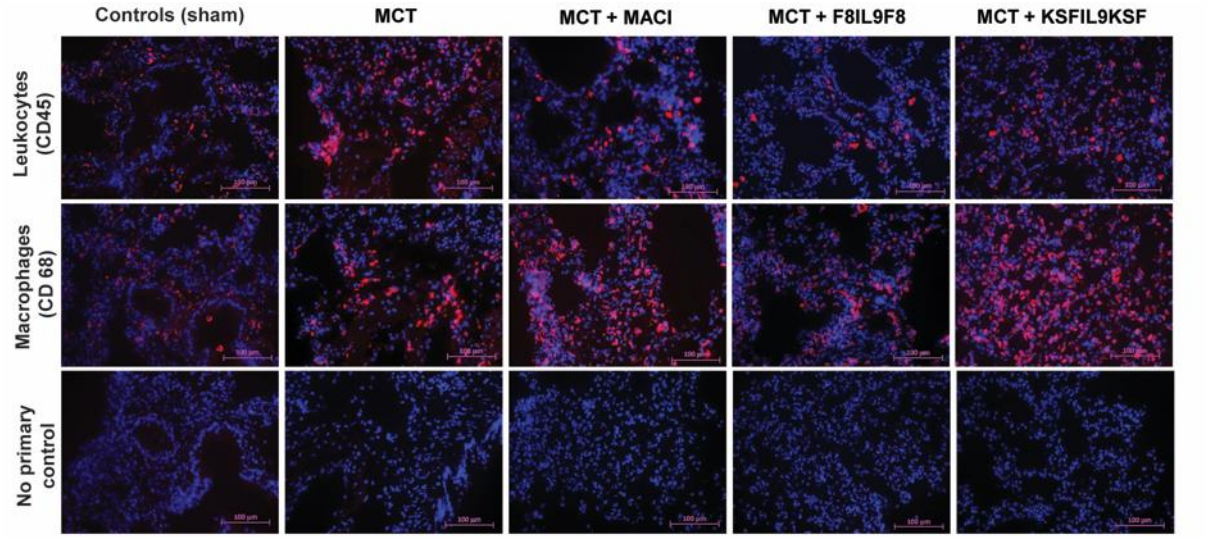

Figure 4.6: Assessment of leukocyte and macrophage accumulation in lung tissue: evaluation of different treatment effects on MCT-induced PH in mice. Lung tissue samples were subjected to immunofluorescence staining of CD45 (red fluorescence, DAPI staining in blue) as common leukocyte marker and CD68 (red fluorescence, DAPI staining in blue) as macrophage marker to quantitatively assess the extent of tissue accumulation to compare IL9-based fusion protein treatment to sham and MACI in MCT-induced PH in mice. The images in the lower row show the corresponding negative controls, in which the primary antibody was omitted.

Effect of IL9 on the accumulation of leukocytes and macrophages in lung and right ventricular cardiac tissue in MCT-induced PH

To further elucidate F8IL9F8 treatment effects on tissue inflammation, detection of CD45 as pan-leukocyte antigen and CD68 as a marker for macrophages was performed by immunofluorescence labeling. Representative samples of microscopic immunofluorescence detection results are given in **Figure 4.6** for lung and in **Figure 4.7** for right ventricular cardiac tissue. As compared to the sham-treated controls, there were significant increases of both leukocyte and macrophage accumulations in the lung and in the RV in all MCT-induced PH groups (i.e., untreated, F8IL9F8, KSFIL9KSF and MACI groups) ($p<0.05$ for all, CD68 in the RV and lung and CD45 in the RV and lung). Compared to the MCT-induced PH untreated group, only the F8IL9F8 group displayed a significant decrease of macrophages and leukocytes accumulation both in lung and RV ($p<0.05$ for all), whereas the MACI treatment group showed a significant decrease only in macrophage accumulation in the RV ($p=0.044$ for all), while no difference could be seen for the KSFIL9KSF treatment group (p=n.s. for all).

Additionally, the KSFIL9KSF treatment group had a significant increase of leukocytes and macrophages accumulation in the RV, compared to the MACI treatment group ($p<0.05$). This increase was even more significant when the KSFIL9KSF was compared to the F8IL9F8 treatment group ($p<0.05$). However, no relevant differences could be noted for leukocyte and macrophages accumulation between the MACI and the F8IL9F8 treatment groups (p=n.s. for all). **Figure 4.8** summarizes the results of the semi-quantitative assessment of leukocyte and macrophage accumulation in the lung (**Figure 4.8A**) and right ventricular cardiac (**Figure 4.8B**) tissue.

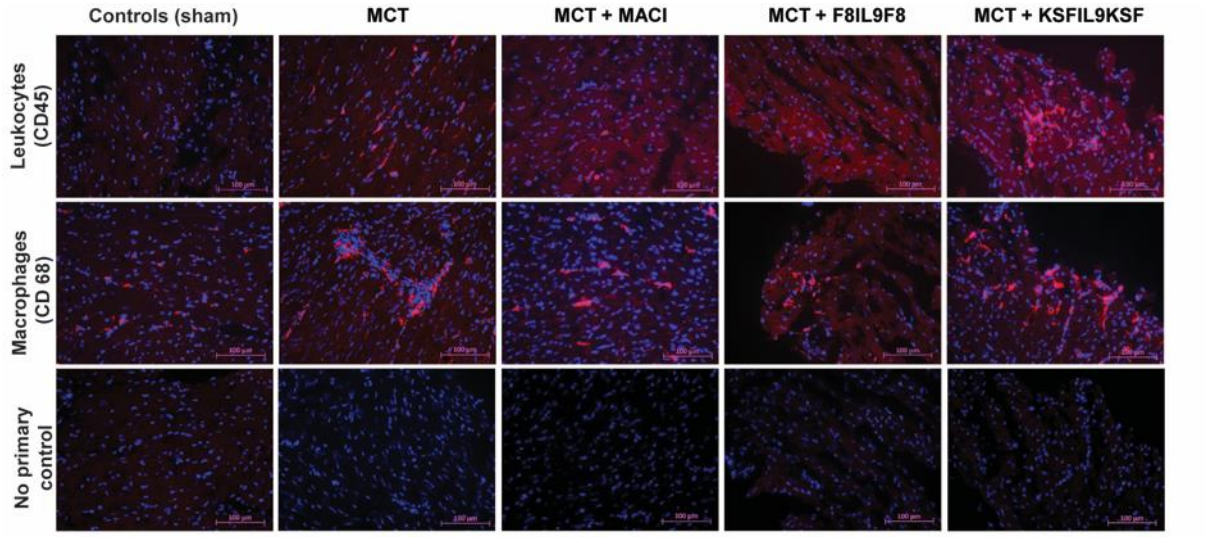

Figure 4.7: Assessment of leukocyte and macrophage accumulation in right ventricular cardiac tissue: evaluation of different treatment effects on MCT-induced PH in mice. Right ventricular cardiac tissue samples were subjected to immunofluorescence staining of CD45 (red fluorescence, DAPI staining in blue) as common leukocyte marker and CD68 (red fluorescence, DAPI staining in blue) as macrophage marker to quantitatively assess the extent of tissue accumulation to compare IL9-based fusion protein treatment to sham and MACI in MCT-induced PH in mice. The images in the lower row show the corresponding negative controls, in which the primary antibody was omitted.

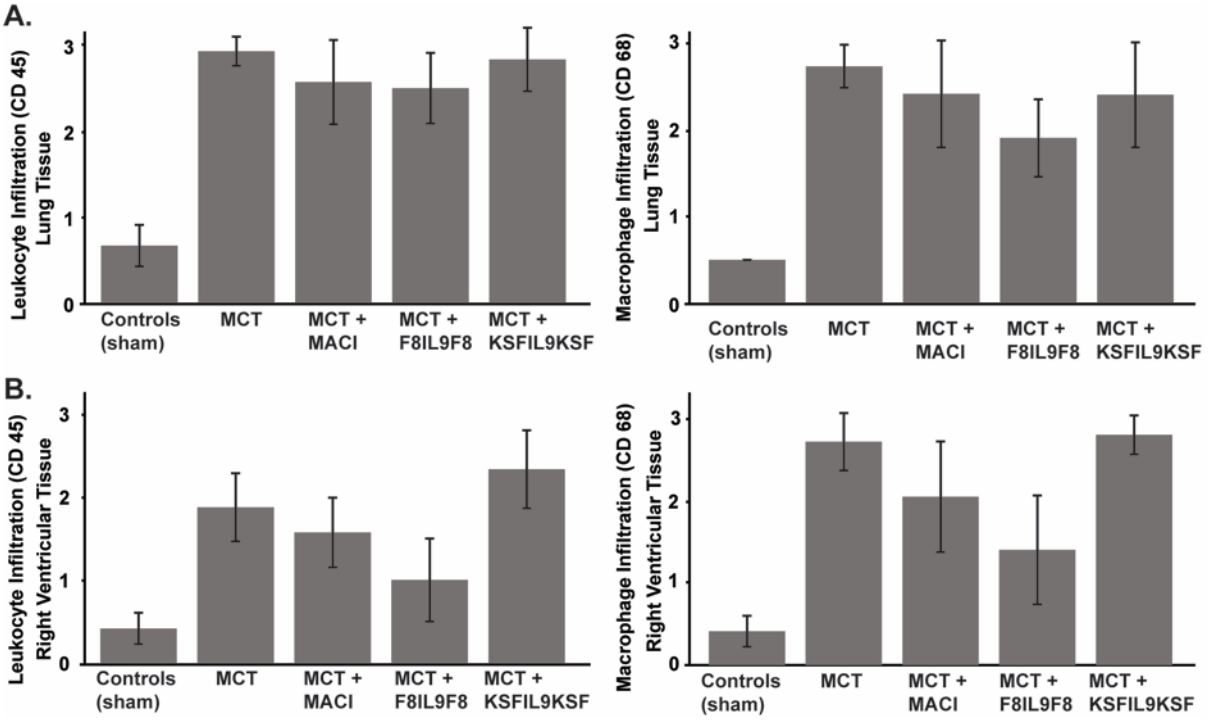

Figure 4.8: Results of semi-quantitative assessment of leukocyte and macrophage accumulation in lung and right ventricular cardiac damage to evaluate the different treatment effects on MCT-induced PH in mice. Graphs show results of the semi-quantitative assessment of leukocyte (CD45) and macrophage (CD68) accumulation in the lung (A) and right ventricular cardiac (B) tissue in comparison of the 5 experimental groups. Results are given as mean ± standard. The assessment score ranged between 0 and 3 as described in the material and methods section.

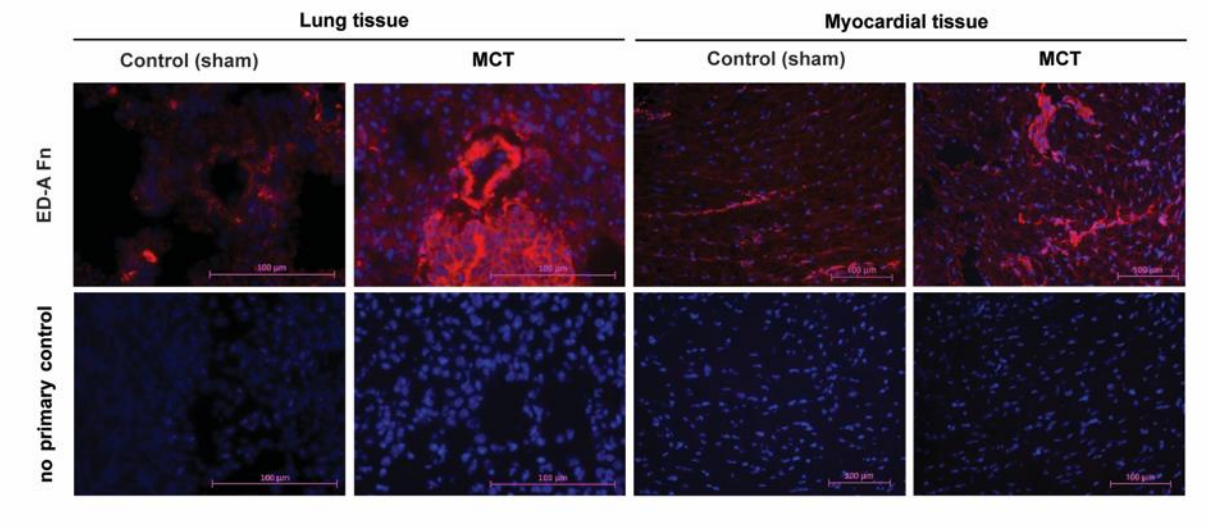

Figure 4.9: Expression of EDA(+) fibronectin as a specific target of the F8 antibody in MCT-induced PH compared to sham-treated mice. Lung and right ventricular cardiac tissue samples were subjected to immunofluorescence staining of EDA(+) fibronectin (red fluorescence, DAPI staining in blue) using the biotinylated antibody SIP-F8 in comparison of sham-treated and MCT-induced PH mice showing a strong up-regulation both with spatial accumulation to lung vessel structures and cardiac interstitial fibrosis. The images in the lower row show the corresponding negative controls, in which the primary antibody was omitted.

EDA(+)-fibronectin expression in lung and right ventricular cardiac tissue in MCT-induced PH compared to sham-treated controls in the mouse model

The concept of F8 based targeted delivery of IL9 to pulmonary vascular as well as right ventricular cardiac tissue remodeling occurring in PH presumes the strong expression of EDA(+) fibronectin, which is the epitope specifically recognized by F8. As proven recently by our group in the rat model of MCT-induced PH [403], we could also demonstrate its strong re-occurrence in PH associated tissue damage in the corresponding mouse model used in this study. As compared to sham-treated controls, in MCT-induced PH, EDA(+) fibronectin is strongly expressed, and its tissue distribution shows, in particular, clear spatial associations to vessel structures in the lung and to cardiac interstitial fibrosis in the RV (**Figure 4.9**).

4.5 Discussion

Available treatments for pulmonary hypertension generally act by decreasing vascular tone and thereby reducing pulmonary artery pressure, but there are no treatments able to stop or reverse PH progression or resolve the damages caused to lung and heart. Therefore, it is of scientific and clinical interest to investigate new therapeutic prototypes for this disease.

In our study, we used an MCT-induced PH model in mouse to evaluate the therapeutic efficacy of the novel immunocytokine F8IL9F8. The MCT model is a well-established and widely accepted animal model of PH, and the majority of drugs currently approved for the treatment of group 1 PH were initially tested in this model [390, 439]. Indeed, the MCT model recapitulates several features of human PAH are including vascular remodeling, the proliferation of smooth muscle cells, functional impairment of the vascular endothelium, upregulation of inflammatory cytokines, and failure of the right ventricle [440].

Pulmonary hypertension is characterized by increased extracellular matrix turnover and pulmonary vascular remodeling [403, 441]. Recently, we have identified EDA(+) fibronectin as a marker of vascular remodeling in the MCT model of PH in rats [403]. Similarly, in our study, we observed a strong EDA overexpression in lung and RV tissues of MCT-induced mice. The specific deposition of EDA(+) fibronectin at PH

lesions offers a perfect target for the antibody-based delivery of therapeutic payloads at the site of disease.

Our group has developed the F8 antibody, specific to the alternatively spliced EDA domain of fibronectin [54]. Over the past decades, we have produced a number of F8-based immunocytokines with different cytokine payloads (e.g., with IL2, IL4, IL6, IL10, IL12, TNF, interferon-alpha), many of which efficiently accumulate at the site of the disease, improving the therapeutic index of the corresponding cytokine payload [107, 111, 115, 117, 118, 349, 422]. In this study, we have used a recently described immunocytokine consisting of IL9 flanked by two moieties of the F8 antibody in single-chain Fv format. As negative control, a non-targeted variant was generated using the irrelevant antibody.

There is increasing evidence demonstrating the role of cytokine and immune cells in the development and pathogenesis of PH, in particular, inflammation has been suggested as a predominant component of pulmonary vascular remodeling in various PH forms [396, 441, 442]. Multiple reports suggest a role of IL9 in lung inflammation and allergy [219, 227, 240, 405]. For example, antibody-mediated neutralization of IL9 has been described to decrease lung inflammation and tissue damages caused by oxidative stress in a murine model of COPD [249] and to suppress lung injury and pulmonary fibrosis in mice that were intranasally exposed to silica [241]. Controversially, a reduction in alveolar fibrosis in IL9 overexpressing mice that were intratracheally treated with silica particles, has also been reported [250].

Therefore, we decided to test the therapeutic efficacy of the targeted delivery of IL9 in the MCT-induced PH mouse model. Disease severity was assessed by a variety of haemodynamic and echocardiographic parameters as well as by the histological analysis of lung and right ventricular cardiac tissues.

Taking into account the functionality and the morphology of lung and heart, F8IL9F8 treatment demonstrated several physiological effects in PH mice compared to untreated controls or mice treated with the untargeted KSFIL9KSF. First, a significant reduction in RVPsys could be achieved associated with a significant improvement in right ventricle morphology and functions. Furthermore, the histological analysis confirmed an attenuation in lung and cardiac tissue damages. In general, disease

improvement mediated by F8IL9F8 was superior to the one observed in mice treated with Macitentan (MACI), the current standard of care for pulmonary arterial hypertension.

In an attempt to understand the implication of immune response on the observed decrease in lung and heart tissue damage and RVPsys improvement by IL9 based therapy, immunofluorescence staining for CD68+ macrophages and CD45+ leukocytes was performed on lung and RV sections. While both CD68+ macrophages and CD45+ leukocytes were increased in all MCT-induced PH groups, they were both reduced in the groups treated with F8IL9F8 or MACI compared to the untreated or KSFIL9KSF treated groups. Moreover, compared to MACI, targeted IL9 delivery induced a stronger reduction in CD45+ leukocyte and CD68+ macrophages infiltration in the heart and in CD68+ macrophages in the lung.

In line with the observed results, CD68+ macrophages have been reported to be abundantly present in the lungs of preclinical PH models and in PAH patients [393, 394, 396, 443, 444]. Moreover, it has been shown that inactivation or depletion of macrophages ameliorates PH conditions in different animal models [444, 445]. Similarly, leukocytes are highly infiltrating the lungs of MCT-induced animals [446], and CD3+ and CD8+ cells are predominant in the lungs of PAH patients where they correlate with disease progression [447]. On the contrary Treg activity may contribute to ameliorating PH disease. Athymic rats, which lack Tregs, are more susceptible to severe PAH than wild rats [448], while Treg immune reconstitution has been reported to be beneficial in a rat model in which PH was induced by the VEGFR2 antagonist SU5416 [399, 449]. It has also been shown that an increased frequency of dysfunctional Treg cells is present in patients with PAH, which suggests that an altered immunosuppressive response may contribute to pulmonary vascular remodeling in PAH [450].

The observed reduction in infiltrating macrophages and leukocytes would suggest an anti-inflammatory role of IL9 in PH. However, a more detailed analysis of their subtypes, especially for M2 macrophages and Tregs, may provide further information on the mechanism by which F8IL9F8 diminishes PH severity. Indeed, IL-9 has been suggested to modulate the activity of macrophages by shifting their phenotype towards a more anti-inflammatory profile and by inducing their production of the anti-

inflammatory TGFB [257, 451]. Furthermore, IL-9 has been proposed to induce the resolution of inflammation in arthritis by promoting ILC2-dependent Treg activation [269]. Since ILC2s are the dominant population of innate lymphoid cells in the lung [452], it would be interesting to investigate whether a similar mechanism may have contributed to the reduce PH severity following F8IL9F8 treatment.

While additional studies are needed to clarify the mechanism by which IL9 promotes amelioration of PH and to investigate the potential of F8IL9F8 to modify the pathological course of PH disease, the results presented in this study provide the first evidence that targeted delivery of IL9, mediated by the F8 antibody, to pulmonary hypertension lesions may represent a potential new treatment for PH.

5 Generation of a small molecule-IL2 conjugate for tumor targeting

Contribution of the authors: In this project I have performed all the experimental work with the exception of the chemical synthesis of the AAZ-LPETG substrate that has been carried out by Jacopo Millul and Samuele Cazzamalli.

Sortase-mediated site-specific modification of interleukin-2 for the generation of a tumor targeting acetazolamide-cytokine conjugate

Baptiste Gouyou[1], Jacopo Millul[1], Alessandra Villa[1], Samuele Cazzamalli[1], Dario Neri[2], Mattia Matasci[1]

Author affiliations:

1) Philochem AG, Libernstrasse 3, 8112 Otelfingen, Switzerland

2) Department of Chemistry and Applied Biosciences, Swiss Federal Institute of Technology, Zurich, Switzerland.

Keywords:

Tumor targeting, Carbonic anhydrase 9, Sortase A, Interleukin-2, Small molecule cytokine conjugate, site specific conjugation

5.1 Abstract

Small ligands specific to tumor-associated antigens can be used as alternatives to antibodies for the delivery of small payloads such as radionuclides, cytotoxic drugs and fluorophores. Their use as delivery moiety of bioactive proteins like cytokines remains largely unexplored. Here, we describe the preparation and *in vivo* characterization of the first small molecule-cytokine conjugate targeting carbonic anhydrase IX (CAIX), a marker of renal cell carcinoma and hypoxia. Site-specific conjugation between interleukin-2 and acetazolamide was obtained by Sortase A-mediated transpeptidation. Binding of the conjugate to the cognate CAIX antigen was confirmed by surface plasmon resonance. The *in vivo* targeting of structures expressing carbonic anhydrase IX was assessed by biodistribution experiments in tumor bearing mice. Optimization of manufacturability and tumor targeting performance of acetazolamide-cytokine products will be required in order to enable industrial applications.

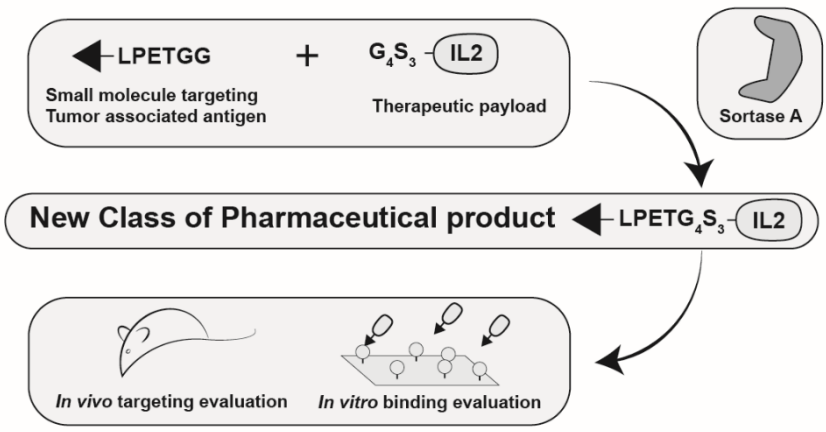

5.2 Introduction

The active delivery of anticancer cytokines to tumor tissue has been extensively explored with the aim to enhance their therapeutic window and circumvent adverse events associated with their systemic administration. To this respect tumor specific antibodies have been used as selective vehicles for the targeted delivery of pro-inflammatory cytokines including interleukin-2 (IL2), intereleukin-12 (IL12) and tumor necrosis factor (TNF) [95, 100, 138, 141, 285, 453]. In several cases antibody-cytokine fusion proteins (i.e., Immunocytokines), have demonstrated selective tumor uptake and anti-tumor activity in murine models of cancer and several products have been advanced into clinical trial [100, 138, 141, 143, 293]. However, the use of antibodies

for pharmacodelivery of bioactive payloads to solid tumors, may be limited by their relatively large size, which can lead to slow extravasation and poor tumor tissue penetration combined with extended systemic half-life[9]. These limitations can be partly counteracted by using small antibody fragments (like scFv or diabodies)[454].

Small organic ligands specific for a list of tumor-associated antigens (e.g., Folate Receptor, Prostate-Specific Membrane Antigen, Somatostatin Receptors and Carbonic Anhydrase IX (CAIX)) [163, 164, 455–457] have been considered as an alternative to antibodies for the targeted delivery of drugs and of therapeutic radionuclides [371, 458–460]. Small molecules can diffuse very rapidly and homogeneously into solid tumors, potentially reaching high tumor-to-organ ratios by combining extended residence time at the tumor site with rapid body clearance [163, 164].

CAIX is a cell-surface non-internalizing marker of tumor hypoxia that is highly expressed in about 90% of clear cell renal cell carcinomas (RCCs) and in other aggressive cancers [370, 371, 373, 459]. In contrast, CAIX is virtually absent in most normal adult tissues, exception made for some structures of the gastro-intestinal tract [370, 372, 373, 459, 460].

Our group has demonstrated that acetazolamide (AAZ), a small molecule binder of CAIX, can be effectively used to deliver radionuclides and cytotoxic drugs to tumors for diagnostic and therapeutic applications in tumor bearing mice[168, 374, 461, 462]. We have recently reported good SPECT-CT imaging results in patients with renal cell carcinoma using a derivative of acetazolamide labeled with the radioactive payload 99mTc [171].

The IL2 cytokine is a potent inducer of cytotoxic T cells and NK cells, and was one of the first immunotherapeutic agents approved by FDA for the treatment of metastatic melanoma and renal cell carcinoma (RCC) [272]. However, its use in RCC at high dose produces durable complete response in a small portion of patients but with severe systemic toxicity[273, 274]. The antibody-based delivery to tumors has shown the potential to improve the therapeutic index of IL2 in immunocompetent mouse models of cancer[100, 138, 141, 285].

Traditional strategies for covalent bioconjugation allow limited control over the site and frequency of the modification, resulting in heterogeneous products with potential loss of biological activity of the modified protein[463]. Sortase A (SrtA) is a sequence-specific transpeptidase that catalyze the ligation between LPXTG-containing polypeptides (Sortag) and oligoglycine terminated moieties[464]. Due to its high specificity for the Sortag and broad substrate tolerance, SrtA-mediated transpeptidation has emerged as a powerful method for the site-specific modification of proteins. Recently SrtA has been used for the site specific conjugation of antibodies to generate products such as imaging probes [464–466], bispecific antibodies[467] and antibody drug conjugates[468].

Here we describe the development and the in vitro and in vivo characterization of the first small-molecule cytokine conjugate (SMCC) targeting CAIX, termed AAZ–IL2, that was generated by SrtA mediated site specific transpeptidation.

5.3 Results and discussion

The aim of this work was to develop a small molecule-cytokine conjugate (SMCC) targeting CAIX and perform a proof-of-concept study to test its tumor targeting performance *in vivo*. IL2, the model bioactive payload of choice, was coupled to AAZ, a known nanomolar binder of CAIX. The product was generated by SrtA mediated conjugation[464–468], which allowed to obtain a site-specific functionalization of the IL2 cytokine with the AAZ targeting ligand (**Figure 5.2A**). A detailed mechanism of the transpeptidation reaction catalyzed by Sortase A is presented in the supplementary **Figure 5.S6**.

AAZ-LPETGG (**Figure 5.1**, compound B) was isolated after a convergent late stage parallel synthesis, mixing on solid phase and in solution chemistry (**Figure 5.S1**), allowing the attachment of the AAZ targeting ligand to the N-terminus of 6-mer LPETGG “Sortag” peptide via a triazole linker. Prior to the enzymatic coupling, the identity and purity of the produced AAZ-LPETGG material was analyzed by LC-MS, confirming the presence of a single peak (MW 986 Da) (**Figure 5.S2**). The histidine-tagged (G4S)3-IL2 cytokine and SrtA enzyme were recombinantly expressed in mammalian cells and bacteria, respectively, and purified via metal affinity chromatography (**Figure 5.S4** and **5.S3**). The mutations T23S and C125S were

introduced in the (G4S)3-IL2 protein in order to avoid glycosylation and the formation of covalent multimers as confirmed by SDS-PAGE and size exclusion chromatography (**Figure 5.S4**).

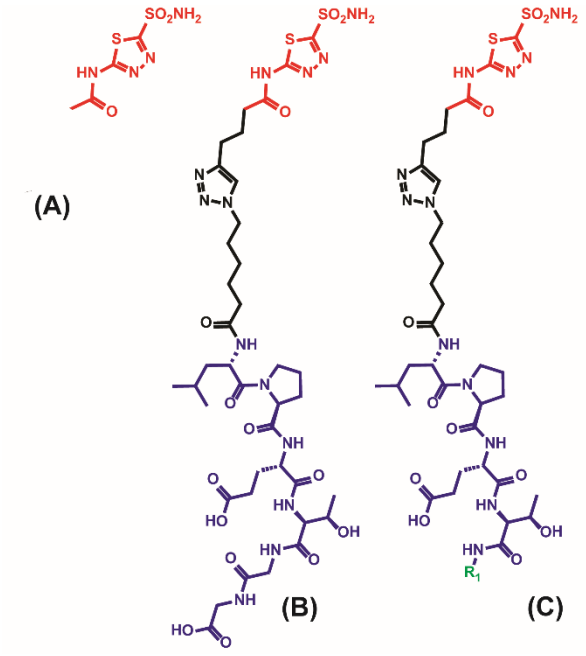

Figure 5.1: Structures of acetazolamide derivatives. The CAIX inhibitor AAZ (A), the sortagged conjugate AAZ-LPETGG (B), and the conjugation product AAZ-IL2 (C) obtained after Sortase A mediated transpeptidation are depicted. Red = acetazolamide (AAZ) black = triazole linker, blue in (B) = LPETGG "Sortag" R1 = (G4S)3-IL2.

Complete conjugation of (G4S)3-IL2 to AAZ-LPETGG, could be obtained upon incubation, for 3h at 4°C with SrtA, using a 20-fold molar excess of the AAZ-LPETGG substrate. **Figure 5.2B** shows the LC-MS analysis of the crude reaction mixture, confirming the virtually complete conversion of the (G4S)3-IL2 substrate (MW 17154 Da) into the final AAZ-IL2 product (MW 18008 Da). Interestingly under these experimental conditions the majority of the SrtA enzyme was still bound to AAZ-LPETGG as covalent thioacyl intermediate (MW 18705 Da) suggesting the possibility for a further optimization of the transpeptidation reaction. The crude reaction product was then subjected to anti-IL2 affinity chromatography to separate the AAZ-IL2 product from unreacted thioacyl intermediate and SrtA. Homogeneity of the purified AAZ-IL2 product was confirmed by LC-MS analysis (**Figure 5.2C**) and gel filtration chromatography (**Figure 5.S5**). Furthermore, the capability of AAZ-IL2 to bind CAIX was tested in vitro by SPR analysis showing a relatively fast kon and koff (**Figure 5.2D**), whereas the non-targeted control (G4S)3-IL2 displayed no binding capacity on the CAIX coated chip (data not shown).

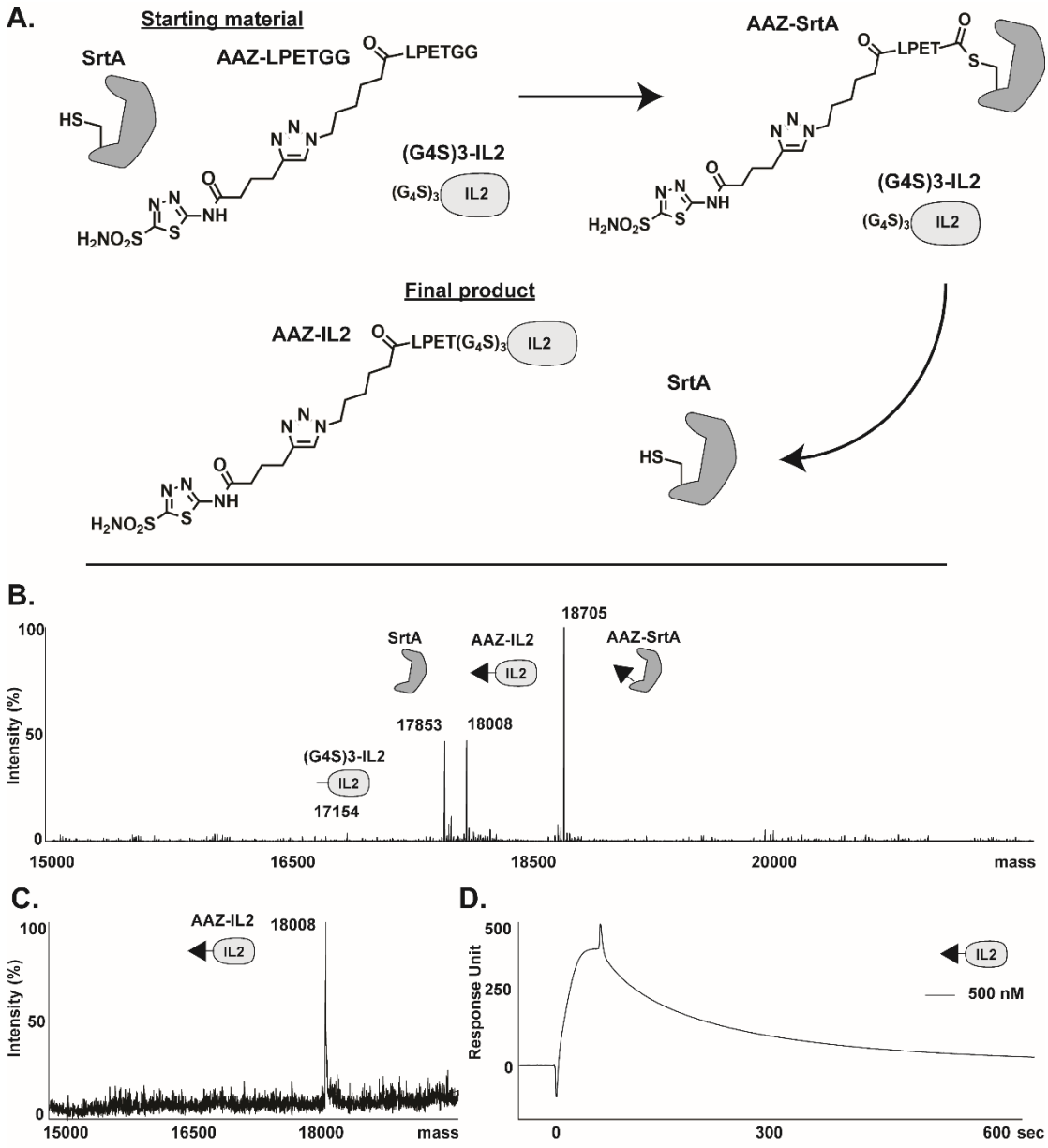

Figure 5.2: Sortase A mediated AAZ-IL2 conjugation and product characterization. (A) Schematic representation of the Sortase A mediated transpeptidation reaction between AAZ-LPETGG and (G4S)3-IL2. (B) ESI-MS profile of the crude reaction mixture after 3h of enzymatic reaction. (C) ESI-MS result of AAZ-IL2 after affinity chromatography purification. (D) SPR sensogram of AAZ-IL2 injected at a concentration of 500nM on CAIX-coated sensor chip.

SrtA mediated transpeptidation resulted in the production of highly homogeneous site specifically conjugated AAZ-IL2 which retained CAIX in vitro binding. However, main limitations in this technology may hamper its application for commercial scale manufacturing, including the need for GMP grade SrtA and reaction substrates, the relatively high amount of SrtA required to achieve complete conversion, and the final purification step necessary to separate the conjugated product from the SrtA enzyme. The use of engineered SrtA variants [469] with increased catalytic activity, combined

with the immobilization of the SrtA to solid supports may contribute to overcome some of these limitations[466].

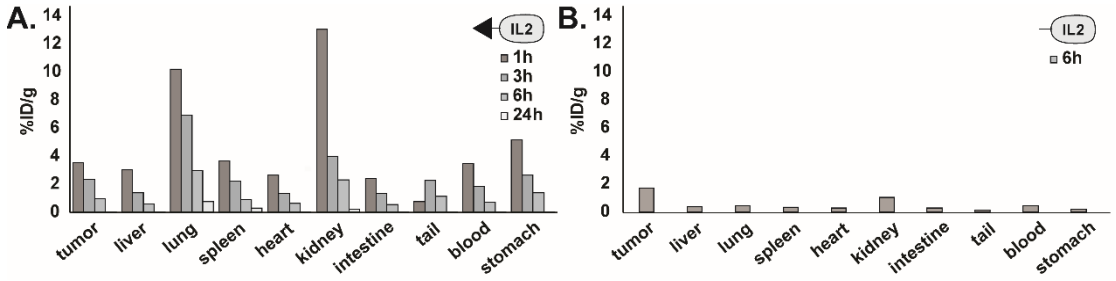

Figure 5.3: Tumor targeting assessment by quantitative biodistribution analysis of radiolabeled AAZ-IL2 (A) and (G4S)3-IL2 (B) in SK-RC-52 bearing nude mice. Organs were collected, weighed, and the radioactivity measured at different timepoints after intravenous injection of the radiolabeled compounds. Results are expressed as percentage of injected dose per gram of tissue (%ID/g n=1 per group).

Pure preparation of AAZ-IL2 was used to study its quantitative biodistribution in nude mice bearing subcutaneously-grafted human SK-RC-52 renal cell carcinomas. The conjugate was radiolabeled with I-125 following previously described methodologies[110] and injected intravenously at a fixed dose of 0.5 mg/Kg. Mice were sacrificed at different time points and radioactivity in tumors and in different healthy organs was counted. Surprisingly AAZ-IL2 failed to preferentially accumulate at the tumor site at any tested time-point (**Figure 5.3A** and **Figure 5.4**). Furthermore, at the earliest timepoints (up to 6h) a nonnegligible accumulation in the kidney, lung, spleen and stomach was observed, whereas at 24h post-injection all organs were virtually free from AAZ-IL2 (with the exception of some weak uptake into lung and spleen). Uptake into kidney, lung, spleen and stomach seems to be an intrinsic property of the AAZ-IL2 product since a similar behavior was not observed for the untargeted control (**Figure 5.3B**). The observed accumulation of AAZ-IL2 in healthy tissues may in part be due to the physiological expression of CAIX in the gastrointestinal tract [372, 459]. Moreover, being AAZ a promiscuous inhibitor of most CA isoforms [370], we may hypothesis that binding to other carbonic anhydrase isoforms that are expressed on the surface of cells in kidney, lung, spleen and stomach [372, 459], may also account for some uptake of AAZ-IL2 in these tissues. A comparable accumulation in the same normal organs was reported for the biodistribution of 99mTc labeled AAZ derivatives [461]. In these studies, showing efficient AAZ tumor uptake at molecular doses comparable to the ones used in our experiments, targeting selectivity could be improved by increasing the injected dose of the CAIX ligands or by preinjecting

unlabeled ligand preparations. It remains to be tested whether a similar approach might be useful to improve the tumor targeting ability of AAZ-IL2.

A substantial lack of preferential tumor uptake was confirmed in ex-vivo immunofluorescence studies. In this case, tumor bearing mice were sacrificed 2h after the injection of 150 µg of FITC labeled AAZ-IL2 or (G4S)3-IL2 and tissue sections were analyzed for the presence of the injected compounds by immunofluorescence. Only a weak presence of AAZ-IL2 could be detected into tumor sections, whereas a relatively stronger staining was again observed in lung, spleen and kidney (**Figure 5.4**). In agreement with the biodistribution results no significant staining was observed for the (G4S)3-IL2 negative control in any of the tissues analyzed.

Our biodistribution studies suggest that AAZ-IL2 reaches the tumor mass already at 1h post injection (earlier time point tested), however no significant specific accumulation could be observed over time. In order to bind the CAIX antigen present on the surface of SK-RC-52 cancer cells, AAZ-IL2 needs to efficiently diffuse within the tumor mass. It may be hypothesized that limitations in extravasation and tumor penetration due to the relatively large size (18 kDa) of AAZ-IL2, may impair its targeting properties. Poor tumor tissue penetration and heterogeneous distribution was indeed observed for AAZ-IL2 by ex vivo immunofluorescence studies at 2h post injection.

In vitro AAZ-IL2 showed binding to CAIX, with a quite low affinity characterized by a fast koff. Enhancing tumor uptake and improving tumor to healthy organs selectivity, may be achieved by increasing the affinity to CAIX antigen expressed on the surface of cancer cells.

In the same SK-RC-52 xenograft model used in our studies, Krall et al reported that a bivalent-AAZ-dye conjugate with improved CAIX binding affinity, had longer residence on the tumor than the corresponding monovalent version[374]. Similarly, an affinity matured version of acetazolamide recovered from DNA encoded library[169], showed substantially improved tumor targeting performances when compared to acetazolamide[164, 169]. Whether the use of a higher affinity CAIX ligand variant would improve also the targeted delivery of IL2 remains to be elucidated.

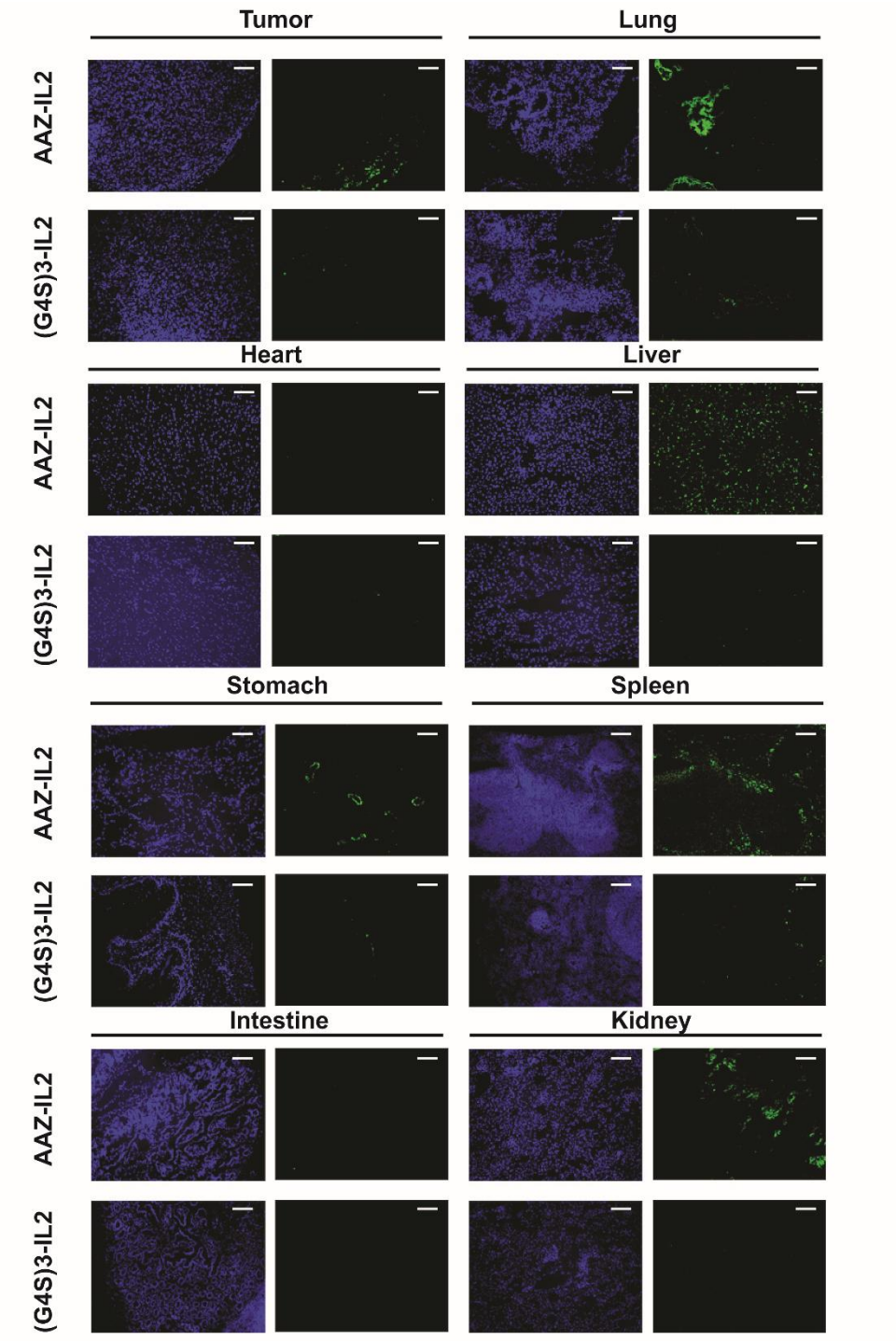

Figure 5.4: Tumor targeting assessment by ex vivo immunofluorescence analysis of AAZ-IL2 and (G4S)3-IL2 in SK-RC-52 bearing mice. Mice were sacrificed 2 hours after intravenous injection of FITC-labeled AAZ-IL2 or (G4S)3-IL2 (untargeted negative control). Tissue sections were stained and analyzed by fluorescence microscopy at a 10x magnification. Green= FITC-labeled compounds, blue = DAPI staining, scale bar = 50 µm.

5.4 Conclusions

To the best of our knowledge, this is the first report of the site-specific conjugation of a small-molecule ligand to a cytokine for tumor targeting purposes. Using SrtA based transpeptidation, we efficiently conjugate the acetazolamide targeting moiety to IL2. This novel small molecule-cytokine conjugate retained binding capacity to CAIX in vitro, but lacked tumor targeting specificity *in vivo*, when tested in the SK-RC-52 xenograft model of renal cell carcinoma. Whereas further optimization of the conjugate product is required to obtain efficient tumor targeting, including the use of AAZ ligand variant with higher affinity for the CAIX antigen, we anticipate that development of efficient SMCC products can make a valuable contribution in the field of cancer immunotherapy.

5.5 Experimental section

5.5.1 AAZ-LPETGG synthesis

AAZ-LPETGG was prepared by convergent late stage parallel synthesis, mixing on solid phase and in solution chemistry (**Figure 5.S1**). The 6-mer peptide LPETGG was grown on solid-phase (SPPS) by using standard Fmoc-strategy procedures.

AAZ was derivatized with an alkyne linker using a previously described procedure[168]. The obtained N-(5-sulfamoyl-1,3,4-thiadiazol-2-yl)hex-5-ynamide (compound 1 in **Figure 5.S1**) was attached to the growing peptide by a CuI-catalyzed azide–alkyne cycloaddition (CuI, TBTA, DMF/THF 1:1, overnight, r.t.). The AAZ-LPETGG compound was cleaved from the resin with a cleavage cocktail composed by TFA (33 %), Triisopropylsilane (14%), mQ water (3%) and dichloromethane (50%). AAZ-LPETGG was purified from the crude via reverse-phase HPLC purification. Fractions containing the purified product were identified by mass spectrometry and lyophilized to obtain the final AAZ-LPETGG product as a white powder (35 mg 35.5 µmol 7.2% yield) LC-MS (ES+) m/z 986.30(M+H)+.

5.5.2 Cloning of (G4S)3-IL2 and Sortase A

A custom-synthesized DNA fragment (Eurofins Genomics) consisting of human IL2 (AA 21-153) carrying a N-terminal (G4S)3 linker and a C125S mutation was used as

template for the generation of the (G4S)3-IL2 expression gene. A leader sequence and an additional T23S mutation were inserted by two round of PCR using the following primer pairs: PCR1-Fw primer: GATCCTCCTGTTCCTCGTCGC-TGTGGCTACAGGTGTGCACTCGGGTGGAGGCGGTTCAGGCGGAGGTGGCTCT GGCGGTGGCGGATCAGCACCTTCTTCA, PCR1Bw primer: ACAGGCGGCC-GCTTATCAATGGTGATGGTG-GTGATGAGTCAGTGTTGAGA, PCR2-Fw primer: TCCAGAAGCTTCCACCATGGGCTGGAGCCTGATCCTCCTGTTCCTCGTCG, PCR2Bw primer: ACAGGCGGCCGCTTATCAATGGTGATGGTGGTGATGAGTCA-GTGTTGAGA.

The final PCR product was HindIII/NotI double digested and ligated into pcDNA3.1 (Invitorgen). The resulting pcDNA3.1-(G4S)3-IL2 plasmid was amplified in bacteria, purified with Nucleobond PC500 purification kit (Macherey-Nagel) and used for mammalian cell transfection.

The Sortase A gene was amplified from a custom synthesized DNA fragment (Eurofins Genomics). In order to insert a C-terminal hexa-Histidine tag, two rounds of PCR amplification were performed using the following primers PCR1-Fw primer: GCCG-CATATGATGCAGGCAAAACCGCAGATTCCGAA, PCR1-Bw primer: ATTAGCG-GCCGCGTGATGGTGATGGTGATGTTCCAGT, PCR2-Fw primer: ATTAGCATGC-AAATTCTATTTCAAGGAGACAGTCATAATGCAGGCAAAACCGCAG, PCR2-bw primer: GCCGGAATTCTTAGTGATGGTGATGGTGATGTTCCAGTTTAACTTCG.

The PCR product was then SphI/EcoRI double digested and ligated into pUC119 plasmid. The resulting pUC119-SrtA plasmid was electroporated in TG1 bacteria for protein production.

5.5.3 Protein expression

For bacterial production of Sortase A, TG1 cultures transformed with the pUC119-SrtA plasmid were induced by IPTG for 16h at 30°C. Bacteria were pelleted by centrifugation and resuspended in lysis buffer (50mM NaH2PO4, 300mM NaCl, 10mM Imidazole, 1mg/mL lysozyme pH 8), and sonicated for 5 minutes. Supernatant was clarified by centrifugation (13000rpm for 15 minutes) and filtered (0.44µm) prior to purification. (G4S)3-IL2 was expressed by transient gene expression in CHO cells[417]. For 1 ml of production, 4 × 106 cells were collected by centrifugation and

resuspended in ProCHO4 media (Lonza) supplemented with 4 mM Ultraglutamine (Lonza). Per million cells, 0.625 µg of plasmid DNAs followed by 2.5 µg polyethylenimine (PEI 1 mg/mL solution in water at pH 7.0, Polysciences) were added to the cells and gently mixed. The transfected cultures were incubated in a shaking incubator at 31°C, 5% CO2, 120 rpm for 6 days.

5.5.4 Protein purification

The His-tagged Sortase A, and (G4S)3-IL2 proteins were purified by immobilized metal affinity chromatography (IMAC). Briefly, clarified supernatants from bacterial (Sortase A) or mammalian cultures ((G4S)3-IL2) were incubated with cOmplete® His-Tag Purification Resin (Roche) for 2h under shaking conditions. The resin was transferred into liquid chromatography columns (Sigma) and washed with 250 mM NaCl, 10 mM Imidazole, in PBS. Proteins were eluted with 250 mM NaCl, 250 mM Imidazole, in PBS, and finally dialyzed against PBS.

5.5.5 Protein characterization

Purified proteins were characterized for their size, homogeneity and purity by SDS-PAGE, size exclusion chromatography and LC-MS, respectively. SDS-PAGE analysis was performed under reducing and non-reducing conditions, using 10 or 12% acrylamide gels (Invitrogen) and Coomassie blue staining. Size-exclusion chromatography was performed on an ÄKTA FPLC system using a Superdex 75 increase 10/300GL column (GE Healthcare). Proteins were characterized by LC-MS using a Waters Xevo G2XS Qtof instrument (ESI-ToF-MS) coupled to a Waters Acquity UPLC H-Class System. An Acquity BEH300 C4 column from Waters (2.1 × 50 mm, 1.7 µm, flow 0.4 mL/min) was used as stationary phase and a gradient of water with 0.1% formic acid (Solvent A) and acetonitrile with 0.1% formic acid (Solvent B), was used as mobile phase. A linear gradient from 5% to 95% solvent B, 4.5 min run was used. AAZ-IL2 binding affinity was evaluated by Surface plasmon resonance on a BIAcore X100 instrument (GE Healthcare) using CM5 chip (GE Healthcare) coated with in house produced recombinant human CAIX.

5.5.6 Sortase A mediated AAZ-IL2 production

For the enzymatic conjugation of the small molecule cytokine conjugate, 100 µM of AAZ-LPETGG were incubated with 5 µM of Sortase A and 5 µM of (G4S)3-IL2, for 3h at 4°C. Following reaction completion, the final product was purified by affinity chromatography. Briefly, the crude mixture was incubated for 2 hours at room temperature with an anti-IL2 resin. The resin was transferred into liquid chromatography columns (Sigma) and washed with Buffer A (100 mM NaCl, 0.5 mM EDTA, 0.1% tween, PBS) followed by Buffer B (500mM NaCl,0.5mM EDTA, PBS). Elution was performed with 0.1M glycine pH 3 and fractions containing the AAZ-IL2 product were pooled and dialyzed against PBS.

5.5.7 *In vivo* experiments

In vivo experiments on tumor models were performed under a project license granted by the cantonal veterinary office (ZH004/18) in agreement with Swiss regulations. SK-RC-52 were grown in RPMI (Life Technologies) supplemented with 10% FBS at 37 °C and 5% CO2, cells were detached using Trypsin-EDTA 0.05% (Invitrogen). Female athymic Balb/c nu/nu mice (8 weeks old, Janvier) were injected on the right flank with 5×106 SK-RC-52 cells. When tumor reached 100mm3 mice were used for tumor targeting experiments.

5.5.8 Biodistribution studies

In vivo tumor targeting was evaluated by biodistribution analysis, as previously described[418]. Proteins were radioiodinated with 125I and Chloramine T hydrate and purified on a PD10 column (GE Healthcare). ~10 µg of radiolabeled proteins were injected intravenously. Mice were sacrificed at different timepoints (1h, 3h, 6h, 24h). Collected organs were weighed and radioactivity was counted using a Packard Cobra gamma counter (Packard, Meriden, CT, USA). Values are reported as percentage of injected dose of radiolabeled protein per gram of tissue (%ID/g). For each time-point a single mouse was used.

5.5.9 Ex-vivo immunofluorescence analysis.

For fluorescent labeling AAZ-IL2 and (G4S)3-IL2 proteins were dialyzed against 0.1 M Sodium Carbonate pH 9 over night at 4°C. 25 µL of a 1 mg/mL solution of FITC (Acros organics) was added to 1 mg of protein for 16h at 4°C under gentle agitation. FITC labeled protein were purified over size exclusion chromatography (PD10, GE Healthcare). For immunofluorescence targeting, mice were injected intravenously with the fluorescent derivatives of AAZ-IL2 and (G4S)3-IL2. Two hours later, mice were sacrificed, and collected organs were embedded and frozen into OCT. Frozen sections (8 µm) were fixed by 4% of Formalin and blocked with 20% FBS in PBS. Detection of the test article was performed using rabbit anti-FITC IgG (Biorad) followed by anti-rabbit IgG Alexa Fluor 488 (Invitrogen) and counter stained with DAPI.

5.6 Supplementary information

5.6.1 General remarks and procedures

Peptide grade *N,N'*-dimethylformamide (DMF) for solid phase synthesis was bought from ABCR. All other solvents were used as supplied by Merck or Sigma Aldrich in HPLC or analytical grade. Gly-2-Chlorotrityl resin was purchased from RAPP Polymere. All other chemicals and solvents (HPLC-grade or reagent-grade quality), were purchased from commercial sources and used without further purification unless noted otherwise.

5.6.1.1 Liquid chromatography - mass spectrometry

Liquid-Chromatography-Mass-Spectrometry (LC-MS) were recorded on an Agilent 6100 Series Single Quadrupole MS system combined with an Agilent 1200 Series LC, using an InfinityLab Poroshell 120 EC-C18 Column, 2.7 µm, 4.6 Å~ 50 mm at a flow rate of 0.6 ml min^{-1}, 10% MeCN in 0.1% aq. FA to 100% MeCN in 6 min.

Alternatively, Ultra Performance Liquid Chromatography - High Resolution Mass Spectrometry (UPLC-HRMS) were recorded on a Waters Acquity UPLC H-Class System with PDA UV detector coupled to a Waters Xevo G2-XS QTOF, using an ACQUITY UPLC BEH C18 Column (130 Å, 50 mm x 2.1 mm, 1.7 µm particle size) at

a flow rate of 0.6 mL/min with linear gradients of solvents A and B (A = H2O with 0.1% FA, B = CH3CN with 0.1% FA).

5.6.1.2 Reversed-phase high-performance liquid chromatography

Preparative RP-HPLC were performed on a Agilent 1200 Series RP-HPLC with PDA UV detector, using a Synergi 4µm, Polar-RP 80Å 10 Å~ 150 mm C18 column at a flow rate of 5 ml min^{-1} with linear gradients of solvents A and B (A = Millipore water with 0.1% trifluoroacetic acid [TFA], B = MeCN with 0.1% trifluoroacetic acid [TFA]).

5.6.1.3 Size-exclusion chromatography

Size-exclusion chromatography was performed using a Superdex 75 Increase 10/300 GL column on an ÄKTA FPLC (GE Healthcare) Fast Protein Liquid Chromatograph equipped with a UV-900 detector system.

5.6.2 Supporting figures

In order to derivatized the targeting ligand acetazolamide (5-Amino-1,3,4-thiadiazole-2-sulfonamide) with an azide linker, 5-hexynoic acid (1.0 eq.) was dissolved in DCM (50 mL) and DMF (50 µL) and cooled to 0 °C. Oxalyl chloride (1.2 eq.) was added dropwise, reaction was stirred until evanescence ceased and then concentrated under reduced pressure. The obtained yellow liquid was added to a solution of 5-Amino-1,3,4-thiadiazole-2-sulfonamide (1.0 eq.), DMAP (0.1 eq.) and TEA (3.0 eq.) in DMF and the reaction allowed to proceed for 3h at r.t.. The solvent was removed under reduced pressure and compound **1** (N-(5-sulfamoyl-1,3,4-thiadiazol-2-yl)hex-5-ynamide) purified by preparative RP-HPLC. In parallel, the LPETGG peptide was synthesized by standard SPPS Fmoc peptide synthesis protocols on Gly-2-Chlorotrityl resin. For each coupling reaction, 3 eq. of Fmoc-AA, 3 eq. of HBTU, 3 eq. of HOBt, 6 eq. of DIPEA and 5 mL of DMF were used. The coupling reaction was allowed to proceed for 1h at rt. Fmoc deprotection was performed by treating the resin-bound peptide with 20% piperidine in DMF (2 × 3 mL) for 15 min at rt, after which the resin was capped using 6-azido hexanoic acid (3 eq.), HOBt (3 eq.) HBTU (3 eq.) and DIPEA (6 eq.) for 1h at r.t.. The targeting ligand was installed by letting the resin reacting with a solution of CuI (0.1 eq.), TBTA (0.3 eq.), and compound **1** (N-(5-sulfamoyl-1,3,4-thiadiazol-2-yl)hex-5-ynamide) (1.0 eq.), in DMF/THF (1:1) overnight

at r.t.. For compound cleavage the resin was suspended in a cocktail composed by TFA (33 %), TIPS (14%), mQ water (3%) and DCM (50%) for 3 h. Following resin removal by filtration the cleaved compound was purified to >95% purity by preparative RP-HPLC and lyophilized overnight to obtain AAZ-LPETGG as a white powder (35 mg 35.5 µmol 7.2% yield). Quality of the pure material was analyzed by mass spectrometry.

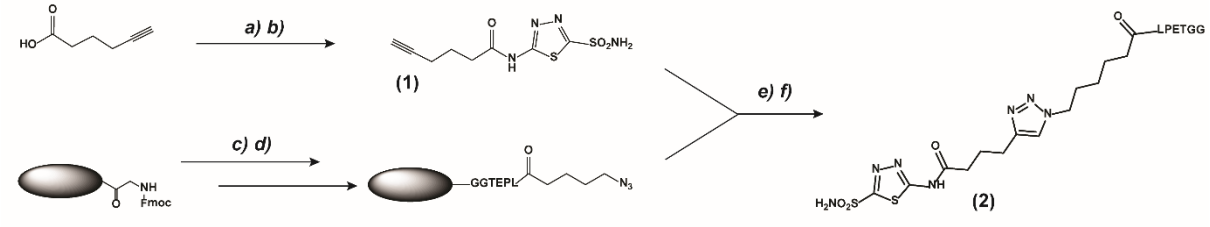

Figure 5.S1: Synthesis route of AAZ-LPETGG. *a)* Oxalyl Chloride, DCM. *b)* 5-amino-1,2,3-thiadiazole-2-sulfonamide, DMAP, TEA, DMF. *c)* Fmoc-Gly-OH, HOBt, HBTU, DIPEA, DMF, 1h, rt Piperdine 20% in DMF, 15 min. (twice) Fmoc-Thr-(tBu)-OH , HOBt, HBTU, DIPEA, DMF, 1h, r.t. Piperdine 20% in DMF, 15 min. (twice) Fmoc-Glu-(OtBu)-OH, HOBt, HBTU, DIPEA, DMF, 1h, r.t. Piperdine 20% in DMF, 15 min. (twice) Fmoc-Pro-OH, HOBt, HBTU, DIPEA, DMF, 1h, r.t. Piperdine 20% in DMF, 15 min. (twice) Fmoc-Leu-OH, HOBt, HBTU, DIPEA, DMF, 1h, r.t. Piperdine 20% in DMF, 15 min. (twice). *d)* 6-azido-hexanoic acid, HOBt, HBTU, DIPEA, DMF, 1h, r.t.. *e)* CuI, TBTA, DMF/THF. *f)* TFA (33%), TIPS (14%), DCM (50%), H_2O (3%).

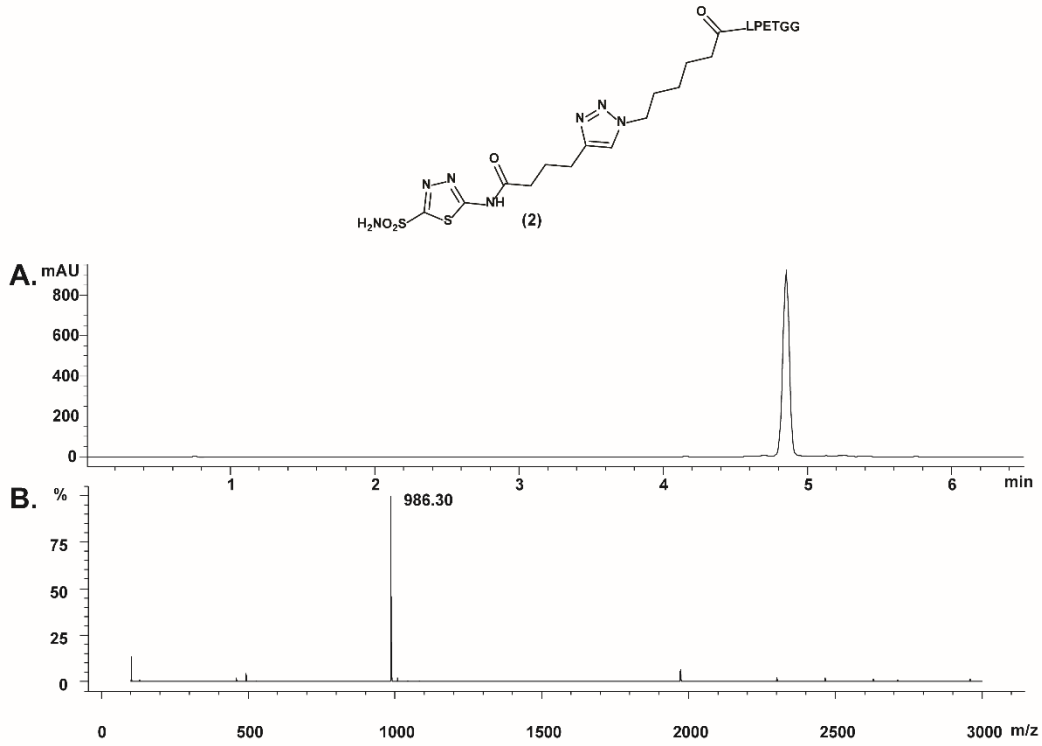

Figure 5.S2: AAZ-LPETGG characterization. (A) HPLC chromatogram (□ = 260 nm). (B) MS spectra of AAZ-LPETGG, MS(ES^+) m/z calculated for $[C38H59N13O14S2]^+$ 986.09 $[M+H]^+$, found 986.30

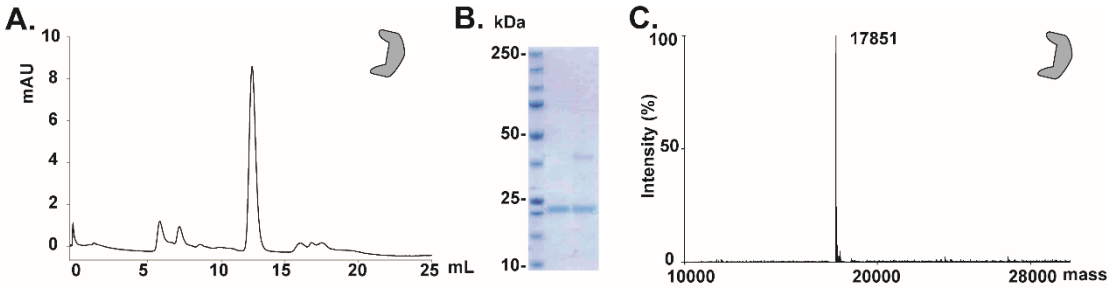

Figure 5.S3: Recombinant Sortase A characterization. Sortase A was recombinantly expressed in bacteria. Following affinity purification by immobilized metal affinity chromatography (IMAC), the protein was characterized by size exclusion chromatography (A) SDS-PAGE (B) and mass spectrometry (C).

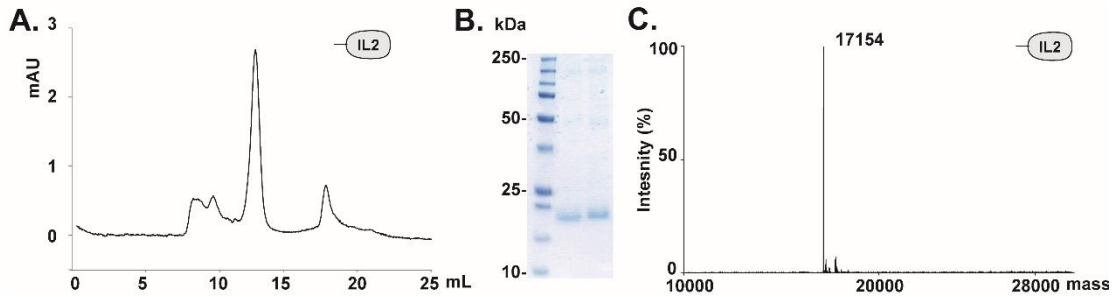

Figure 5.S4: Recombinant (G4S)3-IL2 characterization. (G4S)3-IL2 was recombinantly expressed in CHO cells. Following affinity purification, by IMAC, the (G4S)3-IL2 protein was characterized by size exclusion chromatography (A) SDS-PAGE analysis (B) and mass spectrometry (C).

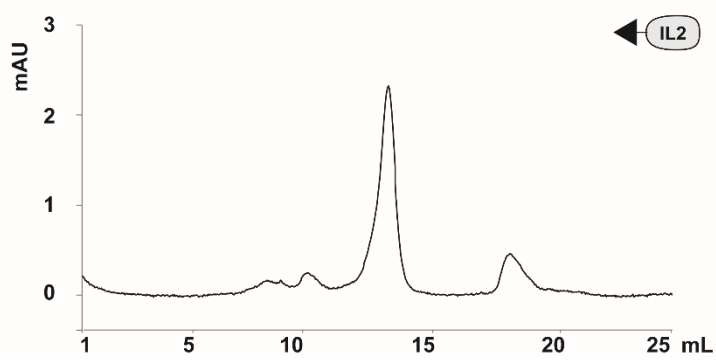

Figure 5.S5: AAZ-IL2 Size exclusion chromatography analysis. The AAZ-IL2 product obtained after Sortase A mediated transpeptidation between the AAZ-LPETGG and (G4S)3-IL2 substrates, was purified by IL2 affinity chromatography and analyzed by size exclusion chromatography.

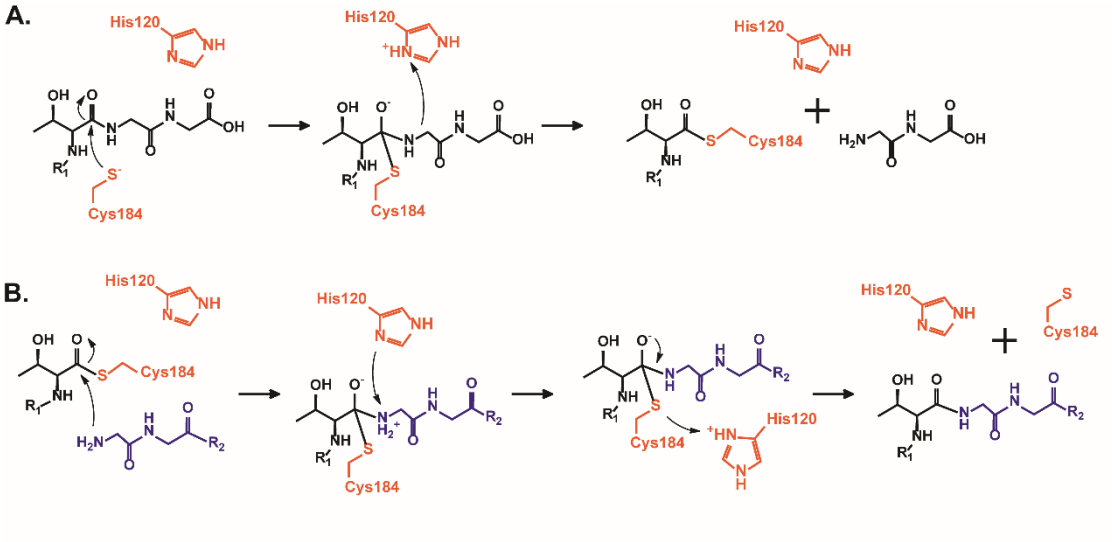

Figure 5.S6: Illustration of the conjugation process between the AAZ-LPETG ligand and the (G4S)3-IL2 engineered cytokine. Site-specific ligation is performed with the aid of the SrtA transpeptidase. (A) The nucleophilic thiol group of the cysteine 184 in the catalytic site of SrtA initiate the traspeptidation by attacking the peptide bound between the threonine and glycine residues of the LPETGG motif in the sortagged-AAZ (AAZ-LPETGG). (B) The resulting thiolester-linked acyl enzyme intermediate is than resolved by a nucleophilic attack mediated the primary amino group of the N-terminal tetraglycine stretch of the (G4S)3-IL2 protein. The positively charged imidazole group of histidine 120 acts as a proton donor/acceptor during the acylation and diacylation steps. The newly formed peptide bond between the threonine and incoming glycine results in the generation of the site-specific ligated product AAZ-IL2, and the release of intact SrtA enzyme. R1= AAZ-LPE R2= GGSGGGGSGGGGS-IL2 StrA= Sortase A.

6 Generation of a small molecule apelin conjugate for half-life extension

Contribution of the authors: In this work I have designed, synthetized and performed the in vitro characterization the three AlbuAPL peptide conjugates. The *in vivo* pharmacokinetic experiment has been performed by the group of Prof. Dr. Philippe Valet from the University of Toulouse. I am grateful to Jacopo Millul and Samuele Cazzamalli for their support during the chemical synthesis of the peptide conjugates.

Generation of Albutag-apelin-13 conjugates with extended serum half-life.

Baptiste Gouyou[1], Le Gonidec Sophie[2], Jacopo Millul[1], Pereira Ophélie[2], Alessandra Villa[1], Samuele Cazzamalli[1], Philippe Valet[2], Dario Neri[3], Mattia Matasci[1]

Author affiliations:

1) Philochem AG, Libernstrasse 3, 8112 Otelfingen, Switzerland

2) Institut des Maladies Métaboliques et Cardiovasculaires, INSERM U1048, Université de Toulouse, UPS, Toulouse, France

3) Department of Chemistry and Applied Biosciences, Swiss Federal Institute of Technology, Zurich, Switzerland.

Keywords:

Apelin, half-life extension, therapeutic peptide, Small molecule albumin binder, Albutag

6.1 Abstract

Apelin is an endogenous peptide hormone with an important role in numerous physiological processes, such as angiogenesis, energy metabolism, and the regulation of fluid homeostasis and the cardiovascular system. Exogenous apelin administration has been shown to be beneficial for the treatment of various diseases including metabolic, and cardiovascular disorders and sarcopenia. Apelin suffers from a very short half-life in blood (i.e., in the range of minutes in human), which in clinical settings translates into the need for frequent administrations to achieve therapeutic efficacy. We describe the generation of three Albutag-apelin-13 derivatives, termed AlbuAPL0C, AlbuAPL1C, and AlbuAPL2C, with extended serum half-life. The structure of the conjugates includes a 4-(p-iodophenyl)butyric acid derivative (termed “Albutag”), a small molecule which binds human and murine serum albumin with similar and high-affinity constants. The novel conjugates were characterized for their improved *in vivo* pharmacokinetic profile in mice.

6.2 Introduction

Albumin is the most abundant protein of the serum, and due to its size and FcRn-mediated recycling, it has an exceptionally long half-life of about 19 days in both humans and mice [22]. Accordingly, strategies to extend the half-life of therapeutic payloads have largely exploited the non-covalent binding to albumin. For example, the AlbudAb® platform, developed by GSK, relies on an antibody fragment (AlbudAb®) that targets albumin and can be fused to diverse therapeutic payloads. This technology has been used in clinical trials to extend the half-life of Extendin-4 (a GLP-1 receptor agonist) from few hours to 6-10 days [470]. The interaction between fatty acids and albumin has been exploited for the generation of long-acting variants of insulin. The commercial insulin analog, insulin detemir, displays a myristic acid at the end of its B-chain and has been described to have an extension of its half-life from few minutes (for human insulin) to about 8 h [196]. Similarly, the Heinis’s research group developed a heptapeptide-palmitoyl tag for half-life extension of therapeutic peptides. Their studies reported a 24-fold extended half-life for a cyclic peptide developed for anti-thrombotic therapy [197].

The Albutag is a portable non-covalent binder to human and mouse albumin that has been developed by our group. Albutag is a small molecular ligand, originally isolated from DNA Encoded Chemical Libraries, which binds human and murine serum albumin with a calculated K_D about 3 µM [181]. The Albutag technology has been proven highly versatile by successfully extending the *in vivo* half-life of small molecules like fluorescein, ^{177}Lu-DTPA [181, 198], and larger proteins, including antibody fragments [198].

Apelin is an endogenous peptide that holds great potential for pharmaceutical applications such as the treatment of metabolic disorders, cardiovascular diseases, and sarcopenia. Various bioactive apelin isoforms resulting from N-terminal processing of the 77 amino acids long immature preproapelin polypeptide have been characterized. Among them [Pyr1]apelin-13, a pyroglutamylated form of apelin-13, represents the major apelin isoform in human plasma [471]. Recently, various Apelin derivatives have shown promising results in preclinical disease models paving the way to clinical trial investigations.

It has recently been shown that old mice suffering from sarcopenia treated with [Pyr1]apelin-13 were recovering their muscle strength and started a regenerative pathway within the aged muscle [316]. Additionally, administration of [Pyr1]apelin-13 in obese insulin-resistant mice (due to high-fat diet) improved insulin sensitivity, increased skeletal muscle glucose intake [320], and decreased insulinemia and abnormal fat retention in a hepatocyte independent manner [317, 319, 472]. Recently, [Pyr1]apelin-13 has been tested in healthy overweight men, which confirmed translatability of these results into the clinic (ClinicalTrials.gov, NCT02033473) [322]. Moreover, apelin has been reported to have beneficial cardiovascular effects on vasorelaxation [323] by decreasing arterial blood pressure and systemic venous tone [324–327] while increasing cardiac contractility [328]. Two clinical trials have been performed to assess cardiovascular effects of apelin in healthy patients and patients with chronic heart failure. In both studies, apelin administration resulted in vasodilatation and decreased blood vessel resistance and increased cardiac output [310, 329]. Apelin has been reported to improve haemodynamic parameters in two preclinical models of pulmonary hypertension (the monocrotaline-induced pulmonary hypertension model in rats and the genetic PPAR-γ knockout model in mice) [331,

332]. Similarly, Brash and collaborators reported a beneficial effect of [Pyr1]apelin-13 infusion in pulmonary hypertension patients, including reduced pulmonary vascular resistance and an overall increased cardiac function. (ClinicalTrials.gov NCT01457170) [333].

The therapeutic use of [Pyr1]apelin-13 remains mainly limited by its extremely short biological half-life, which is less than 8 minutes in men [310], and about 2.3 minutes in rats [473]. Therefore, in clinical trials, its administration required prolonged intravenous infusions [310, 322, 333]. Nevertheless, apelin cardiovascular effects have been reported to rapidly subsides after cessation of administration [474]. Therefore, there is growing interest in the generation of apelin variants with an extended half-life for potential clinical applications. Here we describe the generation and *in vitro* and *in vivo* characterization of three Albutag-apelin-13 variants with improved pharmacokinetic properties.

6.3 Results and discussion

This work main aim was to evaluate the Albutag technology for half-life extension of the small therapeutic peptide Apelin-13. Three fusion variants, termed AlbuAPL0C, AlbuAPL1C, and AlbuAPL2C, respectively, have been generated and characterized for their *in vivo* for pharmacokinetic properties.

Since negative charges have been reported to improve the affinity of 4-(p-iodophenyl)butyric acid derivatives toward albumin [181], three fusion variants were synthesized, which differ in the number of negatively charged residues in the sequence linking the Albutag moiety and the apelin-13 (**Figure 6.1**). The apelin-13 peptide was chemically synthesized in frame with the Albutag via standard solid-phase peptide synthesis (SPPS) (**Figure 6.2**). Negative charges were added by the inclusion of one or two glutamate residues (AlbuAPL1C and AlbuAPL2C, respectively), while the AlbuAPL0C peptide was synthesized without the addition of glutamate (**Figure 6.1 and 6.2**). Pure preparations of AlbuAPL derivatives (>96.6% pure) could be obtained after HPLC purification, followed by lyophilization. Overall production yields were 8.7%, 1.62%, 2.3% for AlbuAPL0C, AlbuAPL1C, and AlbuAPL2C, respectively. The identity and purity of the products were analyzed by LC-MS (**Figure 6.2**).

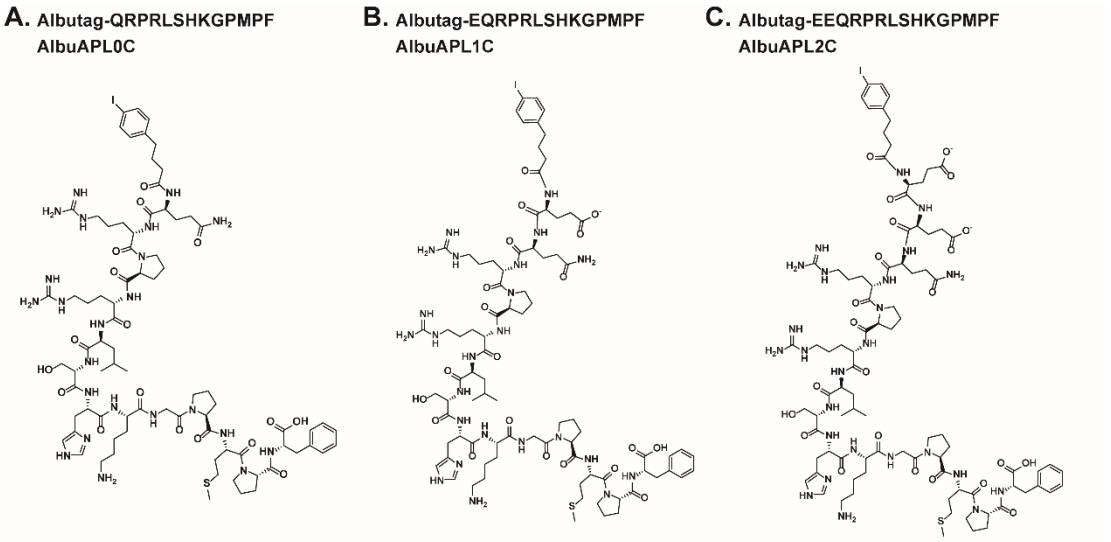

Figure 6.1: Structures of the three AlbuAPL derivatives. The fusion between apelin-13 and the Albutag moiety named AlbuAPL0C (A), Albutag, and apelin-13 separated by one glutamate (AlbuAPL1C B) or by two glutamates (AlbuAPL2C C) for the addition of negative charges next to the Albutag binding moiety.

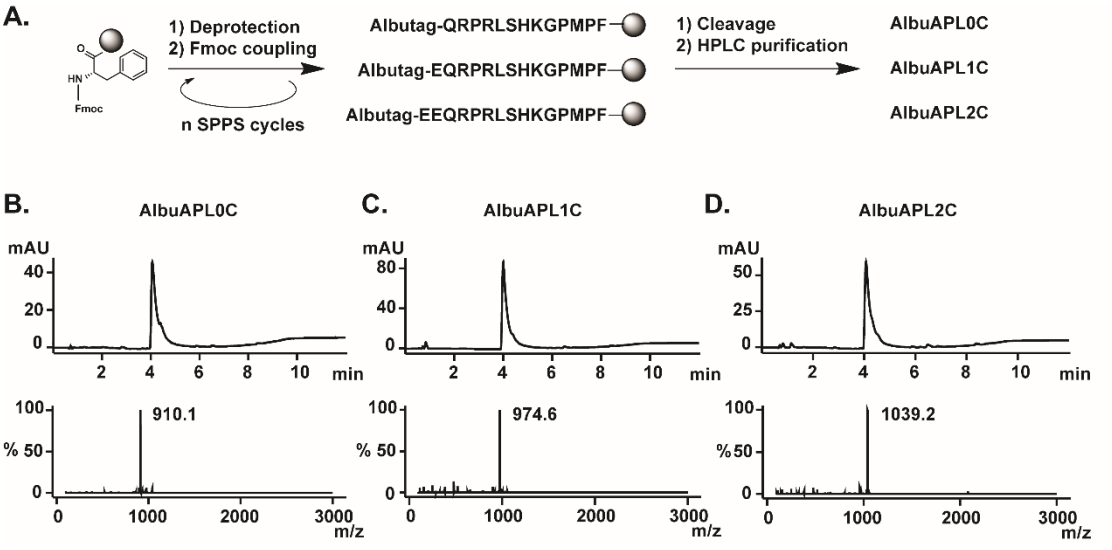

Figure 6.2: Synthesis of AlbuAPL derivatives and mass spectrometry characterization. (A) Schematic representation of the chemical synthesis of the AlbuAPL derivatives. HPLC chromatogram (λ = 260 nm) (upper graphic) and MS spectra (lower graphic) of AlbuAPL derivatives (B-C).

Three orthogonal methodologies assessed the binding toward mouse and human serum albumin (MSA and HSA, respectively). In a first approach, we performed an electrophoretic mobility assay using fluorescently labeled AlbuAPL variants preincubated with HSA or human carbonic anhydrase IX (hCAIX) as a negative control. Acetazolamide (AAZ), a nanomolar binder of hCAIX, was used as an experimental control. As expected, a fluorescently labeled AAZ derivative formed a stable complex with hCAIX while it migrated to the bottom of the gel in the presence of HSA. Similarly, the three AlbuAPL variants freely migrated in presence of the irrelevant target hCAIX. In this case, AlbuAPL0C, AlbuAPL1C and AlbuAPL2C, migrated at different distances accordingly to their number of charges. In the presence of HSA, the AlbuAPL derivatives mainly remained in the stacking portion of the gel, confirming the binding affinity of the three peptide derivatives toward HSA (**Figure 6.3A**).

In fluorescence polarization (FP), AlbuAPL0C, AlbuAPL1C, and AlbuAPL2C showed similar binding affinity toward both MSA and HSA (**Figure 6.3C**). However, in our experimental setting, binding saturation could not be achieved, hampering the precise quantification of their binding affinities. In the last approach, the albumin binding affinity of AlbuAPL0C, AlbuAPL1C, and AlbuAPL2C, was tested by surface plasmon resonance (SPR). Pure bifunctional peptide variants were injected on MSA and HSA coated chips, demonstrating their binding affinity toward both albumin proteins (**Figure 6.3B**). Surprisingly, no differences in the binding affinity between the three variants were observed, despite the presence of variable negative charges of the molecules. The three methodologies used confirmed the ability of AlbuAPL0C, AlbuAPL1C, and AlbuAPL2C to bind human and murine albumin. However, highly variable values for the calculated binding affinities were obtained depending on the approach used. Whereas SPR chromatograms did not allow a consistent calculation of K_D values due to the very rapid dissociation of the three compounds from albumin, K_D values calculated from FP assays were up to 75 fold-higher higher than the 3μM values reported by Dumelin and coworkers for the parental Albutag moiety [181] (**Figure 6.4A**). Therefore, it may be hypothesized that the fusion of apelin-13 to the Albutag may reduce the affinity of the 4-(p-iodophenyl)butyric acid towards albumin.

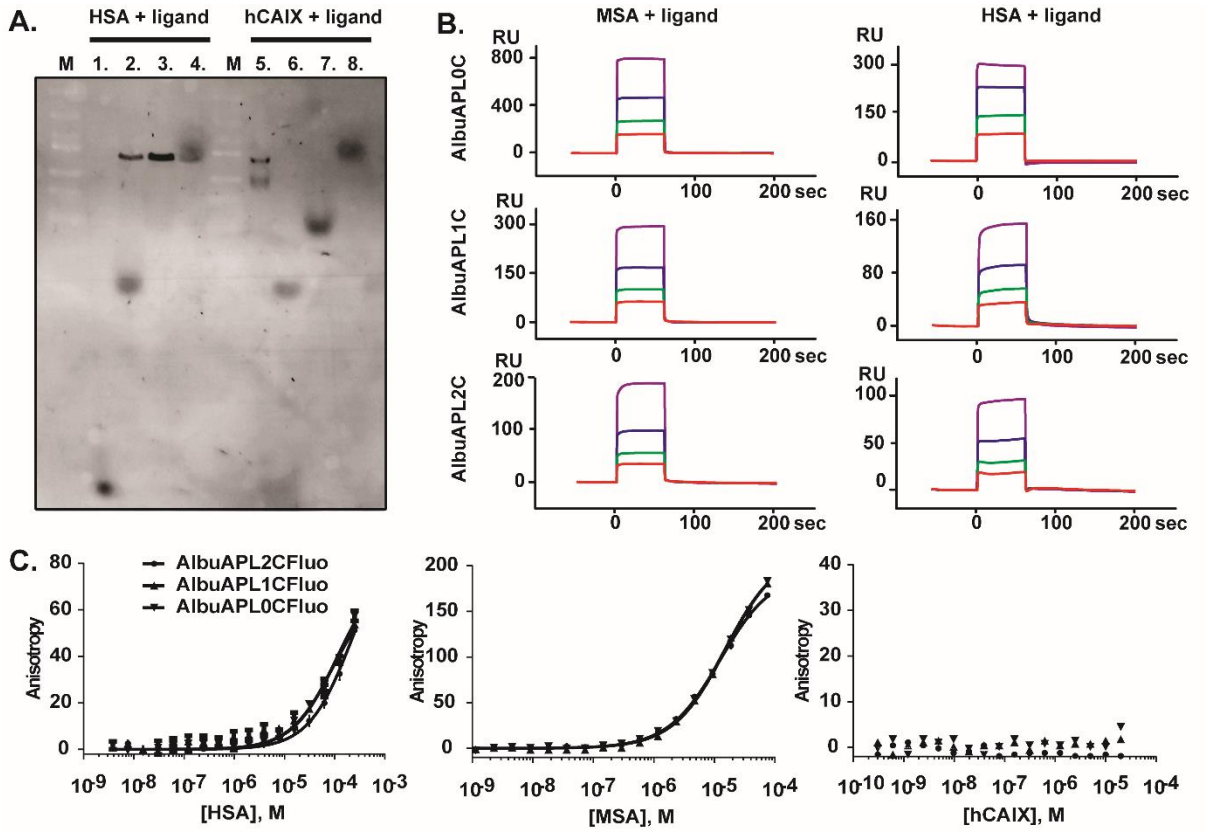

Figure 6.3: ***In vitro*** **binding affinity assessment of the three AlbuAPL variants.** (A) For the electromobility assay, fluorescent variants were incubated for 40 minutes at room temperature and loaded onto a 20%TBE gel. Lane 1: AAZ + HSA, lane 2: AlbuAPL2C + HSA, lane 3: AlbuAPL1C + HSA, lane 4: AlbuAPL0C + HSA, lane 5: AAZ + hCAIX, lane 6: AlbuAPL2C + hCAIX, lane 7: AlbuAPL1C + hCAIX, lane 8: AlbuAPL0C + hCAIX. M is marker Precision Plus Protein™ All Blue Prestained Protein Standards (Biorad). (B) SPR sensogram of AlbuAPL variants on MSA coated chip (left panel) and on HSA coated chip (right panel). Concentration of AlbuAPL variant use were 1000 µM (purple line), 500 µM (blue line), 250 µM (green line) 125 µM (red line). (C) Fluorescence polarization analysis of AlbuAPL variants. After NHS-Fluo coupling on AlbuAPL variants, they were incubated with HSA, MSA, or hCAIX (from left to right) for 1h30 at room temperature.

Calculation of the theoretical steady-state binding in human blood suggests that due to the high concentration of albumin in the human serum, AlbuAPL0C, AlbuAPL1C, and AlbuAPL2C would have extended half-life *in vivo.* Indeed, taking into consideration the experimental K_D values calculated, we can expect that about 85.6% of AlbuAPL0C, 87.4% of AlbuAPL1C, and 74.4% of AlbuAPL2C will bind HSA following injection (**Figure 6.4B**). Accordingly, the portable Albutag would extend the half-life of apelin in clinical conditions.

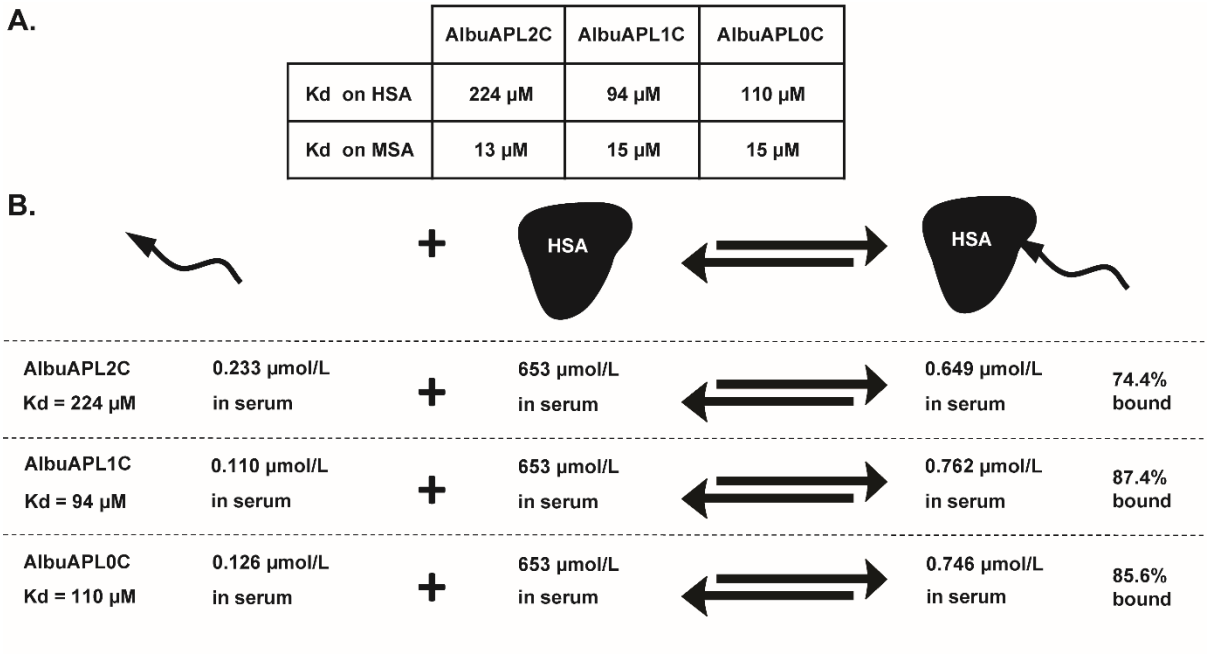

Figure 6.4: Calculated K_D values and theoretical estimation of the binding efficacy of the three AlbuAPL variants in humans. (A) K_D values are calculated from fluorescence polarization. (B) Estimation of steady-state equilibrium of AlbuAPL bound to albumin. % of bound AlbuAPL derivative has been calculated from fluorescence polarization experimental K_Ds in the setting of a 70kg human injected with 30nmol/kg of AlbuAPL conjugates.

In order to validate this hypothesis, healthy mice were injected with 10 nmol of each AlbuAPL derivative, or [Pyr1]apelin-13 to assess the pharmacokinetic parameters of the molecules. Blood samples were taken 30 minutes prior to compound injections and after 5 minutes, 15 minutes, 30 minutes, 45 minutes, 60 minutes, and 90 minutes, and apelin concentration in plasma was determined using a commercial EIA kit.

Experimental values from apelin detection in mouse plasma confirmed an improved pharmacokinetic profile for AlbuAPL0C, AlbuAPL1C, and AlbuAPL2C compared to [Pyr1]apelin-13. Of the three conjugated variants, AlbuAPL2C was the one that was retained longer in the blood compared in agreement with the presence of two additional negative charges in the Albutag structure. [Pyr1]apelin-13 was in principle not detectable at any time point since the measured values corresponded to the one of the uninjected controls (**Figure 6.5**). This result is in agreement with the previously reported half-life for [Pyr1]apelin-13 of less than 2.3 and 8 minutes in rat and human, respectively [310, 473]. 5 minutes after peptides injection values for AlbuAPL0C, AlbuAPL1C and AlbuAPL2C plasma concentration were 41.8 (+/- 13.6), 40.4 (+/- 7.8), 17.1 (+/- 2.9) ng/mL (+/- SEM), respectively. However, assuming a total plasma volume of 1.485 mL in a 25g mouse [475], the maximal theoretical concentrations for

the injection of 10 nmol of each compound would be 13731 ng/mL, 13131 ng/mL, and 12256 ng/ml for AlbuAPL0C, AlbuAPL1C, and AlbuAPL2C respectively. Accordingly, more than 99% of the injected AlbuAPL variants were cleared from the bloodstream within 5 minutes.

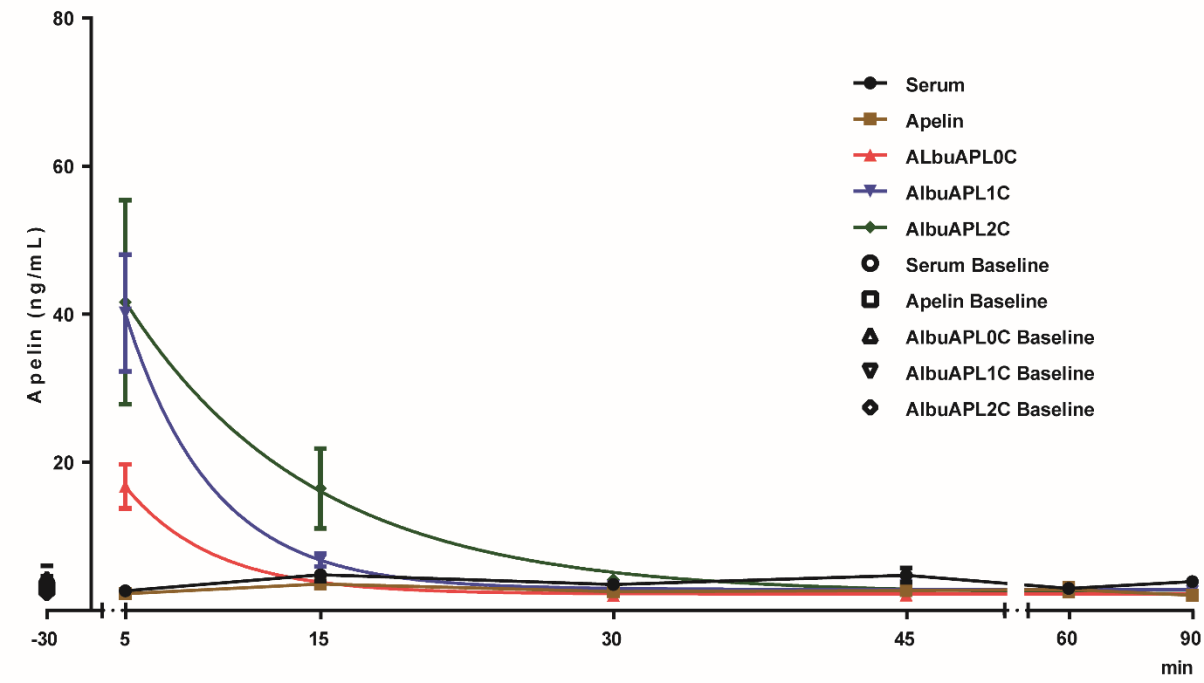

Figure 6.5: Pharmacokinetic evaluation of AlbuAPL variants in mice. Mice were injected intravenously with 10nmol of AlbuAPL derivative (ALbuAPL0C, AlbuAPL1C, AlbuAPL2C), 10nmol of [Pyr1]apelin-13, or physiological serum (Serum). Blood was collected at different time points, and apelin plasma concentration was assessed via the EIA test, which is specific for apelin-12. Non-linear regression one-phase exponential decay was applied to the results and are presented in ng/mL ± SEM.

Whereas the three AlbuAPL variants showed enhanced pharmacokinetic profiles, the improvement was relatively modest, and the three fusion peptides were no more detectable already after 45 minutes. For therapeutic applications, longer blood residence times may be required. Based on the previously reported performances of the Albutag moiety [181, 198, 199], we were expecting better K_D values for the binding of AlbuAPL0C, AlbuAPL1C, and AlbuAPL2C to albumin. Whereas in the original Albutag moiety, a lysine residue was used to enhance albumin binding. In the Albutag versions used in this study, lysine was replaced glutamate residues, possibly accounting for the observed reduced affinity. Alternatively, it is possible that the apelin peptide might interfere with the ability of the Albutag moiety to interact with albumin.

Higher albumin affinity may be achieved by optimization of the linker between the Albutag and apelin. In alternative, an additional Albutag moiety may be combined in the fusion peptide in order to generate a bivalent fusion peptide. The presence of a second binding moiety may increase albumin affinity by an avidity effect. A similar approach has been used to improve the *in vivo* targeting ability of a bivalent AAZ small molecule [374].

Our group has recently described new albumin binding moieties isolated from DECL with a nanomolar affinity toward HSA [180]. Whereas the use of higher affinity ligands might help to improve apelin PK further, it remains to be determined the impact of a very high albumin affinity with respect to apelin bioavailability towards the APJ receptor.

Strategies to extend the half-life and improve the pharmacokinetics of apelin have been extensively explored. For example, an apelin-13 Fc fusion has been developed. Fc-apelin-13 resulted in a half-life of about 33h in obese mice, and the molecule retained biological apelin activity, including improvement of glucose disposal, amelioration of liver stenosis, and heart fibrosis, and increase of cardiac output [315]. Other approaches aimed at minimizing apelin proteolytic degradation make use of apelin variants containing non-natural amino acids and cyclic apelin analogs [307, 476]. Read *et al.*, reported the generation of an apelin mimetic peptide containing unnatural amino acids, termed MM202. The chemical fusion of MM202, to the anti-serum albumin antibody AlbudAb® resulted in a molecule, with an improved half-life, that fully retained *in vitro* and *in vivo* functional activity [314]. The manufacturing of such a bioconjugate may be cumbersome and expensive since it will require both GMP compliant biologic-based and small-molecule manufacturing activities. From a manufacturing point of view, the fusion of apelin to the Albutag may be a better and cheaper option as it fully relies on chemical synthesis.

6.4 Conclusions

Fusion to the portable albumin binder Albutag is a suitable approach to extend apelin half-life. This technology may be of general use to improve pharmacokinetics properties of therapeutic peptides. However, further optimization of the hybrid conjugate product, such as the use of apelin variants containing non-natural amino

acids, cyclization of apelin, or the use of multivalent albumin binders, may be required to obtain a robust product which meets clinical requirements. Therapeutic applications of apelin are strongly limited by its short half-life. We thus anticipate that the development of synthetic apelin conjugates with improved pharmacokinetic properties will be of great interest for pharmaceutical applications in the field of metabolic disorders, aging, and cardiovascular diseases.

6.5 Experimental section

6.5.1 Compound synthesis

Peptide grade N,N'-dimethylformamide (DMF) for solid-phase synthesis, and the 4-(p-Iodophenyl)butyric acid were purchased from ABCR. The Fmoc-Phe-Wang resin, the HBTU (O-(Benzotriazol-1-yl)-N,N,N',N'-tetramethyluronium hexafluorophosphate), the HOBt (1-Hydroxybenzotriazole hydrate), and the protected amino acids were purchased from Chemipex. All other solvents were used as supplied by Merck or Sigma Aldrich in HPLC or analytical grade. All other chemicals and solvents (HPLC-grade or reagent-grade quality) were purchased from commercial sources and used without further purification unless noted otherwise.

AlbuAPL derivatives were synthesized by standard SPPS on Fmoc-Phe-Wang resin. Each coupling reaction was performed for 1h at room temperature (3 equivalents of Fmoc-AA, 3 eq. of HBTU, 3 eq. of HOBt, 6 eq. of DIPEA in 10 mL of DMF). Fmoc deprotection was performed with 20% piperidine in DMF (2 × 15 mL) for 15 min at room temperature. After the final amino acid of each AlbuAPL derivatives, the peptide was coupled with 4-(p-iodophenyl)butyric acid (3 eq.), HOBt (3 eq.) HBTU (3 eq.) and DIPEA (6 eq.) into DMF for 1h at room temperature. Final products were cleaved from the resin using a cleavage cocktail containing TFA (88 %), Triisopropylsilane (2%), mQ water (5%), and phenol (5%). The crude solid material was obtained by precipitation in cold ether. AlbuAPL variants were purified from the crude via reverse-phase HPLC purification. Fractions containing the purified product were identified by mass spectrometry and lyophilized to yield the final product (white powder). For AlbuAPL0C: 80 mg 43.91 µmol 8.7% yield MW: 1822.91Da theoretical LC-MS (ES+) m/z 1821.8(M+H)+. For AlbuAPL1C: 16 mg 10.6 µmol 1.62% yield MW: 1951.02 Da

LC-MS (ES+) m/z 1949.83(M+H)+. For AlbuAPL2C: 24 mg MW: 2079.12 Da 11.54 µmol 2.3% yield LC-MS (ES+) m/z 1039.44(M+H)+.

Preparative RP-HPLC purifications were performed on an Agilent 1200 Series RP-HPLC with PDA UV detector, using a Synergi 4 µm, Polar-RP 80Å 10 Å~ 150 mm C18 column at a flow rate of 5 ml min^{-1} with linear gradients of solvents A and B (A = Millipore water with 0.1% trifluoroacetic acid [TFA], B = MeCN with 0.1% trifluoroacetic acid [TFA]).

Liquid-Chromatography-Mass-Spectrometry (LC-MS) spectra were recorded on an Agilent 6100 Series Single Quadrupole MS system combined with an Agilent 1200 Series LC, using an InfinityLab Poroshell 120 EC-C18 Column, 2.7 µm, 4.6 Å~ 50 mm at a flow rate of 0.6 ml min^{-1}, 10% MeCN in 0.1% aq. FA to 100% MeCN in 12 min.

Liquid phase NHS chemical reaction was used to attach the fluorescein to the free lysine of the apelin moiety. AlbuAPL (1 µmol) conjugate was resuspended in 50 mM borate buffer pH 8.5 (500 µL) and mixed with 1.2 equivalents of NHS-fluorescein pre-dissolved in DMSO. Purification was performed via reverse phase HPLC to obtain the final products as a white powder, as previously described. Fluorescent derivatives were resuspended into DMF then diluted into PBS (pH 7.4). Their concentration was determined by measuring the absorbance at 480 nm (ε = 91,600 M^{-1} cm^{-1}).

6.5.2 Fluorescence polarization

For fluorescence polarization, 1µM PBS diluted fluorescent derivatives were prepared in a 384-wells plate. Whereas the protein was 16 times serial diluted 1:2 starting from 285µM for HSA, 75µM for MSA, and 20 µM for hCAIX. Triplicate samples were used for homogeneous data acquisition. The plate was incubated for 1h30 minutes at room temperature prior to fluorescence measurement on Tecan instrument. Anisotropy values were plotted against the protein molar concentration. K_D calculation was performed using GraphPad prism.

6.5.3 Biacore experiment

The affinity of AlbuAPL variants toward HSA and MSA were confirmed using Surface plasmon resonance (SPR) on a Biacore S200. HSA and MSA were coated on a CM5

chip serie S (GE Healthcare) at 5828 RU 5630 RU, respectively, using 400 mM EDC-HCl, 100 mM N-hydroxysucinimmide (NHS), and 1M Ethanolamine (pH=8.5). Lyophilized AlbuAPL compounds were resuspended into HBS-EP (GE Healthcare) and injected into the Biacore at different concentrations (1000 µM, 500 µM, 250 µM, and 125 µM).

6.5.4 Electro mobility assay

AlbuAPL variant and AAZ fluorescently labeled, final concentration 2.5 µM were incubated in the presence of HSA (75 µM) or hCAIX (3 µM) for 40 minutes at room temperature. Samples were mixed into sucrose loading buffer, and 25 µL of samples with 1% sucrose were loaded into a 20% TBE gel (Invitrogen). 225V was applied onto the TBE gel into TBE buffer (100mM Tris, 100mM boric acid, 0.4mM EDTA) for an hour. The marker Precision Plus Protein™ All Blue Prestained Protein Standards (Biorad) has been used to follow the migration of the gel. A picture of the gel was taken under a UV lamp (TFP-M/WL, λ312nm, Villier Lourmat). Colors were saturated using photoshop for better visualization of the bands.

6.5.5 Calculation of the steady state AlbuAPL bound to HSA in serum

Steady-state equilibrium, formula (1), was estimated for clinical injection of AlbuAPL variants equivalent to 30nmol/kg [322] into a 70kg patient. Concentrations are reported per liter of serum. Therefore, a concentration at injection time has been calculated to be 0.872 µmol/L, defined as [AlbuAPL]init. = x. While K_D used for the calculation are from experimental values of FP measurements on HSA and albumin concentration was estimated at 653 µmol/L, defined as [Albumin]init. =y. Using the following parameters, [Albumin]eq = (y-a) [AlbuAPL]eq = (x-a) [AlbuComplex]eq = a, formula (2) and (3) could be deducted from formula (1) and resolved with a second-order equation, giving the concentration of the complex at equilibrium (a = [AlbuComplex]eq).

(1) [Albumin]eq + [AlbuAPL]eq ↔ [AlbuComplex]eq

(2) $K_D = \frac{[\text{Albumin}]eq \times [\text{AlbuAPL}]eq}{[\text{AlbuComplex}]eq} = \frac{(y-a)\times(x-a)}{a}$

(3) $K_D \times a = (y-a)\times(x-a)$

6.5.6 Pharmacokinetic evaluation

Apelin variants ([Pyr1]apelin-13 and AlbuAPL variants) were injected at a concentration of 10nmol (100μL) retro-orbital intravenous sinus of C57Bl6/J mice. After different time points (-30min, 5min, 15min, 30min, 45min, 1h, 1h30), blood was collected, and plasma was isolated using EDTA cuvettes. Apelin plasma concentration was quantified with the nonselective apelin-12 enzyme immunoassay or the specific human EIA kit (Phoenix Pharmaceuticals) following the manufacturer's instructions. Data have been analyzed on GraphPad prism, and non-linear regression (one exponential phase decay) was applied to the apelin concentration values ± SEM.

7 Discussion and outlook

Multispecific drugs are composed of powerful molecules that, when fused together, may improve each other's therapeutic capabilities. The pharmaceutical interest in multispecific drugs is driven by their potential to be both more specific and more potent than conventional drugs.

Over the past two decades, targeted pharmacodelivery strategies have been extensively explored, and antibodies or small molecules tested as targeting moieties in multispecific drugs. Antibody-cytokine fusion proteins (immunocytokines) have proven to successfully improve the therapeutic index of the cytokine payloads both in preclinical and clinical studies [140, 144, 477, 478], in contrast small molecules have been mainly investigated for their ability to deliver cytotoxic drugs within neoplastic tumor masses [165, 165, 168]. Additionally, multispecific drug approaches have been developed to bypass the short half-life of certain therapeutic proteins and peptides [181, 197, 198, 314]. In this thesis, we reported the development and preclinical evaluation of three bispecific therapeutic candidates consisting of (i) a novel immunocytokine, (ii) a small molecule cytokine conjugate, and (iii) a new bifunctional therapeutic peptide.

Immunocytokines represent a challenging class of multifunctional biopharmaceuticals that has gained growing interest in pharmaceutical applications [23, 24, 453]. During the last twenty years, our company in collaboration with the research group of Prof. Dr. Dario Neri at the ETH Zurich, developed a number of immunocytokines, based on the F8 and L19 antibodies specific for the alternatively spliced EDA and EDB domains of fibronectin, respectively [95, 105–117]. These two extradomains are attractive targets for pharmacodelivery applications since they are highly specific to various pathological conditions. Furthermore, the EDA and EDB sequences are highly conserved between rodents and men, facilitating the translation of preclinical activities into clinical studies. Philogen's immunocytokine prototypes showing promising preclinical therapeutic efficacy have been moved into human clinical trials. For example, candidates based on the pro-inflammatory cytokines, IL2 or TNF, are currently being tested for oncology applications [140, 144, 477, 478], while an immunocytokine based on the anti-inflammatory cytokines IL10 has reached the

clinical stage for the treatment of rheumatoid arthritis [139]. Motivated by the success of these immunocytokines, we are continuously developing new immunocytokine prototypes for the treatment of cancer and autoimmune diseases.

In the projects presented in Chapters 3 and 4 of this thesis, I have developed an IL9 based immunocytokine and characterized it for *in vivo* targeting efficacy and therapeutic activity in cancer, rheumatoid arthritis, and pulmonary hypertension preclinical models. IL9 biological functions are poorly understood; nevertheless, IL9 has been suggested to play an important role in the pathogenesis of various diseases including, for example, cancer, rheumatoid arthritis, and multiple sclerosis, although results for preclinical are often controversial [220, 252–254, 257–260, 263, 263, 264, 267–269, 479].

The F8IL9F8 immunocytokine developed during this thesis has shown excellent disease homing properties. However, in different cancer models tested, F8IL9F8 injection showed only a moderate tumor growth retardation. In agreement with previous reports, anti-cancer activity was tumor type-dependent. It remains to be tested whether the combination of F8IL9F8 with other therapeutic modalities would improve its anti-cancer properties. Nevertheless, the therapeutic efficacy and the levels of CD4+ T cells, CD8+ T cells, and NK cells infiltration promoted by F8IL9F8 monotherapy were substantially lower than the ones observed with other immunocytokines developed by our company based on potent pro-inflammatory cytokines like Il2, Il12, and TNF [107, 111, 115, 117, 118, 349, 422]. Consequently, we do not foresee further development of F8IL9F8 for cancer treatment.

In contrast to the data reported by Rauber and colleagues, the targeted delivery of IL9 to arthritic mice did not show any therapeutic benefit. The use of different preclinical models and therapeutic modalities may in part explain the controversial results. In particular, in the study of Rauber *et al.,* IL9 was delivered by a gene therapy approach prior to the onset of the disease, whereas in our protocol, F8IL9F8 was administered only after the onset of arthritic lesions. IL9 has been postulated to exert its effect on various cell types, thus promoting both anti- and pro-inflammatory responses. Consequently, it may be speculated that during the early phases of the disease, IL9 may promote resolution of the inflammation by boosting ILC2 cells survival, whereas, at later phases, IL9 may support the proliferation of synovial neutrophils, thus

contributing to the worsening of the disease. Additional experiments will be required to better understand the potential role of IL9 in the pathology of arthritis. Such studies may include a prophylactic F8IL9F8 treatment in CIA mice and a timeframe analysis of the IL9 receptor (IL9R) expression to identify which cell types may be activated by IL9 during the pathological progression of arthritis. IL9 concentration and IL9R expression levels may play an important role in modulating its pro- or anti-inflammatory properties. However, in our study, none of the two F8IL9F8 concentrations tested showed therapeutic efficacy against CIA, whereas, in the gene therapy approach used by Rauber *et al.,* IL9 expression levels were not reported.

Our results highlight the importance of the disease models and therapeutic intervention used for the preclinical evaluation of therapeutic candidates. Our investigative approach relies on the targeted delivery of cytokines at the disease site in murine models that mimic as close as possible the human pathological condition. Such an approach can be promptly translated into a clinical protocol. Using this strategy, our company has brought several immunocytokines into clinical development. The same preclinical models described in this study have been previously used for the preclinical validation of several immunocytokine that are currently under clinical development, where for several cases, they could confirm the therapeutic activity observed in mice. The rapid translation of preclinical research into clinical practice is further facilitated by the fact that the prototypes that we use in preclinical studies are often identical or very similar to the final clinical product. Indeed, unless the human cytokine under investigation conserves its activity in mouse, preclinical and clinical immunocytokines are generated, which differ only in the cytokine sequence (that will be either of murine or human origin) while sharing exactly the same antibody moiety. This is possible since we target disease-specific antigens that are highly conserved between mice and humans, allowing us to use the same targeting antibodies for the construction of murine and human immunocytokine surrogates.

F8IL9F8 therapy showed relevant efficacy in the treatment of pulmonary hypertension (PH) in the monocrotaline (MCT) induced model in mice. When compared to untreated controls or mice treated with an untargeted variant of Il9, F8IL9F8 injection resulted in a relevant amelioration of the disease as assessed by a variety of haemodynamic and

echocardiographic parameters. Disease improvement has been at least as good or even better than the one observed in mice treated with Macitentan (MACI), the current standard of care for pulmonary arterial hypertension. Treatment efficacy was further confirmed by histological analysis showing reduced damage in lung and right ventricular cardiac tissues. These results are surprising considering the various reports suggesting a key role played by IL9 in promoting lung inflammation and asthma [240, 244–247, 405]. Indeed, in our study, the reduced infiltration of leukocytes and macrophages observed in lung and right ventricular cardiac tissues of mice treated with F8IL9F8 would suggest an anti-inflammatory role of IL9 in PH. Pulmonary hypertension (PH) is a pathophysiological disorder that can involve multiple clinical conditions and is a complication of most cardiovascular and respiratory diseases. Current treatment options for PH generally act by decreasing vascular tone and reducing pulmonary artery pressure, but no treatment able to stop or reverse PH progression is available. Due to the immunomodulatory properties of IL9, F8IL9F8 hold the promise to modify disease pathogenesis by modulating tissue remodeling in lung vessels and right ventricle, thus potentially stop or even reverse the disease progression. To verify this hypothesis, additional preclinical studies will be needed to determine F8IL9F8 effects during the time course of disease progression. In this regard, the group of Prof Marcus Franz in collaboration with the MRI research group of Prof Reichenbach at Jena University Hospital has established an MRI approach in the rat PH, allowing the time-courses assessment of disease progression and treatment associated reversibility. Such an approach not only may provide information regarding the disease-modifying potential of F8IL9F8 but may also help in defining an optimized treatment schedule and dosing.

After the very promising results of F8IL9F8 in PH, our company is considering the further development of this product in clinical trials. Besides the execution of additional preclinical studies to confirm F8IL9F8 efficacy in PH and understand its mode of action, the next steps towards the clinical testing of F8IL9F8 includes the generation of a manufacturing cell line and the development of an appropriate GMP production process, as well as the execution of safety-toxicology studies in non-human-primates. The exact dose/scheduling approach to be used in humans will be defined only during Phase I clinical trials after the execution of safety-toxicology studies. The dose to be injected into patients are often high for biologics and the production can be challenging

for low yielding proteins. However, in transient gene expression of the human surrogate of F8**h**IL9F8 was produced at yields of about 20mg/L and resulted, after a single step purification by protein A affinity chromatography, in a highly homogeneous protein. From our experience, fusion proteins with this level of transient expression are often resulting in high yielding stable cell lines. Therefore, these preliminary data make us confident about the possibility of producing F8**h**IL9F8 at high levels under GMP manufacturing conditions. During the development of the GMP manufacturing process, a particular emphasis should be taken with regards to F8**h**IL9F8 product glycosylation. The IL9 cytokine is a heavily glycosylated protein, carrying 4 potential N-glycosylation sites. Previous studies using the F8IL9 immunocytokine, based on the diabody format and murine IL9, showed that only protein preparations containing high terminal sialic acid levels were retaining *in vivo* targeting activities [122]. As the glycosylation pattern on recombinant proteins is strongly affected by the production process and media components used for manufacturing, optimization of an F8**h**IL9F8 GMP manufacturing process should not only aim at high production yields but also at obtaining a product with a suitable glycosylation profile. In conclusion, the IL9-based immunocytokine developed during this thesis is currently at a very preliminary stage of development as a therapeutic product but hopefully may reach clinical development in the next couple of years to fulfill the unmet medical need of pulmonary hypertension.

Pharmacodelivery based on antibodies and antibody fragments has proven to be a very promising approach for the selective delivery of cytokines at the site of diseases. IL2-based immunocytokines are among the most advanced immunocytokines in the clinic [100, 102, 134, 138, 143, 286]. The immunomodulatory activity mediated by the IL2 payload led to consistent tumor growth inhibition in various mouse models of cancer [134, 156, 287, 288] and significant objective response in clinical trials [298]. However, due to their relatively large size, some immunocytokines suffer from poor tumor tissue penetration and fairly long half-life, potentially leading to systemic side effects [143, 158, 480]. Small organic ligands can diffuse in a very rapid and homogeneous way into solid tumors, as such they can, potentially reach high tumor:organ ratios and combine extended residence time at the tumor site with rapid body clearance [164, 169, 171, 179]. For these reasons, small organic ligands can be used as an alternative to antibodies for pharmacodelivery purposes. For example, small molecule drug conjugates (SMDCs) based on acetazolamide derivatives, a

small ligand specific to CAIX, have shown excellent biodistribution profiles and promising therapeutic efficacy in preclinical cancer models [165, 169, 171, 461].

The aim of my second project, presented in Chapter 5, was to investigate the possibility of using the AAZ ligand for the targeted delivery of IL2 to tumors that express CAIX. Combination of both beneficial effects of SMDC (rapid diffusion, tissue penetration) and IL2-based targeted delivery (disease homing, strong immunomodulation). Traditional bioconjugation methods often result in a reduction or complete loss of the modified protein's biological activity due to a lack of site-specificity of the conjugation reaction [463]. For this reason, we chose an approach based on the site-specific transpeptidation reaction mediated by the Sortase A (SrtA) enzyme for the generation of the AAZ-IL2 conjugate. The SrtA enzyme has been successfully used for the generation of labeled antibodies [464–466] and antibody-drug conjugates [203, 468], highlighting the effectiveness and versatility of this approach. However, unlike some immunocytokine and SMDC products, we have not been able to achieve an efficient *in vivo* accumulation of AAZ-IL2 within tumors expressing the cognate antigen. Further product optimization has been proposed in Chapter 5. Possible optimization includes the use of an AAZ bivalent ligand [370], in order to increase product avidity toward CAIX, or the use of an affinity matured variant of AAZ [169], to reach a better affinity toward the cognate antigen. These strategies have been successfully applied for various AAZ derivatives resulting in improved *in vivo* targeting efficacy [169, 374]. Whereas the SrtA-based approach chosen for the production of AAZ-IL2 was effective at the lab scale, its use at the commercial manufacturing scale poses several challenges, including the need to produce the three reagents and perform the conjugation reaction under GMP conditions. Nevertheless, NBE Therapeutics recently reported the GMP manufacturing of an ADC product generated by SrtA mediated site-specific conjugation. The corresponding product termed NBE-002 is currently under evaluation in a Phase 1/2 clinical trial for the treatment of advanced solid cancers (NCT04441099) [481, 482]. Our study represents the first report on the site-specific conjugation of a small-molecule ligand to a cytokine for tumor targeting purposes, to the best of our knowledge. Although the tumor-targeting performances of AAZ-IL2 have been insufficient to justify its further industrial development, this pioneering work will hopefully inspire other researchers to develop small molecule cytokine conjugate (SMCC) products.

As described in chapter 2.3.3, the excellent potential for therapeutic applications of the apelin peptide is currently hampered by its brief plasma half-life [309, 310]. Albumin binding moieties represent a suitable methodology for half-life extension of therapeutic molecules (as described in chapter 2.2.4). Our group has developed a portable albumin binder termed Albutag and demonstrated its ability to improve the pharmacokinetic profile of proteins and radionuclides [181, 198]. In Chapter 6, we have reported a strategy for half-life extension of apelin based on a bifunctional peptide generation. Three fully synthetic bifunctional peptides, termed AlbuAPL, were generated. The three peptides retained the ability to recognize the mouse and human albumin, and their half-lives were extended when intravenously injected into mice when compared to [Pyr1]apelin-13. However, the calculated affinity to the albumin of the AlbuAPL variants was somehow lower than the one previously reported for the parental Albutag small molecule. The avidity effect has been demonstrated to improve the *in vivo* targeting ability of a bivalent AAZ small molecule [374]. Similarly, the poor affinity of the AlbuAPL may be compensated by adding a second Albumin binding moiety to these bifunctional molecules. Additionally, our group has recently described other albumin binding moieties isolated from DNA Encoded Libraries (DECLs) with higher affinity toward HSA [180]. Using higher affinity Albumin ligands might be a second alternative to improve the pharmacokinetic profile of apelin further.

With this project, we have demonstrated the possibility to generate an apelin-Albutag fusion peptide with improved pharmacokinetic properties by a chemical synthesis approach. Other groups have developed apelin derivatives with extended half-life using a variety of approaches. For instance, an Fc-apelin fusion has been reported to have a half-life of 33 hours [315]. Similarly, the chemical conjugation of an antibody fragments specific for albumin (AlbudAb) to a modified apelin peptide agonist (MM202) led to an improvement in *ex vivo* plasma half-life over on both its parent compound and endogenous agonist [Pyr^{1}]apelin-13 [314, 483]. While these products showed better pharmacokinetics parameters than the current AlbuAPL variants, their industrial GMP manufacturing may be more laborious and expensive than the full chemical synthesis of the AlbuAPL compounds.

The incorporation of non-natural amino acids in the apelin sequence and the use of cyclic apelin variants have been described to improve resistance to enzymatic

degradation and thus extend *in vivo* half-life of the corresponding apelin analogs [307, 476].

Further optimization of the apelin peptide may arise from the combination of Albutag technology with the use of apelin analogs designed to be resistant to proteolytic cleavage while retaining full biological activity. In summary, in our preliminary work, we demonstrated that Albutag technology effectively improves an apelin peptide's pharmacokinetic profile. However, further optimization of the AlbuAPL derivatives is required to achieve a half-life compatible with clinical applications.

In conclusion, bifunctional molecules based on antibodies or small organic ligands as targeting agents hold great potential for the development of targeted drugs. However, their development faces several challenges in terms of manufacturing and fine-tuning their efficacy, pharmacokinetics, and toxicity profiles. In this thesis, different methodologies have been applied for the generation of bifunctional molecules with therapeutic potential, namely a new immunocytokine (F8IL9F8), a small molecule cytokine conjugate (AAZ-IL2), and a bifunctional peptide (AlbuAPL). Whereas the AAZ-IL2 and AlbuAPL products have shown some limitations that would require additional optimization to be further developed as therapeutic products, F8IL9F8 has shown very promising preclinical therapeutic efficacy in PH and is currently under further investigation.

8 References

1. NobelPrize.org The Nobel Prize in Physiology or Medicine 1901. In: NobelPrize.org. https://www.nobelprize.org/prizes/medicine/1901/behring/article/.

2. Köhler G, Milstein C (1975) Continuous cultures of fused cells secreting antibody of predefined specificity. Nature 256:495–497

3. Leader B, Baca QJ, Golan DE (2008) Protein therapeutics: a summary and pharmacological classification. Nat Rev Drug Discov 7:21–39

4. Dimitrov DS (2012) Therapeutic Proteins. Methods Mol Biol Clifton NJ 899:1–26

5. Kumar SS, Sabu A (2019) Fibrinolytic Enzymes for Thrombolytic Therapy. In: Labrou N (ed) Ther. Enzym. Funct. Clin. Implic. Springer, Singapore, pp 345–381

6. Bianchi ML, Vai S (2019) Alkaline Phosphatase Replacement Therapy. In: Labrou N (ed) Ther. Enzym. Funct. Clin. Implic. Springer, Singapore, pp 201–232

7. Maggi M, Scotti C (2019) Enzymes in Metabolic Anticancer Therapy. In: Labrou N (ed) Ther. Enzym. Funct. Clin. Implic. Springer, Singapore, pp 173–199

8. Lu R-M, Hwang Y-C, Liu I-J, Lee C-C, Tsai H-Z, Li H-J, Wu H-C (2020) Development of therapeutic antibodies for the treatment of diseases. J Biomed Sci. https://doi.org/10.1186/s12929-019-0592-z

9. Klapper JA, Downey SG, Smith FO, Yang JC, Hughes MS, Kammula US, Sherry RM, Royal RE, Steinberg SM, Rosenberg S (2008) High-dose interleukin-2 for the treatment of metastatic renal cell carcinoma : a retrospective analysis of response and survival in patients treated in the surgery branch at the National Cancer Institute between 1986 and 2006. Cancer 113:293–301

10. Rosenberg SA, Yang JC, White DE, Steinberg SM (1998) Durability of complete responses in patients with metastatic cancer treated with high-dose interleukin-2: identification of the antigens mediating response. Ann Surg 228:307–319

11. Atkins MB, Lotze MT, Dutcher JP, et al (1999) High-dose recombinant interleukin 2 therapy for patients with metastatic melanoma: analysis of 270 patients treated between 1985 and 1993. J Clin Oncol Off J Am Soc Clin Oncol 17:2105–2116

12. Fyfe G, Fisher RI, Rosenberg SA, Sznol M, Parkinson DR, Louie AC (1995) Results of treatment of 255 patients with metastatic renal cell carcinoma who received high-dose recombinant interleukin-2 therapy. J Clin Oncol Off J Am Soc Clin Oncol 13:688–696

13. Groopman JE, Gottlieb MS, Goodman J, Mitsuyasu RT, Conant MA, Prince H, Fahey JL, Derezin M, Weinstein WM, Casavante C (1984) Recombinant alpha-

2 interferon therapy for Kaposi's sarcoma associated with the acquired immunodeficiency syndrome. Ann Intern Med 100:671–676

14. Golomb HM, Jacobs A, Fefer A, Ozer H, Thompson J, Portlock C, Ratain M, Golde D, Vardiman J, Burke JS (1986) Alpha-2 interferon therapy of hairy-cell leukemia: a multicenter study of 64 patients. J Clin Oncol Off J Am Soc Clin Oncol 4:900–905

15. Solal-Celigny P, Lepage E, Brousse N, Reyes F, Haioun C, Leporrier M, Peuchmaur M, Bosly A, Parlier Y, Brice P (1993) Recombinant interferon alfa-2b combined with a regimen containing doxorubicin in patients with advanced follicular lymphoma. Groupe d'Etude des Lymphomes de l'Adulte. N Engl J Med 329:1608–1614

16. Kirkwood JM, Strawderman MH, Ernstoff MS, Smith TJ, Borden EC, Blum RH (1996) Interferon alfa-2b adjuvant therapy of high-risk resected cutaneous melanoma: the Eastern Cooperative Oncology Group Trial EST 1684. J Clin Oncol Off J Am Soc Clin Oncol 14:7–17

17. Yamakawa S, Hayashida K (2019) Advances in surgical applications of growth factors for wound healing. Burns Trauma 7:10

18. Rhodes CA, Pei D (2017) Bicyclic Peptides as Next-Generation Therapeutics. Chem Weinh Bergstr Ger 23:12690–12703

19. Chen S, Heinis C (2015) Phage selection of bicyclic peptides based on two disulfide bridges. Methods Mol Biol Clifton NJ 1248:119–137

20. Mathur D, Prakash S, Anand P, Kaur H, Agrawal P, Mehta A, Kumar R, Singh S, Raghava GPS (2016) PEPlife: A Repository of the Half-life of Peptides. Sci Rep 6:36617

21. Narayanan S, Harris DL, Maitra R, Runyon SP (2015) Regulation of the Apelinergic System and Its Potential in Cardiovascular Disease: Peptides and Small Molecules as Tools for Discovery. J Med Chem 58:7913–7927

22. Kontermann RE (2016) Half-life extended biotherapeutics. Expert Opin Biol Ther 16:903–915

23. Kiefer JD, Neri D (2016) Immunocytokines and bispecific antibodies: two complementary strategies for the selective activation of immune cells at the tumor site. Immunol Rev 270:178–192

24. Hess C, Venetz D, Neri D (2014) Emerging classes of armed antibody therapeutics against cancer. MedChemComm 5:408–431

25. Zhao P, Zhang Y, Li W, Jeanty C, Xiang G, Dong Y (2020) Recent advances of antibody drug conjugates for clinical applications. Acta Pharm Sin B 10:1589–1600

26. Steiner M, Neri D (2011) Antibody-Radionuclide Conjugates for Cancer Therapy: Historical Considerations and New Trends. Clin Cancer Res 17:6406–6416

27. Schmier J, Ogden K, Nickman N, Halpern MT, Cifaldi M, Ganguli A, Bao Y, Garg V (2017) Costs of Providing Infusion Therapy for Rheumatoid Arthritis in a Hospital-based Infusion Center Setting. Clin Ther 39:1600–1617

28. Puetz J, Wurm FM (2019) Recombinant Proteins for Industrial versus Pharmaceutical Purposes: A Review of Process and Pricing. Processes 7:476

29. Urquhart L (2020) Top companies and drugs by sales in 2019. Nat Rev Drug Discov 19:228–228

30. Biogen reports record revenues for both the full year and q4 2018. https://investors.biogen.com/static-files/5dcc04ff-a91e-44a5-8298-72b779543563.

31. Novo NordiskAnnual Report 2018. https://www.novonordisk.com/content/dam/Denmark/HQ/investors/irmaterial/annual_report/2019/NN-AR18_UK_Online.pdf.

32. Peptide Therapeutics Market to expand at a CAGR of 7.9% from 2019 to 2027 | TMR. https://www.transparencymarketresearch.com/pressrelease/peptide-therapeutics-market.htm.

33. Fosgerau K, Hoffmann T (2015) Peptide therapeutics: current status and future directions. Drug Discov Today 20:122–128

34. Allhorn M, Olin AI, Nimmerjahn F, Collin M (2008) Human IgG/FcγR Interactions Are Modulated by Streptococcal IgG Glycan Hydrolysis. PLOS ONE 3:e1413

35. Brekke OH, Sandlie I (2003) Therapeutic antibodies for human diseases at the dawn of the twenty-first century. Nat Rev Drug Discov 2:52–62

36. Chames P, Van Regenmortel M, Weiss E, Baty D (2009) Therapeutic antibodies: successes, limitations and hopes for the future. Br J Pharmacol 157:220–233

37. Junghans RP, Anderson CL (1996) The protection receptor for IgG catabolism is the beta2-microglobulin-containing neonatal intestinal transport receptor. Proc Natl Acad Sci U S A 93:5512–5516

38. Raghavan M, Chen MY, Gastinel LN, Bjorkman PJ (1994) Investigation of the interaction between the class I MHC-related Fc receptor and its immunoglobulin G ligand. Immunity 1:303–315

39. West AP, Bjorkman PJ (2000) Crystal structure and immunoglobulin G binding properties of the human major histocompatibility complex-related Fc receptor(,). Biochemistry 39:9698–9708

40. Mitragotri S, Burke PA, Langer R (2014) Overcoming the challenges in administering biopharmaceuticals: formulation and delivery strategies. Nat Rev Drug Discov 13:655–672

41. Patel KR, Nott JD, Barb AW (2019) Primary Human Natural Killer Cells Retain Proinflammatory IgG1 at the Cell Surface and Express CD16a Glycoforms with Donor-dependent Variability. Mol Cell Proteomics MCP 18:2178–2190

42. Vidarsson G, Dekkers G, Rispens T (2014) IgG Subclasses and Allotypes: From Structure to Effector Functions. Front Immunol 5:520

43. Kung P, Goldstein G, Reinherz EL, Schlossman SF (1979) Monoclonal antibodies defining distinctive human T cell surface antigens. Science 206:347–349

44. Hooks MA, Wade CS, Millikan WJ (1991) Muromonab CD-3: A Review of Its Pharmacology, Pharmacokinetics, and Clinical Use in Transplantation. Pharmacother J Hum Pharmacol Drug Ther 11:26–37

45. Baert F, Noman M, Vermeire S, Van Assche G, D' Haens G, Carbonez A, Rutgeerts P (2003) Influence of immunogenicity on the long-term efficacy of infliximab in Crohn's disease. N Engl J Med 348:601–608

46. van Schie KA, Hart MH, de Groot ER, Kruithof S, Aarden LA, Wolbink GJ, Rispens T (2015) The antibody response against human and chimeric anti-TNF therapeutic antibodies primarily targets the TNF binding region. Ann Rheum Dis 74:311–314

47. Bartelds GM, Krieckaert CLM, Nurmohamed MT, van Schouwenburg PA, Lems WF, Twisk JWR, Dijkmans BAC, Aarden L, Wolbink GJ (2011) Development of antidrug antibodies against adalimumab and association with disease activity and treatment failure during long-term follow-up. JAMA 305:1460–1468

48. Morrison SL, Oi VT (1984) Transfer and expression of immunoglobulin genes. Annu Rev Immunol 2:239–256

49. Jones PT, Dear PH, Foote J, Neuberger MS, Winter G (1986) Replacing the complementarity-determining regions in a human antibody with those from a mouse. Nature 321:522–525

50. Verhoeyen M, Milstein C, Winter G (1988) Reshaping human antibodies: grafting an antilysozyme activity. Science 239:1534–1536

51. Lonberg N, Taylor LD, Harding FA, Trounstine M, Higgins KM, Schramm SR, Kuo CC, Mashayekh R, Wymore K, McCabe JG (1994) Antigen-specific human antibodies from mice comprising four distinct genetic modifications. Nature 368:856–859

52. Mendez MJ, Green LL, Corvalan JR, et al (1997) Functional transplant of megabase human immunoglobulin loci recapitulates human antibody response in mice. Nat Genet 15:146–156

53. McCafferty J, Griffiths AD, Winter G, Chiswell DJ (1990) Phage antibodies: filamentous phage displaying antibody variable domains. Nature 348:552–554

54. Villa A, Trachsel E, Kaspar M, Schliemann C, Sommavilla R, Rybak J-N, Rösli C, Borsi L, Neri D (2008) A high-affinity human monoclonal antibody specific to the alternatively spliced EDA domain of fibronectin efficiently targets tumor neo-vasculature in vivo. Int J Cancer 122:2405–2413

55. Pini A, Viti F, Santucci A, Carnemolla B, Zardi L, Neri P, Neri D (1998) Design and use of a phage display library. Human antibodies with subnanomolar affinity against a marker of angiogenesis eluted from a two-dimensional gel. J Biol Chem 273:21769–21776

56. Brack SS, Silacci M, Birchler M, Neri D (2006) Tumor-targeting properties of novel antibodies specific to the large isoform of tenascin-C. Clin Cancer Res Off J Am Assoc Cancer Res 12:3200–3208

57. Huston JS, Levinson D, Mudgett-Hunter M, Tai MS, Novotný J, Margolies MN, Ridge RJ, Bruccoleri RE, Haber E, Crea R (1988) Protein engineering of antibody binding sites: recovery of specific activity in an anti-digoxin single-chain Fv analogue produced in Escherichia coli. Proc Natl Acad Sci U S A 85:5879–5883

58. Viti F, Tarli L, Giovannoni L, Zardi L, Neri D (1999) Increased Binding Affinity and Valence of Recombinant Antibody Fragments Lead to Improved Targeting of Tumoral Angiogenesis. Cancer Res 59:347–352

59. Borsi L, Balza E, Bestagno M, et al (2002) Selective targeting of tumoral vasculature: Comparison of different formats of an antibody (L19) to the ED-B domain of fibronectin. Int J Cancer 102:75–85

60. Gutbrodt KL, Neri D (2012) Immunocytokines. Antibodies 1:70–87

61. Lewis AL, Chaft J, Girotra M, Fischer GW (2020) Immune checkpoint inhibitors: a narrative review of considerations for the anaesthesiologist. Br J Anaesth 124:251–260

62. Robert C (2020) A decade of immune-checkpoint inhibitors in cancer therapy. Nat Commun 11:3801

63. Patel SA, Minn AJ (2018) Combination Cancer Therapy with Immune Checkpoint Blockade: Mechanisms and Strategies. Immunity 48:417–433

64. Valabrega G, Montemurro F, Aglietta M (2007) Trastuzumab: mechanism of action, resistance and future perspectives in HER2-overexpressing breast cancer. Ann Oncol Off J Eur Soc Med Oncol 18:977–984

65. Kazazi-Hyseni F, Beijnen JH, Schellens JHM (2010) Bevacizumab. The Oncologist 15:819–825

66. Klein C, Lammens A, Schäfer W, Georges G, Schwaiger M, Mössner E, Hopfner K-P, Umaña P, Niederfellner G (2013) Epitope interactions of monoclonal

antibodies targeting CD20 and their relationship to functional properties. mAbs 5:22–33

67. Beckman RA, Weiner LM, Davis HM (2007) Antibody constructs in cancer therapy: protein engineering strategies to improve exposure in solid tumors. Cancer 109:170–179

68. Fujimori K, Covell DG, Fletcher JE, Weinstein JN (1990) A modeling analysis of monoclonal antibody percolation through tumors: a binding-site barrier. J Nucl Med Off Publ Soc Nucl Med 31:1191–1198

69. Sforza V, Martinelli E, Ciardiello F, et al (2016) Mechanisms of resistance to anti-epidermal growth factor receptor inhibitors in metastatic colorectal cancer. World J Gastroenterol 22:6345–6361

70. Weng W-K, Levy R (2003) Two immunoglobulin G fragment C receptor polymorphisms independently predict response to rituximab in patients with follicular lymphoma. J Clin Oncol Off J Am Soc Clin Oncol 21:3940–3947

71. Wang Q, Chung C-Y, Chough S, Betenbaugh MJ (2018) Antibody glycoengineering strategies in mammalian cells. Biotechnol Bioeng 115:1378–1393

72. Preithner S, Elm S, Lippold S, Locher M, Wolf A, da Silva AJ, Baeuerle PA, Prang NS (2006) High concentrations of therapeutic IgG1 antibodies are needed to compensate for inhibition of antibody-dependent cellular cytotoxicity by excess endogenous immunoglobulin G. Mol Immunol 43:1183–1193

73. Nimmerjahn F, Ravetch JV (2007) Antibodies, Fc receptors and cancer. Curr Opin Immunol 19:239–245

74. Lucey DR, Clerici M, Shearer GM (1996) Type 1 and type 2 cytokine dysregulation in human infectious, neoplastic, and inflammatory diseases. Clin Microbiol Rev 9:532–562

75. Spolski R, Gromer D, Leonard WJ (2017) The γ c family of cytokines: fine-tuning signals from IL-2 and IL-21 in the regulation of the immune response. F1000Research 6:1872

76. Ng CT, Mendoza JL, Garcia KC, Oldstone MBA (2016) Alpha and Beta Type 1 Interferon Signaling: Passage for Diverse Biologic Outcomes. Cell 164:349–352

77. Kirkwood J (2002) Cancer immunotherapy: The interferon-α experience. Semin Oncol 29:18–26

78. Welsh RM, Bahl K, Marshall HD, Urban SL (2012) Type 1 interferons and antiviral CD8 T-cell responses. PLoS Pathog 8:e1002352

79. Roche Pharma Roferon®-A läuft aus - Pressemeldungen. In: Roche Dtschl. https://www.roche.de/medien/meldungen/roferon-a-laeuft-aus-5083.html.

80. Lipiäinen T, Peltoniemi M, Sarkhel S, Yrjönen T, Vuorela H, Urtti A, Juppo A (2015) Formulation and stability of cytokine therapeutics. J Pharm Sci 104:307–326

81. Baldo BA (2014) Side effects of cytokines approved for therapy. Drug Saf 37:921–943

82. Vazquez-Lombardi R, Roome B, Christ D (2013) Molecular Engineering of Therapeutic Cytokines. Antibodies 2:426–451

83. McCormack PL, Scott LJ (2004) Interferon-β-1b. CNS Drugs 18:521–546

84. Miller CHT, Maher SG, Young HA (2009) Clinical Use of Interferon-gamma. Ann N Y Acad Sci 1182:69–79

85. Bhatia M, Davenport V, Cairo MS (2007) The role of interleukin-11 to prevent chemotherapy-induced thrombocytopenia in patients with solid tumors, lymphoma, acute myeloid leukemia and bone marrow failure syndromes. Leuk Lymphoma 48:9–15

86. Balkwill F (2009) Tumour necrosis factor and cancer. Nat Rev Cancer 9:361–371

87. van Horssen R, Ten Hagen TLM, Eggermont AMM (2006) TNF-alpha in cancer treatment: molecular insights, antitumor effects, and clinical utility. The Oncologist 11:397–408

88. Konrad MW, Hemstreet G, Hersh EM, Mansell PW, Mertelsmann R, Kolitz JE, Bradley EC (1990) Pharmacokinetics of recombinant interleukin 2 in humans. Cancer Res 50:2009–2017

89. Tang A, Harding F (2019) The challenges and molecular approaches surrounding interleukin-2-based therapeutics in cancer. Cytokine X 1:100001

90. Deshaies RJ (2020) Multispecific drugs herald a new era of biopharmaceutical innovation. Nature 580:329–338

91. Carter PJ, Lazar GA (2018) Next generation antibody drugs: pursuit of the “high-hanging fruit.” Nat Rev Drug Discov 17:197–223

92. Neri D (2019) Antibody-Cytokine Fusions: Versatile Products for the Modulation of Anticancer Immunity. Cancer Immunol Res 7:348–354

93. June CH, O’Connor RS, Kawalekar OU, Ghassemi S, Milone MC (2018) CAR T cell immunotherapy for human cancer. Science 359:1361–1365

94. Cazzamalli S, Dal Corso A, Widmayer F, Neri D (2018) Chemically Defined Antibody- and Small Molecule-Drug Conjugates for in Vivo Tumor Targeting Applications: A Comparative Analysis. J Am Chem Soc 140:1617–1621

95. Halin C, Rondini S, Nilsson F, Berndt A, Kosmehl H, Zardi L, Neri D (2002) Enhancement of the antitumor activity of interleukin-12 by targeted delivery to neovasculature. Nat Biotechnol 20:264–269

96. Wang Q, Chen Y, Park J, Liu X, Hu Y, Wang T, McFarland K, Betenbaugh MJ (2019) Design and Production of Bispecific Antibodies. Antibodies Basel Switz 8:43

97. Labrijn AF, Janmaat ML, Reichert JM, Parren PWHI (2019) Bispecific antibodies: a mechanistic review of the pipeline. Nat Rev Drug Discov 18:585–608

98. Bratt, Linderholm, Monroe, Chamow (2017) Therapeutic IgG-Like Bispecific Antibodies: Modular Versatility and Manufacturing Challenges. BioProcess Int.

99. Lipinski CA, Lombardo F, Dominy BW, Feeney PJ (1997) Experimental and computational approaches to estimate solubility and permeability in drug discovery and development settings. Adv Drug Deliv Rev 23:3–25

100. Klein C, Waldhauer I, Nicolini VG, et al (2017) Cergutuzumab amunaleukin (CEA-IL2v), a CEA-targeted IL-2 variant-based immunocytokine for combination cancer immunotherapy: Overcoming limitations of aldesleukin and conventional IL-2-based immunocytokines. Oncoimmunology 6:e1277306

101. Klein C, Waldhauer I, Nicolini V, et al (2013) Novel Tumor-Targeted, Engineered IL-2 Variant (IL2v)-Based Immunocytokines For Immunotherapy Of Cancer. Blood 122:2278–2278

102. Lansigan F, Nakamura R, Quick DP, Vlock D, Raubitschek A, Gillies SD, Bachanova V (2016) DI-Leu16-IL2, an Anti-CD20-Interleukin-2 Immunocytokine, Is Safe and Active in Patients with Relapsed and Refractory B-Cell Lymphoma: A Report of Maximum Tolerated Dose, Optimal Biologic Dose, and Recommended Phase 2 Dose. Blood 128:620–620

103. Fallon J, Tighe R, Kradjian G, Guzman W, Bernhardt A, Neuteboom B, Lan Y, Sabzevari H, Schlom J, Greiner JW (2014) The immunocytokine NHS-IL12 as a potential cancer therapeutic. Oncotarget 5:1869–1884

104. Galeazzi M, Sebastiani G, Voll R, et al (2018) FRI0118 Dekavil (F8IL10) – update on the results of clinical trials investigating the immunocytokine in patients with rheumatoid arthritis. Ann Rheum Dis 77:603–604

105. Hemmerle T, Zgraggen S, Matasci M, Halin C, Detmar M, Neri D (2014) Antibody-mediated delivery of interleukin 4 to the neo-vasculature reduces chronic skin inflammation. J Dermatol Sci 76:96–103

106. Hemmerle T, Doll F, Neri D (2014) Antibody-based delivery of IL4 to the neovasculature cures mice with arthritis. Proc Natl Acad Sci U S A 111:12008–12012

107. Pasche N, Wulhfard S, Pretto F, Carugati E, Neri D (2012) The Antibody-Based Delivery of Interleukin-12 to the Tumor Neovasculature Eradicates Murine

Models of Cancer in Combination with Paclitaxel. Clin Cancer Res 18:4092–4103

108. Hemmerle T, Neri D (2014) The antibody-based targeted delivery of interleukin-4 and 12 to the tumor neovasculature eradicates tumors in three mouse models of cancer. Int J Cancer 134:467–477

109. Lo K-M, Lan Y, Lauder S, Zhang J, Brunkhorst B, Qin G, Verma R, Courtenay-Luck N, Gillies SD (2007) huBC1-IL12, an immunocytokine which targets EDB-containing oncofetal fibronectin in tumors and tumor vasculature, shows potent anti-tumor activity in human tumor models. Cancer Immunol Immunother CII 56:447–457

110. Frey K, Schliemann C, Schwager K, Giavazzi R, Johannsen M, Neri D (2010) The immunocytokine F8-IL2 improves the therapeutic performance of sunitinib in a mouse model of renal cell carcinoma. J Urol 184:2540–2548

111. Hemmerle T, Probst P, Giovannoni L, Green AJ, Meyer T, Neri D (2013) The antibody-based targeted delivery of TNF in combination with doxorubicin eradicates sarcomas in mice and confers protective immunity. Br J Cancer 109:1206–1213

112. Bootz F, Ziffels B, Neri D (2016) Antibody-Based Targeted Delivery of Interleukin-22 Promotes Rapid Clinical Recovery in Mice With DSS-Induced Colitis. Inflamm Bowel Dis 22:2098–2105

113. Schmid AS, Tintor D, Neri D (2018) Novel antibody-cytokine fusion proteins featuring granulocyte-colony stimulating factor, interleukin-3 and interleukin-4 as payloads. J Biotechnol 271:29–36

114. Ongaro T, Matasci M, Cazzamalli S, Gouyou B, De Luca R, Neri D, Villa A (2019) A novel anti-cancer L19-interleukin-12 fusion protein with an optimized peptide linker efficiently localizes in vivo at the site of tumors. J Biotechnol 291:17–25

115. Hess C, Neri D (2014) Tumor-targeting properties of novel immunocytokines based on murine IL1β and IL6. Protein Eng Des Sel 27:207–213

116. Schwager K, Bootz F, Imesch P, Kaspar M, Trachsel E, Neri D (2011) The antibody-mediated targeted delivery of interleukin-10 inhibits endometriosis in a syngeneic mouse model. Hum Reprod Oxf Engl 26:2344–2352

117. Schwager K, Kaspar M, Bootz F, Marcolongo R, Paresce E, Neri D, Trachsel E (2009) Preclinical characterization of DEKAVIL (F8-IL10), a novel clinical-stage immunocytokine which inhibits the progression of collagen-induced arthritis. Arthritis Res Ther 11:R142

118. Hemmerle T, Neri D (2014) The dose-dependent tumor targeting of antibody-IFNγ fusion proteins reveals an unexpected receptor-trapping mechanism in vivo. Cancer Immunol Res 2:559–567

119. Pasche N, Woytschak J, Wulhfard S, Villa A, Frey K, Neri D (2011) Cloning and characterization of novel tumor-targeting immunocytokines based on murine IL7. J Biotechnol 154:84–92

120. Kaspar M, Trachsel E, Neri D (2007) The Antibody-Mediated Targeted Delivery of Interleukin-15 and GM-CSF to the Tumor Neovasculature Inhibits Tumor Growth and Metastasis. Cancer Res 67:4940–4948

121. Hemmerle T, Wulhfard S, Neri D (2012) A critical evaluation of the tumor-targeting properties of bispecific antibodies based on quantitative biodistribution data. Protein Eng Des Sel PEDS 25:851–854

122. Venetz D, Hess C, Lin C, Aebi M, Neri D (2015) Glycosylation profiles determine extravasation and disease-targeting properties of armed antibodies. Proc Natl Acad Sci U S A 112:2000–2005

123. Halin C, Gafner V, Villani ME, Borsi L, Berndt A, Kosmehl H, Zardi L, Neri D (2003) Synergistic Therapeutic Effects of a Tumor Targeting Antibody Fragment, Fused to Interleukin 12 and to Tumor Necrosis Factor α. Cancer Res 63:3202–3210

124. Kontermann RE (2012) Antibody-cytokine fusion proteins. Arch Biochem Biophys 526:194–205

125. Bootz F, Neri D (2016) Immunocytokines: a novel class of products for the treatment of chronic inflammation and autoimmune conditions. Drug Discov Today 21:180–189

126. Ribas A, Kirkwood JM, Atkins MB, Whiteside TL, Gooding W, Kovar A, Gillies SD, Kashala O, Morse MA (2009) Phase I/II open-label study of the biologic effects of the interleukin-2 immunocytokine EMD 273063 (hu14.18-IL2) in patients with metastatic malignant melanoma. J Transl Med 7:68

127. Jain RK, Baxter LT (1988) Mechanisms of heterogeneous distribution of monoclonal antibodies and other macromolecules in tumors: significance of elevated interstitial pressure. Cancer Res 48:7022–7032

128. King DM, Albertini MR, Schalch H, et al (2004) Phase I Clinical Trial of the Immunocytokine EMD 273063 in Melanoma Patients. J Clin Oncol Off J Am Soc Clin Oncol 22:4463–4473

129. Tzeng A, Kwan BH, Opel CF, Navaratna T, Wittrup KD (2015) Antigen specificity can be irrelevant to immunocytokine efficacy and biodistribution. Proc Natl Acad Sci 112:3320–3325

130. Holliger P, Prospero T, Winter G (1993) “Diabodies”: small bivalent and bispecific antibody fragments. Proc Natl Acad Sci U S A 90:6444–6448

131. Borsi L, Balza E, Carnemolla B, et al (2003) Selective targeted delivery of TNFα to tumor blood vessels. Blood 102:4384–4392

132. Wu AM, Chen W, Raubitschek A, Williams LE, Neumaier M, Fischer R, Hu S, Odom-Maryon T, Wong JYC, Shively JE (1996) Tumor localization of anti-CEA single-chain Fvs: improved targeting by non-covalent dimers. Immunotechnology 2:21–36

133. Adams GP, Tai M-S, McCartney JE, Marks JD, Stafford WF, Houston LL, Huston JS, Weiner LM (2006) Avidity-Mediated Enhancement of In vivo Tumor Targeting by Single-Chain Fv Dimers. Clin Cancer Res 12:1599–1605

134. Schwager K, Hemmerle T, Aebischer D, Neri D (2013) The Immunocytokine L19–IL2 Eradicates Cancer When Used in Combination with CTLA-4 Blockade or with L19-TNF. J Invest Dermatol 133:751–758

135. Matsumoto H, Liao S, Arakawa F, Ueno A, Abe H, Awasthi A, Kuroki M, Kuroki M (2002) Targeting of interleukin-2 to human MK-1-expressing carcinoma by fusion with a single-chain Fv of anti-MK-1 antibody. Anticancer Res 22:2001–2007

136. Gafner V, Trachsel E, Neri D (2006) An engineered antibody–interleukin-12 fusion protein with enhanced tumor vascular targeting properties. Int J Cancer 119:2205–2212

137. Sommavilla R, Pasche N, Trachsel E, Giovannoni L, Roesli C, Villa A, Neri D, Kaspar M (2010) Expression, engineering and characterization of the tumor-targeting heterodimeric immunocytokine F8-IL12. Protein Eng Des Sel PEDS 23:653–661

138. van den Heuvel MM, Verheij M, Boshuizen R, Belderbos J, Dingemans A-MC, De Ruysscher D, Laurent J, Tighe R, Haanen J, Quaratino S (2015) NHS-IL2 combined with radiotherapy: preclinical rationale and phase Ib trial results in metastatic non-small cell lung cancer following first-line chemotherapy. J Transl Med 13:32

139. Galeazzi M, Bazzichi L, Sebastiani GD, et al (2014) A phase IB clinical trial with Dekavil (F8-IL10), an immunoregulatory “armed antibody” for the treatment of rheumatoid arthritis, used in combination wIh methotrexate. Isr Med Assoc J IMAJ 16:666

140. Weide B, Eigentler TK, Pflugfelder A, et al (2014) Intralesional treatment of stage III metastatic melanoma patients with L19-IL2 results in sustained clinical and systemic immunologic responses. Cancer Immunol Res 2:668–678

141. Eigentler TK, Weide B, de Braud F, et al (2011) A dose-escalation and signal-generating study of the immunocytokine L19-IL2 in combination with dacarbazine for the therapy of patients with metastatic melanoma. Clin Cancer Res Off J Am Assoc Cancer Res 17:7732–7742

142. Mm van den H, M V, R B, J B, Am D, D DR, J L, R T, J H, S Q (2015) NHS-IL2 combined with radiotherapy: preclinical rationale and phase Ib trial results in metastatic non-small cell lung cancer following first-line chemotherapy. J Transl Med 13:32–32

143. Osenga KL, Hank JA, Albertini MR, et al (2006) A phase I clinical trial of the hu14.18-IL2 (EMD 273063) as a treatment for children with refractory or recurrent neuroblastoma and melanoma: a study of the Children's Oncology Group. Clin Cancer Res Off J Am Assoc Cancer Res 12:1750–1759

144. Danielli R, Patuzzo R, Di Giacomo AM, et al (2015) Intralesional administration of L19-IL2/L19-TNF in stage III or stage IVM1a melanoma patients: results of a phase II study. Cancer Immunol Immunother CII 64:999–1009

145. Gillies SD, Lan Y, Wesolowski JS, Qian X, Reisfeld RA, Holden S, Super M, Lo KM (1998) Antibody-IL-12 fusion proteins are effective in SCID mouse models of prostate and colon carcinoma metastases. J Immunol Baltim Md 1950 160:6195–6203

146. Paoloni M, Mazcko C, Selting K, et al (2015) Defining the Pharmacodynamic Profile and Therapeutic Index of NHS-IL12 Immunocytokine in Dogs with Malignant Melanoma. PloS One 10:e0129954

147. Kim JW, Heery CR, Bilusic M, Singh NK, Madan RA, Sabzevari H, Schlom J, Gulley JL (2012) First-in-human phase I trial of NHS-IL12 in advanced solid tumors. J Clin Oncol 30:TPS2617–TPS2617

148. Borsi L, Carnemolla B, Nicolò G, Spina B, Tanara G, Zardi L (1992) Expression of different tenascin isoforms in normal, hyperplastic and neoplastic human breast tissues. Int J Cancer 52:688–692

149. Midulla M, Verma R, Pignatelli M, Ritter MA, Courtenay-Luck NS, George AJ (2000) Source of oncofetal ED-B-containing fibronectin: implications of production by both tumor and endothelial cells. Cancer Res 60:164–169

150. Mariani G, Lasku A, Balza E, Gaggero B, Motta C, Di Luca L, Dorcaratto A, Viale GA, Neri D, Zardi L (1997) Tumor targeting potential of the monoclonal antibody BC-1 against oncofetal fibronectin in nude mice bearing human tumor implants. Cancer 80:2378–2384

151. Folli S, Pèlegrin A, Chalandon Y, Yao X, Buchegger F, Lienard D, Lejeune F, Mach JP (1993) Tumor-necrosis factor can enhance radio-antibody uptake in human colon carcinoma xenografts by increasing vascular permeability. Int J Cancer 53:829–836

152. Cooke SP, Pedley RB, Boden R, Begent RHJ, Chester KA (2002) In vivo tumor delivery of a recombinant single chain Fv::tumor necrosis factor-alpha fusion [correction of factor: a fusion] protein. Bioconjug Chem 13:7–15

153. Robert B, Mach JP, Mani JC, Ychou M, Folli S, Artus JC, Pèlegrin A (1996) Cytokine targeting in tumors using a bispecific antibody directed against carcinoembryonic antigen and tumor necrosis factor alpha. Cancer Res 56:4758–4765

154. Probst P, Kopp J, Oxenius A, Colombo MP, Ritz D, Fugmann T, Neri D (2017) Sarcoma Eradication by Doxorubicin and Targeted TNF Relies upon CD8+ T-cell Recognition of a Retroviral Antigen. Cancer Res 77:3644–3654

155. Balza E, Mortara L, Sassi F, Monteghirfo S, Carnemolla B, Castellani P, Neri D, Accolla RS, Zardi L, Borsi L (2006) Targeted delivery of tumor necrosis factor-alpha to tumor vessels induces a therapeutic T cell-mediated immune response that protects the host against syngeneic tumors of different histologic origin. Clin Cancer Res Off J Am Assoc Cancer Res 12:2575–2582

156. Pretto F, Elia G, Castioni N, Neri D (2014) Preclinical evaluation of IL2-based immunocytokines supports their use in combination with dacarbazine, paclitaxel and TNF-based immunotherapy. Cancer Immunol Immunother 63:901–910

157. Balza E, Carnemolla B, Mortara L, Castellani P, Soncini D, Accolla RS, Borsi L (2010) Therapy-induced antitumor vaccination in neuroblastomas by the combined targeting of IL-2 and TNFα. Int J Cancer 127:101–110

158. Spitaleri G, Berardi R, Pierantoni C, et al (2013) Phase I/II study of the tumour-targeting human monoclonal antibody–cytokine fusion protein L19-TNF in patients with advanced solid tumours. J Cancer Res Clin Oncol 139:447–455

159. Papadia F, Basso V, Patuzzo R, et al (2013) Isolated limb perfusion with the tumor-targeting human monoclonal antibody-cytokine fusion protein L19-TNF plus melphalan and mild hyperthermia in patients with locally advanced extremity melanoma. J Surg Oncol 107:173–179

160. Lejeune FJ (1995) High dose recombinant tumour necrosis factor (rTNFα) administered by isolation perfusion for advanced tumours of the limbs: a model for biochemotherapy of cancer. Eur J Cancer 31:1009–1016

161. Kaplon H, Reichert JM (2018) Antibodies to watch in 2018. mAbs 10:183–203

162. Weide B, Neri D, Elia G (2017) Intralesional treatment of metastatic melanoma: a review of therapeutic options. Cancer Immunol Immunother 66:647–656

163. Vlahov IR, Leamon CP (2012) Engineering folate-drug conjugates to target cancer: from chemistry to clinic. Bioconjug Chem 23:1357–1369

164. Krall N, Pretto F, Mattarella M, Müller C, Neri D (2016) A 99mTc-Labeled Ligand of Carbonic Anhydrase IX Selectively Targets Renal Cell Carcinoma In Vivo. J Nucl Med 57:943–949

165. Cazzamalli S, Figueras E, Pethő L, Borbély A, Steinkühler C, Neri D, Sewald N (2018) In Vivo Antitumor Activity of a Novel Acetazolamide-Cryptophycin Conjugate for the Treatment of Renal Cell Carcinomas. ACS Omega 3:14726–14731

166. Low PS, Henne WA, Doorneweerd DD (2008) Discovery and Development of Folic-Acid-Based Receptor Targeting for Imaging and Therapy of Cancer and Inflammatory Diseases. Acc Chem Res 41:120–129

167. Kularatne SA, Venkatesh C, Santhapuram H-KR, Wang K, Vaitilingam B, Henne WA, Low PS (2010) Synthesis and Biological Analysis of Prostate-Specific Membrane Antigen-Targeted Anticancer Prodrugs. J Med Chem 53:7767–7777

168. Krall N, Pretto F, Decurtins W, Bernardes GJL, Supuran CT, Neri D (2014) A small-molecule drug conjugate for the treatment of carbonic anhydrase IX expressing tumors. Angew Chem Int Ed Engl 53:4231–4235

169. Wichert M, Krall N, Decurtins W, Franzini RM, Pretto F, Schneider P, Neri D, Scheuermann J (2015) Dual-display of small molecules enables the discovery of ligand pairs and facilitates affinity maturation. Nat Chem 7:241–249

170. Krall N, Scheuermann J, Neri D (2013) Small targeted cytotoxics: current state and promises from DNA-encoded chemical libraries. Angew Chem Int Ed Engl 52:1384–1402

171. Kulterer OC, Pfaff S, Wadsak W, et al (2020) A microdosing study with 99mTc-PHC-102 for the SPECT/CT imaging of primary and metastatic lesions in renal cell carcinoma patients. J Nucl Med jnumed.120.245530

172. Minn I, Koo SM, Lee HS, et al (2016) [64Cu]XYIMSR-06: A dual-motif CAIX ligand for PET imaging of clear cell renal cell carcinoma. Oncotarget 7:56471–56479

173. Yang X, Minn I, Rowe SP, et al (2015) Imaging of carbonic anhydrase IX with an 111In-labeled dual-motif inhibitor. Oncotarget 6:33733–33742

174. Millul J, Krudewig C, Plaza SD, Puca E, Villa A, Neri D, Cazzamalli S (2020) Immunotherapy with immunocytokines and PD-1 blockade enhances the anticancer activity of small molecule-drug conjugates targeting carbonic anhydrase IX. bioRxiv 2020.06.03.129049

175. O'Shannessy DJ, Somers EB, Smale R, Fu Y-S (2013) Expression of folate receptor-α (FRA) in gynecologic malignancies and its relationship to the tumor type. Int J Gynecol Pathol Off J Int Soc Gynecol Pathol 32:258–268

176. O'Shannessy DJ, Yu G, Smale R, Fu Y-S, Singhal S, Thiel RP, Somers EB, Vachani A (2012) Folate receptor alpha expression in lung cancer: diagnostic and prognostic significance. Oncotarget 3:414–425

177. Morris RT, Joyrich RN, Naumann RW, Shah NP, Maurer AH, Strauss HW, Uszler JM, Symanowski JT, Ellis PR, Harb WA (2014) Phase II study of treatment of advanced ovarian cancer with folate-receptor-targeted therapeutic (vintafolide) and companion SPECT-based imaging agent (99mTc-etarfolatide). Ann Oncol Off J Eur Soc Med Oncol 25:852–858

178. Merck and Endocyte Announce Independent DSMB Recommends Vintafolide PROCEED Phase 3 Trial Be Stopped for Futility Following Interim Analysis. Merck.com

179. Rahbar K, Ahmadzadehfar H, Kratochwil C, et al (2017) German Multicenter Study Investigating 177Lu-PSMA-617 Radioligand Therapy in Advanced Prostate Cancer Patients. J Nucl Med Off Publ Soc Nucl Med 58:85–90

180. Favalli N, Biendl S, Hartmann M, et al (2018) A DNA-Encoded Library of Chemical Compounds Based on Common Scaffolding Structures Reveals the

Impact of Ligand Geometry on Protein Recognition. ChemMedChem 13:1303–1307

181. Dumelin CE, Trüssel S, Buller F, et al (2008) A portable albumin binder from a DNA-encoded chemical library. Angew Chem Int Ed Engl 47:3196–3201

182. Brenner S, Lerner RA (1992) Encoded combinatorial chemistry. Proc Natl Acad Sci 89:5381–5383

183. Clark MA, Acharya RA, Arico-Muendel CC, et al (2009) Design, synthesis and selection of DNA-encoded small-molecule libraries. Nat Chem Biol 5:647–654

184. Goodnow RA, Dumelin CE, Keefe AD (2017) DNA-encoded chemistry: enabling the deeper sampling of chemical space. Nat Rev Drug Discov 16:131–147

185. Alqahtani S, Alandas N, Alsultan A (2019) Estimation of apparent clearance of valproic acid in adult Saudi patients. Int J Clin Pharm 41:1056–1061

186. Dozier JK, Distefano MD (2015) Site-Specific PEGylation of Therapeutic Proteins. Int J Mol Sci 16:25831–25864

187. Fishburn CS (2008) The pharmacology of PEGylation: Balancing PD with PK to generate novel therapeutics. J Pharm Sci 97:4167–4183

188. Duivelshof BL, Murisier A, Camperi J, Fekete S, Beck A, Guillarme D, D'Atri V (2020) Therapeutic Fc-fusion proteins: Current analytical strategies. J Sep Sci. https://doi.org/10.1002/jssc.202000765, Advance online publication.

189. Lagassé HAD, Hengel H, Golding B, Sauna ZE (2019) Fc-Fusion Drugs Have FcγR/C1q Binding and Signaling Properties That May Affect Their Immunogenicity. AAPS J 21:62

190. Sand KMK, Bern M, Nilsen J, Noordzij HT, Sandlie I, Andersen JT (2015) Unraveling the Interaction between FcRn and Albumin: Opportunities for Design of Albumin-Based Therapeutics. Front Immunol 5:682

191. Thorneloe KS, Sepp A, Zhang S, et al (2019) The biodistribution and clearance of AlbudAb, a novel biopharmaceutical medicine platform, assessed via PET imaging in humans. EJNMMI Res 9:45

192. O'Connor-Semmes RL, Lin J, Hodge RJ, Andrews S, Chism J, Choudhury A, Nunez DJ (2014) GSK2374697, a novel albumin-binding domain antibody (AlbudAb), extends systemic exposure of exendin-4: first study in humans--PK/PD and safety. Clin Pharmacol Ther 96:704–712

193. Tijink BM, Laeremans T, Budde M, Walsum MS, Dreier T, Haard HJ de, Leemans CR, Dongen GAMS van (2008) Improved tumor targeting of anti–epidermal growth factor receptor Nanobodies through albumin binding: taking advantage of modular Nanobody technology. Mol Cancer Ther 7:2288–2297

194. Lin J, Hodge RJ, O'Connor-Semmes RL, Nunez DJ (2015) GSK2374697, a long duration glucagon-like peptide-1 (GLP-1) receptor agonist, reduces postprandial

circulating endogenous total GLP-1 and peptide YY in healthy subjects. Diabetes Obes Metab 17:1007–1010

195. Hollander PA (2012) Insulin detemir for the treatment of obese patients with type 2 diabetes. Diabetes Metab Syndr Obes Targets Ther 5:11–19

196. Arnolds S, Kuglin B, Kapitza C, Heise T (2010) How pharmacokinetic and pharmacodynamic principles pave the way for optimal basal insulin therapy in type 2 diabetes. Int J Clin Pract 64:1415–1424

197. Zorzi A, Middendorp SJ, Wilbs J, Deyle K, Heinis C (2017) Acylated heptapeptide binds albumin with high affinity and application as tag furnishes long-acting peptides. Nat Commun 8:16092

198. Trüssel S, Dumelin C, Frey K, Villa A, Buller F, Neri D (2009) New strategy for the extension of the serum half-life of antibody fragments. Bioconjug Chem 20:2286–2292

199. Ahlskog JKJ, Dumelin CE, Trüssel S, Mårlind J, Neri D (2009) In vivo targeting of tumor-associated carbonic anhydrases using acetazolamide derivatives. Bioorg Med Chem Lett 19:4851–4856

200. Zimmermann G, Neri D (2016) DNA-encoded chemical libraries: foundations and applications in lead discovery. Drug Discov Today 21:1828–1834

201. Tsuchikama K, An Z (2018) Antibody-drug conjugates: recent advances in conjugation and linker chemistries. Protein Cell 9:33–46

202. Casi G, Neri D (2015) Antibody–Drug Conjugates and Small Molecule–Drug Conjugates: Opportunities and Challenges for the Development of Selective Anticancer Cytotoxic Agents. J Med Chem 58:8751–8761

203. Stefan N, Gébleux R, Waldmeier L, Hell T, Escher M, Wolter FI, Grawunder U, Beerli RR (2017) Highly Potent, Anthracycline-based Antibody–Drug Conjugates Generated by Enzymatic, Site-specific Conjugation. Mol Cancer Ther 16:879–892

204. Baeuerle PA, Reinhardt C (2009) Bispecific T-cell engaging antibodies for cancer therapy. Cancer Res 69:4941–4944

205. Spiess C, Zhai Q, Carter PJ (2015) Alternative molecular formats and therapeutic applications for bispecific antibodies. Mol Immunol 67:95–106

206. Topp MS, Gökbuget N, Stein AS, et al (2015) Safety and activity of blinatumomab for adult patients with relapsed or refractory B-precursor acute lymphoblastic leukaemia: a multicentre, single-arm, phase 2 study. Lancet Oncol 16:57–66

207. Friedberg JW, Fisher RI (2004) Iodine-131 tositumomab (Bexxar): radioimmunoconjugate therapy for indolent and transformed B-cell non-Hodgkin’s lymphoma. Expert Rev Anticancer Ther 4:18–26

208. Puvvada SD, Guillén-Rodríguez JM, Yan J, Inclán L, Heard K, Rivera XI, Anwer F, Mahadevan D, Schatz JH, Persky DO (2018) Yttrium-90-Ibritumomab Tiuxetan (Zevalin®) Radioimmunotherapy after Cytoreduction with ESHAP Chemotherapy in Patients with Relapsed Follicular Non-Hodgkin Lymphoma: Final Results of a Phase II Study. Oncology 94:274–280

209. Noelle RJ, Nowak EC (2010) Cellular sources and immune functions of interleukin-9. Nat Rev Immunol 10:683–7

210. Gessner A, Blum H, Röllinghoff M (1993) Differential regulation of IL-9-expression after infection with Leishmania major in susceptible and resistant mice. Immunobiology 189:419–435

211. Wilhelm C, Hirota K, Stieglitz B, Van Snick J, Tolaini M, Lahl K, Sparwasser T, Helmby H, Stockinger B (2011) An IL-9 fate reporter demonstrates the induction of an innate IL-9 response in lung inflammation. Nat Immunol 12:1071–1077

212. Licona-Limón P, Henao-Mejia J, Temann AU, Gagliani N, Licona-Limón I, Ishigame H, Hao L, Herbert DR, Flavell RA (2013) Th9 Cells Drive Host Immunity against Gastrointestinal Worm Infection. Immunity 39:744–757

213. Tan C, Aziz MK, Lovaas JD, Vistica BP, Shi G, Wawrousek EF, Gery I (2010) Antigen-specific Th9 cells exhibit uniqueness in their kinetics of cytokine production and short retention at the inflammatory site. J Immunol Baltim Md 1950 185:6795–6801

214. Peng Y, Gao X, Yang J, Shekhar S, Wang S, Fan Y, Yang X (2015) Chlamydial Lung Infection Induces Transient IL-9 Production Which Is Redundant for Host Defense against Primary Infection. PLoS ONE 10:e0115195

215. Monteiro M, Agua-Doce A, Almeida CF, Fonseca-Pereira D, Veiga-Fernandes H, Graca L (2015) IL-9 Expression by Invariant NKT Cells Is Not Imprinted during Thymic Development. J Immunol Baltim Md 1950 195:3463–3471

216. Schmitt E, Germann T, Goedert S, Hoehn P, Huels C, Koelsch S, Kühn R, Müller W, Palm N, Rüde E (1994) IL-9 production of naive CD4+ T cells depends on IL-2, is synergistically enhanced by a combination of TGF-beta and IL-4, and is inhibited by IFN-gamma. J Immunol Baltim Md 1950 153:3989–3996

217. Veldhoen M (2009) The role of T helper subsets in autoimmunity and allergy. Curr Opin Immunol 21:606–611

218. Dardalhon V, Korn T, Kuchroo VK, Anderson AC (2008) Role of Th1 and Th17 cells in organ-specific autoimmunity. J Autoimmun 31:252–256

219. Nowak EC, Weaver CT, Turner H, Begum-Haque S, Becher B, Schreiner B, Coyle AJ, Kasper LH, Noelle RJ (2009) IL-9 as a mediator of Th17-driven inflammatory disease. J Exp Med 206:1653–1660

220. Elyaman W, Bradshaw EM, Uyttenhove C, et al (2009) IL-9 induces differentiation of TH17 cells and enhances function of FoxP3+ natural regulatory T cells. Proc Natl Acad Sci U S A 106:12885–12890

221. Lu L-F, Lind EF, Gondek DC, et al (2006) Mast cells are essential intermediaries in regulatory T-cell tolerance. Nature 442:997–1002

222. Hültner L, Kölsch S, Stassen M, Kaspers U, Kremer JP, Mailhammer R, Moeller J, Broszeit H, Schmitt E (2000) In activated mast cells, IL-1 up-regulates the production of several Th2-related cytokines including IL-9. J Immunol Baltim Md 1950 164:5556–5563

223. Gounni AS, Nutku E, Koussih L, Aris F, Louahed J, Levitt RC, Nicolaides NC, Hamid Q (2000) IL-9 expression by human eosinophils: regulation by IL-1beta and TNF-alpha. J Allergy Clin Immunol 106:460–466

224. Turner J-E, Morrison PJ, Wilhelm C, Wilson M, Ahlfors H, Renauld J-C, Panzer U, Helmby H, Stockinger B (2013) IL-9-mediated survival of type 2 innate lymphoid cells promotes damage control in helminth-induced lung inflammation. J Exp Med 210:2951–2965

225. Rochman Y, Spolski R, Leonard WJ (2009) New insights into the regulation of T cells by gamma(c) family cytokines. Nat Rev Immunol 9:480–490

226. Bradley BL, Azzawi M, Jacobson M, Assoufi B, Collins JV, Irani AM, Schwartz LB, Durham SR, Jeffery PK, Kay AB (1991) Eosinophils, T-lymphocytes, mast cells, neutrophils, and macrophages in bronchial biopsy specimens from atopic subjects with asthma: comparison with biopsy specimens from atopic subjects without asthma and normal control subjects and relationship to bronchial hyperresponsiveness. J Allergy Clin Immunol 88:661–674

227. Kay AB (1991) Asthma and inflammation. J Allergy Clin Immunol 87:893–910

228. Weigmann B, Neurath MF (2017) Th9 cells in inflammatory bowel diseases. Semin Immunopathol 39:89–95

229. Wan J, Wu Y, Ji X, Huang L, Cai W, Su Z, Wang S, Xu H (2020) IL-9 and IL-9-producing cells in tumor immunity. Cell Commun Signal 18:50

230. Townsend JM, Fallon GP, Matthews JD, Smith P, Jolin EH, McKenzie NA (2000) IL-9-deficient mice establish fundamental roles for IL-9 in pulmonary mastocytosis and goblet cell hyperplasia but not T cell development. Immunity 13:573–583

231. Schmitt E, Van Brandwijk R, Van Snick J, Siebold B, Rüde E (1989) TCGF III/P40 is produced by naive murine CD4+ T cells but is not a general T cell growth factor. Eur J Immunol 19:2167–2170

232. Uyttenhove C, Simpson RJ, Van Snick J (1988) Functional and structural characterization of P40, a mouse glycoprotein with T-cell growth factor activity. Proc Natl Acad Sci U S A 85:6934–6938

233. Mesplès B, Fontaine RH, Lelièvre V, Launay J-M, Gressens P (2005) Neuronal TGF-beta1 mediates IL-9/mast cell interaction and exacerbates excitotoxicity in newborn mice. Neurobiol Dis 18:193–205

234. Wiener Z, Falus A, Toth S (2004) IL-9 increases the expression of several cytokines in activated mast cells, while the IL-9-induced IL-9 production is inhibited in mast cells of histamine-free transgenic mice. Cytokine 26:122–130

235. Lora JM, Al-Garawi A, Pickard MD, Price KS, Bagga S, Sicoli J, Hodge MR, Gutiérrez-Ramos J-C, Briskin MJ, Boyce JA (2003) FcepsilonRI-dependent gene expression in human mast cells is differentially controlled by T helper type 2 cytokines. J Allergy Clin Immunol 112:1119–1126

236. Chakraborty S, Kubatzky KF, Mitra DK (2019) An Update on Interleukin-9: From Its Cellular Source and Signal Transduction to Its Role in Immunopathogenesis. Int J Mol Sci 20:2113

237. Li J, Chen S, Xiao X, Zhao Y, Ding W, Li XC (2017) IL-9 and Th9 cells in health and diseases—from tolerance to immunopathology. Cytokine Growth Factor Rev 37:47–55

238. Goswami R, Kaplan MH (2011) A brief history of IL-9. J Immunol Baltim Md 1950 186:3283–3288

239. Faulkner H, Renauld J-C, Van Snick J, Grencis RK (1998) Interleukin-9 Enhances Resistance to the Intestinal Nematode Trichuris muris. Infect Immun 66:3832–3840

240. Shimbara A, Christodoulopoulos P, Soussi-Gounni A, et al (2000) IL-9 and its receptor in allergic and nonallergic lung disease: increased expression in asthma. J Allergy Clin Immunol 105:108–115

241. Sugimoto N, Suzukawa M, Nagase H, et al (2019) IL-9 Blockade Suppresses Silica-induced Lung Inflammation and Fibrosis in Mice. Am J Respir Cell Mol Biol 60:232–243

242. Wilhelm C, Turner J-E, Van Snick J, Stockinger B (2012) The many lives of IL-9: a question of survival? Nat Immunol 13:637–641

243. Moretti S, Renga G, Oikonomou V, et al (2017) A mast cell-ILC2-Th9 pathway promotes lung inflammation in cystic fibrosis. Nat Commun 8:14017

244. Temann U-A, Laouar Y, Eynon EE, Homer R, Flavell RA (2007) IL9 leads to airway inflammation by inducing IL13 expression in airway epithelial cells. Int Immunol 19:1–10

245. Temann U-A, Ray P, Flavell RA (2002) Pulmonary overexpression of IL-9 induces Th2 cytokine expression, leading to immune pathology. J Clin Invest 109:29–39

246. Temann UA, Geba GP, Rankin JA, Flavell RA (1998) Expression of interleukin 9 in the lungs of transgenic mice causes airway inflammation, mast cell hyperplasia, and bronchial hyperresponsiveness. J Exp Med 188:1307–1320

247. Whittaker L, Niu N, Temann U-A, Stoddard A, Flavell RA, Ray A, Homer RJ, Cohn L (2002) Interleukin-13 mediates a fundamental pathway for airway

epithelial mucus induced by CD4 T cells and interleukin-9. Am J Respir Cell Mol Biol 27:593–602

248. McMillan SJ, Bishop B, Townsend MJ, McKenzie AN, Lloyd CM (2002) The absence of interleukin 9 does not affect the development of allergen-induced pulmonary inflammation nor airway hyperreactivity. J Exp Med 195:51–57

249. Zou S-C, Pang L-L, Mao Q-S, Wu S-Y, Xiao Q-F (2018) IL-9 exacerbates the development of chronic obstructive pulmonary disease through oxidative stress. Eur Rev Med Pharmacol Sci 22:8877–8884

250. Arras M, Huaux F, Vink A, Delos M, Coutelier JP, Many MC, Barbarin V, Renauld JC, Lison D (2001) Interleukin-9 reduces lung fibrosis and type 2 immune polarization induced by silica particles in a murine model. Am J Respir Cell Mol Biol 24:368–375

251. Oh CK, Leigh R, McLaurin KK, Kim K, Hultquist M, Molfino NA (2013) A randomized, controlled trial to evaluate the effect of an anti-interleukin-9 monoclonal antibody in adults with uncontrolled asthma. Respir Res 14:93

252. Renauld JC, van der Lugt N, Vink A, van Roon M, Godfraind C, Warnier G, Merz H, Feller A, Berns A, Van Snick J (1994) Thymic lymphomas in interleukin 9 transgenic mice. Oncogene 9:1327–1332

253. Zhang J, Wang W, Geng Q-R, Wang L, Chen X-Q, Liu C-C, Lv Y (2014) Serum levels of interleukin-9 correlate with negative prognostic factors in extranodal NK/T-cell lymphoma. PloS One 9:e94637

254. Purwar R, Schlapbach C, Xiao S, et al (2012) Robust tumor immunity to melanoma mediated by interleukin-9-producing T cells. Nat Med 18:1248–1253

255. Do Thi VA, Park SM, Lee H, Kim YS (2018) Ectopically Expressed Membrane-bound Form of IL-9 Exerts Immune-stimulatory Effect on CT26 Colon Carcinoma Cells. Immune Netw 18:e12

256. Wang J, Sun M, Zhao H, Huang Y, Li D, Mao D, Zhang Z, Zhu X, Dong X, Zhao X (2019) IL-9 Exerts Antitumor Effects in Colon Cancer and Transforms the Tumor Microenvironment In Vivo. Technol Cancer Res Treat 18:1533033819857737

257. Donninelli G, Saraf-Sinik I, Mazziotti V, Capone A, Grasso MG, Battistini L, Reynolds R, Magliozzi R, Volpe E (2020) Interleukin-9 regulates macrophage activation in the progressive multiple sclerosis brain. J Neuroinflammation 17:149

258. Dantas AT, Marques CDL, da Rocha Junior LF, et al (2015) Increased Serum Interleukin-9 Levels in Rheumatoid Arthritis and Systemic Lupus Erythematosus: Pathogenic Role or Just an Epiphenomenon? Dis Markers 2015:e519638

259. Matusiewicz M, Neubauer K, Bednarz-Misa I, Gorska S, Krzystek-Korpacka M (2017) Systemic interleukin-9 in inflammatory bowel disease: Association with mucosal healing in ulcerative colitis. World J Gastroenterol 23:4039–4046

260. Ouyang H, Shi Y, Liu Z, Feng S, Li L, Su N, Lu Y, Kong S (2013) Increased interleukin-9 and CD4+IL-9+ T cells in patients with systemic lupus erythematosus. Mol Med Rep 7:1031–1037

261. Kim HS, Chung DH (2013) IL-9-producing invariant NKT cells protect against DSS-induced colitis in an IL-4-dependent manner. Mucosal Immunol 6:347–357

262. Gerlach K, Hwang Y, Nikolaev A, et al (2014) TH9 cells that express the transcription factor PU.1 drive T cell-mediated colitis via IL-9 receptor signaling in intestinal epithelial cells. Nat Immunol 15:676–686

263. Gerlach K, McKenzie AN, Neurath MF, Weigmann B (2015) IL-9 regulates intestinal barrier function in experimental T cell-mediated colitis. Tissue Barriers 3:e983777

264. Li L, Huang S, Wang H, et al (2018) Cytokine IL9 Triggers the Pathogenesis of Inflammatory Bowel Disease Through the miR21-CLDN8 Pathway. Inflamm Bowel Dis 24:2211–2223

265. Li H, Nourbakhsh B, Cullimore M, Zhang G-X, Rostami A (2011) IL-9 is important for T-cell activation and differentiation in autoimmune inflammation of the central nervous system. Eur J Immunol 41:2197–2206

266. Li H, Nourbakhsh B, Ciric B, Zhang G-X, Rostami A (2010) Neutralization of IL-9 Ameliorates Experimental Autoimmune Encephalomyelitis by Decreasing the Effector T Cell Population. J Immunol 185:4095–4100

267. Yoshimura S, Thome R, Konno S, et al (2020) IL-9 Controls Central Nervous System Autoimmunity by Suppressing GM-CSF Production. J Immunol 204:531–539

268. Ciccia F, Guggino G, Rizzo A, et al (2015) Potential involvement of IL-9 and Th9 cells in the pathogenesis of rheumatoid arthritis. Rheumatol Oxf Engl 54:2264–2272

269. Rauber S, Luber M, Weber S, et al (2017) Resolution of inflammation by interleukin-9-producing type 2 innate lymphoid cells. Nat Med 23:938–944

270. Boyman O, Sprent J (2012) The role of interleukin-2 during homeostasis and activation of the immune system. Nat Rev Immunol 12:180–190

271. Matsuoka K, Koreth J, Kim HT, et al (2013) Low-dose interleukin-2 therapy restores regulatory T cell homeostasis in patients with chronic graft-versus-host disease. Sci Transl Med 5:179ra43

272. Rosenberg SA (2014) IL-2: the first effective immunotherapy for human cancer. J Immunol Baltim Md 1950 192:5451–5458

273. Arenas-Ramirez N, Woytschak J, Boyman O (2015) Interleukin-2: Biology, Design and Application. Trends Immunol 36:763–777

274. Chavez AR de V, Buchser W, Basse PH, Liang X, Appleman LJ, Maranchie JK, Zeh H, de Vera ME, Lotze MT (2009) Pharmacologic administration of interleukin-2. Ann N Y Acad Sci 1182:14–27

275. Abbas AK, Trotta E, Simeonov DR, Marson A, Bluestone JA (2018) Revisiting IL-2: Biology and therapeutic prospects. Sci Immunol 3:eaat1482

276. Chen X, Ai X, Wu C, Wang H, Zeng G, Yang P, Liu G (2018) A novel human IL-2 mutein with minimal systemic toxicity exerts greater antitumor efficacy than wild-type IL-2. Cell Death Dis 9:1–12

277. Shanafelt AB, Lin Y, Shanafelt MC, et al (2000) A T-cell-selective interleukin 2 mutein exhibits potent antitumor activity and is well tolerated in vivo. Nat Biotechnol 18:1197–1202

278. Levin AM, Bates DL, Ring AM, et al (2012) Exploiting a natural conformational switch to engineer an interleukin-2 “superkine.” Nature 484:529–533

279. Mitra S, Ring AM, Amarnath S, et al (2015) Interleukin-2 activity can be fine tuned with engineered receptor signaling clamps. Immunity 42:826–838

280. Boyman O, Kovar M, Rubinstein MP, Surh CD, Sprent J (2006) Selective stimulation of T cell subsets with antibody-cytokine immune complexes. Science 311:1924–1927

281. Trotta E, Bessette PH, Silveria SL, et al (2018) A human anti-IL-2 antibody that potentiates regulatory T cells by a structure-based mechanism. Nat Med 24:1005–1014

282. Spangler JB, Tomala J, Luca VC, Jude KM, Dong S, Ring AM, Votavova P, Pepper M, Kovar M, Garcia KC (2015) Antibodies to Interleukin-2 Elicit Selective T Cell Subset Potentiation through Distinct Conformational Mechanisms. Immunity 42:815–825

283. Charych D, Khalili S, Dixit V, et al (2017) Modeling the receptor pharmacology, pharmacokinetics, and pharmacodynamics of NKTR-214, a kinetically-controlled interleukin-2 (IL2) receptor agonist for cancer immunotherapy. PLOS ONE 12:e0179431

284. BMJ Publishing Group L (2017) 32nd Annual Meeting and Pre-Conference Programs of the Society for Immunotherapy of Cancer (SITC 2017): Part One. J Immunother Cancer 5:86

285. De Luca R, Gouyou B, Ongaro T, Villa A, Ziffels B, Sannino A, Buttinoni G, Galeazzi S, Mazzacuva M, Neri D (2019) A Novel Fully-Human Potency-Matched Dual Cytokine-Antibody Fusion Protein Targets Carbonic Anhydrase IX in Renal Cell Carcinomas. Front Oncol 9:1228

286. Sabzevari H, Gillies SD, Mueller BM, Pancook JD, Reisfeld RA (1994) A recombinant antibody-interleukin 2 fusion protein suppresses growth of hepatic human neuroblastoma metastases in severe combined immunodeficiency mice. Proc Natl Acad Sci U S A 91:9626–9630

287. Carnemolla B, Borsi L, Balza E, Castellani P, Meazza R, Berndt A, Ferrini S, Kosmehl H, Neri D, Zardi L (2002) Enhancement of the antitumor properties of interleukin-2 by its targeted delivery to the tumor blood vessel extracellular matrix. Blood 99:1659–1665

288. Wagner K, Schulz P, Scholz A, Wiedenmann B, Menrad A (2008) The targeted immunocytokine L19-IL2 efficiently inhibits the growth of orthotopic pancreatic cancer. Clin Cancer Res Off J Am Assoc Cancer Res 14:4951–4960

289. Mårlind J, Kaspar M, Trachsel E, Sommavilla R, Hindle S, Bacci C, Giovannoni L, Neri D (2008) Antibody-mediated delivery of interleukin-2 to the stroma of breast cancer strongly enhances the potency of chemotherapy. Clin Cancer Res Off J Am Assoc Cancer Res 14:6515–6524

290. Ridgway JB, Presta LG, Carter P (1996) “Knobs-into-holes” engineering of antibody CH3 domains for heavy chain heterodimerization. Protein Eng 9:617–621

291. Gillies SD, Lan Y, Hettmann T, Brunkhorst B, Sun Y, Mueller SO, Lo K-M (2011) A Low-Toxicity IL-2–Based Immunocytokine Retains Antitumor Activity Despite Its High Degree of IL-2 Receptor Selectivity. Clin Cancer Res 17:3673–3685

292. Sharifi, Khawli L, Hu P, King S, Epstein A (2001) Characterization of a phage display-derived human monoclonal antibody (NHS76) counterpart to chimeric TNT-1 directed against necrotic regions of solid tumors. Hybrid Hybridomics 20:305–12

293. Catania C, Maur M, Berardi R, et al (2015) The tumor-targeting immunocytokine F16-IL2 in combination with doxorubicin: dose escalation in patients with advanced solid tumors and expansion into patients with metastatic breast cancer. Cell Adhes Migr 9:14–21

294. Pedretti M, Rancic Z, Soltermann A, Herzog BA, Schliemann C, Lachat M, Neri D, Kaufmann PA (2010) Comparative immunohistochemical staining of atherosclerotic plaques using F16, F8 and L19: Three clinical-grade fully human antibodies. Atherosclerosis 208:382–389

295. Santimaria M, Moscatelli G, Viale GL, et al (2003) Immunoscintigraphic Detection of the ED-B Domain of Fibronectin, a Marker of Angiogenesis, in Patients with Cancer. Clin Cancer Res 9:571–579

296. Poli GL, Bianchi C, Virotta G, Bettini A, Moretti R, Trachsel E, Elia G, Giovannoni L, Neri D, Bruno A (2013) Radretumab radioimmunotherapy in patients with brain metastasis: a 124I-L19SIP dosimetric PET study. Cancer Immunol Res 1:134–143

297. Erba PA, Sollini M, Orciuolo E, et al (2012) Radioimmunotherapy with radretumab in patients with relapsed hematologic malignancies. J Nucl Med 53:922–927

298. Johannsen M, Spitaleri G, Curigliano G, et al (2010) The tumour-targeting human L19-IL2 immunocytokine: Preclinical safety studies, phase I clinical trial in patients with solid tumours and expansion into patients with advanced renal cell carcinoma. Eur J Cancer 46:2926–2935

299. Danielli R, Patuzzo R, Di Giacomo AM, et al (2015) Intralesional administration of L19-IL2/L19-TNF in stage III or stage IVM1a melanoma patients: results of a phase II study. Cancer Immunol Immunother CII 64:999–1009

300. Heuveling DA, de Bree R, Vugts DJ, Huisman MC, Giovannoni L, Hoekstra OS, Leemans CR, Neri D, van Dongen GAMS (2013) Phase 0 microdosing PET study using the human mini antibody F16SIP in head and neck cancer patients. J Nucl Med Off Publ Soc Nucl Med 54:397–401

301. Schliemann C, Gutbrodt KL, Kerkhoff A, et al (2015) Targeting interleukin-2 to the bone marrow stroma for therapy of acute myeloid leukemia relapsing after allogeneic hematopoietic stem cell transplantation. Cancer Immunol Res 3:547–556

302. Tatemoto K, Hosoya M, Habata Y, et al (1998) Isolation and characterization of a novel endogenous peptide ligand for the human APJ receptor. Biochem Biophys Res Commun 251:471–476

303. Pitkin SL, Maguire JJ, Bonner TI, Davenport AP (2010) International Union of Basic and Clinical Pharmacology. LXXIV. Apelin receptor nomenclature, distribution, pharmacology, and function. Pharmacol Rev 62:331–342

304. Shin K, Kenward C, Rainey JK (2017) Apelinergic system structure and function. Compr Physiol 8:407–450

305. Vickers C, Hales P, Kaushik V, et al (2002) Hydrolysis of biological peptides by human angiotensin-converting enzyme-related carboxypeptidase. J Biol Chem 277:14838–14843

306. Yang P, Kuc RE, Brame AL, Dyson A, Singer M, Glen RC, Cheriyan J, Wilkinson IB, Davenport AP, Maguire JJ (2017) [Pyr1]Apelin-13(1–12) Is a Biologically Active ACE2 Metabolite of the Endogenous Cardiovascular Peptide [Pyr1]Apelin-13. Front Neurosci 11:92

307. Murza A, Parent A, Besserer-Offroy E, Tremblay H, Karadereye F, Beaudet N, Leduc R, Sarret P, Marsault É (2012) Elucidation of the Structure–Activity Relationships of Apelin: Influence of Unnatural Amino Acids on Binding, Signaling, and Plasma Stability. ChemMedChem 7:318–325

308. Ma Y, Yue Y, Ma Y, et al (2017) Structural Basis for Apelin Control of the Human Apelin Receptor. Structure 25:858-866.e4

309. Yamaleyeva LM, Shaltout HA, Varagic J (2016) Apelin-13 in blood pressure regulation and cardiovascular disease. Curr Opin Nephrol Hypertens 25:396–403

310. Japp AG, Cruden NL, Amer DAB, et al (2008) Vascular Effects of Apelin In Vivo in Man. J Am Coll Cardiol 52:908–913

311. Evans NA, Groarke DA, Warrack J, Greenwood CJ, Dodgson K, Milligan G, Wilson S (2001) Visualizing differences in ligand-induced beta-arrestin-GFP interactions and trafficking between three recently characterized G protein-coupled receptors. J Neurochem 77:476–485

312. Masri B, Morin N, Pedebernade L, Knibiehler B, Audigier Y (2006) The apelin receptor is coupled to Gi1 or Gi2 protein and is differentially desensitized by apelin fragments. J Biol Chem 281:18317–18326

313. Murza A, Belleville K, Longpré J-M, Sarret P, Marsault É (2014) Stability and degradation patterns of chemically modified analogs of apelin-13 in plasma and cerebrospinal fluid. Pept Sci 102:297–303

314. Read C, Yang P, Kuc RE, et al (2020) Apelin peptides linked to anti-serum albumin domain antibodies retain affinity in vitro and are efficacious receptor agonists in vivo. Basic Clin Pharmacol Toxicol 126 Suppl 6:96–103

315. Wang W, Zhang D, Yang R, et al (2018) Hepatic and cardiac beneficial effects of a long-acting Fc-apelin fusion protein in diet-induced obese mice. Diabetes Metab Res Rev 34:e2997

316. Vinel C, Lukjanenko L, Batut A, et al (2018) The exerkine apelin reverses age-associated sarcopenia. Nat Med 24:1360–1371

317. Bertrand C, Valet P, Castan-Laurell I (2015) Apelin and energy metabolism. Front Physiol 6:115

318. Yue P, Jin H, Xu S, Aillaud M, Deng AC, Azuma J, Kundu RK, Reaven GM, Quertermous T, Tsao PS (2011) Apelin decreases lipolysis via G(q), G(i), and AMPK-Dependent Mechanisms. Endocrinology 152:59–68

319. Higuchi K, Masaki T, Gotoh K, Chiba S, Katsuragi I, Tanaka K, Kakuma T, Yoshimatsu H (2007) Apelin, an APJ Receptor Ligand, Regulates Body Adiposity and Favors the Messenger Ribonucleic Acid Expression of Uncoupling Proteins in Mice. Endocrinology 148:2690–2697

320. Dray C, Knauf C, Daviaud D, et al (2008) Apelin stimulates glucose utilization in normal and obese insulin-resistant mice. Cell Metab 8:437–445

321. Attané C, Daviaud D, Dray C, Dusaulcy R, Masseboeuf M, Prévot D, Carpéné C, Castan-Laurell I, Valet P (2011) Apelin stimulates glucose uptake but not lipolysis in human adipose tissue ex vivo. J Mol Endocrinol 46:21–28

322. Gourdy P, Cazals L, Thalamas C, et al (2018) Apelin administration improves insulin sensitivity in overweight men during hyperinsulinaemic-euglycaemic clamp. Diabetes Obes Metab 20:157–164

323. Salcedo A, Garijo J, Monge L, Fernández N, Luis García-Villalón A, Sánchez Turrión V, Cuervas-Mons V, Diéguez G (2007) Apelin effects in human splanchnic arteries. Role of nitric oxide and prostanoids. Regul Pept 144:50–55

324. Ashley EA, Powers J, Chen M, et al (2005) The endogenous peptide apelin potently improves cardiac contractility and reduces cardiac loading in vivo. Cardiovasc Res 65:73–82

325. Lee DK, Cheng R, Nguyen T, Fan T, Kariyawasam AP, Liu Y, Osmond DH, George SR, O'Dowd BF (2000) Characterization of apelin, the ligand for the APJ receptor. J Neurochem 74:34–41

326. Tatemoto K, Takayama K, Zou MX, Kumaki I, Zhang W, Kumano K, Fujimiya M (2001) The novel peptide apelin lowers blood pressure via a nitric oxide-dependent mechanism. Regul Pept 99:87–92

327. Cheng X, Cheng XS, Pang CCY (2003) Venous dilator effect of apelin, an endogenous peptide ligand for the orphan APJ receptor, in conscious rats. Eur J Pharmacol 470:171–175

328. Berry MF, Pirolli TJ, Jayasankar V, Burdick J, Morine KJ, Gardner TJ, Woo YJ (2004) Apelin has in vivo inotropic effects on normal and failing hearts. Circulation 110:II187-193

329. Japp A.G., Cruden N.L., Barnes G., et al (2010) Acute Cardiovascular Effects of Apelin in Humans. Circulation 121:1818–1827

330. Gomez-Arroyo JG, Farkas L, Alhussaini AA, Farkas D, Kraskauskas D, Voelkel NF, Bogaard HJ (2012) The monocrotaline model of pulmonary hypertension in perspective. Am J Physiol Lung Cell Mol Physiol 302:L363-369

331. Falcão-Pires I, Gonçalves N, Henriques-Coelho T, Moreira-Gonçalves D, Roncon-Albuquerque R, Leite-Moreira AF (2009) Apelin decreases myocardial injury and improves right ventricular function in monocrotaline-induced pulmonary hypertension. Am J Physiol Heart Circ Physiol 296:H2007-2014

332. Alastalo T-P, Li M, de Jesus Perez V, et al (2011) Disruption of PPARγ/β-catenin–mediated regulation of apelin impairs BMP-induced mouse and human pulmonary arterial EC survival. J Clin Invest 121:3735–3746

333. Brash L, Barnes GD, Brewis MJ, et al (2018) Short-Term Hemodynamic Effects of Apelin in Patients With Pulmonary Arterial Hypertension. JACC Basic Transl Sci 3:176–186

334. Gengenbacher N, Singhal M, Augustin HG (2017) Preclinical mouse solid tumour models: status quo, challenges and perspectives. Nat Rev Cancer 17:751–765

335. Herter-Sprie GS, Kung AL, Wong K-K (2013) New cast for a new era: preclinical cancer drug development revisited. J Clin Invest 123:3639–3645

336. Ireson CR, Alavijeh MS, Palmer AM, Fowler ER, Jones HJ (2019) The role of mouse tumour models in the discovery and development of anticancer drugs. Br J Cancer 121:101–108

337. Day C-P, Merlino G, Van Dyke T (2015) Preclinical mouse cancer models: a maze of opportunities and challenges. Cell 163:39–53

338. Corbett TH, Griswold DP, Roberts BJ, Peckham JC, Schabel FM (1975) Tumor induction relationships in development of transplantable cancers of the colon in mice for chemotherapy assays, with a note on carcinogen structure. Cancer Res 35:2434–2439

339. Talmadge JE, Fidler IJ (1982) Enhanced Metastatic Potential of Tumor Cells Harvested From Spontaneous Metastases of Heterogeneous Murine Tumors. JNCI J Natl Cancer Inst 69:975–980

340. Ebert T, Bander NH, Finstad CL, Ramsawak RD, Old LJ (1990) Establishment and Characterization of Human Renal Cancer and Normal Kidney Cell Lines. Cancer Res 50:5531–5536

341. Artzt K, Dubois P, Bennett D, Condamine H, Babinet C, Jacob F (1973) Surface Antigens Common to Mouse Cleavage Embryos and Primitive Teratocarcinoma Cells in Culture. Proc Natl Acad Sci 70:2988–2992

342. Stevens LC (1970) The development of transplantable teratocarcinomas from intratesticular grafts of pre- and postimplantation mouse embryos. Dev Biol 21:364–382

343. Ziffels B, Grötsch A, Al-Bayati L, Neri D (2019) Targeted delivery of calreticulin to ED-A fibronectin leads to tumor-growth retardation. J Biotechnol 290:53–58

344. Dranoff G (2012) Experimental mouse tumour models: what can be learnt about human cancer immunology? Nat Rev Immunol 12:61–66

345. Mosely SIS, Prime JE, Sainson RCA, et al (2017) Rational Selection of Syngeneic Preclinical Tumor Models for Immunotherapeutic Drug Discovery. Cancer Immunol Res 5:29–41

346. Ziffels B, Pretto F, Neri D (2018) Intratumoral administration of IL2 and TNF based fusion proteins cures cancer without establishing protective immunity. Immunotherapy 10:177–188

347. De Luca R, Neri D (2018) Potentiation of PD-L1 blockade with a potency-matched dual cytokine antibody-fusion protein leads to cancer eradication in BALB/c-derived tumors but not in other mouse strains. Cancer Immunol Immunother CII 67:1381–1391

348. Pretto F (2013) Therapeutic activity of anti-cancer immunocytokines in combination with chemotherapy. https://doi.org/10.3929/ethz-a-009787817

349. Hess C, Neri D (2015) The antibody-mediated targeted delivery of interleukin-13 to syngeneic murine tumors mediates a potent anticancer activity. Cancer Immunol Immunother 64:635–644

350. Bonaventura P, Shekarian T, Alcazer V, Valladeau-Guilemond J, Valsesia-Wittmann S, Amigorena S, Caux C, Depil S (2019) Cold Tumors: A Therapeutic Challenge for Immunotherapy. Front Immunol 10:168

351. Quandt D, Zucht HD, Amann A, et al (2017) Implementing liquid biopsies into clinical decision making for cancer immunotherapy. Oncotarget 8:48507–48520

352. Halama N (2019) The next age of immunotherapy: optimisation, stratification and therapeutic synergies. Br J Cancer 120:1–2

353. Petitprez F, Meylan M, de Reyniès A, Sautès-Fridman C, Fridman WH (2020) The Tumor Microenvironment in the Response to Immune Checkpoint Blockade Therapies. Front Immunol 11:784

354. Yu JW, Bhattacharya S, Yanamandra N, et al (2018) Tumor-immune profiling of murine syngeneic tumor models as a framework to guide mechanistic studies and predict therapy response in distinct tumor microenvironments. PLOS ONE 13:e0206223

355. Even-Desrumeaux K, Baty D, Chames P (2011) State of the Art in Tumor Antigen and Biomarker Discovery. Cancers 3:2554–2596

356. Van den Eynde BJ, Scott AM (1998) Tumor Antigens. In: Delves PJ (ed) Encycl. Immunol. Second Ed. Elsevier, Oxford, pp 2424–2431

357. Grainger SJ, Putnam AJ (2013) ECM Remodeling in Angiogenesis. In: Reinhart-King CA (ed) Mech. Chem. Signal. Angiogenesis. Springer, Berlin, Heidelberg, pp 185–209

358. Henke E, Nandigama R, Ergün S (2020) Extracellular Matrix in the Tumor Microenvironment and Its Impact on Cancer Therapy. Front Mol Biosci 6:160

359. Brassart-Pasco S, Brézillon S, Brassart B, Ramont L, Oudart J-B, Monboisse JC (2020) Tumor Microenvironment: Extracellular Matrix Alterations Influence Tumor Progression. Front Oncol 10:397

360. Giussani M, Triulzi T, Sozzi G, Tagliabue E (2019) Tumor Extracellular Matrix Remodeling: New Perspectives as a Circulating Tool in the Diagnosis and Prognosis of Solid Tumors. Cells 8:81

361. Kaspar M, Zardi L, Neri D (2006) Fibronectin as target for tumor therapy. Int J Cancer 118:1331–1339

362. White ES, Baralle FE, Muro AF (2008) New insights into form and function of fibronectin splice variants. J Pathol 216:1–14

363. Rybak J-N, Roesli C, Kaspar M, Villa A, Neri D (2007) The Extra-domain A of Fibronectin Is a Vascular Marker of Solid Tumors and Metastases. Cancer Res 67:10948–10957

364. Venning FA, Wullkopf L, Erler JT (2015) Targeting ECM Disrupts Cancer Progression. Front Oncol 5:224

365. White ES, Muro AF (2011) Fibronectin splice variants: understanding their multiple roles in health and disease using engineered mouse models. IUBMB Life 63:538–546

366. Kumazaki T, Mitsui Y, Hamada K, Sumida H, Nishiyama M (1999) Detection of alternative splicing of fibronectin mRNA in a single cell. J Cell Sci 112:1449–1453

367. Bootz F, Schmid AS, Neri D (2015) Alternatively Spliced EDA Domain of Fibronectin Is a Target for Pharmacodelivery Applications in Inflammatory Bowel Disease. Inflamm Bowel Dis 21:1908–1917

368. Schwager K, Villa A, Rösli C, Neri D, Rösli-Khabas M, Moser G (2011) A comparative immunofluorescence analysis of three clinical-stage antibodies in head and neck cancer. Head Neck Oncol 3:25

369. Sauer S, Erba PA, Petrini M, et al (2009) Expression of the oncofetal ED-B–containing fibronectin isoform in hematologic tumors enables ED-B–targeted 131I-L19SIP radioimmunotherapy in Hodgkin lymphoma patients. Blood 113:2265–2274

370. Supuran CT (2008) Carbonic anhydrases: novel therapeutic applications for inhibitors and activators. Nat Rev Drug Discov 7:168–181

371. Supuran CT (2018) Carbonic anhydrase inhibitors as emerging agents for the treatment and imaging of hypoxic tumors. Expert Opin Investig Drugs 27:963–970

372. Neri D, Supuran CT (2011) Interfering with pH regulation in tumours as a therapeutic strategy. Nat Rev Drug Discov 10:767–777

373. Lv P-C, Roy J, Putt KS, Low PS (2017) Evaluation of Nonpeptidic Ligand Conjugates for the Treatment of Hypoxic and Carbonic Anhydrase IX-Expressing Cancers. Mol Cancer Ther 16:453–460

374. Krall N, Pretto F, Neri D (2014) A bivalent small molecule-drug conjugate directed against carbonic anhydrase IX can elicit complete tumour regression in mice. Chem Sci 5:3640–3644

375. Schett G, Gravallese E (2012) Bone erosion in rheumatoid arthritis: mechanisms, diagnosis and treatment. Nat Rev Rheumatol 8:656–664

376. Shiozawa S, Tsumiyama K, Yoshida K, Hashiramoto A (2011) Pathogenesis of Joint Destruction in Rheumatoid Arthritis. Arch Immunol Ther Exp (Warsz) 59:89–95

377. Sudoł-Szopińska I, Kontny E, Maśliński W, Prochorec-Sobieszek M, Kwiatkowska B, Zaniewicz-Kaniewska K, Warczyńska A (2012) The pathogenesis of rheumatoid arthritis in radiological studies. Part I: Formation of inflammatory infiltrates within the synovial membrane. J Ultrason 12:202–213

378. Makkar R, Behl T, Bungau S, Kumar A, Arora S (2020) Understanding the Role of Inflammasomes in Rheumatoid Arthritis. Inflammation. https://doi.org/10.1007/s10753-020-01301-1, Advance online publication.

379. Izquierdo E, Cañete JD, Celis R, Del Rey MJ, Usategui A, Marsal S, Sanmartí R, Criado G, Pablos JL (2011) Synovial fibroblast hyperplasia in rheumatoid arthritis: clinicopathologic correlations and partial reversal by anti-tumor necrosis factor therapy. Arthritis Rheum 63:2575–2583

380. McInnes IB, Schett G (2011) The pathogenesis of rheumatoid arthritis. N Engl J Med 365:2205–2219

381. Turesson C, Jacobsson L, Bergström U (1999) Extra-articular rheumatoid arthritis: prevalence and mortality. Rheumatol Oxf Engl 38:668–674

382. Moreland L (2005) Unmet needs in rheumatoid arthritis. Arthritis Res Ther 7:S2–S8

383. Courtenay JS, Dallman MJ, Dayan AD, Martin A, Mosedale B (1980) Immunisation against heterologous type II collagen induces arthritis in mice. Nature 283:666–668

384. Brand DD, Latham KA, Rosloniec EF (2007) Collagen-induced arthritis. Nat Protoc 2:1269–1275

385. Williams RO, Mason LJ, Feldmann M, Maini RN (1994) Synergy between anti-CD4 and anti-tumor necrosis factor in the amelioration of established collagen-induced arthritis. Proc Natl Acad Sci U S A 91:2762–2766

386. Kriegsmann J, Berndt A, Hansen T, et al (2004) Expression of fibronectin splice variants and oncofetal glycosylated fibronectin in the synovial membranes of patients with rheumatoid arthritis and osteoarthritis. Rheumatol Int 24:25–33

387. Shiozawa K, Hino K, Shiozawa S (2001) Alternatively spliced EDA-containing fibronectin in synovial fluid as a predictor of rheumatoid joint destruction. Rheumatology 40:739–742

388. Hoeper MM, Bogaard HJ, Condliffe R, et al (2013) Definitions and diagnosis of pulmonary hypertension. J Am Coll Cardiol 62:D42-50

389. Shah M, Patel K, Sehgal PB (2005) Monocrotaline pyrrole-induced endothelial cell megalocytosis involves a Golgi blockade mechanism. Am J Physiol Cell Physiol 288:C850-862

390. Stenmark KR, Meyrick B, Galie N, Mooi WJ, McMurtry IF (2009) Animal models of pulmonary arterial hypertension: the hope for etiological discovery and pharmacological cure. Am J Physiol Lung Cell Mol Physiol 297:L1013-1032

391. Ryan J, Bloch K, Archer SL (2011) Rodent models of pulmonary hypertension: harmonisation with the world health organisation's categorisation of human PH. Int J Clin Pract Suppl 15–34

392. Price LC, Wort SJ, Perros F, Dorfmüller P, Huertas A, Montani D, Cohen-Kaminsky S, Humbert M (2012) Inflammation in pulmonary arterial hypertension. Chest 141:210–221

393. Rabinovitch M, Guignabert C, Humbert M, Nicolls MR (2014) Inflammation and immunity in the pathogenesis of pulmonary arterial hypertension. Circ Res 115:165–175

394. Vergadi Eleni, Chang Mun Seog, Lee Changjin, Liang Olin D., Liu Xianlan, Fernandez-Gonzalez Angeles, Mitsialis S. Alex, Kourembanas Stella (2011) Early Macrophage Recruitment and Alternative Activation Are Critical for the Later Development of Hypoxia-Induced Pulmonary Hypertension. Circulation 123:1986–1995

395. Frid MG, Brunetti JA, Burke DL, Carpenter TC, Davie NJ, Reeves JT, Roedersheimer MT, van Rooijen N, Stenmark KR (2006) Hypoxia-induced pulmonary vascular remodeling requires recruitment of circulating mesenchymal precursors of a monocyte/macrophage lineage. Am J Pathol 168:659–669

396. Dorfmüller P, Perros F, Balabanian K, Humbert M (2003) Inflammation in pulmonary arterial hypertension. Eur Respir J 22:358–363

397. Thienemann F, Henz BM, Babina M (2004) Regulation of mast cell characteristics by cytokines: divergent effects of interleukin-4 on immature mast cell lines versus mature human skin mast cells. Arch Dermatol Res 296:134–138

398. Kumar R, Graham B (2018) How does inflammation contribute to pulmonary hypertension? Eur Respir J 51:1702403

399. Tamosiuniene R, Tian W, Dhillon G, et al (2011) Regulatory T cells limit vascular endothelial injury and prevent pulmonary hypertension. Circ Res 109:867–879

400. Maston LD, Jones DT, Giermakowska W, Howard TA, Cannon JL, Wang W, Wei Y, Xuan W, Resta TC, Gonzalez Bosc LV (2017) Central role of T helper 17 cells in chronic hypoxia-induced pulmonary hypertension. Am J Physiol Lung Cell Mol Physiol 312:L609–L624

401. Hashimoto-Kataoka T, Hosen N, Sonobe T, et al (2015) Interleukin-6/interleukin-21 signaling axis is critical in the pathogenesis of pulmonary arterial hypertension. Proc Natl Acad Sci 112:E2677–E2686

402. Huber LC, Bye H, Brock M, Swiss Society of Pulmonary Hypertension (2015) The pathogenesis of pulmonary hypertension--an update. Swiss Med Wkly 145:w14202

403. Franz M, Grün K, Betge S, et al (2016) Lung tissue remodelling in MCT-induced pulmonary hypertension: a proposal for a novel scoring system and changes in

extracellular matrix and fibrosis associated gene expression. Oncotarget 7:81241–81254

404. Renauld JC, Druez C, Kermouni A, Houssiau F, Uyttenhove C, Van Roost E, Van Snick J (1992) Expression cloning of the murine and human interleukin 9 receptor cDNAs. Proc Natl Acad Sci U S A 89:5690–5694

405. Koch S, Sopel N, Finotto S (2017) Th9 and other IL-9-producing cells in allergic asthma. Semin Immunopathol 39:55–68

406. Hauber H-P, Bergeron C, Hamid Q (2004) IL-9 in allergic inflammation. Int Arch Allergy Immunol 134:79–87

407. Rivera Vargas T, Humblin E, Végran F, Ghiringhelli F, Apetoh L (2017) TH9 cells in anti-tumor immunity. Semin Immunopathol 39:39–46

408. Chen N, Lu K, Li P, Lv X, Wang X (2014) Overexpression of IL-9 induced by STAT6 activation promotes the pathogenesis of chronic lymphocytic leukemia. Int J Clin Exp Pathol 7:2319–2323

409. Neri D, Sondel PM (2016) Immunocytokines for cancer treatment: past, present and future. Curr Opin Immunol 40:96–102

410. Pasche N, Neri D (2012) Immunocytokines: a novel class of potent armed antibodies. Drug Discov Today 17:583–590

411. Rybak J-N, Trachsel E, Scheuermann J, Neri D (2007) Ligand-based vascular targeting of disease. ChemMedChem 2:22–40

412. Schliemann C, Palumbo A, Zuberbühler K, Villa A, Kaspar M, Trachsel E, Klapper W, Menssen HD, Neri D (2009) Complete eradication of human B-cell lymphoma xenografts using rituximab in combination with the immunocytokine L19-IL2. Blood 113:2275–2283

413. Gutbrodt KL, Schliemann C, Giovannoni L, Frey K, Pabst T, Klapper W, Berdel WE, Neri D (2013) Antibody-based delivery of interleukin-2 to neovasculature has potent activity against acute myeloid leukemia. Sci Transl Med 5:201ra118

414. Bootz F, Venetz D, Ziffels B, Neri D (2016) Different tissue distribution properties for glycosylation variants of fusion proteins containing the p40 subunit of murine interleukin-12. Protein Eng Des Sel 29:445–455

415. Doll F, Schwager K, Hemmerle T, Neri D (2013) Murine analogues of etanercept and of F8-IL10 inhibit the progression of collagen-induced arthritis in the mouse. Arthritis Res Ther 15:R138

416. Bruijnen STG, Chandrupatla DMSH, Giovanonni L, et al (2019) F8-IL10: A New Potential Antirheumatic Drug Evaluated by a PET-Guided Translational Approach. Mol Pharm 16:273–281

417. Hacker DL, Kiseljak D, Rajendra Y, Thurnheer S, Baldi L, Wurm FM (2013) Polyethyleneimine-based transient gene expression processes for suspension-adapted HEK-293E and CHO-DG44 cells. Protein Expr Purif 92:67–76

418. Pfaffen S, Frey K, Stutz I, Roesli C, Neri D (2010) Tumour-targeting properties of antibodies specific to MMP-1A, MMP-2 and MMP-3. Eur J Nucl Med Mol Imaging 37:1559–1565

419. Lu Y, Hong S, Li H, et al (2012) Th9 cells promote antitumor immune responses in vivo. J Clin Invest 122:4160–4171

420. Ebbinghaus C, Ronca R, Kaspar M, Grabulovski D, Berndt A, Kosmehl H, Zardi L, Neri D (2005) Engineered vascular-targeting antibody-interferon-gamma fusion protein for cancer therapy. Int J Cancer 116:304–313

421. Puca E, Probst P, Stringhini M, et al (2020) The antibody-based delivery of interleukin-12 to solid tumors boosts NK and CD8+ T cell activity and synergizes with immune checkpoint inhibitors. Int J Cancer 146:2518–2530

422. Hutmacher C, Núñez NG, Liuzzi AR, Becher B, Neri D (2019) Targeted Delivery of IL2 to the Tumor Stroma Potentiates the Action of Immune Checkpoint Inhibitors by Preferential Activation of NK and CD8+ T Cells. Cancer Immunol Res 7:572–583

423. Chen T, Guo J, Cai Z, et al (2020) Th9 Cell Differentiation and Its Dual Effects in Tumor Development. Front Immunol 11:1026

424. Lee JE, Zhu Z, Bai Q, Brady TJ, Xiao H, Wakefield MR, Fang Y (2019) The Role of Interleukin-9 in Cancer. Pathol Oncol Res. https://doi.org/10.1007/s12253-019-00665-6

425. Schmitt E, Klein M, Bopp T (2014) Th9 cells, new players in adaptive immunity. Trends Immunol 35:61–68

426. Ramadan A, Griesenauer B, Adom D, Kapur R, Hanenberg H, Liu C, Kaplan MH, Paczesny S (2017) Specifically differentiated T cell subset promotes tumor immunity over fatal immunity. J Exp Med 214:3577–3596

427. Hu B, Qiu-Lan H, Lei R-E, Shi C, Jiang H-X, Qin S-Y (2017) Interleukin-9 Promotes Pancreatic Cancer Cells Proliferation and Migration via the miR-200a/Beta-Catenin Axis. BioMed Res Int 2017:2831056

428. Tian L, Li Y, Chang R, Zhang P, Zhang J, Huo L (2019) Lentiviral vector-mediated IL-9 overexpression stimulates cell proliferation by targeting c-myc and cyclin D1 in colitis-associated cancer. Oncol Lett 17:175–182

429. Ye Z-J, Zhou Q, Yin W, Yuan M-L, Yang W-B, Xiong X-Z, Zhang J-C, Shi H-Z (2012) Differentiation and immune regulation of IL-9-producing CD4+ T cells in malignant pleural effusion. Am J Respir Crit Care Med 186:1168–1179

430. Park SM, Do-Thi VA, Lee J-O, Lee H, Kim YS (2020) Interleukin-9 Inhibits Lung Metastasis of Melanoma through Stimulating Anti-Tumor M1 Macrophages. Mol Cells 43:479–490

431. Frey K, Zivanovic A, Schwager K, Neri D (2011) Antibody-based targeting of interferon-alpha to the tumor neovasculature: a critical evaluation. Integr Biol Quant Biosci Nano Macro 3:468–478

432. Pasche N, Frey K, Neri D (2012) The targeted delivery of IL17 to the mouse tumor neo-vasculature enhances angiogenesis but does not reduce tumor growth rate. Angiogenesis 15:165–169

433. De Luca R, Gouyou B, Ongaro T, Villa A, Ziffels B, Sannino A, Buttinoni G, Galeazzi S, Mazzacuva M, Neri D (2019) A Novel Fully-Human Potency-Matched Dual Cytokine-Antibody Fusion Protein Targets Carbonic Anhydrase IX in Renal Cell Carcinomas. Front Oncol 9:1228

434. Omata Y, Frech M, Primbs T, et al (2018) Group 2 Innate Lymphoid Cells Attenuate Inflammatory Arthritis and Protect from Bone Destruction in Mice. Cell Rep 24:169–180

435. Galiè N, Humbert M, Vachiery J-L, et al (2016) 2015 ESC/ERS Guidelines for the Diagnosis and Treatment of Pulmonary Hypertension. Rev Espanola Cardiol Engl Ed 69:177

436. Perros F, Humbert M (2005) [Physiopathology of pulmonary arterial hypertension. Cellular and molecular aspects]. Presse Medicale Paris Fr 1983 34:232–242

437. Gouyou B, Ongaro T, Cazzamalli S, Luca RD, Kerschenmeyer A, Valet P, Villa A, Neri D, Matasci M (2020) Antibody-based delivery of Interleukin-9 to neovascular structures: therapeutic evaluation in cancer and arthritis. bioRxiv 2020.08.26.268292

438. Rohm I, Grün K, Müller LM, et al (2019) Cellular inflammation in pulmonary hypertension: Detailed analysis of lung and right ventricular tissue, circulating immune cells and effects of a dual endothelin receptor antagonist. Clin Hemorheol Microcirc 73:497–522

439. Maarman G, Lecour S, Butrous G, Thienemann F, Sliwa K (2013) A comprehensive review: the evolution of animal models in pulmonary hypertension research; are we there yet? Pulm Circ 3:739–756

440. Nogueira-Ferreira R, Vitorino R, Ferreira R, Henriques-Coelho T (2015) Exploring the monocrotaline animal model for the study of pulmonary arterial hypertension: A network approach. Pulm Pharmacol Ther 35:8–16

441. Hassoun PM, Mouthon L, Barberà JA, et al (2009) Inflammation, growth factors, and pulmonary vascular remodeling. J Am Coll Cardiol 54:S10-19

442. Pullamsetti SS, Savai R, Janssen W, Dahal BK, Seeger W, Grimminger F, Ghofrani HA, Weissmann N, Schermuly RT (2011) Inflammation, immunological

reaction and role of infection in pulmonary hypertension. Clin Microbiol Infect 17:7–14

443. Tuder RM, Groves B, Badesch DB, Voelkel NF (1994) Exuberant endothelial cell growth and elements of inflammation are present in plexiform lesions of pulmonary hypertension. Am J Pathol 144:275–285

444. Thenappan T, Goel A, Marsboom G, et al (2011) A central role for CD68(+) macrophages in hepatopulmonary syndrome. Reversal by macrophage depletion. Am J Respir Crit Care Med 183:1080–1091

445. Tian W, Jiang X, Tamosiuniene R, et al (2013) Blocking macrophage leukotriene b4 prevents endothelial injury and reverses pulmonary hypertension. Sci Transl Med 5:200ra117

446. Cuttica MJ, Langenickel T, Noguchi A, Machado RF, Gladwin MT, Boehm M (2011) Perivascular T-Cell Infiltration Leads to Sustained Pulmonary Artery Remodeling after Endothelial Cell Damage. Am J Respir Cell Mol Biol 45:62–71

447. Austin ED, Rock MT, Mosse CA, Vnencak-Jones CL, Yoder SM, Robbins IM, Loyd JE, Meyrick BO (2010) T lymphocyte subset abnormalities in the blood and lung in pulmonary arterial hypertension. Respir Med 104:454–462

448. Nicolls MR, Mizuno S, Taraseviciene-Stewart L, Farkas L, Drake JI, Al Husseini A, Gomez-Arroyo JG, Voelkel NF, Bogaard HJ (2012) New models of pulmonary hypertension based on VEGF receptor blockade-induced endothelial cell apoptosis. Pulm Circ 2:434–442

449. Tamosiuniene R, Manouvakhova O, Mesange P, et al (2018) Dominant Role for Regulatory T Cells in Protecting Females Against Pulmonary Hypertension. Circ Res 122:1689–1702

450. Sada Y, Dohi Y, Uga S, Higashi A, Kinoshita H, Kihara Y (2016) Non-suppressive regulatory T cell subset expansion in pulmonary arterial hypertension. Heart Vessels 31:1319–1326

451. Pilette C, Ouadrhiri Y, Van Snick J, Renauld JC, Staquet P, Vaerman JP, Sibille Y (2002) Oxidative burst in lipopolysaccharide-activated human alveolar macrophages is inhibited by interleukin-9. Eur Respir J 20:1198–1205

452. Mindt BC, Fritz JH, Duerr CU (2018) Group 2 Innate Lymphoid Cells in Pulmonary Immunity and Tissue Homeostasis. Front Immunol 9:840

453. Murer P, Neri D (2019) Antibody-cytokine fusion proteins: A novel class of biopharmaceuticals for the therapy of cancer and of chronic inflammation. New Biotechnol 52:42–53

454. List T, Neri D (2013) Immunocytokines: a review of molecules in clinical development for cancer therapy. Clin Pharmacol Adv Appl 5:29–45

455. Hillier SM, Maresca KP, Lu G, Merkin RD, Marquis JC, Zimmerman CN, Eckelman WC, Joyal JL, Babich JW (2013) 99mTc-Labeled Small-Molecule

Inhibitors of Prostate-Specific Membrane Antigen for Molecular Imaging of Prostate Cancer. J Nucl Med 54:1369–1376

456. Ginj M, Zhang H, Waser B, Cescato R, Wild D, Wang X, Erchegyi J, Rivier J, Mäcke HR, Reubi JC (2006) Radiolabeled somatostatin receptor antagonists are preferable to agonists for in vivo peptide receptor targeting of tumors. Proc Natl Acad Sci 103:16436–16441

457. Supuran CT (2020) Exploring the multiple binding modes of inhibitors to carbonic anhydrases for novel drug discovery. Expert Opin Drug Discov 15:671–686

458. Cazzamalli S, Corso AD, Neri D (2017) Linker stability influences the anti-tumor activity of acetazolamide-drug conjugates for the therapy of renal cell carcinoma. J Control Release Off J Control Release Soc 246:39–45

459. Supuran CT, Alterio V, Di Fiore A, D' Ambrosio K, Carta F, Monti SM, De Simone G (2018) Inhibition of carbonic anhydrase IX targets primary tumors, metastases, and cancer stem cells: Three for the price of one. Med Res Rev 38:1799–1836

460. van Kuijk SJA, Parvathaneni NK, Niemans R, et al (2017) New approach of delivering cytotoxic drugs towards CAIX expressing cells: A concept of dual-target drugs. Eur J Med Chem 127:691–702

461. Cazzamalli S, Dal Corso A, Neri D (2016) Acetazolamide Serves as Selective Delivery Vehicle for Dipeptide-Linked Drugs to Renal Cell Carcinoma. Mol Cancer Ther 15:2926–2935

462. Cazzamalli S, Ziffels B, Widmayer F, Murer P, Pellegrini G, Pretto F, Wulhfard S, Neri D (2018) Enhanced Therapeutic Activity of Non-Internalizing Small-Molecule-Drug Conjugates Targeting Carbonic Anhydrase IX in Combination with Targeted Interleukin-2. Clin Cancer Res Off J Am Assoc Cancer Res 24:3656–3667

463. Kalia V, Sarkar S, Subramaniam S, Haining WN, Smith KA, Ahmed R (2010) Prolonged interleukin-2Ralpha expression on virus-specific CD8+ T cells favors terminal-effector differentiation in vivo. Immunity 32:91–103

464. Popp MW, Antos JM, Grotenbreg GM, Spooner E, Ploegh HL (2007) Sortagging: a versatile method for protein labeling. Nat Chem Biol 3:707–708

465. Rashidian M, Keliher EJ, Dougan M, et al (2015) Use of 18F-2-Fluorodeoxyglucose to Label Antibody Fragments for Immuno-Positron Emission Tomography of Pancreatic Cancer. ACS Cent Sci 1:142–147

466. Witte MD, Wu T, Guimaraes CP, Theile CS, Blom AEM, Ingram JR, Li Z, Kundrat L, Goldberg SD, Ploegh HL (2015) Site-specific protein modification using immobilized sortase in batch and continuous-flow systems. Nat Protoc 10:508–516

467. Bartels L, Ploegh HL, Spits H, Wagner K (2019) Preparation of bispecific antibody-protein adducts by site-specific chemo-enzymatic conjugation. Methods San Diego Calif 154:93–101

468. Gébleux R, Briendl M, Grawunder U, Beerli RR (2019) Sortase A Enzyme-Mediated Generation of Site-Specifically Conjugated Antibody-Drug Conjugates. Methods Mol Biol Clifton NJ 2012:1–13

469. Chen L, Cohen J, Song X, Zhao A, Ye Z, Feulner CJ, Doonan P, Somers W, Lin L, Chen PR (2016) Improved variants of SrtA for site-specific conjugation on antibodies and proteins with high efficiency. Sci Rep 6:31899

470. O'Connor-Semmes RL, Lin J, Hodge RJ, Andrews S, Chism J, Choudhury A, Nunez DJ (2014) GSK2374697, a novel albumin-binding domain antibody (AlbudAb), extends systemic exposure of exendin-4: first study in humans--PK/PD and safety. Clin Pharmacol Ther 96:704–12

471. Zhen EY, Higgs RE, Gutierrez JA (2013) Pyroglutamyl apelin-13 identified as the major apelin isoform in human plasma. Anal Biochem 442:1–9

472. Yue P, Jin H, Xu S, Aillaud M, Deng A, Azuma J, Kundu R, Reaven G, Quertermous T, Tsao P (2011) Apelin decreases lipolysis via G(q), G(i), and AMPK-Dependent Mechanisms. Endocrinology 152:58–68

473. Brame AL, Maguire JJ, Yang P, Dyson A, Torella R, Cheriyan J, Singer M, Glen RC, Wilkinson IB, Davenport AP (2015) Design, Characterization, and First-In-Human Study of the Vascular Actions of a Novel Biased Apelin Receptor Agonist. Hypertension 65:834–840

474. Jia ZQ, Hou L, Leger A, Wu I, Kudej AB, Stefano J, Jiang C, Pan CQ, Akita GY (2012) Cardiovascular effects of a PEGylated apelin. Peptides 38:181–188

475. Riches AC, Sharp JG, Thomas DB, Smith SV (1973) Blood volume determination in the mouse. J Physiol 228:279–284

476. Trân K, Murza A, Sainsily X, et al (2018) A Systematic Exploration of Macrocyclization in Apelin-13: Impact on Binding, Signaling, Stability, and Cardiovascular Effects. J Med Chem 61:2266–2277

477. Catania C, Maur M, Berardi R, et al (2015) The tumor-targeting immunocytokine F16-IL2 in combination with doxorubicin: dose escalation in patients with advanced solid tumors and expansion into patients with metastatic breast cancer. Cell Adhes Migr 9:14–21

478. Spitaleri G, Berardi R, Pierantoni C, et al (2013) Phase I/II study of the tumour-targeting human monoclonal antibody–cytokine fusion protein L19-TNF in patients with advanced solid tumours. J Cancer Res Clin Oncol 139:447–455

479. Elyaman W, Khoury SJ (2017) Th9 cells in the pathogenesis of EAE and multiple sclerosis. Semin Immunopathol 39:79–87

480. Rudman SM, Jameson MB, McKeage MJ, Savage P, Jodrell DI, Harries M, Acton G, Erlandsson F, Spicer JF (2011) A phase 1 study of AS1409, a novel antibody-cytokine fusion protein, in patients with malignant melanoma or renal cell carcinoma. Clin Cancer Res Off J Am Assoc Cancer Res 17:1998–2005

481. NBE Therapeutics (2020) NBE Therapeutics Company Facts sheet January 2020. 1

482. NBE Therapeutics (2020) NBE-Therapeutics closes a USD 22M Series C financing round. In: NBE Ther. https://www.nbe-therapeutics.com/newsroom/news-press-releases/2020/2020-01-10.

483. Read C (2019) The Identification and Pharmacological Characterisation of Novel Apelin Receptor Agonists In Vitro and In Vivo. PhD Thesis of the University of Cambridge. https://doi.org/10.17863/CAM.35320